Design of a Regional Hybrid Transport Aircraft

A Project Presented to
The Faculty of the Department of Aerospace Engineering
San Jose State University

In Partial Fulfillment to the Requirements of the Degree
Master of Science in Aerospace Engineering

By

Rupa Sindhu Gunnam

Approved by

Dr. Nikos J. Mourtos
Faculty Advisor

TABLE OF CONTENTS

LIST OF SYMBOLS

Symbol	**Definition**
AAA	Advanced Aircraft Analysis
AR	Aspect Ratio
A, B	Regression line constants
b	Span of the wing
$\bar{c}$	Mean aerodynamic chord
C_r	Root chord length of the wing
C_t	Tip chord length of the wing
C_f	Equivalent skin friction coefficient
C_P	Specific fuel consumption
C_D	Drag coefficient
C_{D_o}	Zero lift drag coefficient
C_L	Lift Coefficient
$C_{L_{max_{TO}}}$	Maximum takeoff lift coefficient
$C_{L_{max_L}}$	Maximum landing lift coefficient
$\frac{c_f}{c}$	Ratio of flap chord length to the wing chord length
CG	Center of gravity
CGR	Climb gradient
CGRP	Climb gradient parameter
D	$W_{PL} + W_{Crew} + W_{Bat}$
D_P	Diameter of the propeller
e	Oswald's efficiency factor
E	Endurance
E^{climb}	Energy required to climb
E^{cruise}	Energy required to cruise
E^{loiter}	Energy required to loiter

E^*	Battery energy density
f	Equivalent parasite area
f_e	Fraction of empty weight to takeoff weight
f_p	Fraction of payload weight to takeoff weight
FAR 25	Federal Aviation Regulations part 25
F	Weight sensitivity
g	Acceleration of gravity
h	Altitude
$i_{W_{root}}$	Incidence angle of wing root
$i_{W_{tip}}$	Incidence angle of wing tip
I_P	Power index
L	Lift
L/D	Lift-to-drag ratio
M_{ff}	Mission fuel fraction
nm	Nautical mile (6,076 ft)
NACA	National Advisory Committee for Aeronautics
P	Power
P_{max}	Maximum power per engine
P_{bl}	Power loading per blade
p	Power density of the battery
P_r^{climb}	Power required to climb
P_r^{cruise}	Power required to cruise
P_r^{loiter}	Power required to loiter
R	Range
RC	Rate of climb
sm	Statute mile (5,280 ft)
S	Wing area
S_{wet}	Wetted area

S_{FL}	Landing field length
S_{TOFL}	Takeoff field length
S_{wf}	Wing flap area
$\left(\frac{t}{c}\right)_r$	Thickness to chord ratio of wing root
$\left(\frac{t}{c}\right)_t$	Thickness to chord ratio of wing tip
TTC	Time to climb
T^{cruise}	Time to cruise
T^{loiter}	Time to loiter
V	Velocity of the aircraft
V_A	Approach speed
V_{S_L}	Landing stall speed
V_{cr}	Cruise speed
V^{climb}	Velocity to climb
V^{cruise}	Cruise velocity
V^{loiter}	Loiter velocity
W	Weight
$\frac{W}{S}$	Wing loading
$\frac{W}{P}$	Power loading or weight-to-power ratio
W_{TO}	Takeoff weight
W_{OE}	Operating empty weight
W_E	Empty weight
W_F	Fuel weight
W_{PL}	Payload weight
W_{Crew}	Crew weight
W_{Bat}	Battery weight

$W_{F_{used}}$	Used fuel weight
$W_{F_{res}}$	Reserve fuel weight
W_{tfo}	Weight of all trapped fuel and oil
V_{cr}	Cruise speed
V_{Wf}	Wing fuel volume
$\bar{Y}$	Span wise location of the mean aerodynamic chord
ρ	air density
π	product or 3.142
η_{toal}	Total system efficiency
η_p	propeller efficiency
σ	Density ratio
μ	Dynamic viscosity
λ_W	Taper Ratio of the wing
Λ_{LE}	Leading-edge sweep angle
Λ_{TE}	Trailing-edge sweep angle
$\Lambda_{c/4}$	Quarter chord sweep angle
ε_t	Geometric twist angle
α_{aero}	Aerodynamic twist angle
$\delta_{f_{TO}}$	Take-off flap angle
δ_{f_L}	Landing flap angle

LIST OF FIGURES

LIST OF TABLES

CHAPTER 1: MISSION SPECIFICATION AND COMPARATIVE STUDY

1.1 INTRODUCTION

Aviation industry uses fossil fuels in greater ratio for propulsion system and subsystems. The rise in demand for fossil fuels leads to more energy consumption by next few decades resulting in increased prices (Robertson, 2015). The increased density of energy in hydrocarbon fuels used for gas-turbine engines, reciprocating engines produces polluted emissions and noise. Hence, this chapter presents a hybrid-electric turboprop aircraft RUP-27N as an alternative to conventional gasoline turboprop aircraft. RUP-27N uses a combination of electric and gasoline for the mission to reduce fuel consumption and emissions in environment. The electric motors have high efficiency and power to weight ratio as compared to gas-turbine engines. Hybrid aircraft have advantages of the following:

- Increased fuel efficiency
- Increased power
- Less polluted emissions
- Suppression of noise during take-off and landing

A comparative study can be performed for RUP-27N with existing aircraft ATR 72-600, ATR 42-600, Fokker 50 and Bombardier Q400 in terms of fuel consumption, maintenance cost and operating cost. The main challenge of hybrid-electric aircraft is the storage of high amount of electric energy at low weight and volume (Stuckl, 2012). In this chapter rechargeable batteries are considered for the design. Using conventional turboprop aircraft as reference, RUP-27N hybrid electric aircraft will be designed with parallel propulsion system. RUP-27N aircraft can use electric power at specific flight phases for propulsion and batteries are used to replace fossil fuels partly.

1.2 MOTIVATION

Air travel has increased in recent years, a trend that will continue to rise in coming decades (ATAG, 2018). The number of airplanes has grown in response to the rising energy demands of the public. Currently, the aviation industry uses fossil-fuel-dependent propulsion systems;

gas-turbine and internal combustion engine powered systems are most prevalent in the industry. These engines produce toxic gases during operation that can severely impact the environment and human life. The demands of air travel continue to rise as do fossil fuel prices and environmental concerns (Friedrich, 2014). Environmental concerns surrounding global warming, air pollution, and depletion of energy resources like fossil fuels necessitate greater attention to protect the earth. To address and improve these environmental concerns, research for an alternative to fossil fuel has been started by many companies—including National Aeronautics and Space Administration (NASA) (Anticliff, 2018).

The two primary alternatives for fossil fuels are electric propulsion and hybrid-electric propulsion systems (Jansen, 2017). Electrical airplanes are highly efficient with negligible emission levels. Replacing fuel-based propulsion systems with electrical propulsion is advantageous, but current battery energy densities complicate the transition (Stuckl, 2012). Hence, this chapter presents an alternative solution—hybrid-electric propulsion. A hybrid system combines both fuel and battery-based propulsion systems. The advantages of hybrid-electric propulsion are decreased fuel consumption, fewer emissions, increased power, and reduced aircraft noise. Use of small regional aircraft (up to 40 passengers) can encourage airlines to reestablish service at smaller airports, open new markets, and increase passenger mobility and connectivity. To meet these requirements, hybrid-electric propulsion systems are the ideal technology.

1.3 LITERATURE REVIEW

Road vehicles using electrical and hybrid engines have now become a standard in the automotive industry, but the use of electric and hybrid propulsion systems in aviation is still under development for regional aircraft. There are several successful electrical aircraft on the market that can transport up to 4 passengers, but regional aircraft are still in development. The main drawback of purely electric propulsion is the size of the energy storage systems—specifically battery size and weight. Current battery technology limits the use of strictly electrical aircraft to small, light aircraft.

Accommodating the energy-to-mass and energy-to-volume densities required in electrical systems can impact the takeoff weight and aircraft size—a challenge to the industry. To overcome this challenge a partial replacement of fuel with battery power reduces fuel

consumption and emissions, without a significant impact on aircraft size and weight. Recent improvements in battery technology have allowed the combination of fuel and battery in hybrid-electric aircraft through a parallel propulsion system. A hybrid plane with rechargeable batteries and a parallel hybrid engine, funded by Boeing, has been designed and tested by a team of engineers based at the University of Cambridge in the United Kingdom (Cambridge, 2014). This is the first plane capable of recharging its lithium-polymer batteries in mid-flight and uses 30% less fuel than a conventional aircraft (Cambridge, 2014). This aircraft is a single-seater and uses a Honda 4-stroke piston engine in parallel with a lightweight electric motor or generator to drive the propeller (Cambridge, 2014).

The Zunum Aero's startup plans to conduct their first hybrid-electric test flight for regional travel in 2019 (Knapp, 2018). Zunum Aero is building a hybrid-electric short-haul aircraft for Boeing and Jetblue. This aircraft combines a gas-turbine engine with batteries, where cruising power is generated by a gas-turbine linked to a generator and stores lithium-ion batteries in the wing for extra power during takeoff (Knapp, 2018). This is a 12-passenger regional hybrid-electric aircraft with a range of 1125 km—the existing battery technology limits passenger capacity. Figure 1 shows the schematic diagram of Zunum Aero's hybrid-electric aircraft.

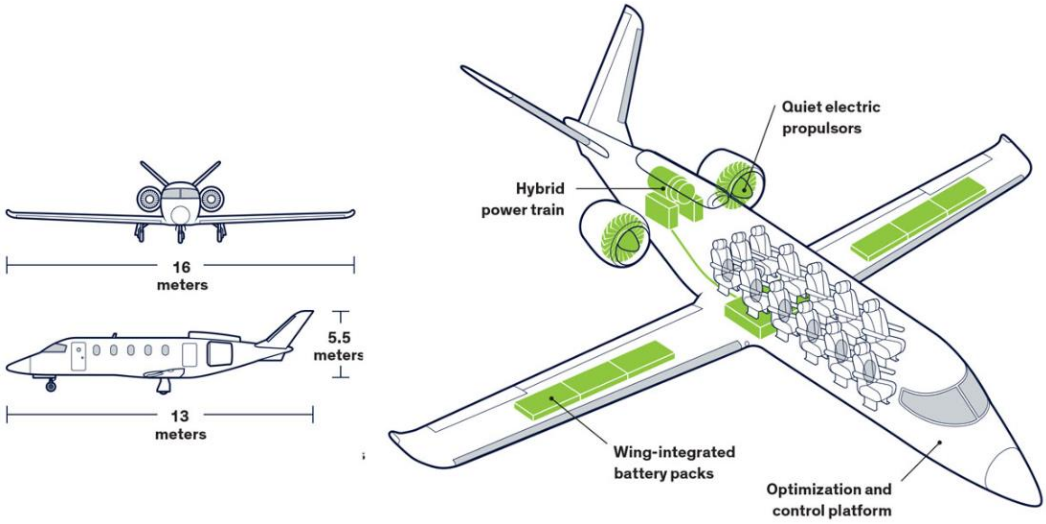

Figure 1: Zunum Aero's regional hybrid-electric plane

The critical requirement of battery technology is energy storage. The most important parameters for energy storage in aircraft is energy per mass and energy per volume. The parameters for various energy storage systems are shown in Figure 2 (Hepperle, 2012). While Figure 2 shows that kerosene is the most efficient energy storage system compared to current battery systems, it has a mass-specific energy density factor of 60 (Hepperle, 2012). The additional weight to the aircraft's wings and fuselage to accommodate additional energy pods leads to loss of efficiency due to the large wetted area. The aircraft is less affected by a lower volume specific energy content than higher volume specific energy. The fuel cells of hydrogen can be stored in metal, but the increased weight makes it unsuitable for aviation. Unfortunately, due to lack of high-power technology conversion for high energy density bio-fuels, like cream or milk, they are currently not useful to the aviation industry.

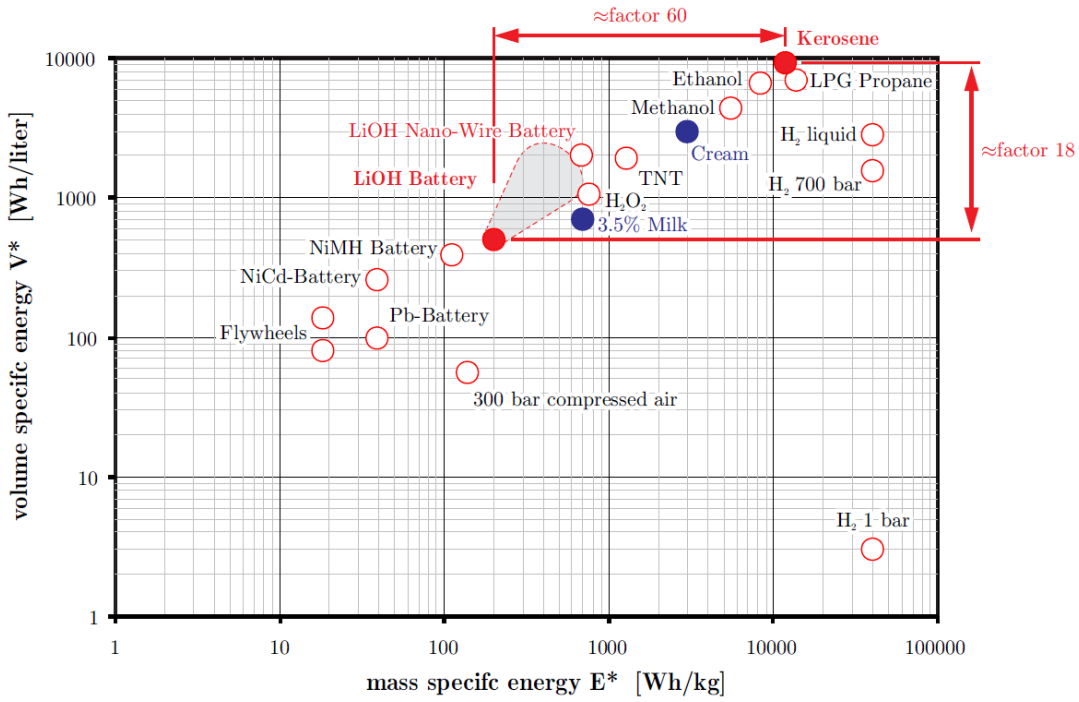

Figure 2: Mass specific energy and volume specific energy characteristics for various energy storage systems

Kerosene can be stored in tanks placed in the fuselage or wings like conventional fuel. Kerosene tanks are integrated with the structure, so they are of low mass compared to other storage systems. Hydrogen, both gas and liquid forms, requires pressure tanks for storage, increasing the weight of the aircraft and in turn drag, compared to conventional fuels.

Batteries also require casings with temperature-control systems, further increasing the weight of the electric-based systems.

Most electric aircraft use lithium-ion batteries as they are relatively cheap compared to other battery systems and can be scaled to fit larger systems with high energy capacity (Hepperle, 2012). Figure 3 shows the current and projected developments in battery systems (Hepperle, 2012). Currently, most battery energy storage systems are lithium-based but based on the survey of battery system development, sulfur-based systems are expected to be predominant in the next 20 years (Luongo, 2014). The currently available specific energy density of the lithium-ion battery system is 200 Wh/kg and is expected to improve to 250 Wh/kg. Lithium-sulfur and lithium-oxygen battery systems research is in active development but shows limited practicality for oxygen-based systems.

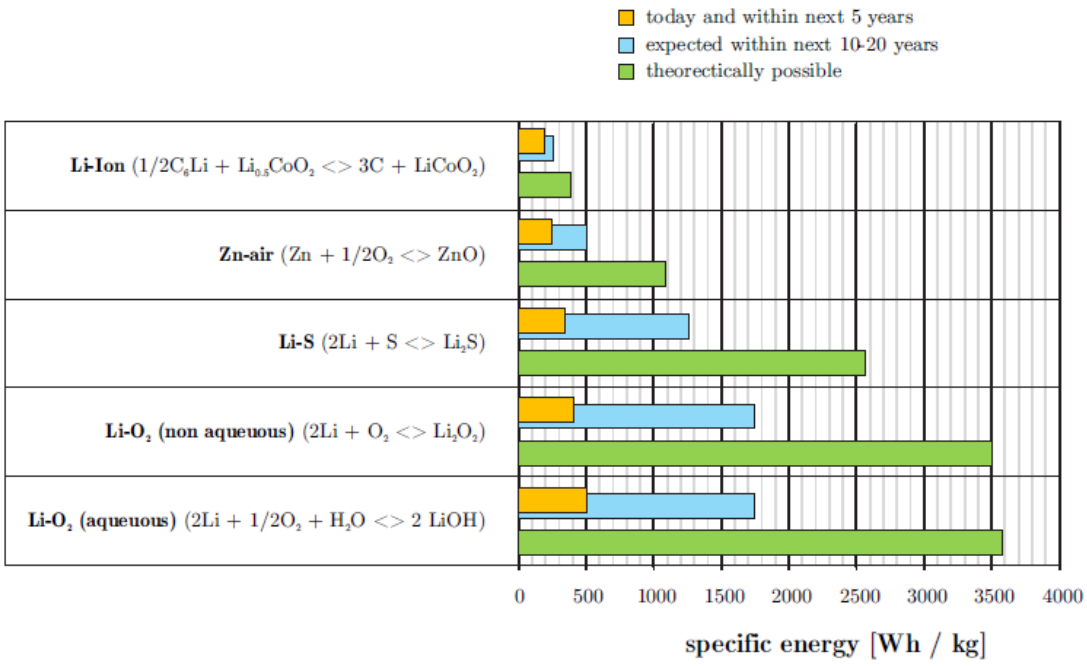

Figure 3: Current and future expected developments in battery technology

Boeing commenced research on a Subsonic Ultra Green Aircraft (SUGAR) for NASA based on a hybrid-electric design (Bradley, 2015). SUGAR is proposed to carry 154 passengers with a dual-class cabin using a hybrid-electric technology, the expected timeline for completion is 2030-2035 (Bradley, 2015). Current SUGAR plans have the aircraft using a battery specific energy of 750 Wh/kg obtained from battery pods located under the wing, distributing the

battery pods across the wing for weight balance. SUGAR is one of the largest ongoing research projects to increase aircraft passenger capacity using a hybrid-electric design, by using battery power in addition to gas-turbine power during take-off. Electric motors placed below the wings generate the battery power required for take-off. Boeing's SUGAR project strives to reduce fuel consumption, emissions, and noise level of the aircraft.

1.4 MISSION SPECIFICATION

1.4.1 Mission Specification

RUP-27N hybrid aircraft is mainly for regional commercial transport with capacity of 40 passengers. The mission requirements for the proposed aircraft design RUP-27N are given below

Table 1: Mission specifications

Pay Load Capacity	Passengers: 40 (175 lbs passenger weight plus 30 lbs baggage weight)
Crew	2 Pilots, 2 Cabin crew
Range	1575 km (850 nmi)
Cruise Speed	510 km/hr (275 knots)
Mach Number	0.42
Cruise Altitude	7600 m
Take-off Field Length	1367 m
Landing Field Length	1300 m
Approach Speed	209.3 km/hr (113 knots)

1.4.2 Mission Profile

The mission phases and profile for the proposed design is shown below

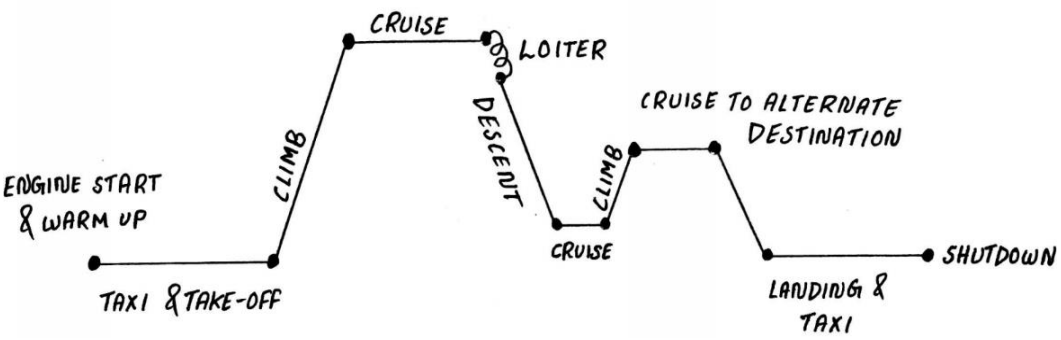

Figure 4: Mission profile for RUP-27N hybrid electric aircraft

1.4.3 Market Analysis

The aviation industry is tremendously growing since last few years and future predictions shows that the air transport further increases (ATAG, 2018). The main goal of an aircraft industry is to keep up the growth by offering the capability in an economical, safe and eco-friendly way. NASA predicts the fuel saving of 26% to 56% for the hybrid aircraft as compared to conventional aircraft (Jansen, 2017). Environmental concern for global warming is a major factor to be considered in aircraft market analysis. Airliners compare the aircraft based on the large number of seats with less operating and maintenance cost. The motivation for designing RUP-27N hybrid electric aircraft is to reduce harmful emissions, save fuel and reduce maintenance cost. The need for such aircraft is for economic saving and environmental benefits. The current market is potentially looking for more electric transportation rather than the fuel transportation for safety, conservation of energy and conservation of earth. This trend for electric transport has grown for aviation industry since last few years.

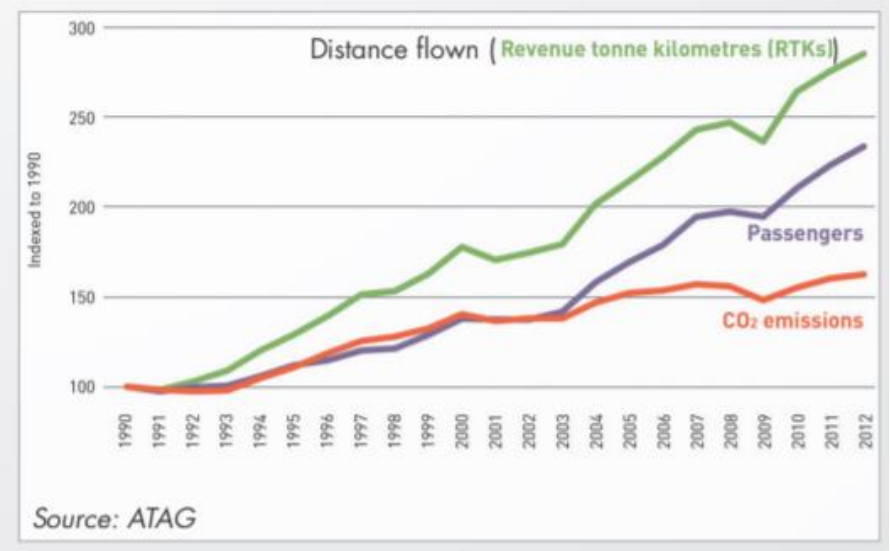

Figure 5: Passengers growth and distance growth with respect to CO2 emissions

RUP-27N can be designed using ATR 72-600 turboprop aircraft as reference aircraft and according to the ATR brochure the following emissions data is provided (ATR, 2014).

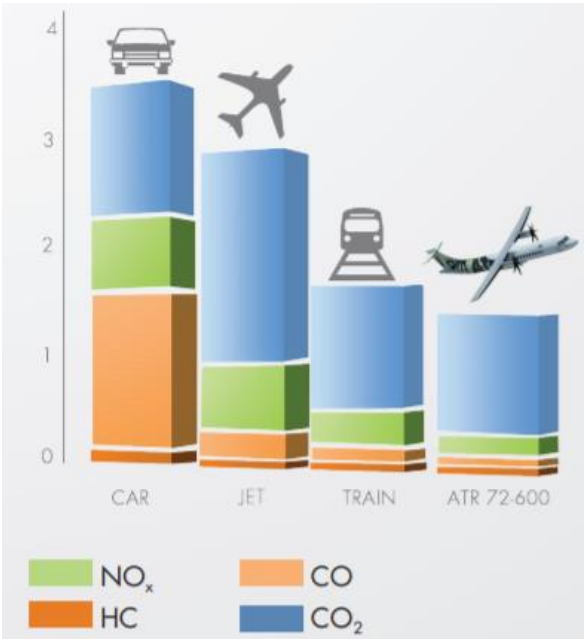

Figure 6: Emissions per passenger per km

The size of the market prediction for RUP-27N hybrid aircraft is 2000 deliveries over 10 years with a capacity of 30 to 50 passengers for regional transportation. In relation to the

market development there is a huge demand for hybrid aircraft with capacity of 30 to 90 passengers for short distance travel (Knapp, 2018).

1.4.4 Technical and Economic Feasibility

RUP-27N aircraft is best suitable for short distance and medium/low demand routes about 850 nautical miles range. Even though airliners have number of options for regional aircraft, hybrid electric aircraft is best one for low cost carrier and quietest aircraft. Turboprop aircraft travels at low altitudes results in less pollution without affecting the ozone layer. The hybrid design requires more components such as batteries, motors, generators, gearboxes, power electronics, cables and inverters which add to take-off mass and increases the acquisition cost. However, this additional mass and cost does not affect much for short distance travel.

Battery power is used only during take-off, missed approaches and peak flight operation demands. The battery can be recharged during cruise phase using propulsors for economic feasibility. The excess power from generators is stored in batteries and used during high demand of power. However, in conventional aircraft there are no extra power sources like in hybrid aircraft.

1.4.5 Critical Mission Requirements

The hybrid aircraft carries additional components like batteries, generators, motors etc. resulting in increase of mass where the payload capacity requirement becomes crucial. Electric power partly replacing the gas-turbine power is critical with high range. High power is required during take-off with maximum payload, so take-off field length is also a critical requirement. The critical mission requirements for the proposed design are as follows:

- Payload Capacity
- Range of 850 nautical miles
- Take-off field length

1.5 COMPARATIVE STUDY OF SIMILAR AIRPLANES

1.5.1 Mission Capabilities and Configuration Selection

- **ATR 72-600**

ATR 72-600 is a regional twin engine turboprop aircraft with capacity of 70 to 78 passengers (ATR , 2014). This aircraft is known for low emissions and low maintenance cost with less speed. ATR 72-600 travels at low Mach number and used for short duration flights.

Figure 7: ATR 72-600 aircraft model

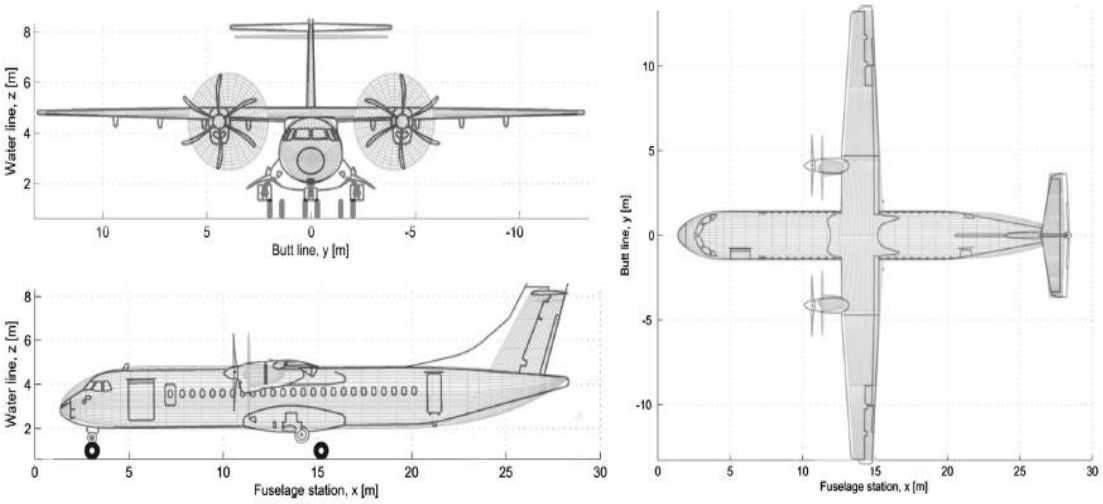

Figure 8: Line drawing of ATR 72-600 aircraft

Table 2: Mission capabilities of ATR 72-600 aircraft

Pay Load Capacity	70 passengers
Crew	2 pilots
Range	1567 km

Cruise Speed	510 km/hr (275 knots)
Take-off field length	1333 m
Landing field length	1067 m

- **ATR 42-600**

  ATR 42-600 is the lower version of ATR 72-600 with less payload capacity and lower range. This aircraft carries 48 passengers with a cruise speed of 556 km/hr (ATR , 2014). It is featured with five wide LCD screens and a glass cockpit flight deck.

Figure 9: ATR 42-600 aircraft model

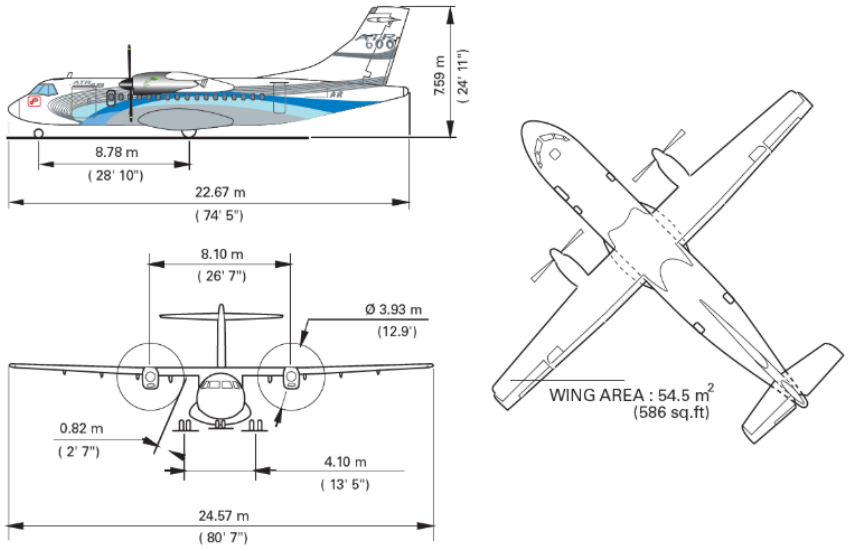

Figure 10: Line drawing of ATR 42-600

Table 3: Mission capabilities of ATR 42-600 aircraft

Pay Load Capacity	48 passengers
Crew	2 pilots
Range	1326 km
Cruise Speed	556 km/hr (300 knots)
Take-off field length	1165 m
Landing field length	1126 m

- **BOMBARDIER Q400**

  Bombardier Q400 aircraft is the fastest and largest turboprop modern technology model with maximum capacity of 82 passengers (Bombardier Inc., 2017). This aircraft has highest cruise speed compared to other Q series airplanes.

Figure 11: Bombardier Q400 aircraft model

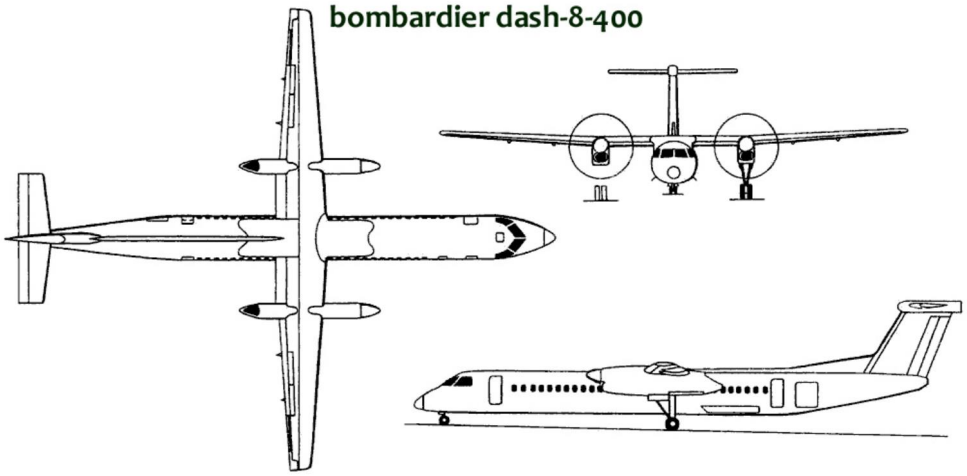

Figure 12: Line drawing of Bombardier Q400

Table 4: Mission capabilities of Bombardier Q400

Pay Load Capacity	82 passengers
Crew	2 pilots, 2-3 cabin crew
Range	2040 km
Cruise Speed	667 km/hr (360knots)
Take-off field length	1300 m
Landing field length	1268 m

- **FOKKER 50**

  This aircraft is popular for high operational feasibility and quiet cabin with turboprop twin engines. Fokker 50 is more reliable with best structure and capable of carrying 50 to 58 passengers (Palt, 2017).

Figure 13: Fokker 50 aircraft model

Table 5: Mission capabilities for Fokker 50

Pay Load Capacity	50-58 passengers
Crew	2 pilots, 2 cabin crew
Range	3000 km
Cruise Speed	530 km/hr (286 knots)
Take-off field length	1050 m
Landing field length	1120 m

- **EADS CASA C-295**

  C-295 is a tactical military transport twin engine turboprop aircraft with a capacity of 71 troops and sometimes it is used purely for carrying missiles (Palt, 2017).

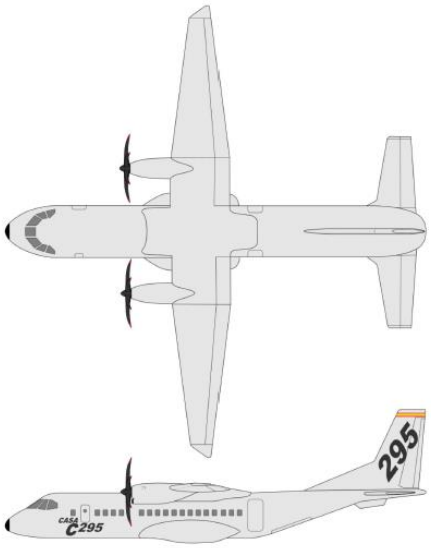

Figure 14: EADS CASA C-295 aircraft model

Table 6: Mission capabilities for C-295

Pay Load Capacity	71 Troops
Crew	2 pilots
Range	1333 km (720 nmi)
Cruise Speed	480 km/hr (260 knots)
Take-off field length	670 m (2200 feet)
Landing field length	320 m (1050 feet)

1.5.2 Comparison of Important Design Parameters

The comparison of important design parameters of similar aircraft models is shown in below table

Table 7: Comparison of important design parameters

Aircraft Model	**ATR 72-600**	**ATR 42-600**	**Bombardier Q400**	**Fokker 50**	**CASA C-295**
Take-off Weight (W_{TO})	22800 kg	18600 kg	30481 kg	20820 kg	23200 kg

Payload Weight (W_{PL})	7500 kg	5300 kg	8489 kg	5500 kg	9250 kg
Empty Weight (W_E)	13311 kg	11550 kg	17819 kg	12520 kg	11000 kg
Fuel Weight (W_F)	5000 kg	4500 kg	5400 kg	4120 kg	6426 kg
Cruise Speed (V_{cr})	510 km/hr	556 km/hr	667 km/hr	530 km/hr	480 km/hr
Range (R)	1528 km (825 nmi)	1326 km (716 nmi)	2040 km (1100 nmi)	3000 km (1620 nmi)	1333 km (720 nmi)
Cruise Altitude (h_{cr})	7600 m	7600 m	8230 m	7620 m	9100 m
Wing Area (S)	61 m^2	54.5 m^2	64 m^2	70 m^2	59 m^2
Wing Span (b)	27.05 m	24.57 m	28.4 m	29 m	25.81 m
Aspect Ratio (AR)	12	11.08	12.6	12	11.3
Type of Payload	Passengers and cargo	Passengers and cargo	Passengers and cargo	Passengers and cargo	Troops and cargo

1.5.3 Discussion

A comparative study of proposed RUP-27N is performed with the similar aircraft models as shown in table 7. All the similar aircraft models use two turboprop engines with different payload capacities whereas RUP-27N uses hybrid electric turboprop engine with parallel propulsion system. Bombardier Q400 has maximum take-off weight with high speed. All the above airplanes have high wing configuration design with horizontal stabilizer on the top of the tail section except for Fokker 50 and CASA C-295. RUP-27N uses a configuration like ATR 72-600/ATR 42-600. High wing configuration offers a better visibility and ground clearance with higher center of lift which is greatly feasible for RUP-27N.

The range is high for Bombardier Q400 and Fokker 50 as compared to other airplanes whereas RUP-27N forecast to achieve range of 1575 km (850 nmi) with more of electric power. The payload weight is high for CASA C-295 as it is used for tactical

military transportation. The wing span and wing area is more for Fokker 50 and less for ATR 42-600. The cruise altitude is relatively less for turboprop engines compared to jet engines results in environmental benefits. The necessity for energy, environmental benefits with low operating cost makes this hybrid aircraft more reliable with the present aviation market.

1.6 CONCLUSIONS AND RECOMMENDATIONS

1.6.1 Conclusions

A detailed chapter of proposed design with mission requirements and comparative study of similar airplanes has been presented. Aviation market analysis and the need for hybrid aircraft is detailed in this chapter. Critical mission requirements for this design are maximum payload capacity and the range of the aircraft as these are crucial to achieve with more of electric power than gasoline. Replacing the fossil fuels completely with electric power is quiet challenging so hybrid design helps in utilizing the combination of both electric power and gasoline. This proposed design is mainly for regional transportation with hybrid power. Summing up the entire discussion and comparison, hybrid design is better in terms of low fuel consumption, safety, ozone layer protection, minimum operating and maintenance cost than the conventional design.

1.6.2 Recommendations

Though hybrid design has many advantages, practically achieving the design and utilizing the maximum electric power in combination with gasoline is challenging. A further study is required to improve the payload capacity and range of the aircraft with hybrid engine. The present aviation market is in the need of better hybrid engines with more passengers. The improvement of battery efficiency needs a further detailed study and analysis.

CHAPTER 2: CONFIGURATION SELECTION

2.1 INTRODUCTION

Configuration design is an iterative and non-unique process (Roskam, 2005). For a given set of mission requirements, it is possible that more than one and sometimes radically different configurations can be selected to satisfy the mission specification (Roskam, 2005). This chapter presents a detailed selection process of wing, empennage, integration of propulsion system, landing gear disposition and overall configuration for the proposed design. Configuration design is very important in design process as 90 percent of life cycle cost gets locked during the early configuration phases of an aircraft. Each configuration has its own advantages and disadvantages but the basic idea behind the ideal configuration is that the center of gravity of empty weight, fuel weight and payload weight are all at the same longitudinal location. It is difficult to practically achieve ideal configuration but can be achieved as close as possible. The main advantage of ideal configuration is that it limits the center of gravity travel and reduces wet area due to less need for trim control power. The location of critical parts such as wing, engines and stabilizer is determined by the mission specification.

A comparative study of configuration can be performed for ATR 72-600, ATR 42-600, Bombardier Q400, Fokker 50 and CASA C-295 to determine the best configuration for the proposed design that satisfy the given mission requirements. Even though configuration design is determined by lot of technical considerations, it is also determined by styling, marketing and emotional considerations. Ideally, approximation should be made for weight and balance, stability and control, drag and other factors involved in the selection process of configuration to achieve efficient configuration. Based on mission requirements specified for the proposed design of RUP-27N aircraft earlier and comparing with similar airplanes, the configuration selection for RUP-27N is proposed in this chapter.

2.2 COMPARATIVE STUDY OF AIRPLANES WITH SIMILAR MISSION PERFORMANCE

2.2.1 Comparison of Weights, Performance and Geometry of Similar Airplanes

Table 8: Comparison of weights, performance and geometry of similar airplanes

Aircraft Model	**ATR 72-600**	**ATR 42-600**	**Bombardier Q400**	**Fokker 50**	**CASA C-295**
Take-off Weight (W_{TO})	22800 kg	18600 kg	30481 kg	20820 kg	23200 kg
Payload Weight (W_{PL})	7500 kg	5300 kg	8489 kg	5500 kg	9250 kg
Empty Weight (W_E)	13311 kg	11550 kg	17819 kg	12520 kg	11000 kg
Fuel Weight (W_F)	5000 kg	4500 kg	5400 kg	4120 kg	6426 kg
Cruise Speed (V_{cr})	510 km/hr	556 km/hr	667 km/hr	530 km/hr	480 km/hr
Range (R)	1528 km (825 nmi)	1326 km (716 nmi)	2040 km (1100 nmi)	3000 km (1620 nmi)	1333 km (720 nmi)
Cruise Altitude (h_{cr})	7600 m	7600 m	8230 m	7620 m	9100 m
Take-off Field Length	1333 m	1165 m	1300 m	1050 m	670 m
Landing Field Length	1067 m	1126 m	1268 m	1120 m	320 m
Aircraft Length (l)	27.16 m	22.67 m	32.8 m	25.25 m	24.45 m
Aircraft Height (h)	7.65 m	7.59 m	8.4 m	8.32 m	8.60 m
Wing Area (S)	61 m^2	54.5 m^2	64 m^2	70 m^2	59 m^2
Wing Span (b)	27.05 m	24.57 m	28.4 m	29 m	25.81 m
Aspect Ratio (AR)	12	11.08	12.6	12	11.3
Type of Payload	Passengers and cargo	Passengers and cargo	Passengers and cargo	Passengers and cargo	Troops and cargo

2.2.2 Configuration Comparison of Similar Airplanes

- **ATR 72-600**

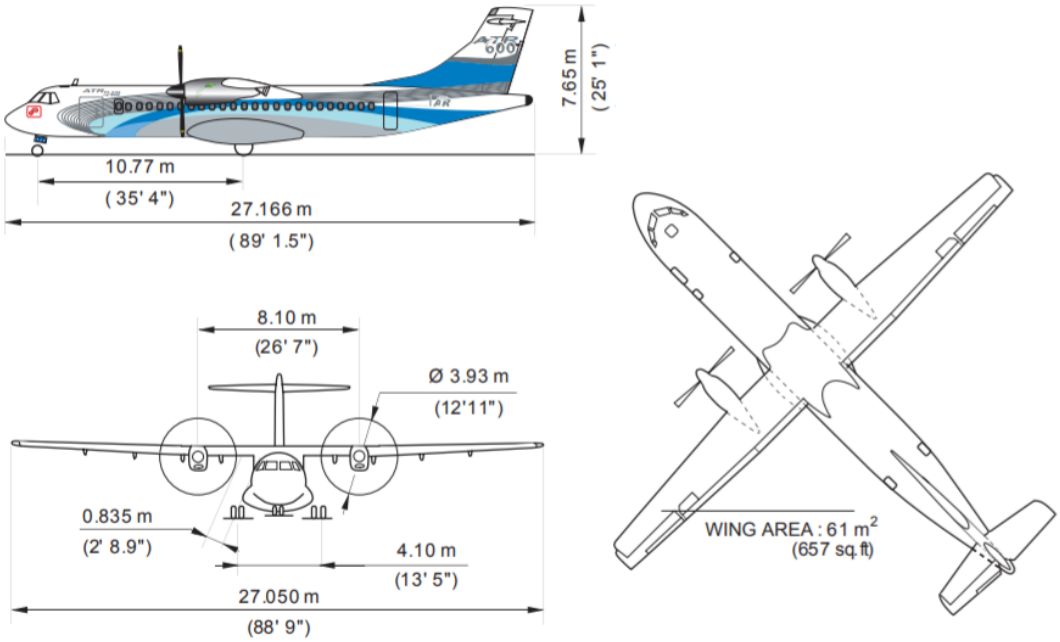

Figure 15: Line drawing of ATR 72-600

- **ATR 42-600**

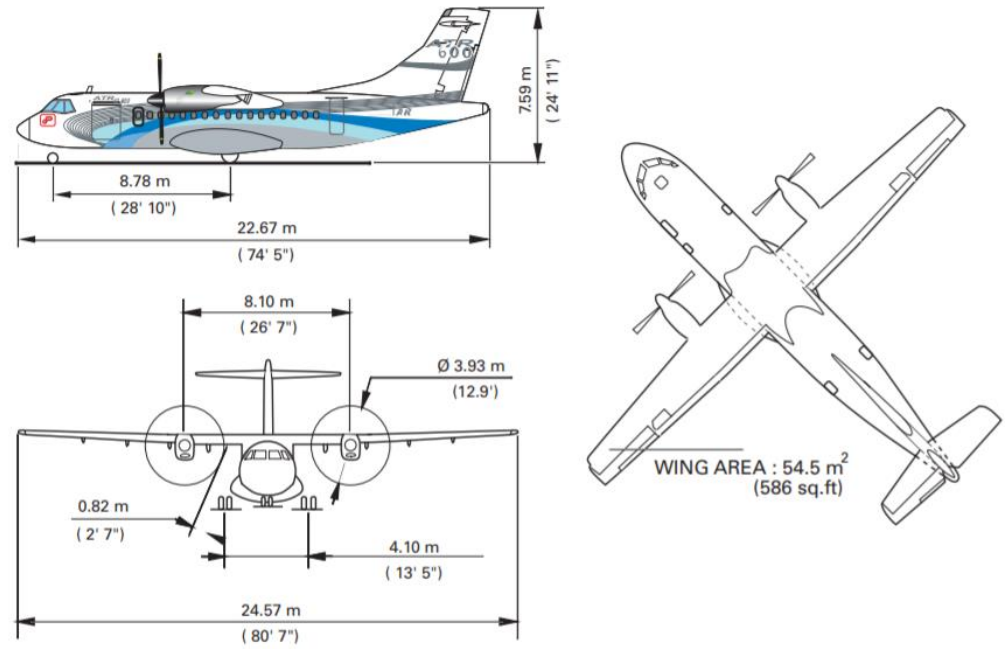

Figure 16: Line drawing of ATR 42-600

- **BOMBARDIER Q400**

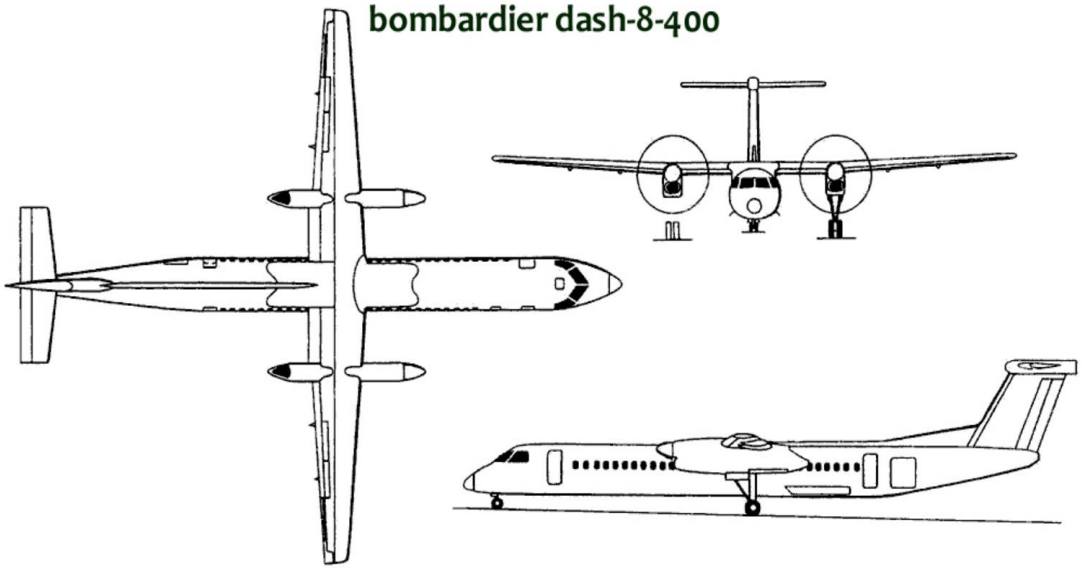

Figure 17: Line drawing of Bombardier Q400

- **FOKKER 50**

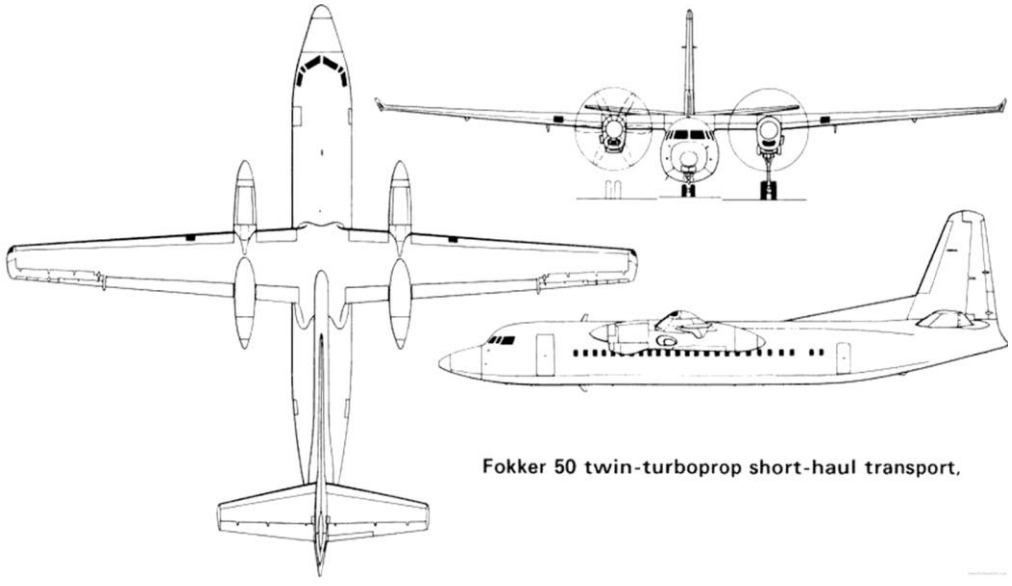

Figure 18: Line drawing of Fokker 50

- **EADS CASA C-295**

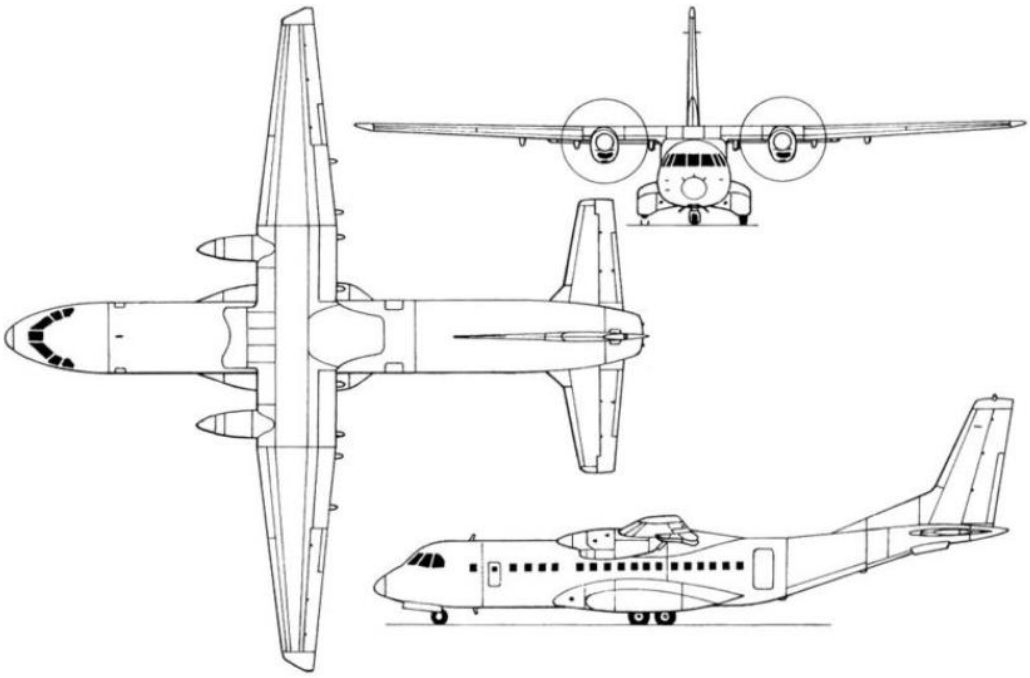

Figure 19: Line drawing of CASA C-295

2.2.3 Discussion

All the similar aircraft models have high wing configuration with conventional fuselage. High wing configuration have advantages of easy loading and unloading, better ground clearance and good visibility below the aircraft. ATR 72-600, ATR 42-600, Bombardier Q400 have T-tail Empennages while Fokker 50 and CASA C-295 have conventional tail arrangement. The wing configuration of all the similar airplanes from a structural point of view is of cantilever construction. From a tail fatigue and handling quality point of views, the location of horizontal tail with respect to slipstream of the propeller is quite important. The distance of propeller to the ground and landing gear length determines the integration of nacelle into a wing.

Bombardier Q400 and Fokker 50 have the nacelles installed in their wings. The disposition of engines of all the above five models are of tractor type where the point of thrust application is ahead of center of gravity. There are 2 engines used in all the five airplanes which are integrated below the wing symmetrically and the type of engine used

is twin engine turboprop. Bombardier Q400 has highest aspect ratio wing and ATR 42-600 has the lowest aspect ratio wing. The landing gear used in ATR 72-600, ATR 42-600, Bombardier Q400, Fokker 50 and C-295 is hydraulically retractable tricycle type. As all the similar airplanes uses a high wing configuration, it is difficult to integrate the landing gear with the wing as it results in longer landing gear. So, ATR 72-600, ATR 42-600 and CASA C-295 have fairings under the fuselage for retraction of landing gear while Bombardier Q400 and Fokker 50 retract landing gear into nacelle below the engines. These fairings produce high drag, but this is acceptable for low speed aircraft.

2.3 CONFIGURATION SELECTION

2.3.1 Overall Configuration

The proposed design RUP-27N is a land-based aircraft mainly for low speed regional commuting. The critical components in general configuration selection are fuselage, wing, engines, empennage and landing gear. As per the given mission requirements and comparing with competitor aircraft in the market with similar mission, the overall configuration is selected as follows:

Table 9: Overall configuration selection for proposed design

RUP-27N CONFIGURATION SELECTION	
Type	Land Based
Fuselage Configuration	Conventional
Wing Configuration	High Wing • Cantilever Wing • Zero or Negligible Sweep
Engine Configuration	Twin Engine Turboprop • Tractor Arrangement • Podded in the wing

	• Engines placed below the wing symmetrically
Empennage Configuration	Horizontal Tail • T-tail Installation (Mounted on Vertical Tail) Vertical Tail • Single Vertical Tail Mounted on Fuselage
Landing Gear Configuration	Retractable Tricycle Gear • Retracted into the Undercarriage Fairing of the Fuselage • Single Main Gear Strut • Two tires per each gear • One nose wheel gear and Two gears at undercarriage fuselage fairing.

The pros and cons for each selection of configuration is explained in detail in below sections

2.3.2 Wing Configuration

The wing configuration can be divided into high wing, mid wing and low wing based on the type of arrangement (Roskam, 2005). It is again classified as cantilever wing and braced wing based on the structural view. Cantilever wing is a conventional configuration and most of the aircraft in the aviation market are of this type. Braced wing is having an additional strut to withstand tension and compression and due to the strut, it results in producing more drag than the cantilever wing.

The main advantage of high wing is easy for loading and unloading, better visibility of ground below the aircraft, good ground clearance and best for shorter take-off and

landing. The main disadvantage of high wing is retraction of landing gear. As the wing is high it is too long and heavy for retraction into wing which adds more weight to wing and for retraction into fuselage it needs an undercarriage fairing which will add to drag. The mid wing is best for low interference drag, best maneuverability, wing is continuous to fuselage and landing gear retraction. The main disadvantage of mid wing is reduced internal useful fuselage volume. The low wing has an advantage of short landing gear which results in less weight and efficient use of undercarriage space but has disadvantage of high interference drag, loading needs additional aids, requires dihedral for longitudinal stability. Based on the above discussion of important aspects of all the types of wings, high wing configuration is selected for the proposed design. As the design uses turboprop hybrid engines it is good to have propeller tip to ground clearance. High wing is suitable for low speed regional aircraft comparing to existing designs in market. Zero or negligible sweep angle is selected with high wing configuration as the proposed design is for low speed commuting aircraft for about 1567 km range. Small sweep has small critical Mach number, large maximum lift coefficient and large lift curve slope. Zero sweep has almost no risk of tip stall and pitch up compared to aft sweep.

2.3.3 Empennage Configuration

Empennage configuration is classified as horizontal tail, vertical tail and canard (Roskam, 2005). T-tail empennage configuration is selected for the proposed design where horizontal tail is mounted on vertical tail as T-tail installation and vertical tail is mounted on fuselage. T-tail is selected because the exhaust flow from the turboprop engine will not disturb flow over the vertical tail. As the propellers are placed in the high wing, the position of horizontal tail with respect to slipstream of the propeller is better with T-tail from handling quality and tail fatigue point of view compared to conventional horizontal tail. T-tail have advantages of less interference drag, better lift slope, excellent glide ratio, less affected by fuselage and wing slipstream over the other empennages (Velupillai, 2014). T-tail has disadvantages of deep stall and maintenance issues. Considering all the pros and cons of different empennage configurations, T-tail is the reasonable choice for regional commuting aircraft.

2.3.4 Integration of the Propulsion System

Engines can be placed in three different ways such as Tractor, Pusher and Combination of both (Roskam, 2005). As the proposed design need point of thrust application ahead of the center of gravity, therefore Tractor type of arrangement was chosen. Moreover, placing the engine propeller at trailing edge of the wing may result in vertical tail inefficiency as the flow disturbs. Hence, engine propellers are placed ahead of the leading edge. The engines are podded into the wing for easy engine accessibility for maintenance and mass of the engine reduces the wing root bending moment. The podded engines placed below the wing have a disadvantage of high drag. The buried installation of engine into the wing has an advantage of less drag but has disadvantage of increased stress on the wing and it might damage wing when engine fails or burns. The placement of engines in the wing symmetrically improves the slipstream and safer against stall compared to other placements. The main disadvantage of this kind of placement is variation of engine power can change the downwash on the tail and engine failure may cause high windmilling drag. This disadvantage can be mitigated by maintaining same engine power using fuel and batteries during the mission. Ideally proposed hybrid aircraft is designed in such a way that there is no variation in engine power, but practically it is achievable only with improved battery density. Regional turboprop airplanes available in the market mostly are of tractor type. Considering the pros and cons of all the types, tractor arrangement podded into the wing symmetrically was chosen to be suitable for hybrid aircraft.

2.3.5 Landing Gear Disposition

Landing gear can be divided into non-retractable or fixed and retractable from a system point of view (Roskam, 2005). The layout of the landing gear can be conventional, taildraggers, tandem and outrigger (Roskam, 2005). The retractable conventional or tricycle type of landing gear is selected for the proposed design. Fixed landing gear increases drag over the retractable. The taildraggers are inherently unstable and violent braking will tip the aircraft to its nose. The outrigger is also unstable as compared to tricycle landing gear. The main advantage of conventional landing gear is braking force acts behind the center of gravity which is stable and uses full braking power. The main disadvantage of conventional landing gear is heavy nosewheel as it takes 30% of the weight under steady braking conditions. The proposed design uses a high wing where the landing retraction into

the wing is long and heavy which increases weight. Hence, the proposed design uses a landing retraction into the fuselage which has advantage of short landing gear with less weight but has a disadvantage of additional undercarriage fairings which increases drag. As per the important aspects discussed above, conventional retractable landing gear is used for the proposed design.

2.3.6 Proposed Configuration

The proposed configuration based on Table 9 data has been conceptually designed in SketchUp CAD software and the 3D model sketches are shown below.

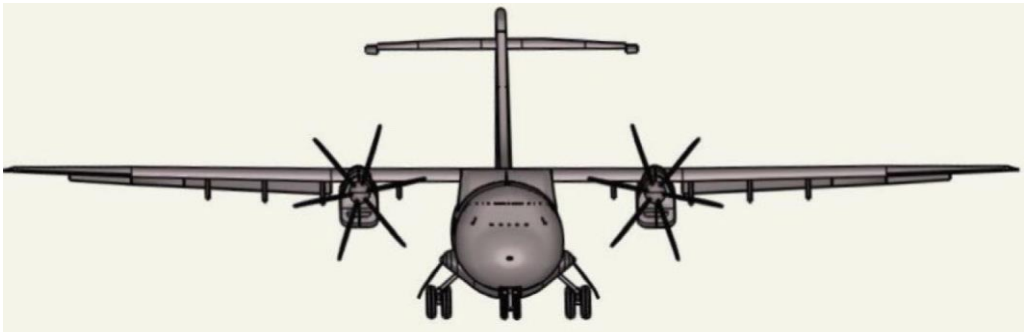

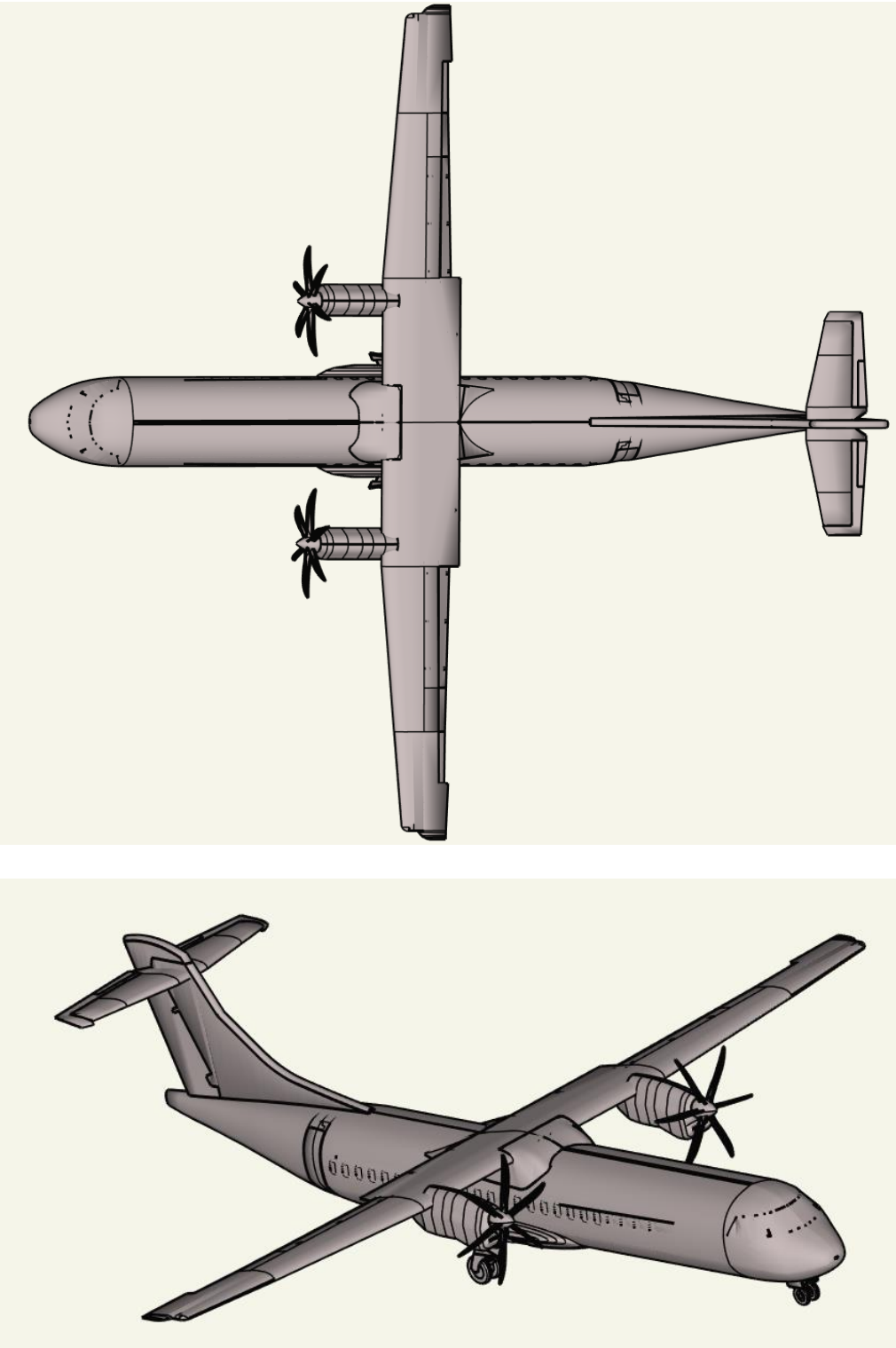

Figure 20: 3D models of proposed configuration

CHAPTER 3: WEIGHT SIZING AND WEIGHT SENSITIVITIES

3.1 INTRODUCTION

This chapter presents weight sizing, weight sensitivities and range sensitivities for the proposed aircraft design. Fuel based airplanes have a standard procedure to calculate weight sizing and weight sensitivities whereas hybrid airplanes are still under research. The proposed design uses both fuel-based aircraft procedure and electrical procedure for calculating the weight sizing weight and range sensitivities. The proposed design uses fuel for engine start and warm up, taxi, takeoff and climb whereas battery power is used for cruise, loiter, descent, fly to alternate location and descent and landing. So, the proposed design relies majorly on battery power for the mission. This chapter presents an estimation method for a given mission specification for the following weights

- Takeoff Weight, W_{TO}
- Empty Weight, W_E
- Mission Fuel Weight, W_F
- Battery Weight, W_{Bat}

The battery weight is calculated by using Hepperle and compared with Riboldi's method. The hybrid airplanes in the aviation market are still under research so, a family of conventional regional aircraft with similar mission are used as reference for calculations. The motor is integrated with the engine, so the weight of the motor is combined with engine weight where it includes in empty weight. The weight sensitivity studies are conducted for the fuel mission phases and range sensitivity studies are conducted for the battery mission phases. The trade studies are performed for takeoff weight versus critical parameters and range versus critical parameters in the final once we get the mission weights and sensitivities.

3.2 MISSION WEIGHT ESTIMATES

The mission weight estimates are primarily to predict the minimum aircraft weight, fuel weight and battery weight needed to accomplish the given mission requirements.

3.2.1 Data Base for Takeoff Weights and Empty Weights of Similar Airplanes

The following table shows the database for takeoff weights and empty weights of similar airplanes

Table 10: Database for takeoff weights and empty weights of similar airplanes

S.No	Name of The Airplane	Gross Take-off Weight, W_{TO} (lbs)	Empty Weight, W_E (lbs)
1	ATR 72-600	50265	29346
2	ATR 42-600	41006	25463
3	Bombardier Q400	67199	39284
4	Fokker 50	45900	27600
5	CASA C-295	51147	24251
6	DeHavilland DHC-7	44000	27000
7	Gulfstream IC	36000	23693
8	Saab-Fairchild 340	26000	15510
9	Antonov 28	14330	7716
10	Piper PA-42	11200	6389

3.2.2 Determination of Regression Coefficients A and B

Based on the above database for takeoff weights and empty weights of similar airplanes, the following graph has been plotted using Excel and compared with AAA program.

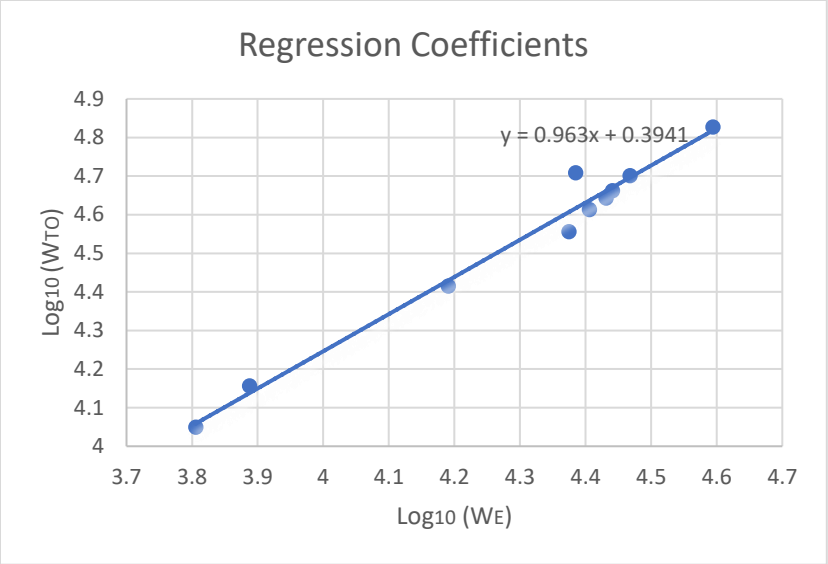

Figure 21: Graph of take-off weights versus empty weights of similar airplanes

Regression Coefficients are determined by using the following equation in comparison with the above graph

$$log_{10}W_{TO} = A + Blog_{10}W_E \quad (3.1)$$

From the above graph, the regression coefficients are calculated as follows

A = 0.3941, B = 0.9630 (3.2)

The AAA program also gives the same values for A and B as shown below

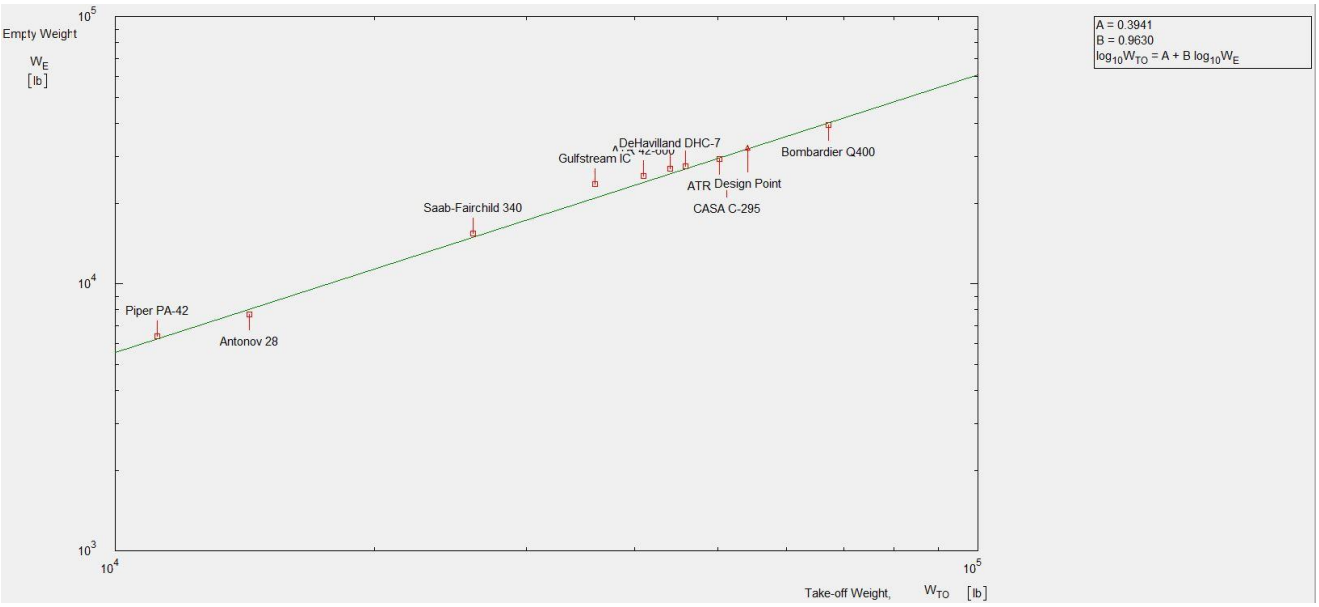

Figure 22: Take-off weights versus empty weights using AAA program

3.2.3 Determination of Mission Weights

The mission weights are calculated by using Roskam procedure (Roskam, 2005) manually and compared with AAA program. The battery weight is calculated using Hepperle and Riboldi's methods.

3.2.3.1 Manual Calculation of Mission Weights

As per the Roskam (Roskam, 2005), the mission weights are calculated by using the following steps

- **Mission Payload Weight**

The Mission requirements specify the passenger capacity of 30-50, 2 cabin crew and 2 cockpit crew. The proposed hybrid-electric design carries 40 passengers with 2 cabin crew and 2 cockpit crew. The average weight of 175 lbs per person and 30 lbs of baggage is considered for commercial airplane using Roskam data (Roskam, 2005).

Weight of the 40 passengers with baggage = $40(175 + 30) = 8200\ lbs$

Payload Weight, $W_{PL} = 8200\ lbs$

Crew Weight, $W_{crew} = 4(175 + 30) = 820\ lbs$

- **Battery Weight**

The battery weight is calculated by using the range equation derived by martin Hepperle (Hepperle, 2012) as follows

$$R = E^* * \eta_{total} * \left(\frac{1}{g}\right) * \left(\frac{L}{D}\right) * \left(\frac{W_{Bat}}{W_{TO}}\right) \qquad (3.3)$$

Where,

R = Range of the Aircraft

E^* = Specific Energy Density of the Battery

η_{total} = Total System Efficiency

$\frac{L}{D}$ = Lift-to-Drag Ratio

$\frac{W_{Bat}}{W_{TO}}$ = The Ratio of Battery Weight to the Total Weight

g = Acceleration due to Gravity

The above equation clearly indicates the aircraft range is dependent on lift-to-drag ratio, available energy, total system efficiency and weight of the aircraft. To calculate the battery weight, specific energy density E^* of present and future chemical battery systems needs to be reviewed. The below table shows a theoretical possible value of specific energy and expected values in future based on complete survey of battery systems specified by Hepperle (Hepperle, 2012).

Table 11: Specific energy density of present and future chemical battery system

System	**Theoretical Specific Energy**	**Expected in 2025**
Li-Ion (2012)	390 Wh/kg	250 Wh/kg
Zn-air	1090 Wh/kg	400-500 Wh/kg
Li-S	2570 Wh/kg	500-1250 Wh/kg

Li-O_2	3500 Wh/kg	800-1750 Wh/kg

As the hybrid airplanes are still under research stage in market, the proposed aircraft can be designed based on the future battery system. Based on the above table, ten years from now it is a reasonable assumption of E^* with 1500 Wh/kg.

The below diagram shows the different propulsion system efficiencies. Battery propulsion system has highest efficiency as compared to conventional turboprop, turbofan and fuel cell. Ten years from now if the battery efficiency increases from 73% to 90 % then it is a reasonable assumption of η_{total} as 90%.

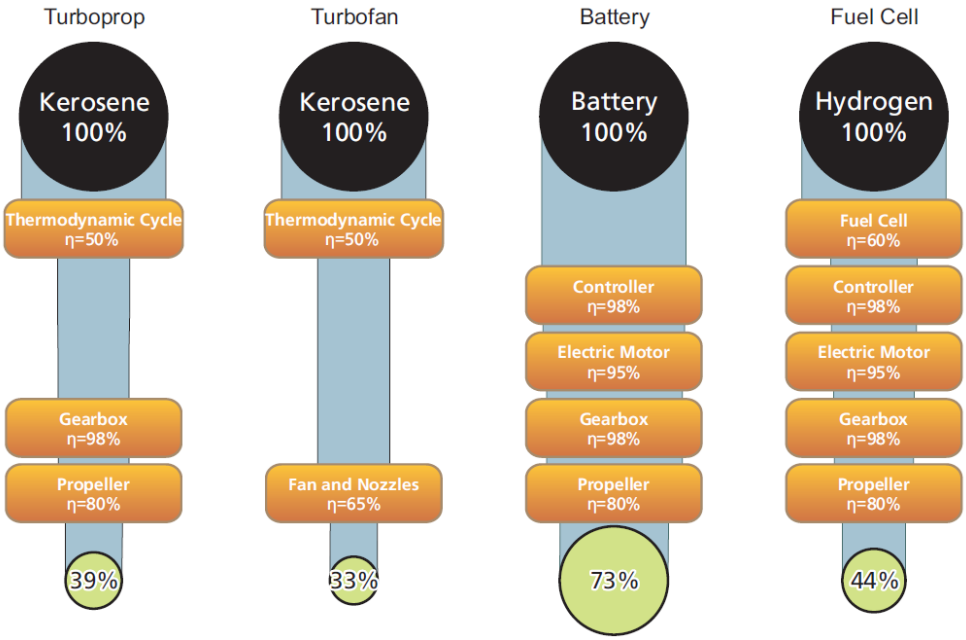

Figure 23: Different propulsion system efficiencies

The Range of the aircraft is specified as 1575 km in mission specification. The comparable reference aircraft ATR-42 600 range is 1326 km. Based on the existing battery technology, L/D ratio and future developments, attainable range is 1400 km to 1500 km. The range for the proposed hybrid design is considered as 1500 km for the calculation of battery weight. The L/D ratio is shown for the reference aircraft ATR 42-600 as 15 in the below figure of historical data (Babikian, 2001). The data from Roskam (Roskam, 2005) shows that L/D ratio for cruise is 11-13. Comparing these data, L/D ratio is assumed to be 15, as the hybrid design is proposed with developments in future.

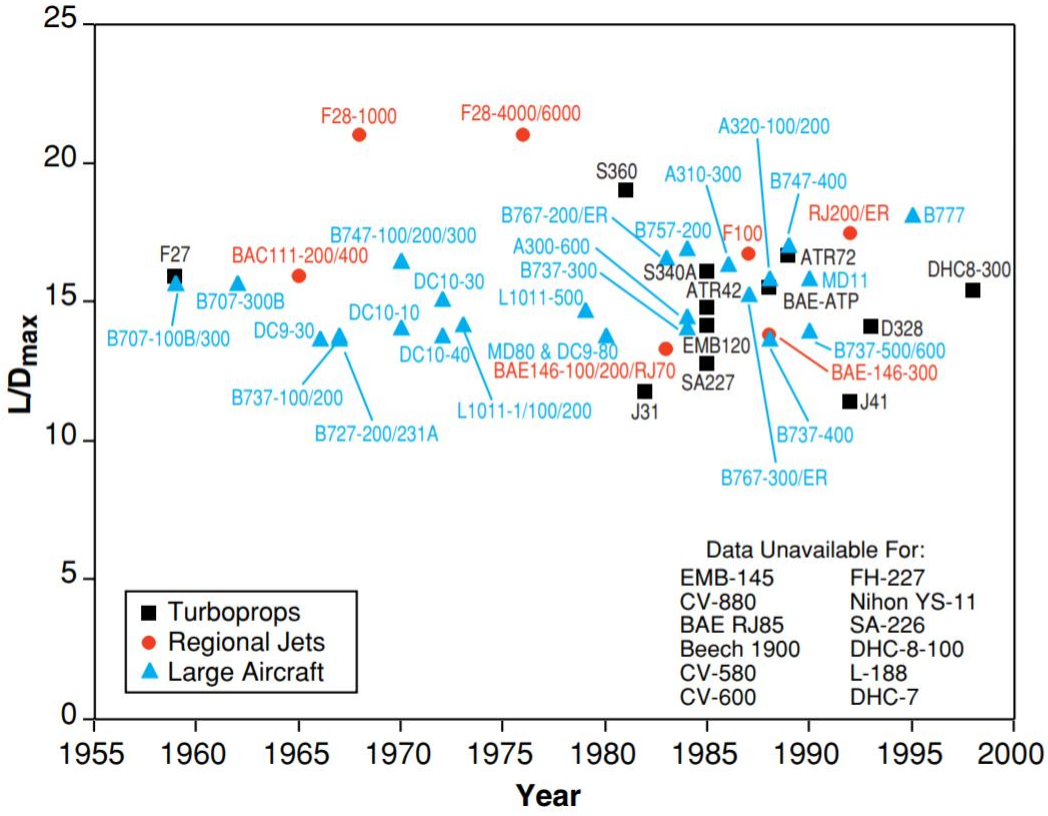

Figure 24: Historical aerodynamic data of lift-to-drag ratio for cruise

Table 2.2 Suggested Values For L/D, c_j, η_p, And For c_p For Several Mission Phases

	Cruise				Loiter			
Mission Phase No. (See Fig. 2.1)	L/D	c_j lbs/lbs/hr 5	c_p lbs/hp/hr	η_p	L/D	c_j lbs/lbs/hr 6	c_p lbs/hp/hr	η_p
Airplane Type								
1. Homebuilt	8-10*		0.6-0.8	0.7	10-12		0.5-0.7	0.6
2. Single Engine	8-10		0.5-0.7	0.8	10-12		0.5-0.7	0.7
3. Twin Engine	8-10		0.5-0.7	0.82	9-11		0.5-0.7	0.72
4. Agricultural	5-7		0.5-0.7	0.82	8-10		0.5-0.7	0.72
5. Business Jets	10-12	0.5-0.9			12-14	0.4-0.6		
6. Regional TBP's	11-13		0.4-0.6	0.85	14-16		0.5-0.7	0.77
7. Transport Jets	13-15	0.5-0.9			14-18	0.4-0.6		
8. Military Trainers	8-10	0.5-1.0	0.4-0.6	0.82	10-14	0.4-0.6	0.5-0.7	0.77
9. Fighters	4-7	0.6-1.4	0.5-0.7	0.82	6-9	0.6-0.8	0.5-0.7	0.77
10. Mil. Patrol, Bomb, Transport	13-15	0.5-0.9	0.4-0.7	0.82	14-18	0.4-0.6	0.5-0.7	0.77
11. Flying Boats, Amphibious, Float Airplanes	10-12	0.5-0.9	0.5-0.7	0.82	13-15	0.4-0.6	0.5-0.7	0.77
12. Supersonic Cruise	4-6	0.7-1.5			7-9	0.6-0.8		

Figure 25: Lift-to-drag ratio for different airplanes

The following values are considered for the calculation of battery weight based on the above discussed assumptions

R = 1500 km or 4921260 ft

L/D = 15

$\eta_{total} = 0.90$

$E^* = 1500 \frac{Wh}{kg} or\ 7.53 * 10^{14}\ \frac{ft^2}{hr^2}$

$g = 9.81 \frac{m}{s^2}\ or\ 416696000 \frac{ft}{hr^2}$

By substituting the above values in range equation,

$$4921260 = 7.53 * 10^{14} * 0.90 * \left(\frac{1}{416696000}\right) * (15) * (\frac{W_{Bat}}{W_{TO}})$$

$$W_{Bat} = 0.20172\ W_{TO} \qquad (3.4)$$

- **Take-off Weight**

The Take-off Weight is calculated by

$$W_{TO} = W_{OE} + W_F + W_{PL} + W_{Bat} \qquad (3.5)$$

By guessing a likely value of take-off weight by looking at the data of similar aircraft.

$$W_{TO} = 50300\ lbs$$

- **Mission Fuel Weight**

The Mission fuel weight is a combination of fuel used during the mission and fuel reserves required for the mission. It can be calculated as

$$W_F = W_{F\,used} + W_{F\,res} \qquad (3.6)$$

The hybrid design uses a combination of fuel and battery power during specific mission profile. The fuel reserves are assumed to be 25% of the used mission fuel for the proposed design. The calculation of $W_{F\,used}$ is carried out by breaking the airplane mission into several mission phases in mission profile as shown below.

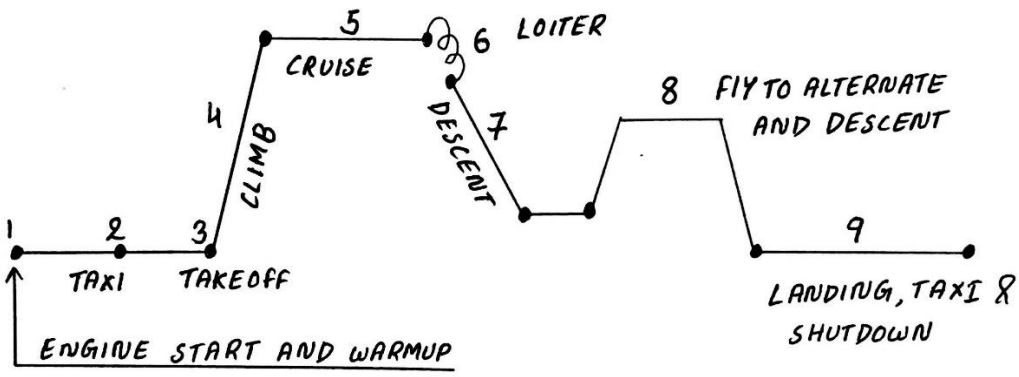

Figure 26: Mission profile

The fuel used during each mission phase is calculated. The Proposed design of hybrid-electric aircraft uses fuel for the following specific mission phases:

- Engine start and warm up
- Taxi
- Takeoff
- Climb

whereas battery power is used for mission phases as follows:

- Cruise
- Loiter
- Descent
- Fly to Alternate Location and Descend
- Landing and Taxi

The weight of fuel changes from one mission phase to another mission phase hence, the fuel-fraction method is used for calculations. The battery weight remains constant throughout the specified mission phases, so the weight fractions remains constant.

Climb

The fuel weight fraction of climb mission phase can be calculated from Breguet's endurance equation for propeller driven aircraft as shown below

$$E_{cl} = 375\left(\frac{1}{V_{cl}}\right)\left(\frac{\eta_p}{c_p}\right)_{cl}\left(\frac{L}{D}\right)_{cl}\ln\left(\frac{W_3}{W_4}\right) \qquad (3.7)$$

The E_{cl} is equal to the time to climb, usually expressed as

$$E_{cl} = \frac{\text{Cruise Altitude}}{\text{Rate of climb}}$$

The cruise altitude is specified as 7600 m or 24934.38 ft in mission specifications and the rate of climb is estimated from reference aircraft as 1355 ft/min.

$$E_{cl} = \frac{24934.38}{1355} = 18.4\ min$$

The following values have been obtained using reference aircraft (ATR , 2014) and Roskam (Roskam, 2005) by reasonable assumptions

- The E_{cl} is estimated from the reference aircraft as 18.4 min or 0.30667 hours
- The climb speed V_{cl} is estimated from reference aircraft as 170 knots or 195.633 mph
- The propeller efficiency is estimated to be 0.77
- The c_p is assumed to be 0.6 lbs/hp/hr
- The lift-to-drag ratio is assumed to be 15

By substituting all the above values in Breguet's endurance equation, we get

$$0.30667 = 375\left(\frac{1}{195.633}\right)\left(\frac{0.77}{0.6}\right)_{cl}(15)_{cl}\ln(\frac{W_3}{W_4})$$

$$\left(\frac{W_4}{W_3}\right) = 0.9917$$

The mission fuel weight fractions are determined for the mission phases which uses fuel whereas the weight fractions remain constant for the mission phases which uses battery power. Below table shows the suggested values from Roskam (Roskam, 2005) and calculated value of climb and constant values for the mission phases with battery power.

Table 12: Mission fuel weight fractions

Mission phase	**Mission Fuel weight Fraction**

Engine start and warm up	$\left(\frac{W_1}{W_{TO}}\right) = 0.99$
Taxi	$\left(\frac{W_2}{W_1}\right) = 0.995$
Take-off	$\left(\frac{W_3}{W_2}\right) = 0.995$
Climb	$\left(\frac{W_4}{W_3}\right) = 0.9917$
Cruise	$\left(\frac{W_5}{W_4}\right) = 1$
Loiter	$\left(\frac{W_6}{W_5}\right) = 1$
Descent	$\left(\frac{W_7}{W_6}\right) = 1$
Fly to Alternate Location and Descent	$\left(\frac{W_8}{W_7}\right) = 1$
Landing, Taxi and Shutdown	$\left(\frac{W_9}{W_8}\right) = 1$

The mission fuel fraction is given by

$$M_{ff} = \left\{\frac{W_9}{W_8}\frac{W_8}{W_7}\frac{W_7}{W_6}\frac{W_6}{W_5}\frac{W_5}{W_4}\frac{W_4}{W_3}\frac{W_3}{W_2}\frac{W_2}{W_1}\frac{W_1}{W_{TO}}\right\} \qquad (3.8)$$

M_{ff} = (1) (1) (1) (1) (1) (1) (0.9917) (0.995) (0.995) (0.99)

$$M_{ff} = 0.97199$$

The fuel used during the mission phases is given by

$$W_{F\,used} = \left(1 - M_{ff}\right)W_{TO} \qquad (3.9)$$

$$W_{F\,used} = (1 - 0.97199)W_{TO} = 0.02801\ W_{TO}$$

The fuel reserves are assumed to be 25% of the used fuel.

$$W_{F\,res} = 0.25\,W_{F\,used} \tag{3.10}$$

The mission Fuel weight is determined by

$$W_F = W_{F\,used} + W_{F\,res} \tag{3.11}$$

$$W_F = 1.25 W_{F\,used} = 0.03501\,W_{TO}$$

- **Tentative Value for Operating Empty Weight**

  The tentative value for operating empty weight is calculated by

$$W_{OE\,tent} = W_{TO\,guess} - W_F - W_{PL} - W_{Bat} \tag{3.12}$$

- **Tentative Value for Empty Weight**

  The tentative value for empty weight is calculated by

$$W_{E\,tent} = W_{OE\,tent} - W_{tfo} - W_{Crew} \tag{3.13}$$

  As per the Roskam data for airplane design the W_{tfo} can be 0.5% or more of W_{TO}. Assuming it is 0.5% of takeoff weight then,

$$W_{tfo} = 0.005\,W_{TO} \tag{3.14}$$

- **Allowable Value of Empty Weight**

  The allowable value of empty weight can be obtained from the following equation,

$$W_E = inv.log_{10}\left\{\frac{(log_{10}W_{TO}) - A}{B}\right\} \tag{3.15}$$

- **Comparing the Allowable and Tentative Empty Weights**

  Comparing the allowable W_E and tentative $W_{E\,tent}$ empty weights and adjusting guess take-off weight by iterative process till the difference is within 0.5% tolerance. The following mission weights are obtained using the above discussed equations.

Table 13: Results of mission weights

Take-off Weight, W_{TO} (lbs)	54000
Empty Weight, W_E (lbs)	31926
Payload Weight, W_{PL} (lbs)	8200

Used Fuel Weight, $W_{F\,used}$ (lbs)	1513
Fuel Weight, W_F (lbs)	1891
Crew Weight, W_{crew}	820
Mission Fuel Fraction, M_{ff}	0.972
Operating Empty Weight, W_{OE} (lbs)	33016
Battery Weight, W_{Bat} (lbs)	10893

- **Battery Weight Calculation by using Riboldi's Method**

  The battery weight can also be calculated by using Riboldi's (Riboldi, 2016) method. This method is described for fully electric aircraft. Assuming all the three mission phases climb, cruise and loiter uses battery power, then the weight of the battery for mission profile is given by (Riboldi, 2016)

$$W_{Bat\,MP} = \frac{g}{\eta_p}\max\{\frac{\left(E^{climb} + E^{cruise} + E^{loiter}\right)}{E^*}, \frac{\max\left(P_r^{climb}, P_r^{cruise} P_r^{loiter}\right)}{p}\} \quad (3.16)$$

  Where,

  The power and energy required to climb is given by

$$P_r^{climb} = W_{TO}RC + \frac{1}{2}\rho^{climb}V^{climb^3}SC_D^{climb} \quad (3.17)$$

$$E^{climb} = P_r^{climb}\,TTC \quad (3.18)$$

  Time to climb is given by

$$TTC = \frac{h^{cruise}}{RC} \quad (3.19)$$

  The power and energy to cruise is given by

$$P_r^{cruise} = \frac{1}{2}\rho^{cruise}V^{cruise^3}SC_D^{cruise} \quad (3.20)$$

$$E^{cruise} = P_r^{cruise}\,T^{cruise} \quad (3.21)$$

  Time to cruise is given by

$$T^{cruise} = \frac{R}{V^{cruise}} \quad (3.22)$$

  The power and energy required to loiter is given by

$$P_r^{loiter} = \frac{1}{2}\rho^{loiter}V^{loiter^3}SC_D^{loiter} \quad (3.23)$$

$$E^{loiter} = P_r^{loiter}\, T^{loiter} \quad (3.24)$$

The drag coefficient is calculated by

$$C_D = C_{D_O} + KC_L^2 \quad (3.25)$$

Where,

$$K = \frac{1}{\pi ARe} \quad (3.26)$$

and

$$C_{D_o} = \frac{f}{S} \quad (3.27)$$

Equivalent parasite area, f is calculated by relating to wetted area S_{wet} as shown in figure below. The skin friction coefficient, C_f is obtained as 0.0040 from the similar turboprop airplane data in Roskam (Roskam, 2005). Hence, the related a and b are obtained as -2.3979 and 1.000.

Equivalent Skin Friction Coefficient, c_f	a	b
0.0090	-2.0458	1.0000
0.0080	-2.0969	1.0000
0.0070	-2.1549	1.0000
0.0060	-2.2218	1.0000
0.0050	-2.3010	1.0000
0.0040	-2.3979	1.0000
0.0030	-2.5229	1.0000
0.0020	-2.6990	1.0000

Figure 27: Correlation coefficients for parasite area versus wetted area

The above figure is represented with the following empirically obtained equation

$$log_{10}f = a + blog_{10}S_{wet} \quad (3.28)$$

The constants c and d are the regression constants obtained by relating take-off weight to the wetted area.

$$log_{10}S_{wet} = c + dlog_{10}W_{TO} \quad (3.29)$$

The c and d constants are considered as -0.0866 and 0.8099 from regional turboprop airplane data in the table shown below.

Airplane Type	c	d
1. Homebuilts	1.2362	0.4319
2. Single Engine Propeller Driven	1.0892	0.5147
3. Twin Engine Propeller Driven	0.8635	0.5632
4. Agricultural	1.0447	0.5326
5. Business Jets	0.2263	0.6977
6. Regional Turboprops	-0.0866	0.8099
7. Transport Jets	0.0199	0.7531
8. Military Trainers*	0.8565	0.5423
9. Fighters*	-0.1289	0.7506
10. Mil. Patrol, Bomb and Transport	0.1628	0.7316
11. Flying Boats, Amph. and Float	0.6295	0.6708
12. Supersonic Cruise Airplanes	-1.1868	0.9609

Figure 28: Regression line coefficients for takeoff weight versus wetted area

The lift coefficient is given by

$$C_L = \frac{2W_{TO}}{\rho V^2 S} \qquad (3.30)$$

Where density, ρ and velocity V are different for climb, cruise and loiter phases. The cruise velocity is considered from mission requirements. The range is considered same for Hepperle's and Riboldi's methods. Wing area, Aspect ratio, Oswald coefficient, Rate of climb and Loiter time are chosen from the reference aircraft (ATR , 2014). Based on cruise altitude specified in mission requirements as 7600 m, the cruise density is chosen. The following data is considered for calculation of battery weight by few assumptions and mission requirements.

Table 14: Assumptions and mission requirements for the calculation of battery weight

Wing Area, S	657 sq. ft
Aspect Ratio, AR	12
Oswald Coefficient, e	0.85

Battery Energy density, E^* (Hepperle, 2012)	7.53e+14 ft^2/hr^2 or 1500 Wh/kg
Power Density, p (Hepperle, 2012)	4.77e+14 ft^2/hr^3 or 950 W/kg
Acceleration due to gravity, g	416696000 ft/hr^2 or 9.81 m/s^2
Cruise Velocity, V^{cruise}	1670929.92 ft/hr or 316.464 mph
Climb Velocity, V^{climb} (ATR , 2014)	1032942.24 ft/hr or 195.633 mph
Loiter Velocity, V^{loiter} (Gary, 2018)	1215223.68 ft/hr or 230.156 mph
Cruise Density, ρ^{cruise} (Engineering, 2003)	0.034297 lb/cu.ft
Climb Density, ρ^{climb} (Engineering, 2003)	0.056497 lb/cu.ft
Loiter Density, ρ^{loiter} (Engineering, 2003)	0.03539 lb/cu.ft
Rate of Climb, RC	81300 ft/hr or 1355 ft/min
Loiter Time, T^{loiter}	15 min or 0.25 hr
Range, R	4921260 ft or 1500 km

Based on the above data, the battery weight is calculated by using MATLAB programming and calculations are shown in Appendix A. The results of power, energy and battery weight are shown below.

Table 15: Results of power, energy and battery weight

Results	
Power Required to Climb, P_r^{climb}	1.518e+18 $lb.\frac{ft^2}{hr^3}$ or 1372 KW
Power Required to Cruise, P_r^{cruise}	2.623e+18 $lb.\frac{ft^2}{hr^3}$ or 2369 KW

Power Required to Loiter, P_r^{loiter}	1.826e+18 $lb.\frac{ft^2}{hr^3}$ or 1650 KW
Energy Required to Climb, E^{climb}	4.656e+17 $lb.\frac{ft^2}{hr^2}$ or 421 KWh
Energy Required to Cruise, E^{cruise}	7.725e+18 $lb.\frac{ft^2}{hr^2}$ or 6978 KWh
Energy Required to Loiter, E^{loiter}	4.566e+17 $lb.\frac{ft^2}{hr^2}$ or 412 KWh
Battery Weight, W_{bat}	12761 lbs

The above results clearly indicate that the cruise phase requires more power and energy as compared to other two mission phases. The battery weight calculated as 12761 lbs by Riboldi's method (Riboldi, 2016) is almost reasonable as compared to Hepperle's (Hepperle, 2012) method of calculation of battery weight 10893 lbs. Hepperle's method of battery weight calculation is mainly based on the range of the aircraft which includes mainly cruise and loiter phase. As we can see by Riboldi's method, most of the battery energy is required by cruise phase, so the battery weight estimation is reasonable with chosen assumptions.

3.2.3.2 Calculation of Mission Weights using AAA Program

The mission weight calculations are shown below using AAA program

Input Parameters

A	0.3941	$W_{TO_{est}}$	54000.0	lb	$W_{\Sigma crew}$	820.0	lb	M_{tfo}	0.500	%	$W_{TO_{min}}$	45000.0	lb
B	0.9630	$W_{\Sigma pax}$	7000	lb	$W_{\Sigma cargo}$	12093.3	lb	$M_{F_{res}}$	25.000	%	$W_{TO_{max}}$	70000.0	lb

Output Parameters

M_{ff}	0.9720	W_F	1896.1	lb	$W_{F_{res}}$	379.2	lb	W_{PL}	19093.3	lb	W_E	32118.1	lb
$W_{F_{used}}$	1516.9	lb	$W_{F_{max}}$	1896.1	lb	W_{tfo}	271.0	lb	W_{useful}	21809.5	lb	W_{TO}	54198.5	lb

Mission Profile Table: Output

	Mission Profile	W_{begin} lb	$\Delta W_{F_{used}}$ lb	$W_{F_{begin}}$ lb
1	Warmup	54198.5	542.0	1896.1
2	Taxi	53656.6	268.3	1354.1
3	Take-off	53388.3	266.9	1085.9
4	Climb	53121.3	439.7	818.9
5	Cruise	52681.6	0.0	379.2
6	Loiter	52681.6	0.0	379.2
7	Turn	52681.6	0.0	379.2
8	Descent	52681.6	0.0	379.2
9	Land/Taxi	52681.6	0.0	379.2

Figure 29: Calculation of mission weights using AAA program

The design point is plotted using the similar airplanes database for take-off weights and empty weights as shown below

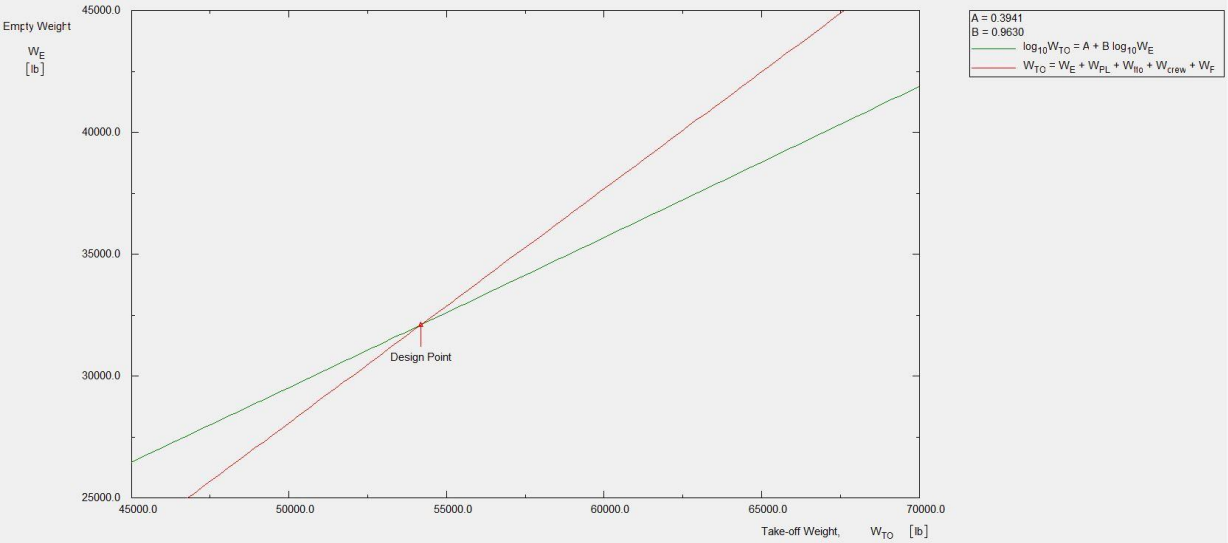

Figure 30: Graph of design point

3.3 TAKE-OFF WEIGHT SENSITIVITIES

Sensitivity Studies are conducted mainly to find out which parameters drive the design and to determine which areas of technological change must be pursued to achieve some new mission capability. Takeoff Weight sensitivities are calculated manually and then compared with AAA

program. The proposed design uses a combination of fuel till climb and battery for the remaining phases. Hence the weight sensitivities are calculated for fuel mission phase and range sensitivities are calculated for battery mission phases. AAA program gives us only weight sensitivities but not range sensitivities to compare.

3.3.1 Manual Calculation of Takeoff Weight Sensitivities

Takeoff weight sensitivities can be obtained by using regression coefficients A, B and parameters C and D. The parameters C and D are given by

$$W_E = CW_{TO} - D \tag{3.31}$$

Where,

$$C = 1 - (1 + M_{res})\left(1 - M_{ff}\right) - M_{tfo} \tag{3.32}$$

From Table 13, we get

$$C = 1 - (1 + 0.25)(1 - 0.97199) - 0.005$$

$$C = 0.9599$$

and

$$D = W_{PL} + W_{crew} + W_{bat} \tag{3.33}$$

$$D = 8200 + 820 + 10893$$

$$D = 19913\ lbs$$

The values of A = 0.3941, B = 0.9630 are already obtained

- **Sensitivity of Take-off Weight to Payload Weight**

The sensitivity of take-off weight to payload weight is given by

$$\frac{\partial W_{TO}}{\partial W_{PL}} = \frac{BW_{TO}}{D - C(1 - B)W_{TO}} \tag{3.34}$$

Where,

A = 0.3941, B = 0.9630

C = 0.9599, D = 19913

$W_{TO} = 54199\ lbs$ obtained from weight sizing

By substituting A, B, C, D and W_{TO} in $\frac{\partial W_{TO}}{\partial W_{PL}}$, we get

$$\frac{\partial W_{TO}}{\partial W_{PL}} = \frac{0.9630 * 54199}{19913 - 0.9599(1 - 0.9630)54199}$$

$$\frac{\partial W_{TO}}{\partial W_{PL}} = 2.90$$

This means, that for each pound of payload added, the airplane take-off weight will have to be increased by 2.9 lbs. The factor 2.9 is called the growth factor due to payload.

- **Sensitivity of Takeoff Weight to Empty Weight**

The sensitivity of takeoff weight to empty weight is expressed as

$$\frac{\partial W_{TO}}{\partial W_E} = \frac{BW_{TO}}{inv\ log_{10}\{\frac{log_{10}W_{TO} - A}{B}\}} \qquad (3.35)$$

$$\frac{\partial W_{TO}}{\partial W_E} = \frac{0.9630 * 54199}{inv\ log_{10}\{\frac{log_{10}54199 - 0.3941}{0.9630}\}}$$

$$\frac{\partial W_{TO}}{\partial W_E} = 1.63$$

This means that take-off weight must be increased by 1.63 lbs for each lbs of increase in empty weight to keep the mission performance same.

- **Sensitivity of Takeoff Weight to Endurance for Climb**

The sensitivity of takeoff weight to endurance for climb is given by

$$\frac{\partial W_{TO}}{\partial E} = \frac{FVC_P}{375n_p(\frac{L}{D})} \qquad (3.36)$$

Where,

$$F = -\frac{BW_{TO}^2(1+M_{res})M_{ff}}{CW_{TO}(1-B)-D} \qquad (3.37)$$

L/D = 15, $n_p = 0.77$, $C_p = 0.6$ lbs/hp/hr are considered for climb from Roskam (Roskam, 2005), takeoff weight taken from AAA program as 54199 lbs. $M_{ff} = 0.972$ and $M_{res} = 0.25$ are obtained from mission weights. Velocity to climb V is considered as 195.633 mph and Endurance E is calculated as 0.307 hr from reference aircraft rate of climb 1355 ft/min and cruise altitude 7600 m or 24943.38 ft from mission requirements (ATR , 2014).

By substituting all the values in F, we get

$$F = 191064.54\ lbs$$

$$\frac{\partial W_{TO}}{\partial E} = \frac{191064.54 * 195.633 * 0.6}{375 * 0.77 * 15}$$

$$\frac{\partial W_{TO}}{\partial E} = 5178\ \frac{lbs}{hr}$$

These values of L/D, n_p, C_p, and F are used for the remaining sensitivity studies for climb

- **Sensitivity of Takeoff Weight to Specific fuel Consumption for Climb**

The sensitivity of takeoff weight to specific fuel consumption is given by

$$\frac{\partial W_{TO}}{\partial C_p} = \frac{FEV}{375 n_p (\frac{L}{D})} \qquad (3.38)$$

$$\frac{\partial W_{TO}}{\partial C_p} = \frac{191064.54\ * 0.307 * 195.633}{375 * 0.77 * 15}$$

$$\frac{\partial W_{TO}}{\partial C_p} = 2650\ \frac{lbs}{\frac{lbs}{hp}/hr}$$

This means if the specific fuel consumption decreases from 0.6 to 0.55 then, takeoff weight would decrease by 0.05*2650 = 132.5 lbs.

- **Sensitivity of Takeoff Weight to Propeller Efficiency for Climb**

The sensitivity of takeoff weight to propeller efficiency is given by

$$\frac{\partial W_{TO}}{\partial n_p} = \frac{-FEVC_P}{375 n_p^2 (\frac{L}{D})} \quad (3.39)$$

$$\frac{\partial W_{TO}}{\partial n_p} = \frac{-191064.54 * 0.307 * 195.33 * 0.6}{375 * 15 * 0.77^2}$$

$$\frac{\partial W_{TO}}{\partial n_p} = -2061\ lbs$$

This means if the propeller efficiency increases from 0.77 to 0.79 then, the takeoff weight decreases by 0.02*2061 = 40 lbs.

- **Sensitivity of Takeoff Weight to Lift-to-Drag Ratio for Climb**

  The sensitivity of takeoff weight to lift-to-drag ratio is given by

$$\frac{\partial W_{TO}}{\partial (\frac{L}{D})} = \frac{-FEVC_P}{375 n_p (L/D)^2} \quad (3.40)$$

$$\frac{\partial W_{TO}}{\partial (\frac{L}{D})} = \frac{-191064.54 * 0.307 * 195.33 * 0.6}{375 * 0.77 * 15^2}$$

$$\frac{\partial W_{TO}}{\partial (\frac{L}{D})} = -107\ lbs$$

This means if L/D increases from 15 to 16 then, the takeoff weight would decrease by 107 lbs.

The below table shows the summary of results of weight sensitivities

Table 16: Results of weight sensitivities

$\frac{\partial W_{TO}}{\partial W_{PL}}$	2.90
$\frac{\partial W_{TO}}{\partial W_E}$	1.63
$\frac{\partial W_{TO}}{\partial E}$	5178 lbs/hr

$\frac{\partial W_{TO}}{\partial C_p}$	2649 lbs/lbs/hp/hr
$\frac{\partial W_{TO}}{\partial n_p}$	-2061 lbs
$\frac{\partial W_{TO}}{\partial (\frac{L}{D})}$	-107 lbs

3.3.2 Manual Calculation of Range Sensitivities

Range sensitivities are calculated based on the cruise parameters and assumptions made in battery weight calculation by Hepperle's method. Fraction of empty to takeoff weight and payload weight to takeoff weight are calculated using empty weight from mission weights data and take-off weight from AAA program. The following parameters are used for the calculation of range sensitivities

Table 17: Parameters used for range sensitivities calculation

Lift-to-Drag Ratio, L/D	15
Battery Energy Density, E^*	7.53e+14 ft^2/hr^2 or 1500 Wh/kg
Total system Efficiency, n_{total}	0.90
Fraction of Empty Weight to Takeoff Weight, $f_e = W_{Empty}/W_{TO}$	0.59
Fraction of Payload Weight to Takeoff Weight, $f_p = W_{PL}/W_{TO}$	0.15
Battery Weight, W_{Bat}	10893 lbs
Acceleration due to gravity, g	416696000 ft$/hr^2$ or 9.81 m$/s^2$
Takeoff Weight, W_{TO} (from AAA program)	54199

The following equation corresponds to range reduction imposed by the total weight growth limit.

$$\frac{\partial W_{TO}}{\partial R} = \frac{1}{4200} * W_{TO}^{1.27} \quad \left[\frac{kg}{km}\right] \qquad (3.41)$$

- **Sensitivity of Range to Takeoff Weight**

  The sensitivity of range to takeoff weight is given by hepperle (Hepperle, 2012) as

$$\frac{\partial R}{\partial W_{TO}} = -E^* n_{total} \left(\frac{L}{D}\right)\left(\frac{1}{g}\right)\left(\frac{W_{bat}}{W_{TO}^2}\right) \qquad (3.42)$$

- **Sensitivity of Range to Lift-to-Drag Ratio**

  The sensitivity of range to lift-to-drag ratio is given by

$$\frac{\partial R}{\partial \left(\frac{L}{D}\right)} = \left(1 - f_e - f_p\right)\left(\frac{1}{g}\right) E^* n_{total} \qquad (3.43)$$

- **Sensitivity of Range to Battery Energy Density**

  The Sensitivity of range to battery energy density is given by

$$\frac{\partial R}{\partial E^*} = \left(1 - f_e - f_p\right)\left(\frac{1}{g}\right)\left(\frac{L}{D}\right) n_{total} \qquad (3.44)$$

- **Sensitivity of Range to Fraction of Empty weight and Takeoff Weight**

  The sensitivity of range to fraction of empty weight and takeoff weight is given by

$$\frac{\partial R}{\partial f_e} = -E^* n_{total} \left(\frac{L}{D}\right)\left(\frac{1}{g}\right) \qquad (3.45)$$

The results of range sensitivities are obtained by using above equations as follows

Table 18: Results of range sensitivities

Growth limit, $\frac{\partial W_{TO}}{\partial R}$	0.060 lbs/ft or 89.3 kg/km
$\frac{\partial R}{\partial \left(\frac{L}{D}\right)}$	422855.03 ft or 128.8 km
$\frac{\partial R}{\partial E^*}$	8.375e-9 hr^2/ft or 0.356 s^2/m

$\frac{\partial f_e}{\partial R}$	-4.099e-8 per ft or 0.0003048 per km
$\frac{\partial R}{\partial W_{TO}}$	-90.43 ft/lbs or -0.0607 km/kg

3.3.3 Calculation of Takeoff Weight Sensitivities using the AAA Program

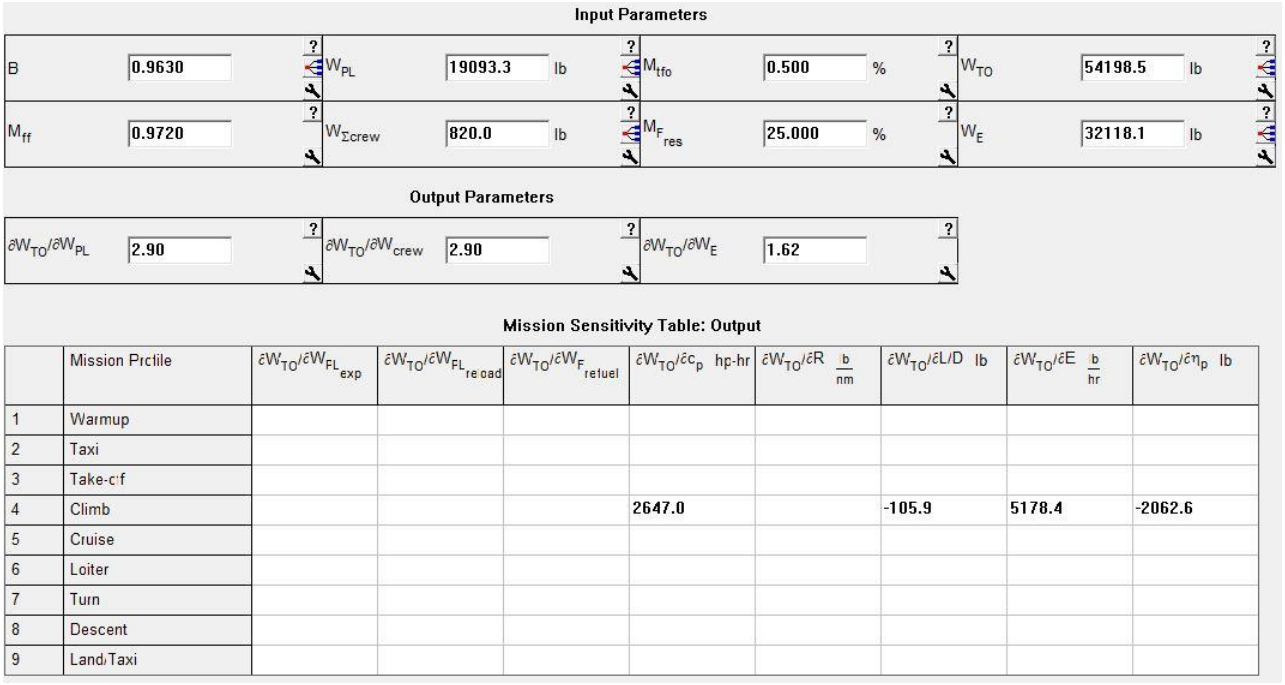

Input Parameters

B	0.9630		W_{PL}	19093.3	lb	M_{tfo}	0.500	%	W_{TO}	54198.5	lb
M_{ff}	0.9720		$W_{\Sigma crew}$	820.0	lb	$M_{F_{res}}$	25.000	%	W_E	32118.1	lb

Output Parameters

$\partial W_{TO}/\partial W_{PL}$	2.90	$\partial W_{TO}/\partial W_{crew}$	2.90	$\partial W_{TO}/\partial W_E$	1.62

Mission Sensitivity Table: Output

	Mission Prctile	$\partial W_{TO}/\partial W_{FL_{exp}}$	$\partial W_{TO}/\partial W_{FL_{reload}}$	$\partial W_{TO}/\partial W_{F_{refuel}}$	$\partial W_{TO}/\partial c_p$ hp-hr	$\partial W_{TO}/\partial R$ $\frac{lb}{nm}$	$\partial W_{TO}/\partial L/D$ lb	$\partial W_{TO}/\partial E$ $\frac{lb}{hr}$	$\partial W_{TO}/\partial \eta_p$ lb
1	Warmup								
2	Taxi								
3	Take-off								
4	Climb				2647.0		-105.9	5178.4	-2062.6
5	Cruise								
6	Loiter								
7	Turn								
8	Descent								
9	Land/Taxi								

Figure 31: Takeoff weight sensitivities calculation using AAA program

3.3.4 Trade Studies

The trade studies are performed for various parameters with respect to takeoff weight and range as shown below

- **Takeoff Weight Versus Payload Weight**

  As we know takeoff weight is directly proportional to payload weight, so the below graph clearly indicates that take-off weight increases with increase in payload weight.

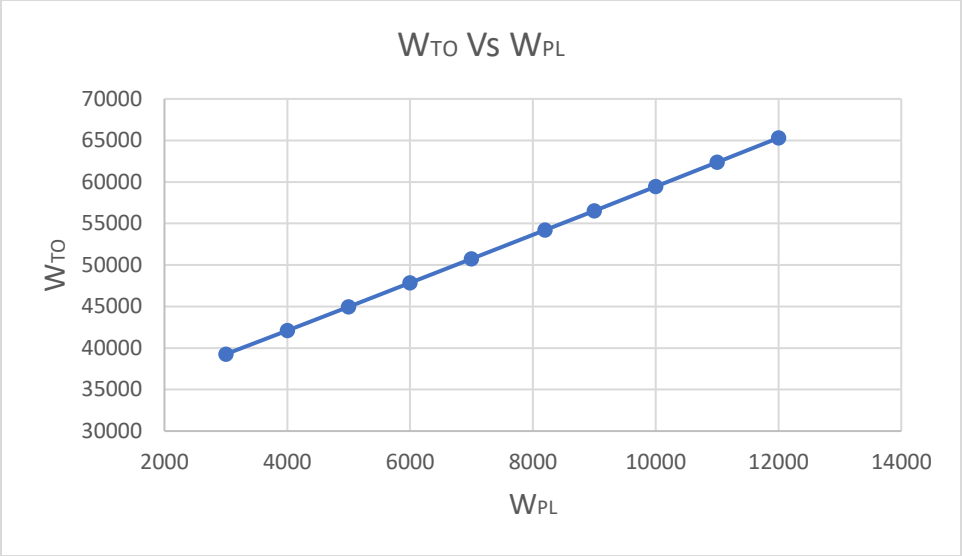

Figure 32: Takeoff weight versus payload weight

- **Takeoff Weight Versus Lift-to-Drag Ratio for Climb**

  The Takeoff weight decreases with increase in lift-to-drag ratio

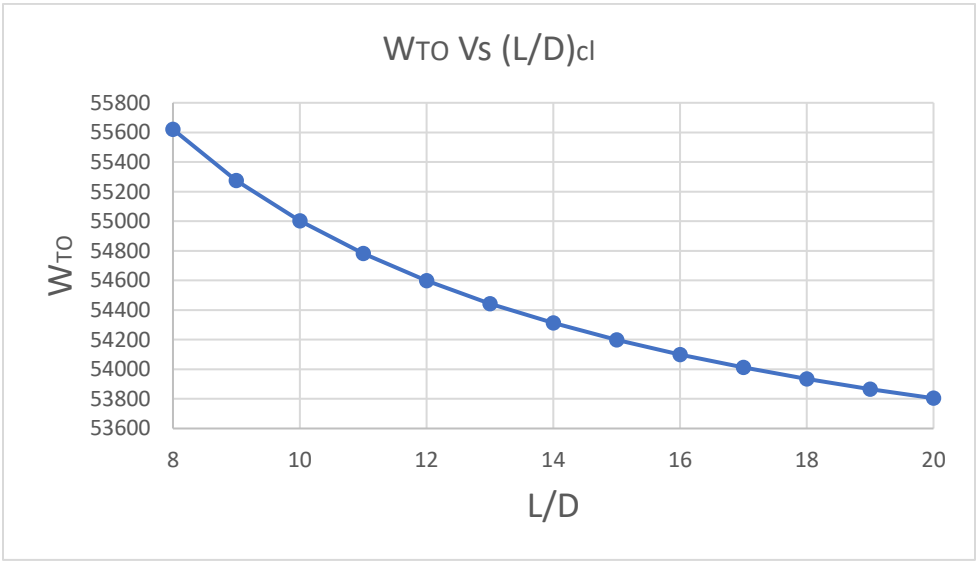

Figure 33: Takeoff weight versus lift-to-drag ratio

- **Takeoff Weight Versus Propeller Efficiency for Climb**

  As the propeller efficiency increases the takeoff weight decreases

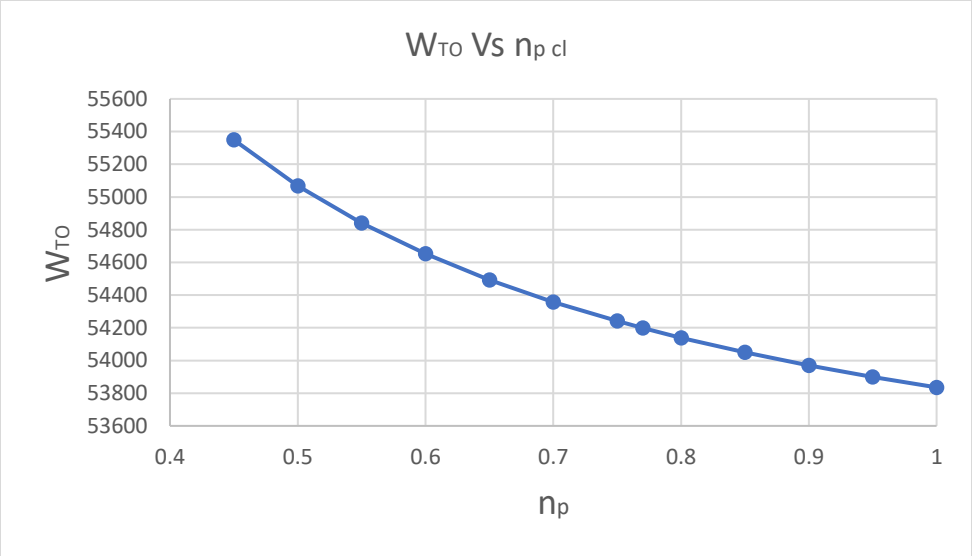

Figure 34: Takeoff weight versus propeller efficiency

- **Takeoff Weight Versus Specific Fuel Consumption for Climb**

  The Takeoff Weight increases with increase in specific fuel consumption for propeller.

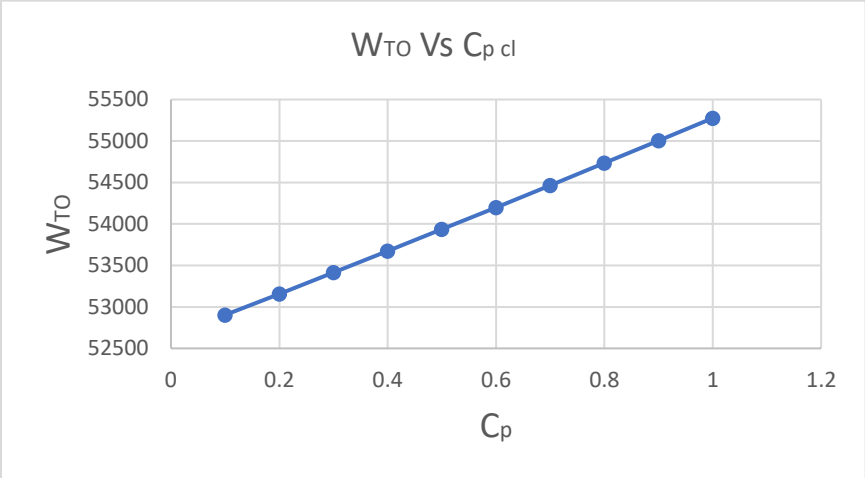

Figure 35: Takeoff weight versus specific fuel consumption

- **Range Versus Payload Weight for Cruise**

  The trade study for range versus payload is based on the range equation. The below graph shows the three zones of maximum payload range, tradeoff between fuel and payload and

tradeoff between payload range. The three lines are the payload limit, maximum take-off weight limit, fuel volume limit.

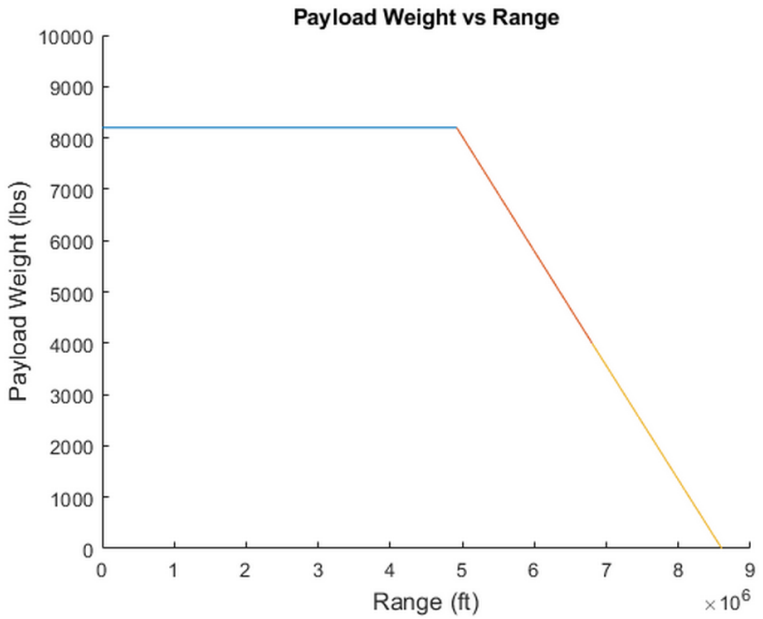

Figure 36: Range versus payload weight

- **Range Versus Lift-to-Drag Ratio for Cruise**

  The range is directly proportional to lift-to-drag ratio, so the range increases with increase in lift-to-drag ratio.

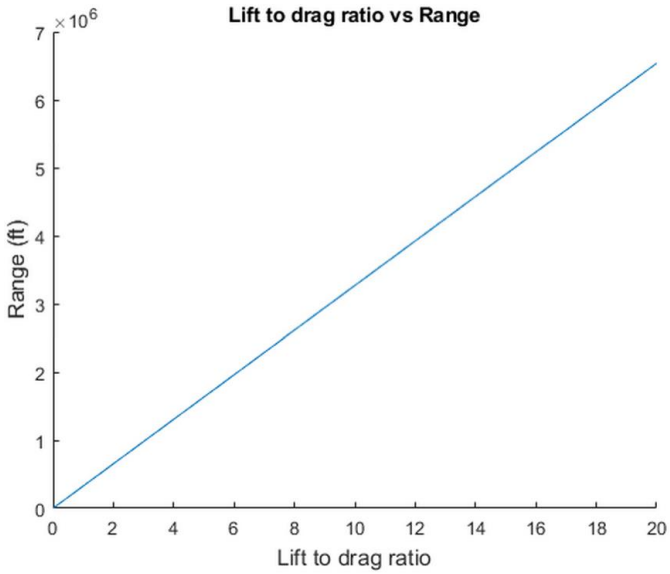

Figure 37: Range versus lift-to-drag ratio

- **Range Versus Propeller Efficiency for Cruise**

  The propeller efficiency is directly proportional to range and hence, the below figure clearly indicates the range increases with increase in propeller efficiency.

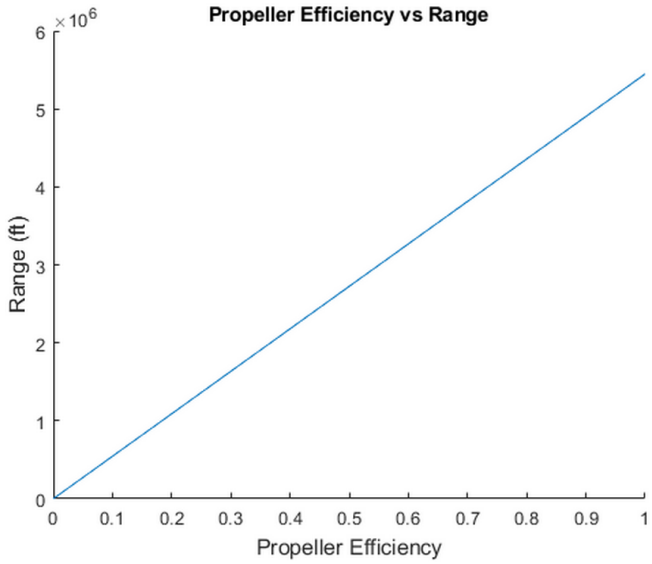

Figure 38: Range versus propeller efficiency

- **Comparison of Hybrid, Fuel and Electrical Aircraft for Range Versus Payload Weight**

  The below graph is plotted as comparison of hybrid, fuel and electrical aircraft for range versus payload weight. The fuel aircraft data is considered from reference conventional aircraft (ATR , 2014). The reference aircraft carries 48 passengers whereas hybrid and electrical carries 40 passengers. The electrical aircraft uses Riboldi's battery weight in the range equation for plotting range versus payload weight. The hybrid aircraft graph is plotted as per the calculated data. Comparing these three plots, the hybrid aircraft can reach maximum range than fuel and electrical aircraft. Electrical aircraft has the minimum range with same payload limit as hybrid. The payload limit for conventional aircraft is more compared to hybrid and electrical.

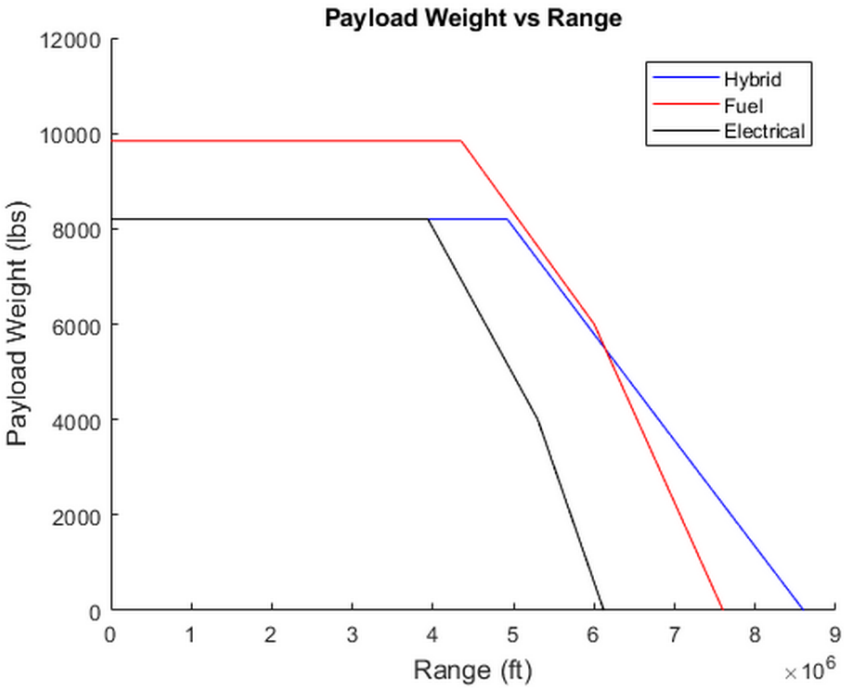

Figure 39: Range versus payload weight comparison for hybrid, fuel and electric aircraft

3.4 DISCUSSION

This chapter presented a class 1 preliminary weight estimation for the hybrid aircraft. The regression constants calculation is the key factor for calculating the allowable aircraft weight. The Takeoff weight is estimated as 54000 lbs manually while AAA program gives the design takeoff weight as 54199 lbs. The mission weights calculated manually are reasonably close enough to AAA program. The battery weight calculated using Hepperle's method is 10893 lbs whereas Riboldi's method gives 12761 lbs. Hepperle's method is mainly for the range of the aircraft whereas Riboldi's method is for complete electric aircraft. As from the power results we can see the cruise mission phase requires more power than other phases. As the proposed design uses fuel for climb and battery power for cruise and loiter, Hepperle's method is quite relevant for the proposed design. The assumptions made for battery weight calculations ten years from now seems to be reasonable. The fuel weight calculation shows that for proposed design the fuel usage is much less as compared to battery weight. The AAA program does not have option for hybrid aircraft, so the battery weight is included in cargo which shows in payload. The output payload visible in AAA includes the battery weight as well. The weight

sensitivities are closely matching with the AAA program. The range sensitivities are calculated manually using Hepperle's equations and AAA does not have range sensitivities.

The trade studies are performed for important parameters with respect to takeoff weight and range. Trade studies shows that takeoff weight increases as payload and specific fuel consumption increases whereas takeoff weight decreases as lift-to-drag and propeller efficiency increases. The range increases with increase in lift-to-drag ratio and propeller efficiency whereas range decreases with increase in takeoff weight. The range versus payload weight graph shows the proposed design can fly a given combination of payload and range to achieve a specified mission.

3.5 CONCLUSION AND RECOMMENDATIONS

3.5.1 Conclusions

The calculated mission weights of proposed design are close to conventional reference fuel aircraft ATR. This indicates that a conventional aircraft can be replaced with hybrid design with less fuel consumption and emissions. The battery weight can be reduced by optimizing the battery energy density and power density. By the optimization of battery technology, the range of the aircraft can be improved. The weight sensitivity studies are closely matching with the AAA program and the values are quite sensible. The range sensitivities are reasonable with appropriate assumptions. The range is directly affected by lift-to-drag ratio and battery energy density, and hence assuming an appropriate lift-to-drag ratio and battery energy density is very important.

3.5.2 Recommendations

The battery technology needs a further research as the range of the aircraft depends on battery energy density. The battery weight needs to be reduced to carry more payload which requires a further study to improve. The battery weight is calculated on certain assumptions which require detailed analysis of reasoning them.

CHAPTER 4: PERFORMANCE CONSTRAINT ANALYSIS

4.1 INTRODUCTION

The mission specifications, configuration selection and weight sizing with weight sensitivities were already presented in previous chapters. This chapter presents performance constraint analysis for the proposed design with the use of data obtained in all the above-mentioned chapters. Range and cruise speed are already specified in mission requirements. In addition to these the following performance constraints will be analyzed in this chapter.

- Stall Speed
- Take-off distance
- Landing distance
- Cruise Speed
- Climb requirements

The performance constraints are calculated both manually and using AAA program. As the proposed design is hybrid, there is no option for hybrid in AAA program so the calculated data will be more accurate. The proposed design carries 40 passengers with obtained take-off weight 54199 lbs from weight sizing so, it is considered as FAR 25 certified aircraft. This chapter follows FAR 25 guidelines specified in Roskam (Roskam, 2005) for calculating the allowable values of wing loading and power loading to meet the performance constraints requirements. The type of propulsion system required for the proposed design will be selected in this chapter. The required number of engines will be selected based on the determination of required power from the matching plot. The propeller sizing will be carried out as per the guidelines and equations provided in Roskam (Roskam, 2005).

4.2 MANUAL CALCULATION OF PERFORMANCE CONSTRAINTS

4.2.1 Stall Speed

As per the Roskam (Roskam, 2005), there are no minimum stall speed requirements for FAR 25 certified airplanes.

4.2.2 Takeoff Distance

Takeoff distance of the proposed design is determined by the following factors (Roskam, 2005):

- Takeoff Weight
- Takeoff Speed also called lift-off speed
- Takeoff weight-to-power ratio and the corresponding propeller characteristics
- Aerodynamic drag coefficient and ground friction coefficient
- Pilot technique

The FAR field length for a passenger aircraft should be less than 5000 ft. The mission requirements specify the take-off field length S_{TOFL} as 1367 m or 4484.908 ft. As per the Roskam (Roskam, 2005), the take-off field length is proportional to take-off wing loading, takeoff thrust-to-weight ratio or take-off weight-to-power ratio and to the maximum take-off lift coefficient. The below figure defines various parameters important to FAR 25 S_{TOFL} requirements (Roskam, 2005).

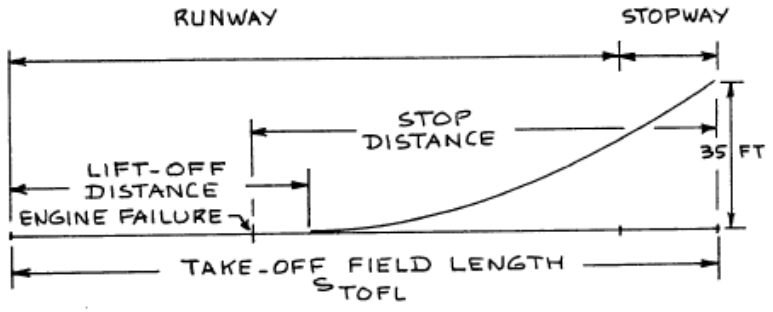

Figure 40: FAR 25 takeoff distance definition

FAR certified airplanes can be both propeller-driven or jet-driven. The following equation is obtained from Roskam (Roskam, 2005) for FAR 25 takeoff field length.

$$S_{TOFL} = 37.5\, TOP_{25} \qquad (4.1)$$

$$TOP_{25} = \frac{4484.908}{37.5} = 119.5975\ \frac{\text{lbs}}{\text{ft}^2}$$

where, TOP_{25} is the take-off parameter for FAR 25 certified airplanes determined as follows

$$TOP_{25} = \frac{\left(\frac{W}{S}\right)_{TO}}{\sigma C_{L_{max_{TO}}} \left(\frac{T}{W}\right)_{TO}} \qquad (4.2)$$

The above equation is for jet driven airplane and as the proposed design uses propeller driven, so the above equation is converted by using the relation as T=2.9 P_{TO} from following graph (Roskam, 2005).

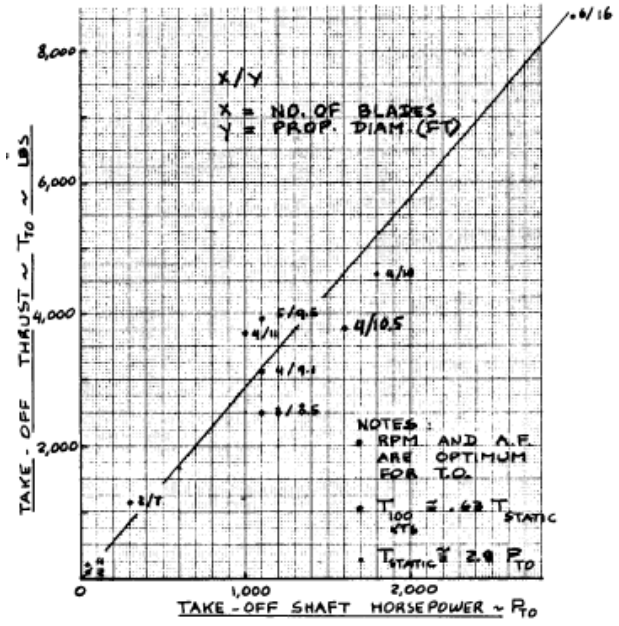

Figure 41: Effect of shaft horsepower on takeoff thrust

So, TOP_{25} for the propeller driven is given by

$$TOP_{25} = \frac{\left(\frac{W}{S}\right)_{TO}}{\sigma C_{L_{max_{TO}}} \left(\frac{2.9P}{W}\right)_{TO}} \qquad (4.3)$$

Using the above relation, we get the takeoff power loading in terms of wing loading as follows

$$\left(\frac{W}{P}\right)_{TO} = \frac{2.9 * TOP_{25} * \sigma * C_{L_{max_{TO}}}}{\left(\frac{W}{S}\right)_{TO}} \qquad (4.4)$$

Where,

$\left(\frac{W}{S}\right)_{TO}$ = Takeoff Wing Loading

$\left(\frac{W}{P}\right)_{TO}$ = Takeoff Power Loading

$C_{L_{max_{TO}}}$ = Maximum Takeoff Lift Coefficient

σ = Ratio of Density at an Altitude to Density at Sealevel

As per the Roskam (Roskam, 2005) data, the regional turboprops have a range of 1.7 to 2.1 maximum takeoff lift coefficient. Assuming the takeoff field length is calculated from sea-level and at sea-level, σ is calculated as 1 (Engineering, 2003).

Airplane Type	$C_{L_{max}}$	$C_{L_{max_{TO}}}$	$C_{L_{max_L}}$
1. Homebuilts	1.2 - 1.8	1.2 - 1.8	1.2 - 2.0*
2. Single Engine Propeller Driven	1.3 - 1.9	1.3 - 1.9	1.6 - 2.3
3. Twin Engine Propeller Driven	1.2 - 1.8	1.4 - 2.0	1.6 - 2.5
4. Agricultural	1.3 - 1.9	1.3 - 1.9	1.3 - 1.9
5. Business Jets	1.4 - 1.8	1.6 - 2.2	1.6 - 2.6
6. Regional TBP	1.5 - 1.9	1.7 - 2.1	1.9 - 3.3
7. Transport Jets	1.2 - 1.8	1.6 - 2.2	1.8 - 2.8
8. Military Trainers	1.2 - 1.8	1.4 - 2.0	1.6 - 2.2
9. Fighters	1.2 - 1.8	1.4 - 2.0	1.6 - 2.6
10. Mil. Patrol, Bomb and Transports	1.2 - 1.8	1.6 - 2.2	1.8 - 3.0
11. Flying Boats, Amphibious and Float Airplanes	1.2 - 1.8	1.6 - 2.2	1.8 - 3.4
12. Supersonic Cruise Airplanes	1.2 - 1.8	1.6 - 2.0	1.8 - 2.2

Figure 42: Maximum lift coefficient values for various type of airplanes

Based on the above assumption and discussion, the following values are obtained

$$TOP_{25} = 119.5975$$

At sea-level,

$$\sigma = 1$$

By substituting all the obtained values in equation (4.4), we get

$$\left(\frac{W}{P}\right)_{TO} = \frac{2.9 * 119.5975 * 1 * C_{L_{max_{TO}}}}{\left(\frac{W}{S}\right)_{TO}}$$

$$\left(\frac{W}{P}\right)_{TO} = \frac{346.832\ C_{L_{max_{TO}}}}{\left(\frac{W}{S}\right)_{TO}} \qquad (4.5)$$

The above equation is plotted with $C_{L_{max_{TO}}}$ varying from 1.5 to 2.1

<u>At Sea-Level</u>

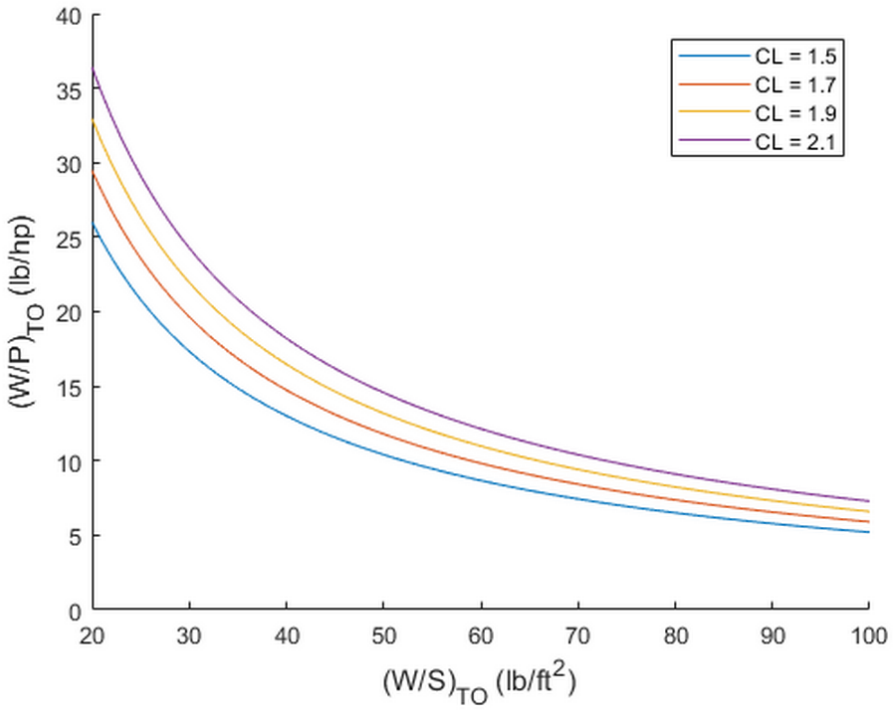

Figure 43: Effect of maximum takeoff lift coefficient and takeoff wing loading on takeoff weight-to-power ratio at sea-level

<u>At an Altitude of 5000 ft</u>

The density ratio at an altitude of 5000 ft is 0.8617 and by substituting the σ in equation (4.4), we get

$$\left(\frac{W}{P}\right)_{TO} = \frac{2.9 * 119.5975 * 0.8617 * C_{L_{max_{TO}}}}{\left(\frac{W}{S}\right)_{TO}}$$

$$\left(\frac{W}{P}\right)_{TO} = \frac{298.86 * C_{L_{max_{TO}}}}{\left(\frac{W}{S}\right)_{TO}} \qquad (4.6)$$

The above equation is plotted with $C_{L_{max_{TO}}}$ varying from 1.5 to 2.1

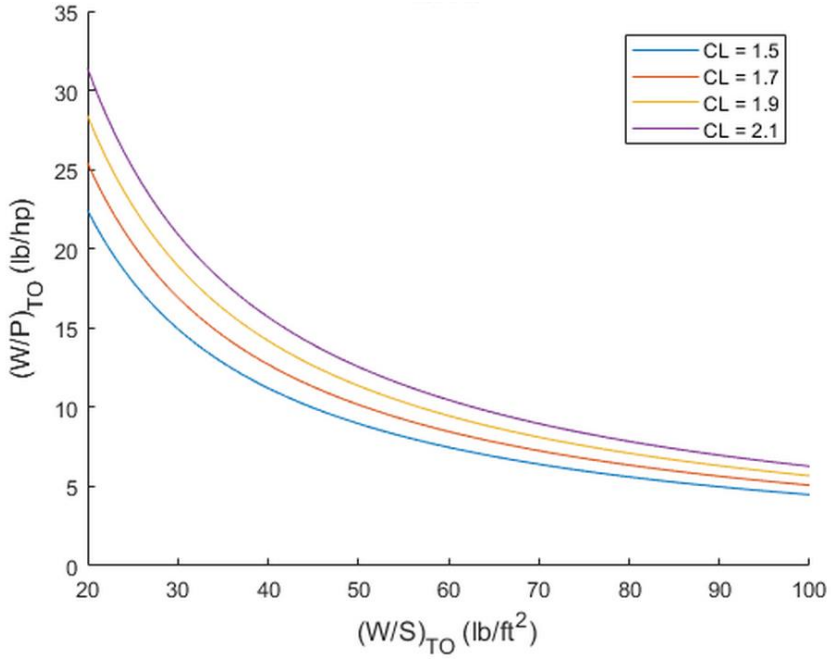

Figure 44: Effect of maximum takeoff lift coefficient and takeoff wing loading on takeoff weight-to-power ratio at 5000 ft altitude

At an Altitude of 8000 ft

The density ratio at an altitude of 8000 ft is 0.7860 and by substituting the σ in equation (4.4), we get

$$\left(\frac{W}{P}\right)_{TO} = \frac{2.9 * 119.5975 * 0.7860 * C_{L_{max_{TO}}}}{\left(\frac{W}{S}\right)_{TO}}$$

$$\left(\frac{W}{P}\right)_{TO} = \frac{272.61 * C_{L_{max_{TO}}}}{\left(\frac{W}{S}\right)_{TO}} \qquad (4.7)$$

The above equation is plotted with $C_{L_{max_{TO}}}$ varying from 1.5 to 2.1

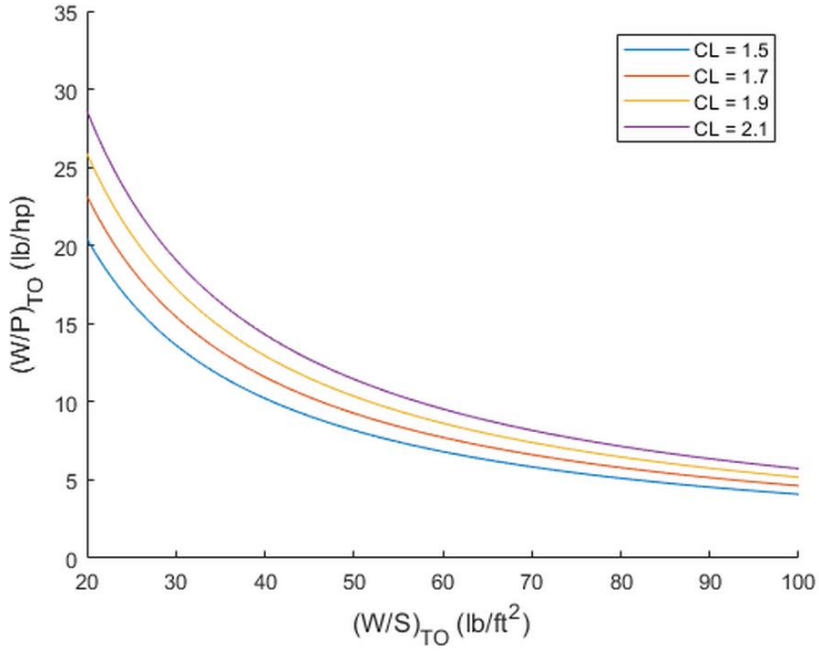

Figure 45: Effect of maximum takeoff lift coefficient and takeoff wing loading on takeoff weight-to-power ratio at sea-level at 8000 ft altitude

4.2.3 Landing Distance

Landing distance of the proposed design is determined by five factors as follows (Roskam, 2005)

- Approach Speed
- Landing Weight
- Deceleration Method Used
- Flying Qualities of the Airplane
- Pilot Technique

The below figure defines the parameters which are important in FAR 25 landing field length requirements (Roskam, 2005).

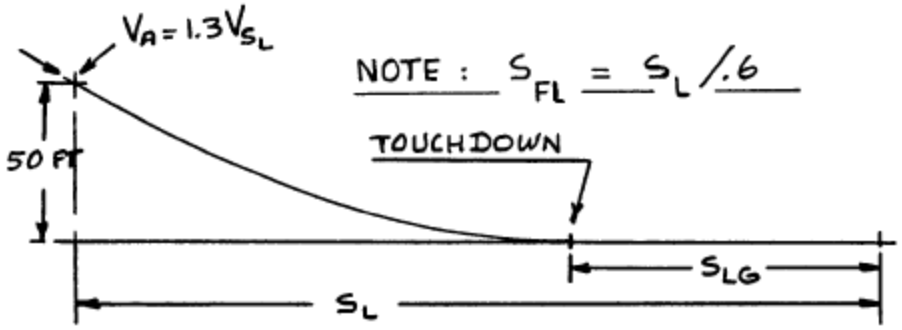

Figure 46: FAR 25 landing distance definition

As per the Roskam (Roskam, 2005), the FAR 25 landing field length in terms of approach speed is given by

$$S_{FL} = 0.3V_A^2 \qquad (4.8)$$

and the approach speed is defined as

$$V_A = 1.3V_{S_L} \qquad (4.9)$$

Where,

$S_{FL} = \text{Landing Field Length}$

$V_A = \text{Approach Speed}$

$V_{S_L} = \text{Landing Stall Speed}$

The landing field length is specified as 1300 m or 4265.092 ft in mission requirements. Therefore, from equation (4.8)

$$4265.092 = 0.3V_A^2$$

$$V_A = \sqrt{\frac{4265.092}{0.3}} = 119.2349 \text{ knots (or) } 201.2459 \ \frac{\text{ft}}{\text{sec}}$$

From equation (4.9), we get

$$V_{S_L} = \frac{119.2349}{1.3} = 91.719 \text{ knots (or) } 154.804 \ \frac{\text{ft}}{\text{sec}}$$

The landing stall speed is determined by using the below equation from Roskam (Roskam, 2005),

$$V_{S_L} = \sqrt{\frac{2\left(\frac{W}{S}\right)_L}{\rho C_{L_{max_L}}}} \qquad (4.10)$$

It is required to size the proposed design for a specified landing field length in mission requirements at sea-level on a standard day.

At the sea-level the density, $\rho = 0.002377 \ \frac{\text{Slugs}}{\text{ft}^3}$

By substituting ρ and V_{S_L} in the above equation, we get

$$154.8045 = \sqrt{\frac{2\left(\frac{W}{S}\right)_L}{0.002377 * C_{L_{max_L}}}}$$

$$\left(\frac{W}{S}\right)_L = 28.48 \ C_{L_{max_L}} \qquad (4.11)$$

The below figure shows the relation of W_L and W_{TO} for different airplanes (Roskam, 2005). The data shows a minimum ratio of 0.92 and maximum ratio of 1 for regional turboprop airplane. The mission fuel fraction obtained in weight sizing as 0.972 for the proposed design which is within the range of 0.92 to 1 as shown in below figure. Hence, the landing weight to take-off weight ratio is considered as 0.972.

$$\frac{W_L}{W_{TO}} = 0.972$$

Therefore, from equation (4.11) we get

$$\left(\frac{W}{S}\right)_{TO} = \frac{28.48 \ C_{L_{max_L}}}{0.972} = 29.3 \ C_{L_{max_L}} \qquad (4.12)$$

The above equation clearly shows the relation between $\left(\frac{W}{S}\right)_{TO}$ and $C_{L_{max_L}}$ to meet the field length requirements.

Airplane Type	W_L/W_{TO} Minimum	Average	Maximum
1. Homebuilts	0.96	1.0	1.0
2. Single Engine Propeller Driven	0.95	0.997	1.0
3. Twin Engine Propeller Driven	0.88	0.99	1.0
4. Agricultural	0.7	0.94	1.0
5. Business Jets	0.69	0.88	0.96
6. Regional TBP	0.92	0.98	1.0
7. Transport Jets	0.65	0.84	1.0
8. Military Trainers	0.87	0.99	1.1
9. Fighters (jets)	0.78	insufficient	1.0
(tbp's)	0.57	data	1.0
10. Mil. Patrol, Bomb and Transports (jets)	0.68	0.76	0.83
(tbp's)	0.77	0.84	1.0
11. Flying Boats, Amphibious and Float Airplanes (land)	0.79	insufficient	0.95
(water)	0.98	data	1.0
12. Supersonic Cruise Airplanes	0.63	0.75	0.88

Figure 47: The ratio of landing weight to takeoff weight for various airplanes

The equation (4.12) is plotted for different $C_{L_{max_L}}$ values using the data for regional turboprop ranging from 1.9 to 2.5.

At Sea-level

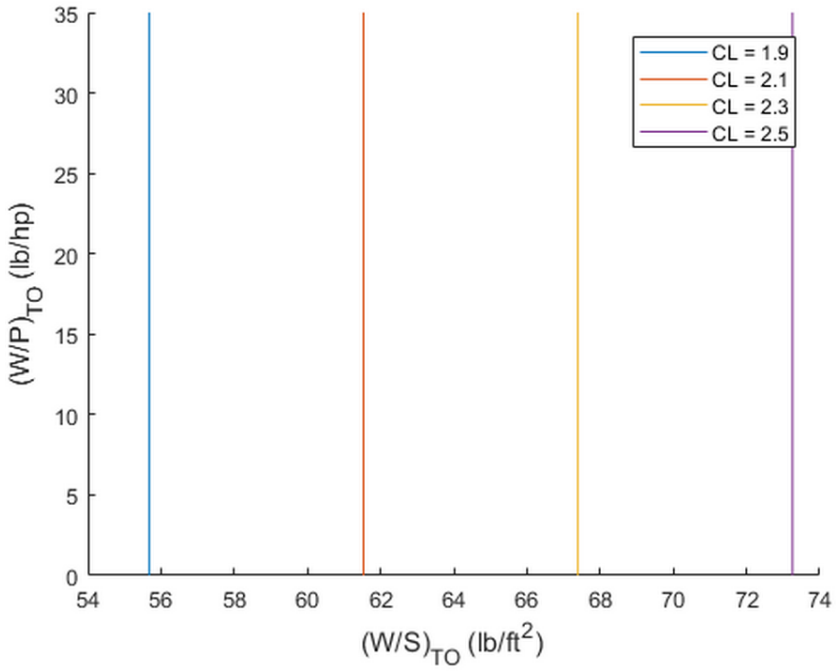

Figure 48: Plot of allowable wing loading to meet field length requirement at sea-level

At an Altitude of 5000 ft

The density at an altitude of 5000 ft is 0.002048 slugs/ft^3 and substituting it in equation (4.10), We get

$$154.8045 = \sqrt{\frac{2\left(\frac{W}{S}\right)_L}{0.002048 * C_{L_{max_L}}}}$$

$$\left(\frac{W}{S}\right)_L = 24.53\, C_{L_{max_L}}$$

By using landing weight to take-off weight ratio as 0.972, we get

$$\left(\frac{W}{S}\right)_{TO} = \frac{24.53\, C_{L_{max_L}}}{0.972} = 25.25\, C_{L_{max_L}} \qquad (4.13)$$

The above equation is plotted for different $C_{L_{max_L}}$ values using the data for regional turboprop ranging from 1.9 to 2.5.

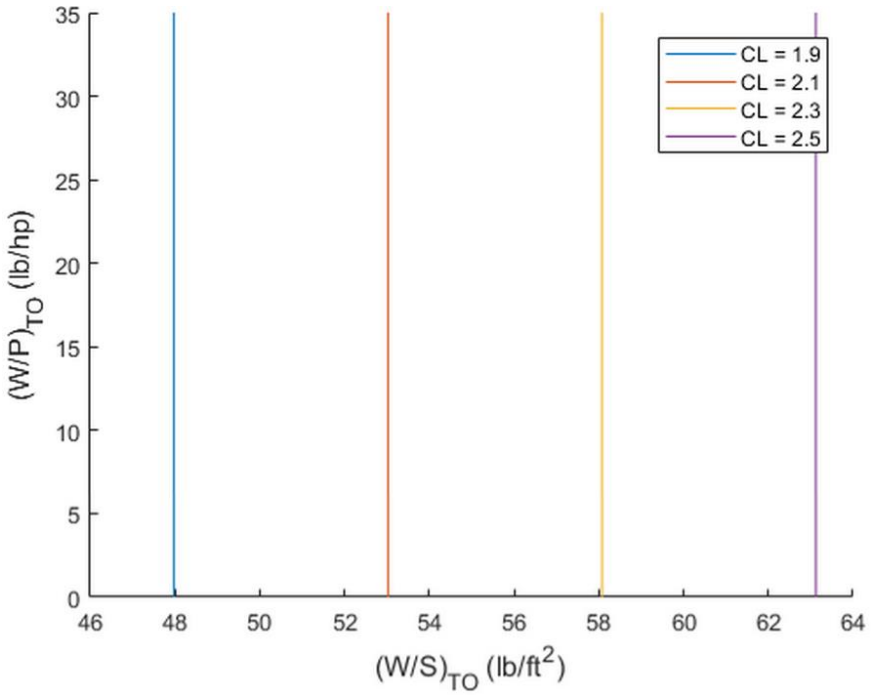

Figure 49: Plot of allowable wing loading to meet field length requirement at an altitude of 5000 ft

At an Altitude of 8000 ft

The density at an altitude of 5000 ft is 0.002048 slugs/ft^3 and substituting it in equation (4.10),

We get

$$154.8045 = \sqrt{\frac{2\left(\frac{W}{S}\right)_L}{0.001868 * C_{L_{max_L}}}}$$

$$\left(\frac{W}{S}\right)_L = 22.39\ C_{L_{max_L}}$$

By using landing weight to take-off weight ratio as 0.972, we get

$$\left(\frac{W}{S}\right)_{TO} = \frac{22.39\ C_{L_{max_L}}}{0.972} = 23.03\ C_{L_{max_L}} \qquad (4.14)$$

The above equation is plotted for different $C_{L_{max_L}}$ values using the data for regional turboprop ranging from 1.9 to 2.5.

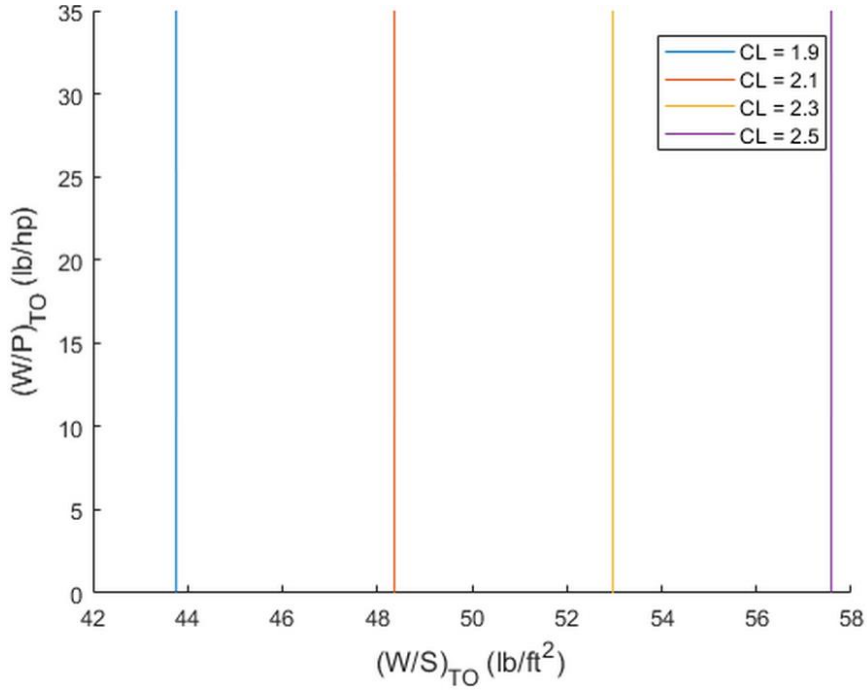

Figure 50: Plot of allowable wing loading to meet field length requirement at an altitude of 8000 ft

4.2.4 Drag Polar Estimation

The drag coefficient of an airplane can be written as

$$C_D = C_{D_O} + \frac{C_L^2}{\pi ARe} \qquad (4.15)$$

Where, C_{D_O}= Zero-Lift Drag Coefficient

AR = Aspect Ratio

e = Oswald Coefficient

Zero-Lift Drag Coefficient can be determined by

$$C_{D_O} = \frac{f}{S} \qquad (4.16)$$

The Equivalent parasite area f is determined from

$$log_{10} f = a + b log_{10} S_{wet} \qquad (4.17)$$

and wetted area S_{wet} is determined from

$$log_{10}S_{wet} = c + dlog_{10}W_{TO} \qquad (4.18)$$

The correlation coefficients a and b are function of the equivalent skin friction coefficient, C_f. The value of C_f chosen as 0.0040 as per the Roskam (Roskam, 2005) data in weight sizing and weight sensitivities section where a and b are obtained as -2.3979 and 1.00. The regression line constants c and d are obtained as -0.0866 and 0.8099. The design takeoff weight is obtained as 54199 lbs from weight sizing and weight sensitivities.

By substituting a,b,c,d and W_{TO} in equation (4.17) and equation (4.18), we get

$$S_{wet} = 5573.98\, sq.ft$$

$$f = 22.29\, sq.ft$$

Assuming the wing area, S from the reference aircraft (ATR , 2014) as 657 sq.ft we get equation (4.16) as

$$C_{D_O} = \frac{22.29}{657} = 0.0339$$

The aspect ratio, AR is assumed to be 12 from the reference aircraft (ATR , 2014) and Oswald coefficient for clean configuration is assumed as 0.85 from the below figure given by Roskam (Roskam, 2005).

Configuration	ΔC_{D_o}	e
Clean	0	0.80 - 0.85
Take-off flaps	0.010 - 0.020	0.75 - 0.80
Landing Flaps	0.055 - 0.075	0.70 - 0.75
Landing Gear	0.015 - 0.025	no effect

Figure 51: First estimates for ΔC_{D_O} and e with flaps and gear down

Based on the above assumptions, the clean configuration drag polar at low speed is calculated from equation (4.15) as

$$C_D = 0.0339 + \frac{C_L^2}{\pi * 12 * 0.85}$$

$$C_D = 0.0339 + 0.0312\, C_L^2$$

The additional zero-lift drag coefficient due to gear and due to flaps are assumed from the above figure as follows

Table 19: Assumptions of ΔC_{D_O} and e for different configurations

Configuration	ΔC_{D_O}	**e**
Clean	0	0.85
Takeoff Flaps	0.015	0.80
Landing Flaps	0.060	0.75
Landing Gear	0.020	-

Using the above assumptions, drag polar for different configurations are obtained as follows

Table 20: Results of drag polar for different configurations

Configuration	C_D
Clean	$0.0339 + 0.0312\ C_L^2$
Takeoff, gear up	$0.0489 + 0.03315\ C_L^2$
Takeoff, gear down	$0.0689 + 0.03315\ C_L^2$
Landing, gear up	$0.0939 + 0.03536\ C_L^2$
Landing, gear down	$0.1139 + 0.03536\ C_L^2$

4.2.5 Climb Constraints

The FAR 25 climb requirements are given for takeoff and balked landing flight conditions. These requirements must be fulfilled with the power available minus losses caused by accessory operation and installation losses. The climb constraints are calculated at sea-level and propeller efficiency is assumed to be 0.85 from Roskam (Roskam, 2005) data for all the climb requirements.

- **Takeoff Climb Requirements**

The takeoff climb requirements are summarized at maximum takeoff weight with ambient atmospheric conditions.

- **FAR 25.111 (OEI)**

This requirement is called initial climb segment requirement. The proposed design uses two engines and the climb gradient with the critical engine inoperative must be at least 1.2 percent for two-engine airplanes i.e CGR > 0.012 in the following configuration (Roskam, 2005):

1. Takeoff flaps
2. Landing gear up or retracted
3. Speed $V_2 = 1.2\ V_{S_{TO}}$
4. Takeoff power on remaining engines
5. Ground effect between 35 ft and 400 ft

The sizing method for FAR 25 propeller driven aircraft climb requirement uses the following equation.

$$CGRP = \text{Climb gradient parameter} = \frac{\{CGR + (L/D)^{-1}\}}{\sqrt{C_L}} \qquad (4.19)$$

Where,

$$CGRP = \frac{18.97\ \eta_p \sqrt{\sigma}}{\left(\frac{W}{S}\right)\sqrt{\left(\frac{W}{P}\right)}} \qquad (4.20)$$

Therefore,

$$CGRP = \frac{18.97\ \eta_p \sqrt{\sigma}}{\left(\frac{W}{S}\right)\sqrt{\left(\frac{W}{P}\right)}} = \frac{\{CGR + (L/D)^{-1}\}}{\sqrt{C_L}} \qquad (4.21)$$

Assuming the propeller efficiency η_p as 0.85 from Roskam (Roskam, 2005) data mentioned in weight sizing and weight sensitivities section and at sea-level σ is 1. The $C_{L_{max_{TO}}}$ is assumed for takeoff flaps, gear up as 1.7.

Using equation (4.10) in terms of takeoff divided by this flight condition, we get

$$\frac{V_{S_{TO}}^2}{V_2^2} = \frac{C_L}{C_{L_{max_{TO}}}} \qquad (4.22)$$

$$\frac{V_{S_{TO}}^2}{(1.2\,V_{S_{TO}})^2} = \frac{C_L}{C_{L_{max_{TO}}}}$$

The lift coefficient in this flight condition is given by

$$C_L = \frac{1.7}{1.2^2} = 1.1806$$

The drag polar equation from Table 20 used for this flight condition takeoff flaps, gear up is

$$C_D = 0.0489 + 0.03315\,C_L^2$$

By substituting C_L, we get $C_D = 0.0951$

Therefore, lift-to-drag ratio is calculated as

$$\left(\frac{L}{D}\right) = \frac{1.1806}{0.0951} = 12.41$$

Substituting $\left(\frac{L}{D}\right) = 12.53,\ C_L = 1.1806, \eta_p = 0.85,\ \sigma = 1$ and CGR = 0.012 in equation (4.21), we get

$$\frac{18.97 * 0.85 * \sqrt{1}}{\left(\frac{W}{S}\right)_{TO}\sqrt{\left(\frac{W}{P}\right)_{TO}}} = \frac{\{0.012 + (12.41)^{-1}\}}{\sqrt{1.1806}}$$

$$\left(\frac{W}{S}\right)_{TO}\sqrt{\left(\frac{W}{P}\right)_{TO}} = 189.29 \qquad (4.23)$$

- **FAR 25.121 (OEI)**

  This requirement is called transition segment climb requirement. The climb gradient with the critical engine inoperative must be at least positive i.e CGR > 0 for the two-engine airplanes in the following configuration (Roskam, 2005).

  1. Takeoff flaps
  2. Landing gear down
  3. Takeoff power on remaining engines

4. Ground Effect
5. Speed between V_{LOF} and $1.2V_{S_{TO}}$

This requirement needs to be checked for two speeds at V_{LOF} and at $1.2V_{S_{TO}}$. Assuming the speed V_{LOF} is $1.1V_{S_{TO}}$ as it is less than $1.2V_{S_{TO}}$

- **FAR 25.121 (OEI)**

  This requirement is called second segment climb requirement demands a climb gradient no less than 2.4 percent i.e CGR > 0.024 with one engine inoperative for two-engine airplanes in the following configuration (Roskam, 2005).

  1. Takeoff flaps
  2. Landing gear retracted
  3. No ground effect
  4. Takeoff power on remaining engines
  5. Speed at $V_2 = 1.2V_{S_{TO}}$

- **FAR 25.121 (OEI)**

  This is enroute climb requirement demands climb gradient no less than 1.2 percent i.e CGR > 0.012 with one engine inoperative for two-engine airplanes in the following configuration (Roskam, 2005).

  1. Flaps up
  2. Landing gear up
  3. Enroute climb altitude
  4. Maximum continuous power on remaining engines
  5. Speed at $1.25V_S$

The below table shows the parameters used in calculation of takeoff climb requirements based on Table 20 and specifications mentioned in takeoff climb requirements. The maximum takeoff lift coefficient is assumed from Roskam data for each requirement based on the configuration.

Table 21: Parameters used in calculation of takeoff climb requirements

Takeoff Climb Requirements	**Configuration**	**Drag Polar Equation**	$C_{L_{max_{TO}}}$	**CGR**

FAR 25.111 (OEI)	Takeoff flaps Gear up Ground effect	$0.0489 + 0.03315\ C_L^2$	1.7	0.012
FAR 25.121 (OEI)	Takeoff flaps Gear down Ground effect	$0.0689 + 0.03315\ C_L^2$	1.7	0
FAR 25.121 (OEI)	Takeoff flaps Gear up No ground effect	$0.0489 + 0.03315\ C_L^2$	1.7	0.024
FAR 25.121 (OEI)	Flaps up Gear up	$0.0339 + 0.0312\ C_L^2$	1.5	0.012

The below table shows the results of takeoff climb requirements in terms of relation between wing loading and weight-to-power ratio. The speeds and climb gradients are chosen as per the FAR requirements discussed above. The lift coefficient for each flight condition is calculated by using equation (4.10) and (4.21). The below values are calculated in a similar procedure as shown in FAR 25.111 (OEI) section.

Table 22: Results of takeoff climb requirements

Takeoff Climb Requirements	**Speed**	$\boldsymbol{C_L}$	$\boldsymbol{C_D}$	$\boldsymbol{\frac{L}{D}}$	**CGRP**	$\boldsymbol{\left(\frac{W}{S}\right)_{TO}\sqrt{\left(\frac{W}{P}\right)_{TO}}}$
FAR 25.111 (OEI)	1.2	$\frac{1.7}{1.2^2} = 1.1806$	0.095	12.41	0.0852	189.29
FAR 25.121 (OEI)	1.1	$\frac{1.7}{1.1^2} = 1.4049$	0.134	10.46	0.0806	199.89

	1.2	$\frac{1.7}{1.2^2} = 1.1806$	0.115	10.26	0.0897	179.69
FAR 25.121 (OEI)	1.2	$\frac{1.7}{1.2^2} = 1.1806$	0.095	12.41	0.0962	167.56
FAR 25.121 (OEI)	1.25	$\frac{1.5}{1.25^2} = 0.96$	0.063	15.32	0.0789	204.48

- **Landing Climb Requirements**

  The landing climb requirements are summarized at maximum design landing weight with ambient atmospheric conditions (Roskam, 2005).

- **FAR 25.119 (AEO)**

  This requirement demands climb gradient no less than 3.2 percent i.e CGR > 0.032 at a power level corresponding to that obtained 8 seconds after moving the throttles from minimum flight idle to the takeoff position (Roskam, 2005).

  1. Landing flaps
  2. Landing gear down
  3. Speed at $1.3V_S$
  4. Takeoff power on all engines

- **FAR 25.121 (OEI)**

  The climb gradient may not be less than 2.1 percent i.e CGR > 0.021 with critical engine inoperative for two-engine airplanes in the following configuration (Roskam, 2005).

  1. Approach flaps
  2. Landing gear down
  3. Takeoff power on remaining engines
  4. Speed at no more than $1.5V_{S_A}$

  The below table shows the parameters used in calculation of landing climb requirements based on Table 20 and specifications mentioned in landing climb requirements. The maximum landing lift coefficient is assumed from Roskam data for each requirement based on the configuration.

Table 23: Parameters used for calculation of landing climb requirements

Landing Climb Requirements	**Configuration**	**Drag Polar Equation**	$C_{L_{max_L}}$	**CGR**
FAR 25.119 (AEO)	Landing flaps Gear down	$0.1139 + 0.03536\ C_L^2$	2.1	0.032
FAR 25.121 (OEI)	Approach flaps Gear down	$0.0864 + 0.03536\ C_L^2$	1.9	0.021

The below table shows the results of landing climb requirements in terms of relation between wing loading and weight-to-power ratio. The speeds and climb gradients are chosen as per the FAR requirements discussed above. The lift coefficient for each flight condition is calculated by using equation (4.10) and (4.21). The ratio of landing weight to takeoff weight is obtained as 0.972 from weight sizing from mission fuel fraction. The below values are calculated in a similar procedure as shown in FAR 25.111 (OEI) section and using landing weight to takeoff weight ratio.

Table 24: Results of landing climb requirements

Landing Climb Requirements	**Speed**	C_L	C_D	$\frac{L}{D}$	**CGRP**	$\left(\frac{W}{S}\right)_{TO}\sqrt{\left(\frac{W}{P}\right)_{TO}}$
FAR 25.119 (AEO)	1.3	$\frac{2.1}{1.3^2} = 1.243$	0.168	7.374	0.15	111.91
FAR 25.121 (OEI)	1.5	$\frac{1.9}{1.5^2} = 0.844$	0.112	7.566	0.167	100.95

The results of take-off and landing climb requirements from Table 22 and Table 24 are plotted below using the relationship between take-off wing loading and take-off power loading.

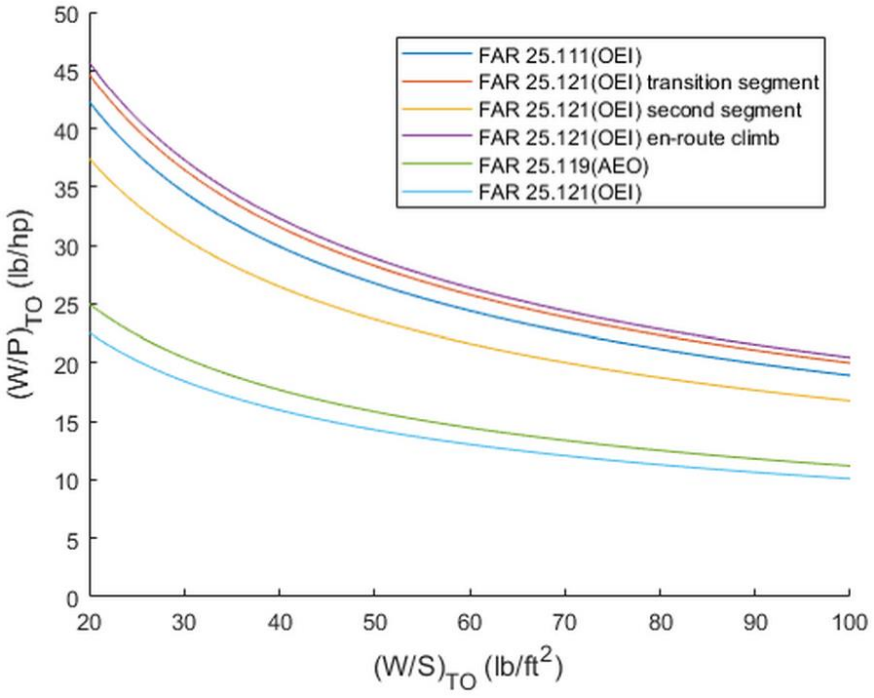

Figure 52: Take-off and landing climb requirements

4.2.6 Cruise Speed Constraint

As per the Roskam (Roskam, 2005), Cruise speed for propeller driven airplanes are calculated at 75 to 80 percent power and hence the cruise speed turns out to be proportional to power index.

$$V_{cr} \propto \left\{ \frac{\left(\frac{W}{S}\right)}{\left(\frac{W}{P}\right)} * \frac{\sigma C_{D_o}}{\eta_P} \right\}^{\frac{1}{3}} \qquad (4.24)$$

$$V_{cr} \propto I_P$$

Where,

$$I_P = \left\{ \frac{\left(\frac{W}{S}\right)}{\sigma\left(\frac{W}{P}\right)} \right\}^{1/3} \qquad (4.25)$$

The cruise speed is considered as 275 knots or 316.464 mph at cruising altitude 24934.38 ft from mission requirements. The below graph from Roskam (Roskam, 2005) shows the

correlation between cruise speed and power index for retractable gear with cantilevered wing configuration. Using the below graph for the cruise speed of 316.464 mph, the power index is calculated as 1.7. The density ratio, σ at sea-level is 1.

Therefore, from equation (4.25) we get

$$1.7 = \left\{ \frac{\left(\frac{W}{S}\right)}{1 * \left(\frac{W}{P}\right)} \right\}^{1/3}$$

$$\frac{\left(\frac{W}{S}\right)}{\left(\frac{W}{P}\right)} = 4.91 \qquad (4.26)$$

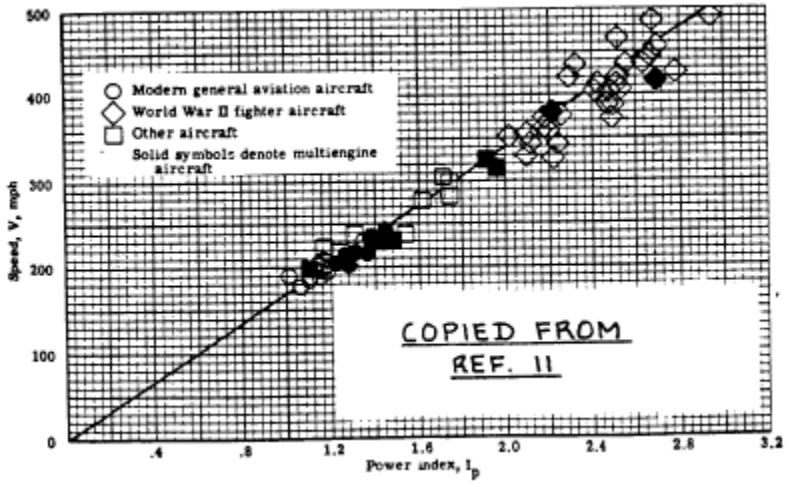

Figure 53: Cruise speed and power index correlation for retractable gear, cantilevered wing configuration

The equation (4.26) is plotted at sea-level which gives allowable values of wing loading and power loading to meet a given cruise speed.

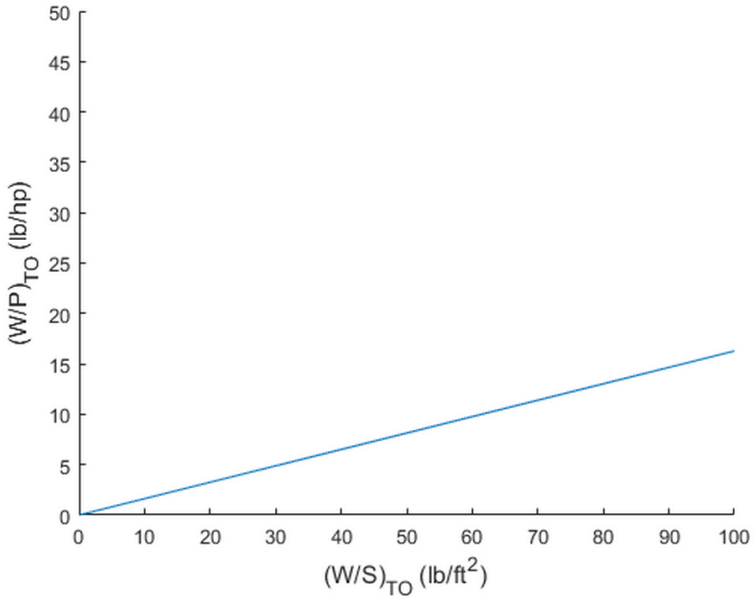

Figure 54: Cruise speed sizing

4.3 CALCULATION OF PERFORMANCE CONSTRAINTS WITH THE AAA PROGRAM

The calculation of the performance constraints using AAA program are shown below.

4.3.1 Takeoff Distance

The inputs of take-off distance are shown below where take-off field length is considered from the mission requirements and maximum lift coefficient is considered from Roskam.

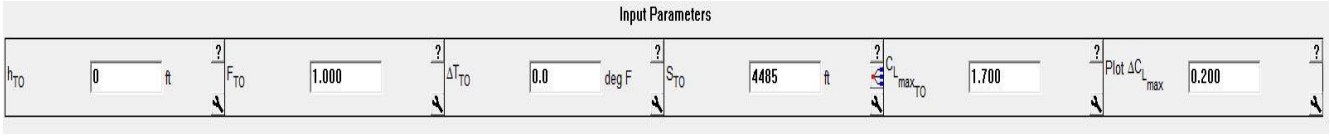

Figure 55: Inputs of take-off distance in AAA program

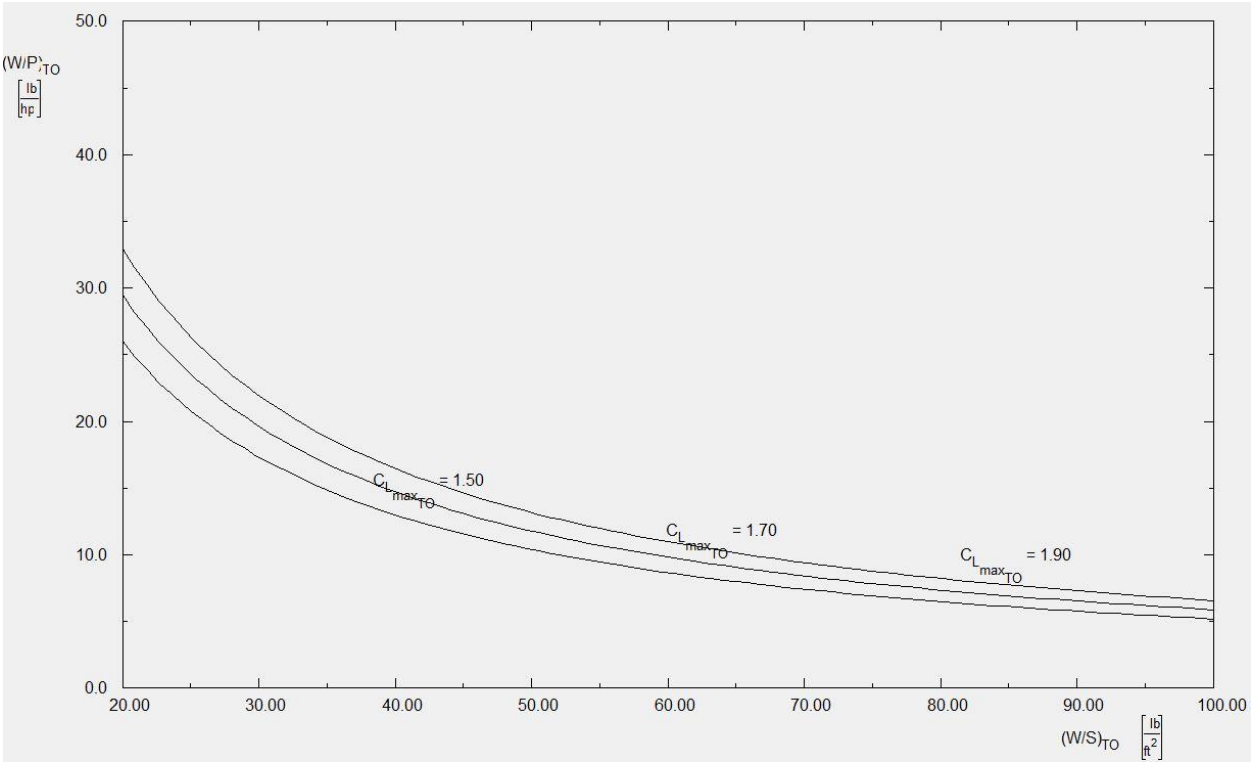

Figure 56: Graph of take-off distance requirement at different lift coefficient values

4.3.2 Landing Distance

The landing distance inputs are shown below where the maximum lift coefficient for landing is considered from Roskam and the calculated landing field length is perfectly matching with the mission requirement.

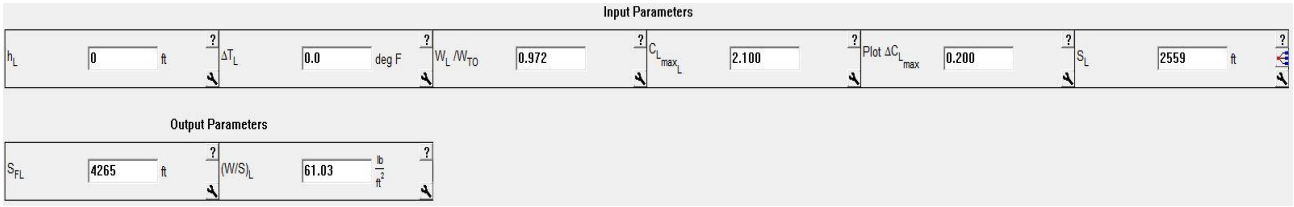

Figure 57: Inputs of landing distance in AAA program

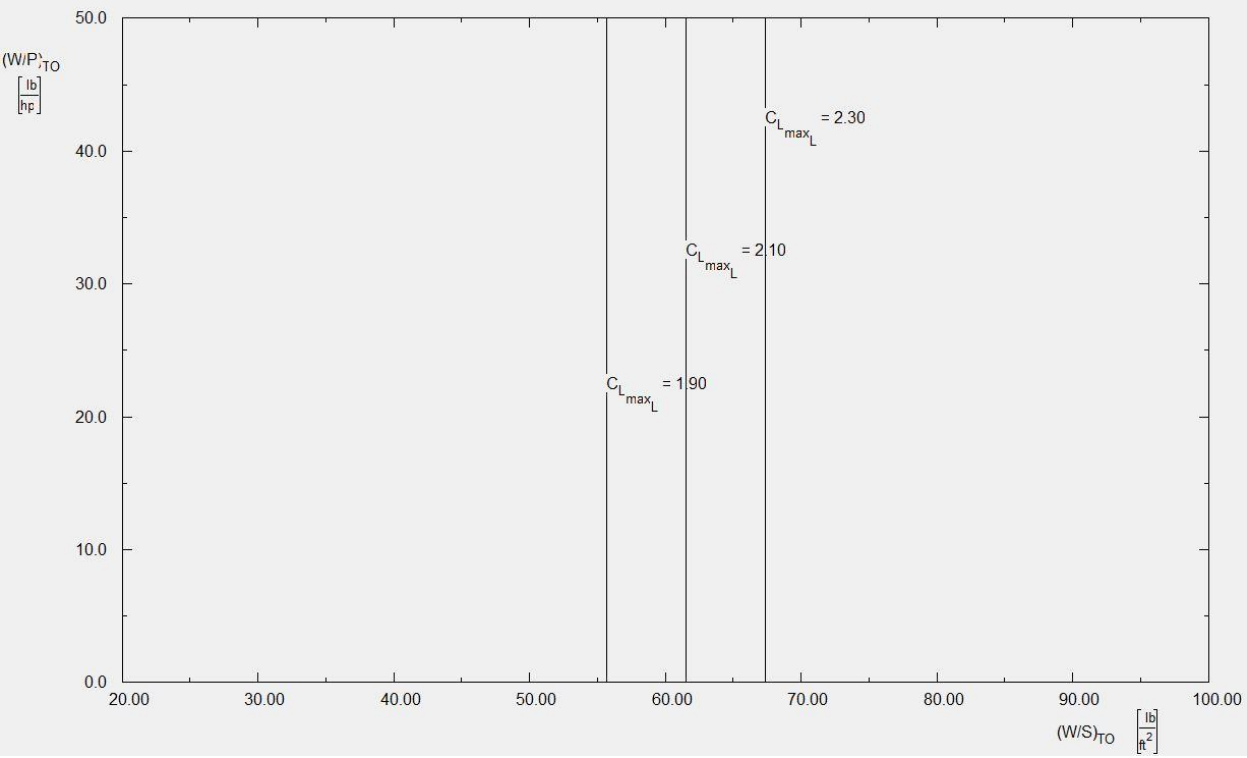

Figure 58: Graph of allowable wing loadings to meet a landing distance requirement in AAA program

4.3.3 Climb Constraints

The inputs of climb constraints in AAA program are given based on the obtained drag polar data for different climb configurations. The propeller efficiency is considered as 0.85 from the Roskam data (Roskam, 2005).

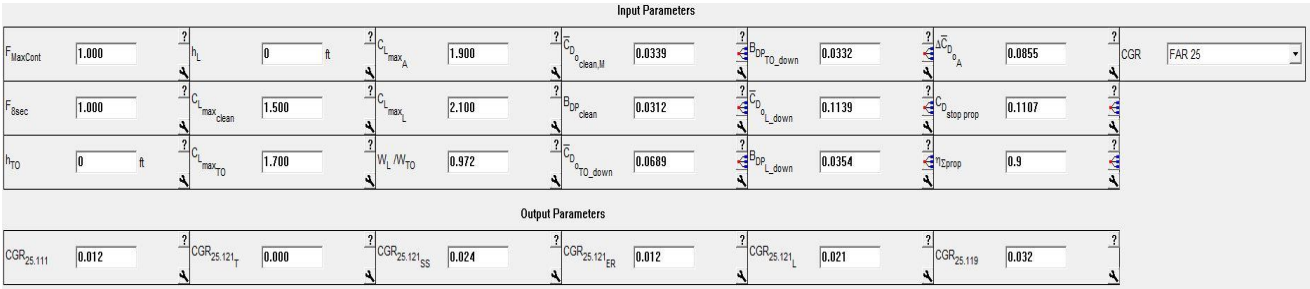

Figure 59: Inputs of climb constraints in AAA program

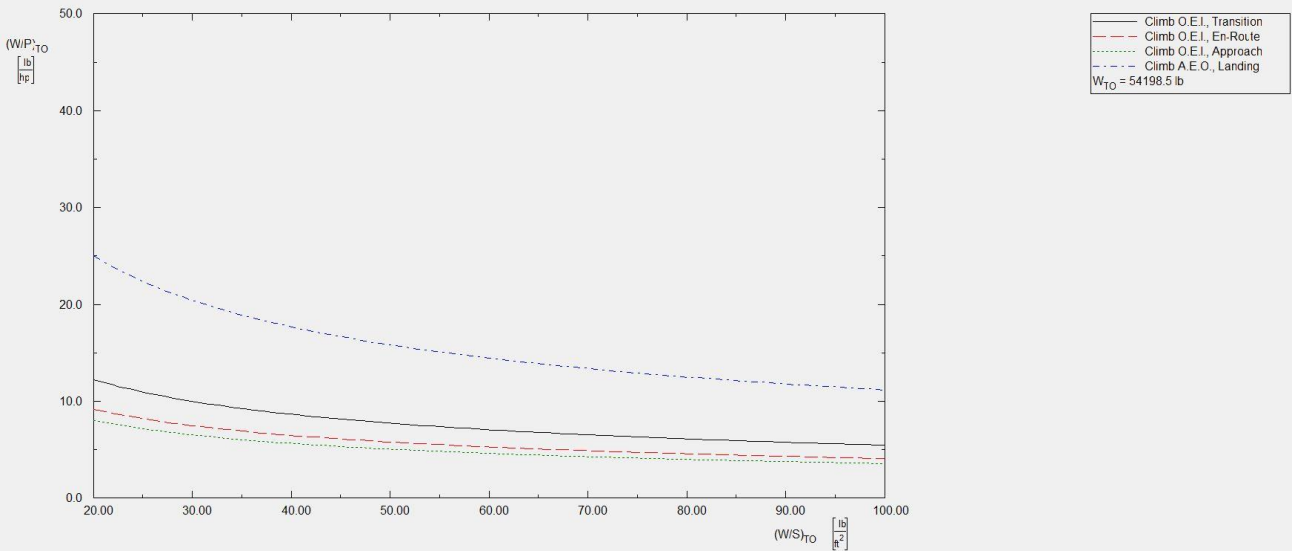

Figure 60: Graph of climb requirements in AAA program

4.3.4 Cruise Speed Constraint

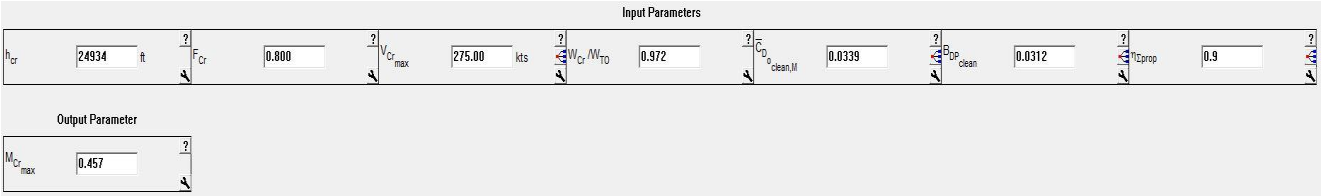

Figure 61: Inputs of cruise speed constraint in AAA program

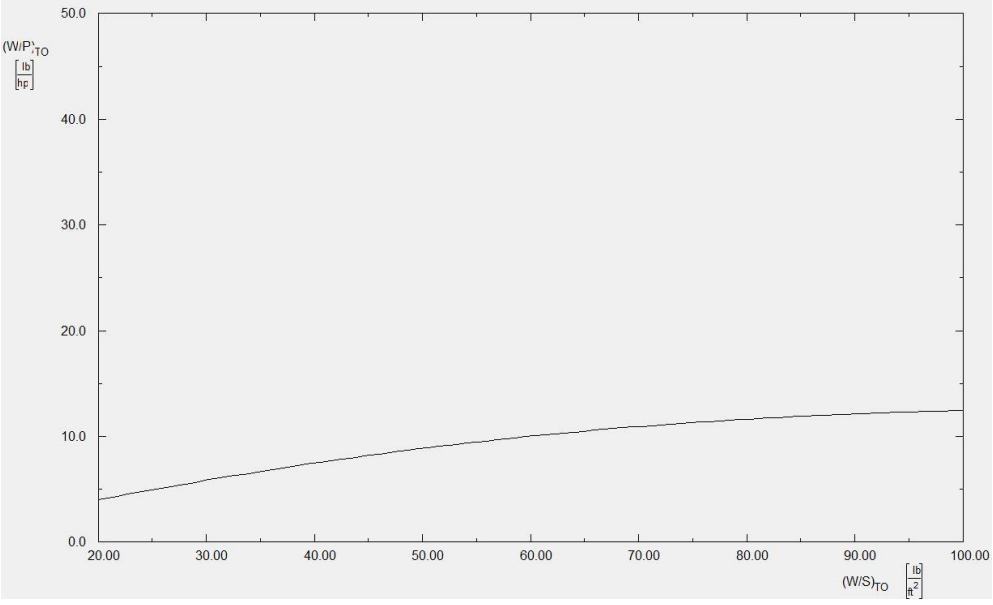

Figure 62: Graph of cruise speed requirement in AAA program

4.3.5 Summary of Performance Constraints

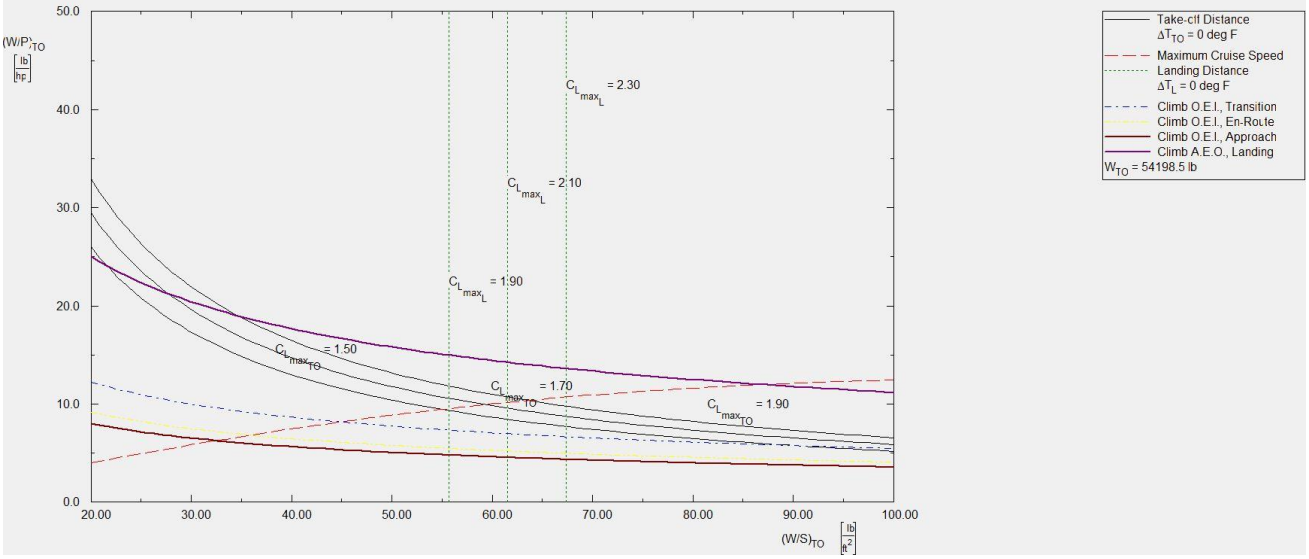

Figure 63: Performance constraints sizing graph in AAA program

The matching graph of all the performance constraints are plotted below using MATLAB programming attached in Appendix B.

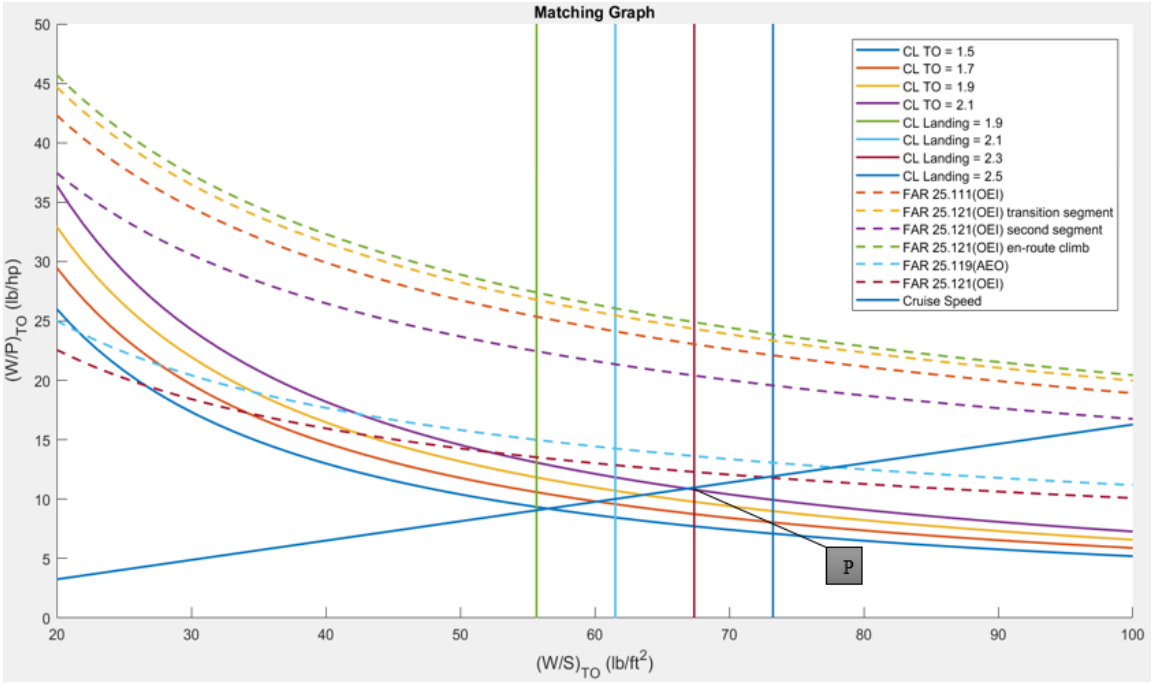

Figure 64: Performance sizing graph of manual calculation

The cleaned-up version of the above matching plot with one curve per constraint is as follows

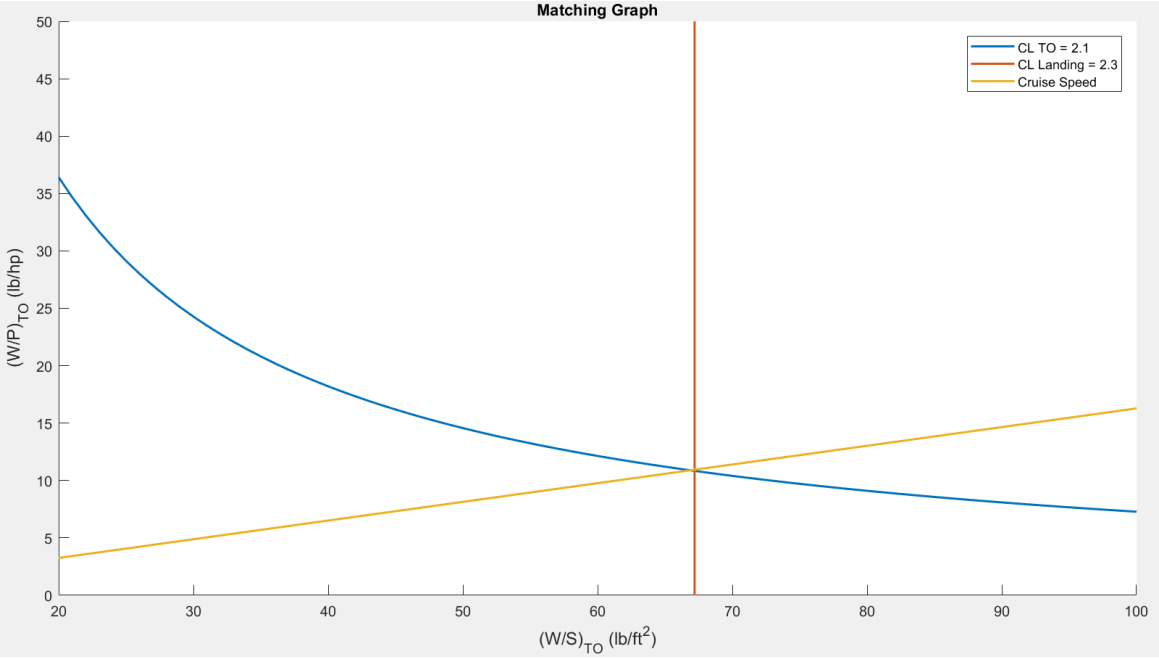

Figure 65: Cleaned-up version of matching plot

The design point is selected from the combination of the highest possible wing loading and the lowest possible power loading that still meets all the performance requirements results in an airplane with lowest weight and the lowest cost. From the above MATLAB plot the design point 'P' is considered at take-off wing loading of 67 psf and take-off power loading of 12 lbs/hp with take-off lift coefficient of 2.1 and landing lift coefficient of 2.3. With this choice, the hybrid design is now characterized by the following design parameters:

Take-off Weight: 54199 lbs

Empty Weight: 31926 lbs

Fuel Weight: 1891 lbs

The above weights are already obtained from weight sizing.

Maximum lift coefficients:

Clean: $C_{L_{max}} = 1.5$

Take-off: $C_{L_{max_{TO}}} = 2.1$

Landing: $C_{L_{max_L}} = 2.3$

Aspect Ratio: 12

Take-off wing loading: 67 psf

Wing area: 54199/67= 809 sq.ft

Take-off Power loading: 12 lbs/hp

Take-off Power: 54199/12= 4517 hp

4.4 SELECTION OF PROPULSION SYSTEM

The selection and integration of the propulsion system involves the following three decisions:

- Selection of the type of propulsion system
- Selection of number of engines to be used
- Integration of these engines into the aircraft configuration

4.4.1 Selection of Propulsion System Type

The selection of propulsion system type for the proposed design is based on the following factors (Roskam, 2005)

- Battery energy density
- Battery power density
- Required cruise speed
- Required maximum operating altitude
- Required Range
- Fuel amount needed
- Fuel cost
- Safety
- Reliability and Maintainability

The aircraft design is proposed for hybrid electric propulsion of regional turboprop in mission specifications. The reference conventional regional turboprop aircraft ATR 42-600 with similar mission uses Pratt and Whitney 127M engine. As the hybrid electric propulsion system is still under research and development in the market, the proposed design uses conceptual model of Pratt and Whitney 127M engine with parallel hybrid architecture. Even though the proposed

design uses hybrid propulsion system to reduce fuel consumption and emissions, it will fall under a family of conventional regional turboprop airplanes in terms of mission profile and number of passengers. NASA did a conceptual sizing of the hybrid propulsion system using PW 127E like engine and compared with current state of art as shown below (Anticliff, 2018).

	SOA	Advanced
η Diffuser	0.975	0.975
η LPC	0.86	0.88
η HPC	0.86	0.88
HPC-IGV Cooling (%)	5.0	0
HPC-HPT Cooling (%)	2.5	2.5
LPC-LPT Cooling (%)	3.5	3.5
η Burner	0.95	0.98
Burner Pressure Loss (%)	7.0	7.0
T4 (°R)	2860	2860
η HPT	0.85	0.88
η LPT	0.85	0.88
η PT	0.85	0.88
η Nozzle	0.975	0.985

Figure 66: Results of NASA numerical propulsion system simulation

As the NASA performed propulsion system sizing analysis close enough to the proposed engine of PW127M (Anticliff, 2018). Based on these results the selection of PW127M with parallel hybrid architecture is reasonable for the proposed aircraft. Note that the electric motor system is installed within the engine pods.

Mechanical Design Parameter	SOA Turboprop 2400 SHP	Advanced Turboprop 2400 SHP	Advanced Hybrid-Electric Turboprop Gas Turbine + Electric Motor		
			1800 + 600 SHP	1200 + 1200 SHP	600 + 1800 SHP
Turbine engine + Gearbox weight (lb)	1054	1010	819	626	410
Propeller system + Nacelle weight (lb)	782	781	766	752	737
Electrical system weight (lb)	-	-	135	270	405
Total engine weight (lb)	1836	1791	1720	1648	1552
Engine pod length (ft)	7.0	7.0	6.1	5.3	4.2
Maximum Propeller Diameter (ft)	12.8	12.8	12.8	12.8	12.8
Nacelle Diameter (ft)	3.3	3.3	3.3	3.3	3.3

Figure 67: Summary of NASA propulsion system sizing

4.4.2 Selection of Number of Engines

The selection of number of engines is based on the required take-off power and engine capacity. The takeoff power obtained from manual calculation of performance constraints as 4517 HP. From below figure Pratt and Whitney PW 127M engine (Pratt and Whitney, 2018) can produce power of 2750 HP, but the takeoff power required is 4517 HP. Hence, total two engines are required. Each engine can now produce 2259 HP to meet the takeoff power requirement.

	Thermodynamic Power Class* (ESHP***)	Mechanical Power Class* (SHP)	Propeller Speed (Max. RPM)	Height** (Inches)	Width** (Inches)	Length** (Inches)
PW150 Series	6,200	5,000	1,020	44	30	95
PW127 Series	3,200	2,750	1,200	33	26	84
PW123/124 Series	3,000	2,400	1,200	33	26	84
PW120 Series	2,400	2,100	1,200	31	25	84
PW118 Series	2,180	1,800	1,300	31	25	81

Figure 68: Pratt and Whitney engine specifications

4.4.3 Propeller Sizing

The proposed design uses twin engine turboprop for the hybrid-electric propulsion where the propeller sizing is dependent on maximum required power by each engine. As per Roskam, the propeller diameter can be determined by using the following equation

$$D_p = \sqrt{\frac{4P_{max}}{\pi n_p P_{bl}}} \qquad (4.27)$$

Where,

D_p = Propeller Diameter

P_{max}= Maximum power per engine

n_p= Number of propeller blades

P_{bl}= Power loading per blade

The number of blades is assumed to be 6 from reference aircraft data (ATR , 2014) and P_{max} obtained as 2259 HP for one engine. P_{bl} is assumed to be 5.0 from the below Roskam data (Roskam, 2005).

Therefore,

$$D_p = \sqrt{\frac{4 * 2259}{\pi * 6 * 5}} = 9.79 \text{ ft}$$

$$D_p = 9.79 \text{ ft}$$

Comparing to the reference aircraft ATR-42-600 propeller diameter of 13 ft, the calculated diameter of the propeller seems to be very less because we are assuming the power loading per blade. The database provided by Roskam below is only for ten airplanes. The assumption of power loading per blade seems to be unreasonable as compared to reference aircraft and hence, the diameter of the propeller for the proposed design is assumed to be 13 ft.

$$D_p = 13 \text{ ft}$$

Airplane Type	Prop. Pitch	Max. Power per Engine, P_{max}, hp	Prop. Diam., D_p, ft	Number of Prop. Blades, n_p,	Power Loading per Blade, P_{bl}, hp/ft^2
Twin Engine FAR23 Certified Airplanes					
PIPER					
PA-31 Navajo	C.Spd	325	6.7	3	3.1
PA-31T Chey. II	C.Spd	620	7.8	3	4.3
CESSNA					
T303	C.Spd	250	6.2	3	2.8
340A	C.Spd	310	6.4	3	3.2
Conquest I	C.Spd	450	7.8	3	3.1
Conquest II	C.Spd	636	7.5	3	4.8
BEECH					
Baron 95-B55	C.Spd	260	6.5	2	3.9
Duke B60	C.Spd	380	6.2	3	4.2
King Air C90-1	C.Spd	550	7.8	3	3.8
BN2B Islander	C.Spd	260	6.5	2	3.9
				P_{bl} range:	2.8-4.8
Regional Turbopropeller Driven Airplanes					
EMB-110 Bandar.	C.Spd	750	7.8	3	5.2
EMB-120 Brasil.	C.Spd	1,500	10.5	4	4.3
SF-340	C.Spd	1,630	10.5	4	4.7
Fokker F27-200	C.Spd	2,140	11.5	4	5.2
Brit.Aer. 748	C.Spd	2,280	12.0	4	5.0
Casa Nurt. 235	C.Spd	1,700	10.8	4	4.6
Beech C99	C.Spd	715	7.8	3	5.0
Beech 1900	C.Spd	1,100	9.1	4	4.2
ATR-42	C.Spd	1,800	13.0	4	3.4
IAI Arava 201	C.Spd	750	8.5	3	4.4
				P_{bl} range:	3.4-5.2

Note: $P_{bl} = 4P_{max}/\pi n_p D_p^2$

Figure 69: Relation between different parameters of propeller for regional turboprop airplanes

4.5 DISCUSSION

The performance constraints obtained manually are reasonable when compared to the reference aircraft (ATR , 2014). The performance constraints calculated manually and by using AAA program are closely matching for take-off distance and landing distance. The cruise speed and climb requirements are slightly varying from AAA program as the AAA does not account for hybrid. The design point was chosen based on the best possible way to meet the FAR 25 requirements. The critical performance constraints are take-off distance, landing distance and cruise speed for the proposed design so, the matching point which fulfills all the three requirements is selected as design point. The maximum lift coefficients obtained for clean, take-off and landing as 1.5, 2.1 and 2.3 which are within the range of specified values in Roskam.

The take-off wing loading obtained for the proposed design is 67 psf whereas comparable aircraft have a range of wing loadings from 60 to 80 psf. The wing loading of 67 psf gives a wing area of 809 sq.ft which is quite reasonable when compared to the reference aircraft (ATR , 2014). The take-off power loading obtained for the proposed design is 12 lbs/hp which gives a take-off power of 4517 HP. Each engine now must provide a take-off power of 2259 HP. This take-off power is reasonable for carrying 40 passengers with take-off weight of 54199 lbs. Based on these obtained performance parameters, the type of propulsion system was chosen as Pratt and Whitney 127M engine with hybrid architecture. The number of engines required to produce a take-off power of 4517 HP are two where each engine provides take-off power of 2259 HP.

4.6 CONCLUSIONS AND RECOMMENDATIONS

4.6.1 Conclusions

The performance constraints calculations obtained for the proposed design are reasonable as compared to reference aircraft database. The most critical parameters are take-off and landing distance for the proposed design for the selection of design point. The required take-off power can be achieved by the proposed propulsion system.

4.6.2 Recommendations

The proposed design requires a hybrid engine for hybrid-electric propulsion and the hybrid engines are still under research in the market so, a further study is required to select a better hybrid engine. The critical performance constraints like take-off distance and landing distance are dependent on the maximum lift coefficients hence, a further study is required on different airfoils which may provide a better lift.

CHAPTER 5: FUSELAGE DESIGN

5.1 INTRODUCTION

The preliminary estimates of mission weights and performance constraints are obtained in previous chapters. This chapter presents a design of fuselage using the mission requirements. The following factors are considered for the design of fuselage.

- Payload Capacity
- Maximum Take-off Weight
- Wing Placement
- Engine Placement
- Landing Gear Location
- Fuel Storage

The preliminary and scaled drawings of cockpit and fuselage layouts are presented using the guidelines provided by Roskam (Roskam, 2005). The realistic cockpit layout is generated based on the visibility, human factors in terms of control and instrument placement and crew seats. The fuselage layout is generated based on the effect of fuselage shape on drag, window and exit placement, passenger seating arrangements, loading, unloading and servicing.

5.2 LAYOUT DESIGN OF THE COCKPIT

The cockpit layout is designed based on the following considerations (Roskam, 2005)

- The pilots and other crew members must be positioned so that they can reach all controls comfortable, from some reference position.
- The pilots and other crew members must be able to see all flight essential instruments without undue effort.
- Communication by voice or by touch must be possible without undue effort.
- Visibility from the cockpit must adhere to certain minimum standards.

Dimensions and Weights for Crew Members

The layout design of the cockpit depends on the dimensions and weights for the crew members. The proposed design assumes two male crew members as the female crew member dimensions are

less than the male crew member. The proposed design uses a wheel control system. The weight of the crew member is considered as 175 lbs without helmet. The body widths are specified as below

- Body width across shoulders: 533 mm
- Body width across hips: 457 mm
- Body width across elbows: 561 mm

The below figures show the male crew member dimensions in standing position. The below figure from Roskam specifies the dimensions of the male crew member. For female crew member all the weight and dimension data must be multiplied by 0.85.

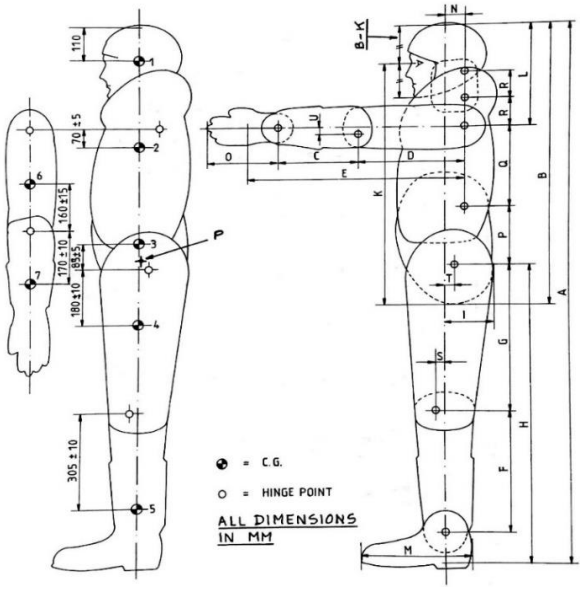

Figure 70: Dimensions of male crew member in standing position

A	B	C	D	E	F	G	H	I	K	L
1,600	870	230	300	620	350	435	850	140	760	300
1,750	920	255	335	685	390	475	950	150	805	330
1,900	990	280	370	750	430	515	1,050	160	875	360

A	M	N	O	P	Q	R	S	T	U
1,600	300	50	200	190	260	80	25	20	20
1,750	325	60	220	200	270	90	30	30	20
1,900	350	70	240	210	280	100	30	30	20

Figure 71: Dimensions of the male crew member

The dimensions of male crew member in sitting position for wheel type controllers are provided in below figures based on the Roskam data.

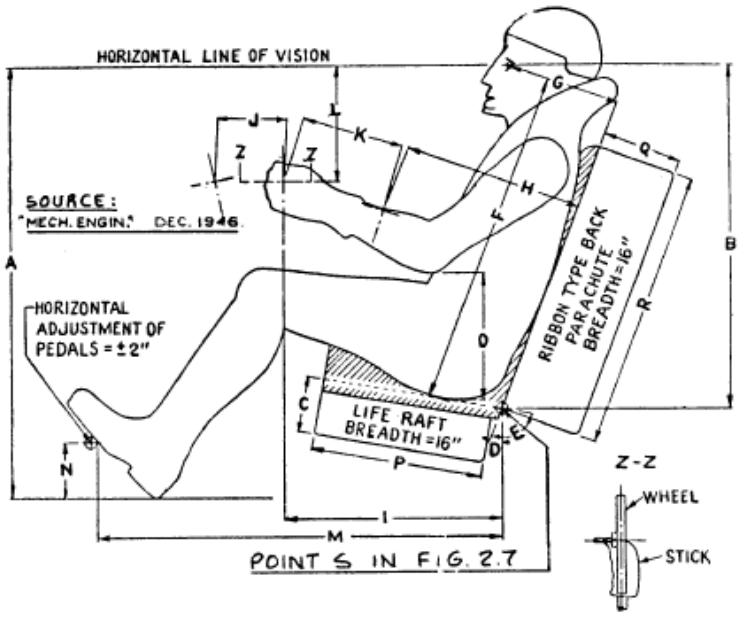

Figure 72: Dimensions of male crew member in sitting position

For Wheel Type Controllers:

A	B	C	D deg.	E deg.	F	G	H	I	J	K
37	30.25	5	21	101	29.75	10.00	16.63	19	6	9
39	30.75	5	19	101	30.25	9.75	15.75	19	6	9
41	31.50	5	16	101	31.00	9.75	15.13	19	6	9
43	31.75	5	16	101	31.25	10.00	15.13	19	6	9

A	L	M	N	O	P	Q	R
37	10.00	36.0	5	9.25	15	7	25
39	10.50	35.0	5	9.25	15	7	25
41	10.75	34.5	5	9.25	15	7	25
43	11.00	34.5	5	9.25	15	7	25

Figure 73: Dimensions of male crew member

Layout of Cockpit Seating and Cockpit Controls

The proposed design is a civil aircraft which has a civil cockpit layout. The cockpit layout accounts for dimensional limitation of human body. The dimensional variations are accomplished by arranging for seat position adjustments. The below figures show the recommended seat

arrangement for civil aircraft with wheel and center-stick controlled airplanes from Roskam. The dimensions specified in Figure 75 are based on the Figure 74 symbols with all the linear dimensions are in cm and all angular dimensions are in degrees.

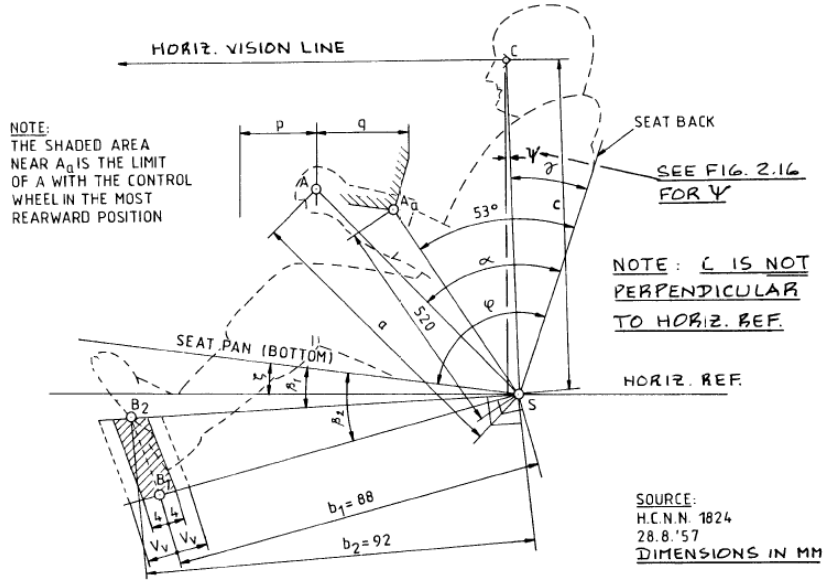

Figure 74: Typical seat arrangement for civil airplanes with wheel and center-stick controlled system

Symbol	Wheel Control	Stick Control
a	67 (+/- 4)	63 (+/- 4)
ξ	7° (+/- 2°)	7° (+/- 2°)
p = Forward motion of point A:	18 (+/- 2)	16 (+/- 2)
q = Rearward motion of point A:	22 (+/- 2)	20 (+/- 2)
r = Sidewise motion of point A from center*:	-----	15 (+/- 2)
d = Distance between handgrips of wheel*:	38 (+/- 5)	-----
ε = Wheel rotation from center*:	85° (max.)	-----
v = Distance between rudder pedal center lines*:	38 (+/- 12)	45 (+/- 5)
α	64° (+/- 3°)	70° (+/- 3°)
β_1	22°	same
β_2	10°	same
c	77 (+/- 2)	same
γ	21° (+/- 1°)	same
φ	102° (+/- 2°)	same
V_v = Adjustment range of pedals from center position B:	7 (+/- 2)	same
U_v = Forward and aft pedal motion from center position B*:	10 (+/- 2)	same
S_h = Horizontal adjustment range of S from center position*:	< 10	same
S_v = Vertical adjustment range of S from center position*:	8 (+/- 1)	same

Figure 75: Dimensions for civil cockpit controls and for seat adjustments

Determination of Visibility from the Cockpit

The cockpit visibility is quite important to observe obstructions and conflicting traffic. The cockpit visibility is defined as the angular area obtained by intersecting the airplane cockpit with radial vectors emanating from the eyes of the pilot. These radial vectors are assumed to be centered on the pilot's head. The cockpit with good visibility is essential for the following reasons:

- A pilot must have good visibility of the immediate surroundings during take-off and landing operations.
- During en-route operations the pilot must be able to observe the conflicting traffic.

Even though the pilots see through both the eyes, it is customary to construct the visibility pattern by assuming the point C is center of the vision as shown in below figure.

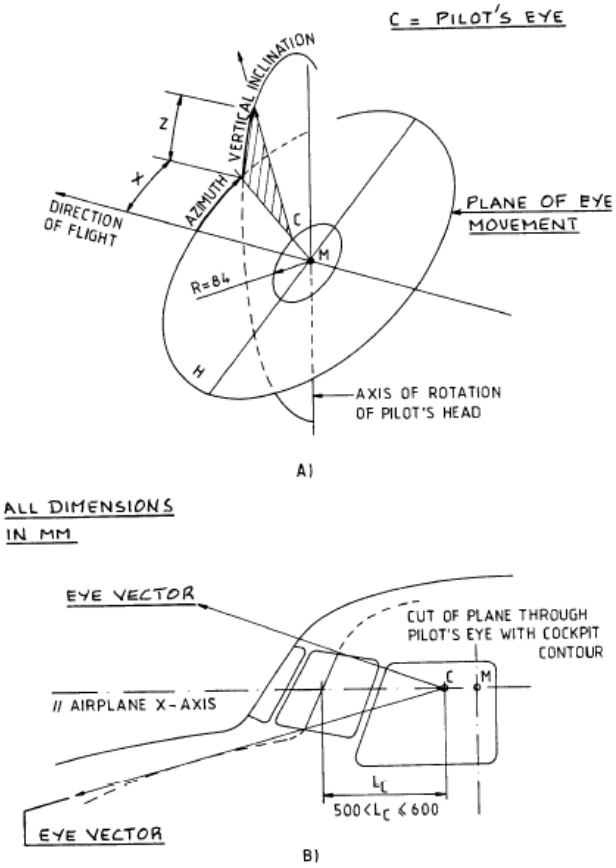

Figure 76: Radial eye vectors definition

The process of laying out a cockpit for acceptable visibility is broken down into the following steps:

- Point C needs to be located on the horizontal vision axis.
- The distance labelled L_C in above figure should be within the indicated range.
- Draw the angle ψ as 8.75 degrees
- With the help of the distance ‘c’, locate point S. The maximum allowable value of c is 80 cm.
- Orient the pilot seat in accordance with the dimensions.
- Draw in the areas required for seat motions, adjustments and cockpit control.
- The minimum required visibility needs to be checked with the visibility rules.

There shall be no obstructing window frames in the area from 30-degree starboard and 20-degree port with side by side pilot seating in transport airplanes. The window frames may not be wider than 2.5 inches in the area from 20-degree port to 60-degree port.

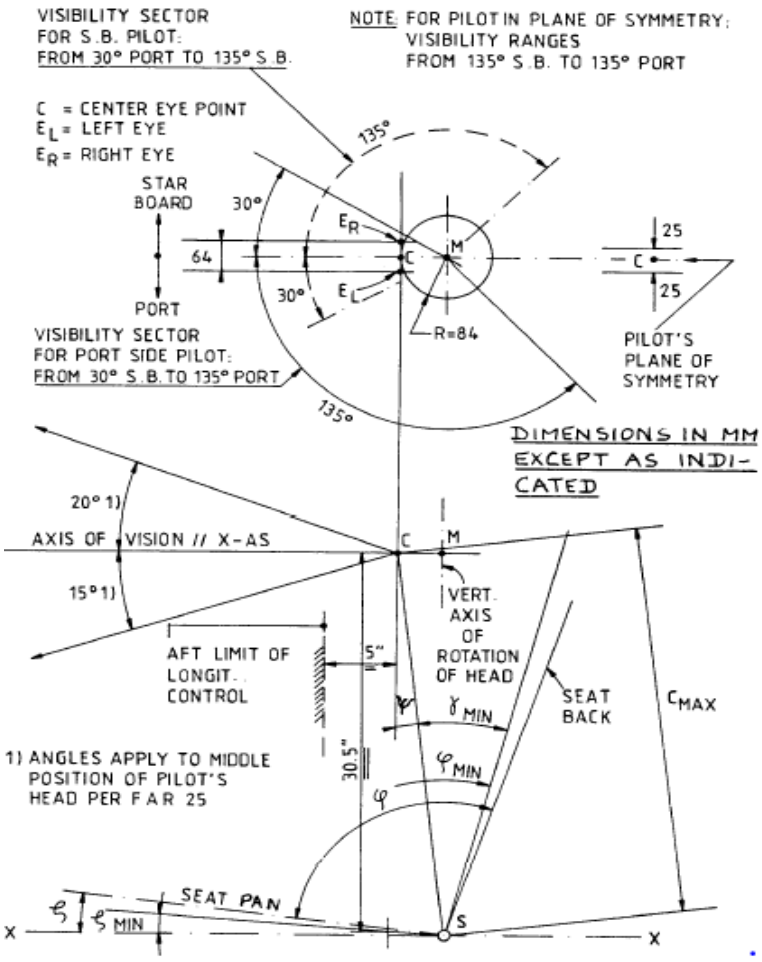

Figure 77: Visibility requirements for the port and for the starboard side and the connection with acceptable seat arrangements

The proposed aircraft layout design of the cockpit is considered same as the reference aircraft (ATR , 2014) as shown below.

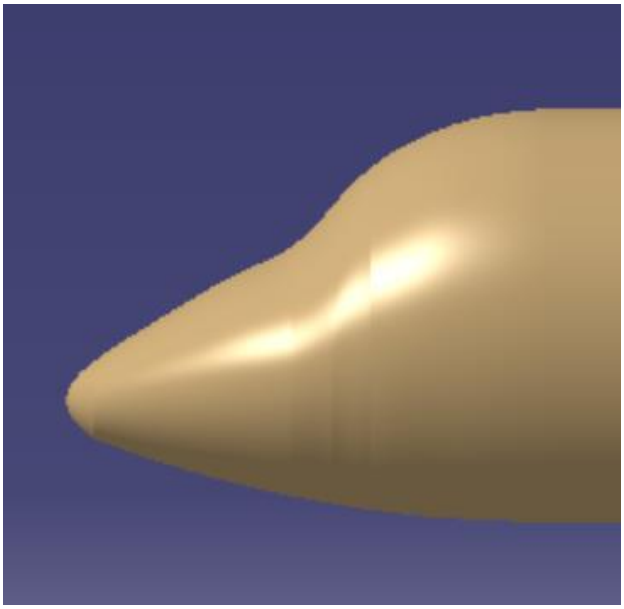

Figure 78: Front view of the cockpit

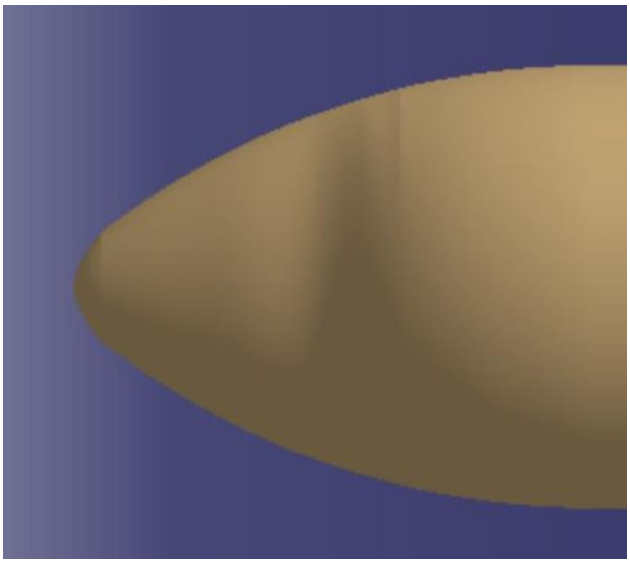

Figure 79: Top view of the cockpit

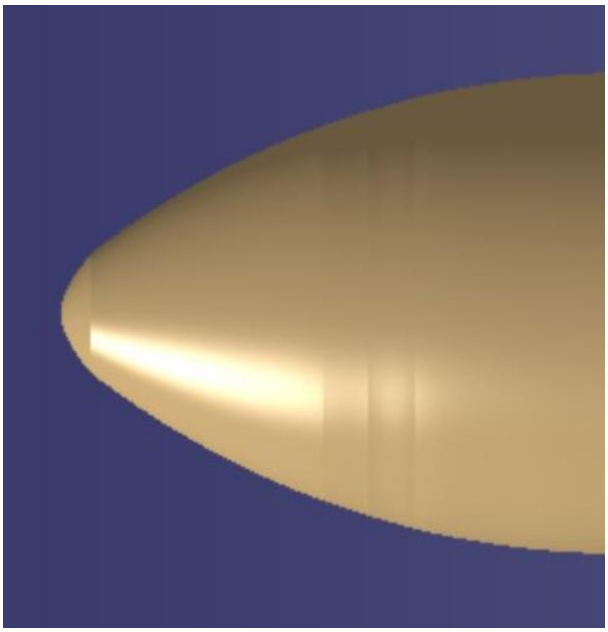

Figure 80: Bottom view of the cockpit

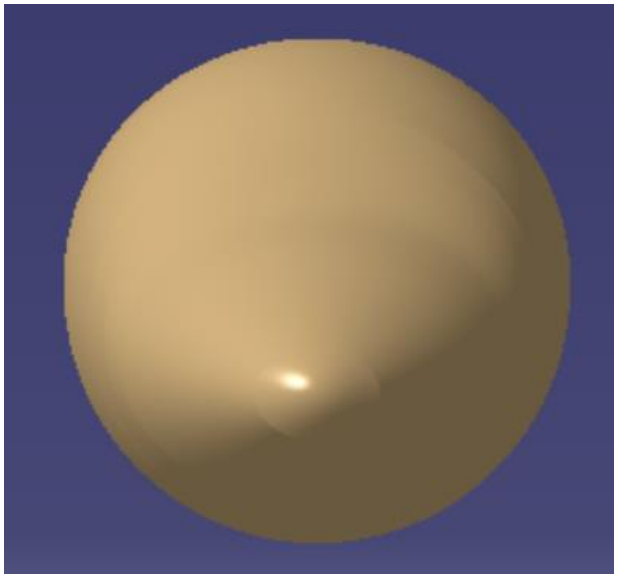

Figure 81: Left side view of the cockpit

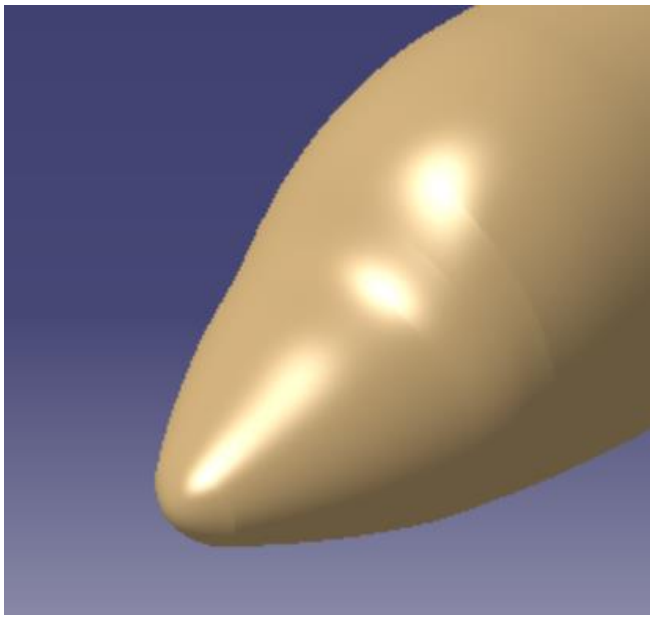

Figure 82: Isometric view of the cockpit

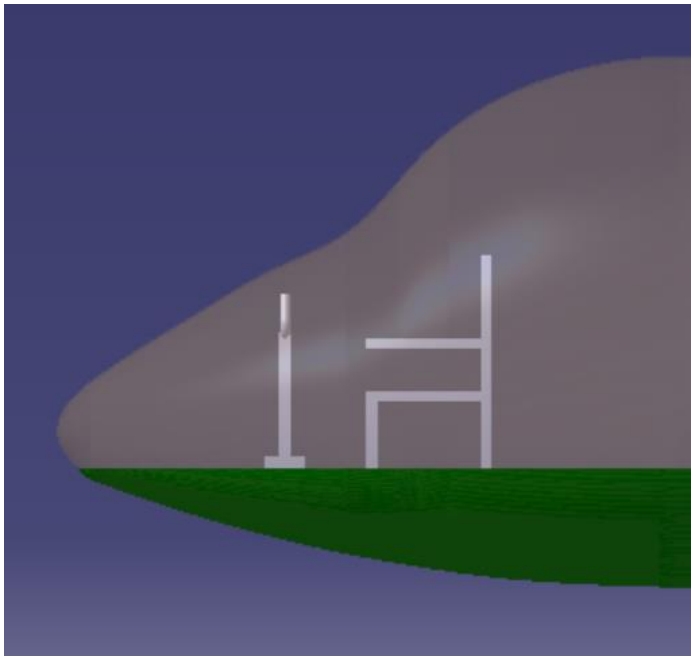

Figure 83: Front view of interior layout of the cockpit

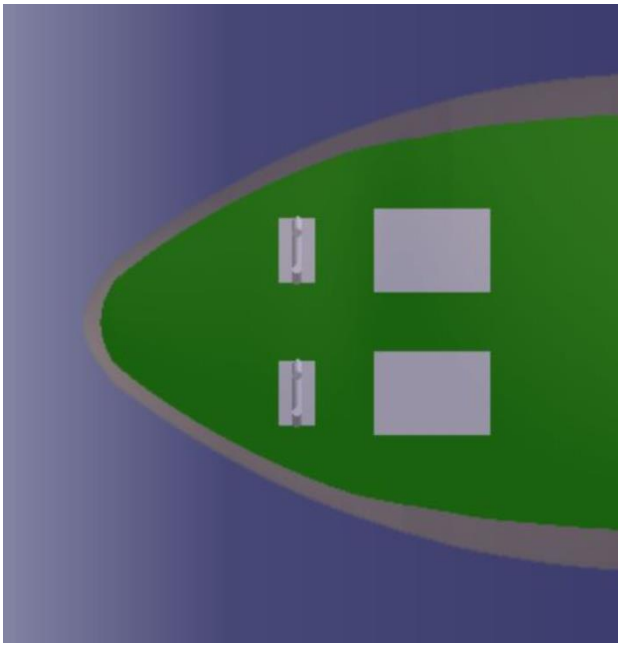

Figure 84: Top view of interior layout of the cockpit

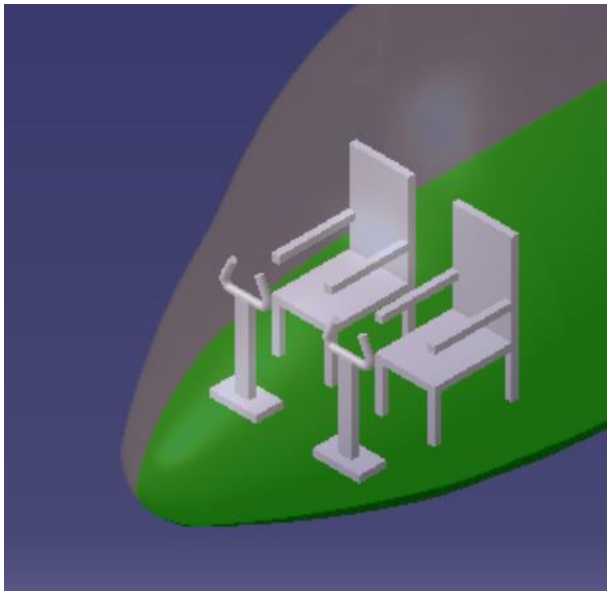

Figure 85: Isometric view of the cockpit

5.3 LAYOUT DESIGN OF THE FUSELAGE

The proposed aircraft uses a fuselage layout design similar to the reference regional aircraft (ATR , 2014). The below figure shows important geometric parameters for the fuselage.

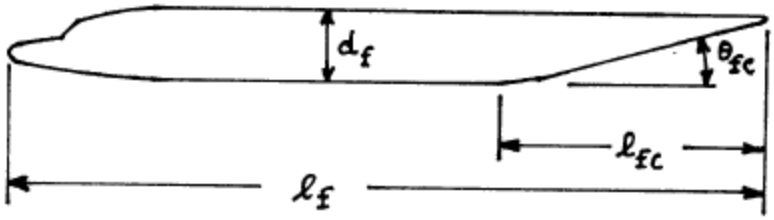

Figure 86: Definition of geometric fuselage parameters

The below figure shows the range of values of the above geometric parameters for different airplanes.

Airplane Type	l_f/d_f	l_{fc}/d_f	θ_{fc} (deg)
Homebuilts	4 - 8	3*	2 - 9
Single Engine	5 - 8	3 - 4	3 - 9
Twins	3.6** - 8	2.6 - 4	6 - 13
Agricultural	5 - 8	3 - 4	1 - 7
Business Jets	7 - 9.5	2.5 - 5	6 - 11
Regionals	5.6 - 10	2 - 4	15 - 19***
Jet Transports	6.8 - 11.5	2.6 - 4	11 - 16
Mil. Trainers	5.4 - 7.5	3*	up to 14
Fighters	7 - 11	3 - 5*	0 - 8
Mil. Transports, Bombers and Patrol Airplanes	6 - 13	2.5 - 6	7 - 25****
Flying Boats	6 - 11	3 - 6	8 - 14
Supersonics	12 - 25	6 - 8	2 - 9

Figure 87: Geometric fuselage parameters currently employed for different airplanes

The length of the fuselage can be calculated from the following equation as shown in below figure (Raymer, 2012). The take-off weight obtained in weight sizing is 54199 lbs and for the transport aircraft a and C are considered as 0.67 and 0.43.

Length of the Fuselage = aW_{TO}^{C} = 0.67*$54199^{0.43}$ = 72.7ft or 22.2 m

Length = aW_F^C	a	C
Sailplane—unpowered	0.86	0.48
Sailplane—powered	0.71	0.48
Homebuilt—metal/wood	3.68	0.23
Homebuilt—composite	3.50	0.23
General aviation—single engine	4.37	0.23
General aviation—twin engine	0.86	0.42
Agricultural aircraft	4.04	0.23
Twin turboprop	0.37	0.51
Flying boat	1.05	0.40
Jet trainer	0.79	0.41
Jet fighter	0.93	0.39
Military cargo/bomber	0.23	0.50
Jet transport	0.67	0.43

Figure 88: Length of the fuselage with respect to maximum take-off weight for different airplanes

Aerodynamic Drag Considerations

The sizing of the fuselage depends on the aerodynamic drag considerations. A large percentage of the overall drag is produced by the fuselage. The fuselage should be sized and shaped with minimum drag. The following types of drag are generated by fuselage:

- Friction Drag
- Profile Drag
- Base Drag
- Compressibility Drag
- Induced Drag

The wetted area is directly related to the length of the and perimeter of the fuselage and the friction drag is directly proportional to wetted area. The friction drag can be minimized by using the below options:

- Shape the fuselage so that laminar flow is possible
- Reduce the perimeter and length as much as possible

Profile and base drag are a function of front and aft fuselage body shape where blunt aft bodies and front bodies increase the flow separations which lead to raise in profile and base drag. Fore-body bluntness is caused by

- Poor Cockpit Window or Canopy Shaping
- Requirement for front end loading

So, by improving the canopy shaping fore-body the profile and base drag can be reduced. Compressibility drag occurs for very high subsonic Mach numbers of fuselage alone. It does not affect until the fuselage experiences very high subsonic Mach numbers. Generally, the compressibility drag comes from the presence of shocks on the fuselage. As the proposed design fly at low Mach number so, there are no compressibility drag effects. The fuselage contributes to induced drag primarily because of its adverse effect on wing span load distribution.

Fuselage Layout Design

The length of the fuselage obtained as 72.7 ft and the inner diameter of the fuselage is assumed as 8.43 ft from the reference aircraft. The rear fuselage angle is considered as 18 degrees as per the Roskam data (Roskam, 2005). The below table clearly indicates the fineness ratio is within the range of the Roskam data (Roskam, 2005). Based on the aerodynamic drag considerations and definition of fuselage geometric parameters given by Roskam, the proposed design fuselage layout is shown below with the following dimensions.

Table 25: Fuselage dimensions

Fuselage Parameter	**Dimension**
Length of the Fuselage, l_f	72.7 ft or 22.2 m
Inner Diameter of the Fuselage, d_f	8.43 ft or 2.57 m
Rear Fuselage Angle, θ_{fc}	18 degrees
Fuselage Fineness Ratio, $\frac{l_f}{d_f}$	8.63

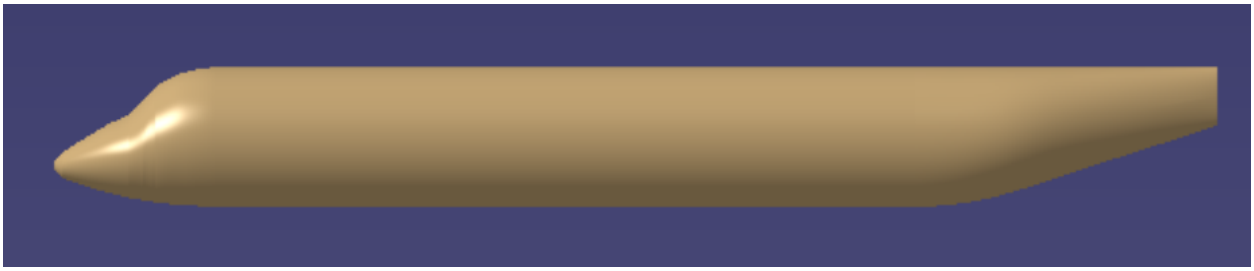

Figure 89: Front view of the fuselage

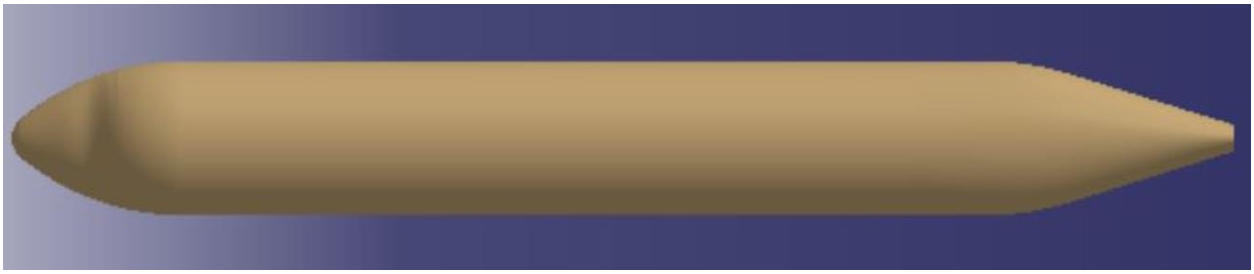

Figure 90: Top view of the fuselage

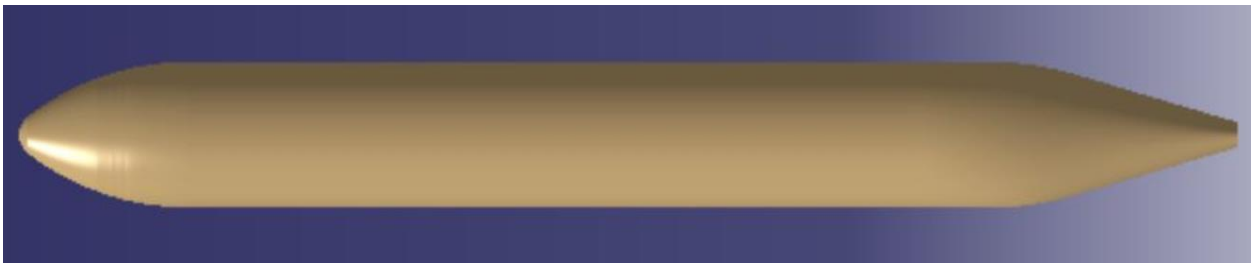

Figure 91: Bottom view of the fuselage

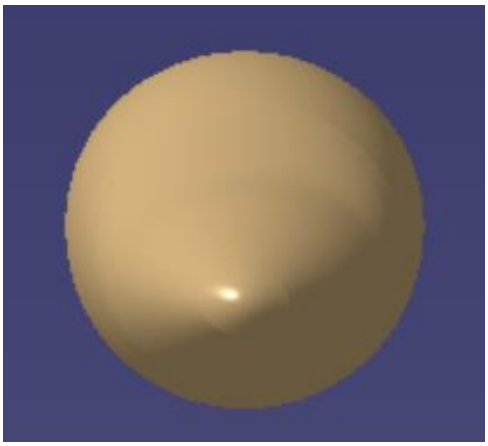

Figure 92: Left side view of the fuselage

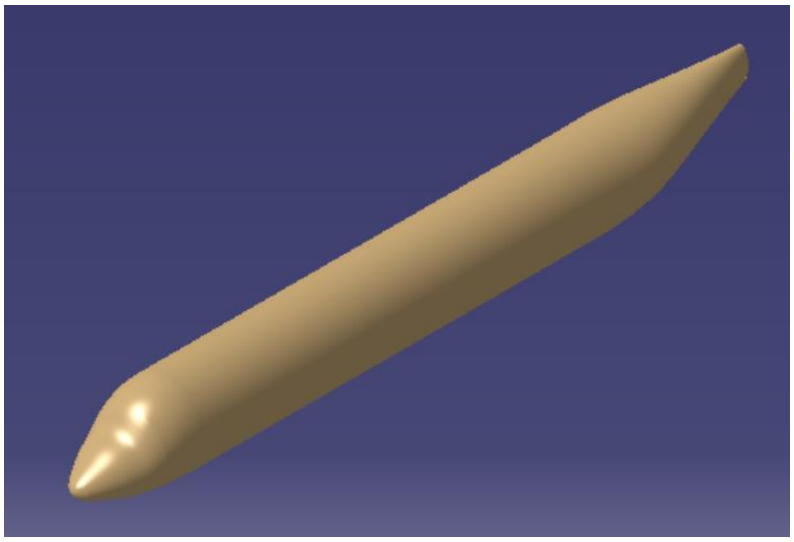

Figure 93: Isometric view of the fuselage

Interior Layout Design of the Fuselage

The interior layout design of the fuselage and the seat arrangement for the proposed design is considered same as the reference aircraft with seat pitch of 30 inches or 2.5 ft as shown below. The passenger access door is located on the port side and servicing access doors are located on the starboard side. For the airplane carrying less than 80 passengers, one passenger access door is normally enough. The passenger door size is considered as 50.9 x 62.8 inches or 4.2 x 5.2 ft from the reference aircraft (ATR , 2014). The attendant seat, galley, toilet, baggage and emergency exit locations are considered same as the reference aircraft.

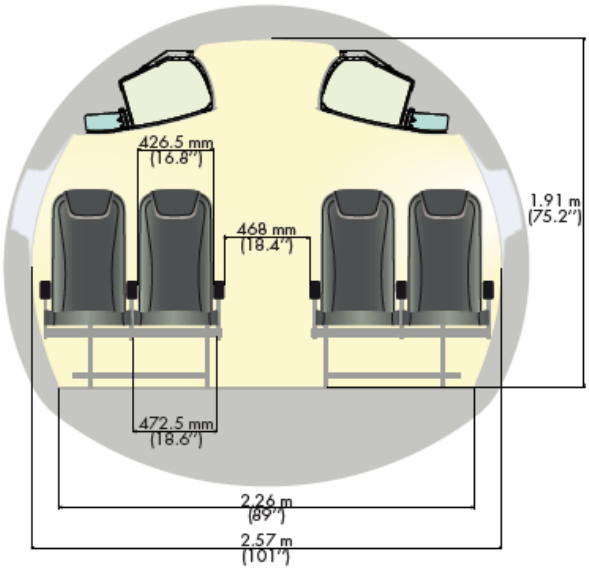

Figure 94: Cross-section of fuselage interior

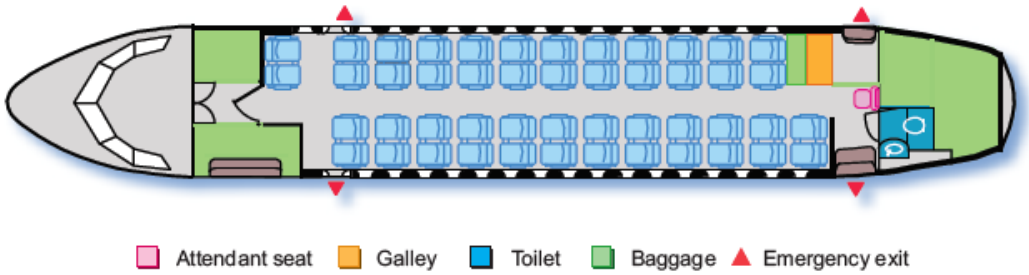

Figure 95: Interior layout of the fuselage

The proposed aircraft interior layout design of the fuselage with respect to the assumed reference aircraft data is shown below using CATIA V5 CAD software.

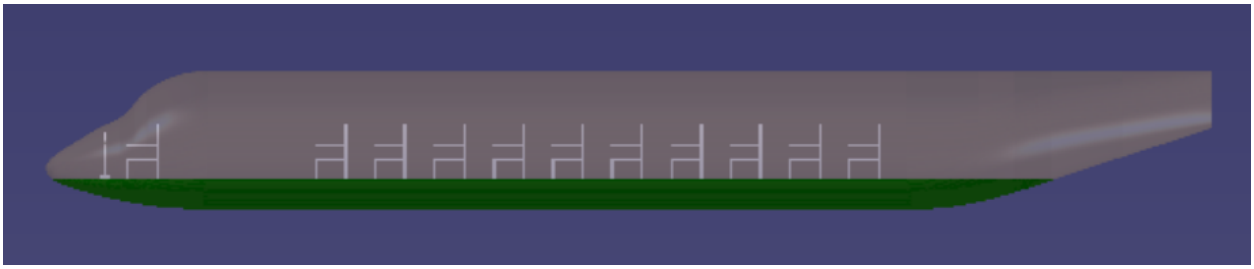

Figure 96: Front view of interior layout of the fuselage

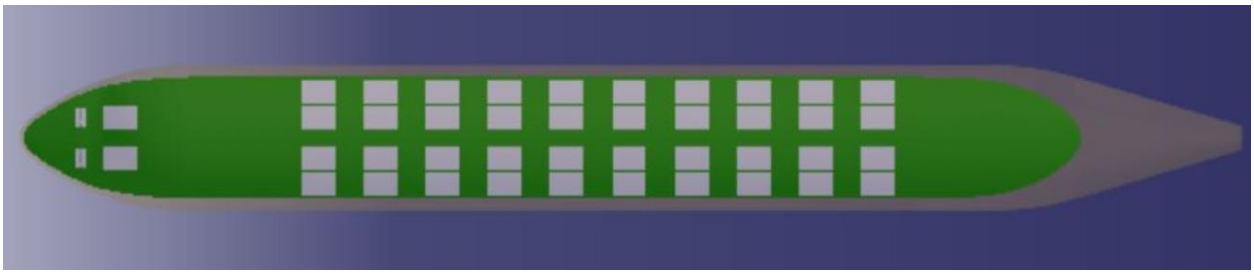

Figure 97: Top view of interior layout of the fuselage

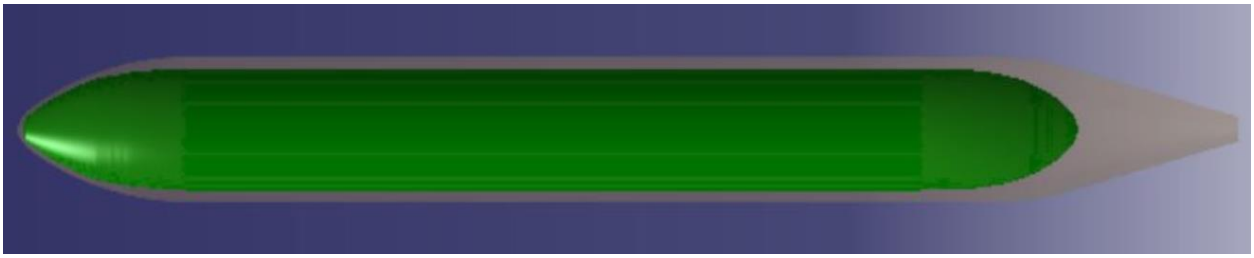

Figure 98: Bottom view of interior layout of the fuselage

Figure 99: Side view of interior layout of the fuselage

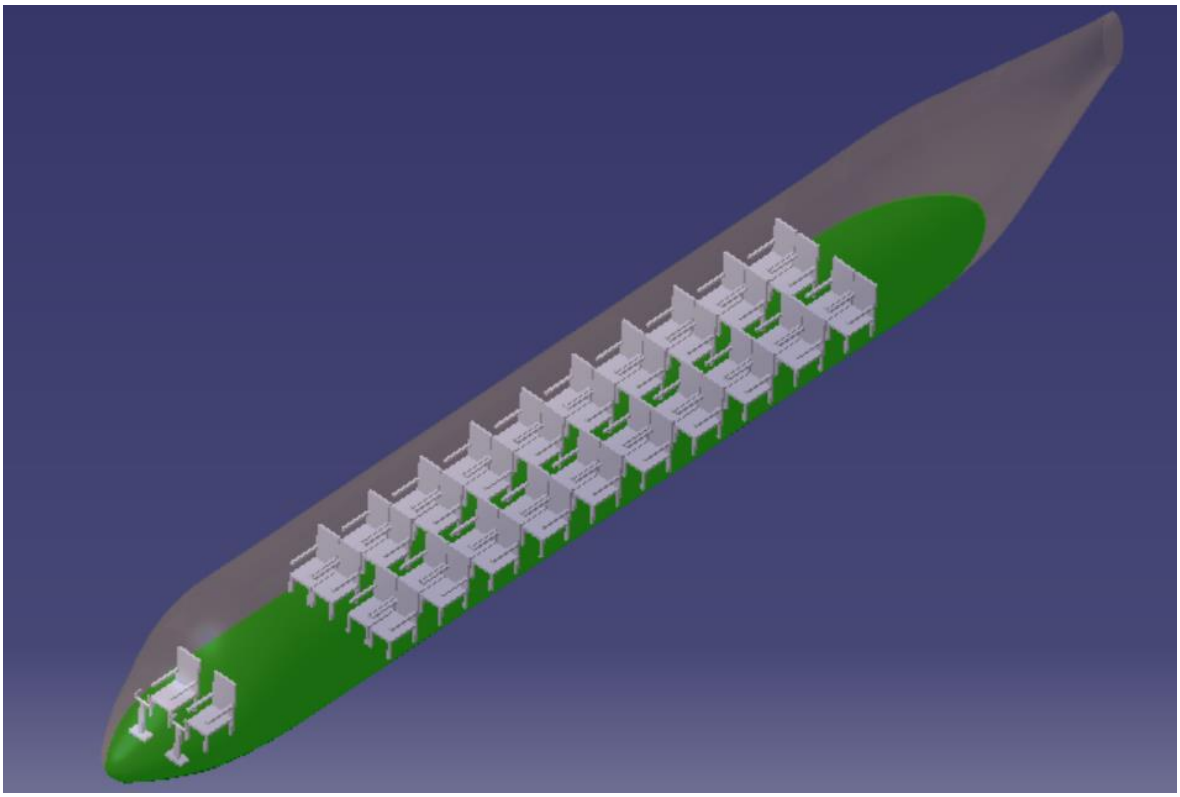

Figure 100: Isometric view of interior layout of the fuselage

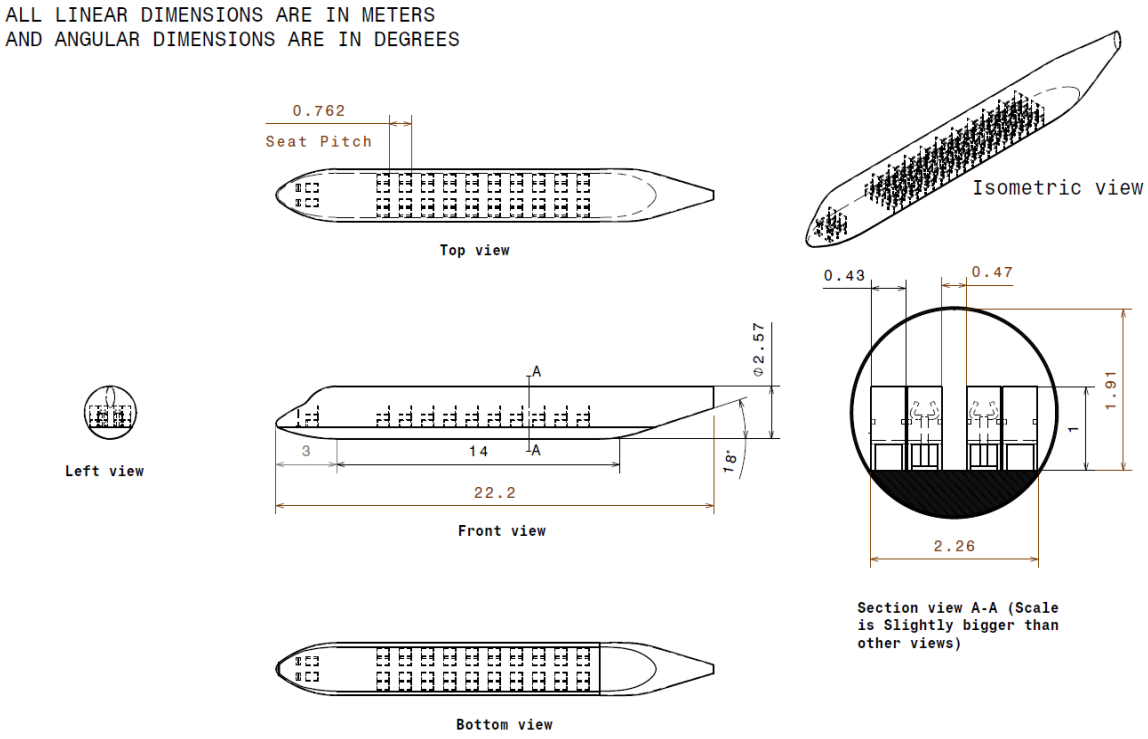

Figure 101: Drawing of the fuselage layout

5.4 DISCUSSION

This chapter presented a detailed approach for layout design of the cockpit and the fuselage of the proposed aircraft. The fuselage length is calculated using Raymer's Equation. The diameter of the fuselage is assumed from the reference aircraft. The calculated fineness ratio is within the given range of values by Roskam. The layout design of the cockpit and fuselage are considered based on the reference aircraft data. The reference aircraft ATR 42-600 fuselage length is 74.5 ft with 48 passengers and the proposed aircraft calculated fuselage length is 72.7 ft with 40 passengers which seems to be reasonable in comparison. The interior layout design of the fuselage is selected same as the reference aircraft for the proposed design. The seat arrangement and sizing are selected same as the ATR-42-600 aircraft. There is only one passenger access door for the proposed aircraft as it carries only 40 passengers. The layout design of cockpit and fuselage of the proposed aircraft are shown using CATIA V5 (Computer Aided Three-Dimensional Interactive Application Version 5) CAD software. The complete design of proposed aircraft till date is shown in fuselage section.

CHAPTER 6: WING, HIGH-LIFT SYSTEM AND LATERAL CONTROL DESIGN

6.1 INTRODUCTION

This chapter presents a wing planform design with required lateral control surface and high lift devices based on the obtained weight sizing, performance sizing and configuration selection. This chapter presents a detailed methodology for calculating the following characteristics of wing planform design (Roskam, 2005).

- Sweep Angle
- Dihedral Angle
- Incidence Angle
- Twist Angle
- Type of Airfoil
- Taper Ratio
- Thickness Ratio
- Lateral Control Surface Layout

The wing area of 809 sq.ft and aspect ratio of 12 are obtained in performance sizing chapter. The overall configuration selected as conventional with cantilevered high wing in configuration design chapter. The obtained parameters in previous chapters are used for determining the wing geometry parameters. The wing sizing is determined based on the performance required by the proposed design. The type of airfoil is selected based on the thickness to chord ratio required for wing root and tip and maximum lift coefficient needed. The high lift devices are selected based on the required maximum lift coefficients for clean, take-off and landing obtained in performance sizing. The hybrid design uses more of batteries than fuel for the mission and the required fuel weight is just 1891 lbs which is quite less in terms of fuel volume placed in the wing.

6.2 WING PLANFORM DESIGN

The proposed uses a monoplane wing cantilevered high wing obtained from configuration selection. The area of the wing is calculated as 809 sq.ft from the wing loading of 67 psf with

aspect ratio of 12 in performance sizing. Now the taper ratio and dihedral angle will be selected based on the reference regional aircraft data given by Roskam as shown below (Roskam, 2005).

Table 6.6 Regional Turbopropeller Driven Airplanes: Wing Geometric Data

Type	Dihedral Angle, Γ_w, deg.	Incidence Angle, i_w, root/tip deg.	Aspect Ratio, A	Sweep Angle, $\Lambda_{c/4}$, deg.	Taper Ratio, λ_w	Max. Speed, V_{max}, kts	Wing Type
CASA C-212-200							
SHORTS							
330	3 (outer)	NA	12.3	0	1.0	190(10K)	brcd/high
360							
BEECH							
1900	6	3.5/-1.1	9.8	0	0.42	263(8K)	ctl/low
B99	7	4.8	7.5	0	0.5	247(12K)	ctl/low
CESSNA CONQUEST							
I							
II							
GA Gulfstr. Ic							
GAF N22B							
Fokker F27-200	2.5	3.5	12.0	0	0.41	259(20K)	ctl/high
DeHAVILLAND CANADA							
DHC-6-300							
DHC-7	4.5	3	10.0	0	0.44	231(8K)	ctl/high
DHC-8	2.5 (out)	NA	12.3	0	0.45	270(15K)	ctl/high
EMB 110	7	3	9.9	0	0.50	248(8K))	ctl/low
EMB 120	6.5	2	9.9	0	0.50	NA	ctl/low
BRITISH AEROSPACE							
Jetstream 31	7	2	10.0	0.5	0.37	263(20K)	ctl/low
748	7	3	12.7	2.9	0.36	244(15K)	ctl/low

ctl = cantilever (30K) = 30,000 ft altitude

Figure 102: Wing geometric data for different regional turboprop airplanes

The taper ratio is defined as the ratio of root chord length to the tip chord length. Tapered wing is efficient for giving lower induced drag and smaller the taper ratio, lighter the wing structure. Smaller taper ratio produces more lift at the wing root.

$$\lambda_W = \frac{C_{tip}}{C_{root}} \qquad (6.1)$$

The dihedral angle is defined as the upward angle from the wing root to the wing tip of an aircraft wing. The dihedral effect produces a lateral stability or inherent stability along the roll axis. The proposed aircraft is a high wing configuration where the center of gravity is below the wing so, a smaller dihedral angle is required for lateral stability.

The proposed design uses a cantilevered conventional high wing and by comparing with the above data it is reasonable to assume the taper ratio as 0.41 and dihedral angle as 2.5 degrees. The span of the wing is calculated by the following equation

$$b = \sqrt{AS} \tag{6.2}$$

Where, A is Aspect ratio and S is Wing area

$$b = \sqrt{12 * 809} = 98.53 \text{ ft}$$

Root chord is calculated by the following equation from Raymer (Raymer, 2012)

$$C_r = \frac{2S}{b(1 + \lambda_W)} \tag{6.3}$$

$$C_r = \frac{2 * 809}{98.53(1 + 0.41)} = 11.64\text{ft}$$

Tip chord is calculated by using equation (6.1),

$$C_t = \lambda_W * C_r \tag{6.4}$$

$$C_t = 0.41 * 11.64 = 4.77 \text{ ft}$$

The mean aerodynamic chord can be determined by using the following equation from Raymer (Raymer, 2012)

$$\bar{c} = \left(\frac{2}{3}\right) C_{root} \left(\frac{1 + \lambda_W + {\lambda_W}^2}{1 + \lambda_W}\right) \tag{6.5}$$

$$\bar{c} = \left(\frac{2}{3}\right) * 11.64 \left(\frac{1 + 0.41 + 0.41^2}{1 + 0.41}\right) = 8.685$$

The span wise location of mean aerodynamic chord is determined as

$$\bar{Y} = \left(\frac{b}{6}\right)\left(\frac{1 + 2\lambda_W}{1 + \lambda_W}\right) \tag{6.6}$$

$$\bar{Y} = \left(\frac{98.53}{6}\right)\left(\frac{1 + 2 * 0.41}{1 + 0.41}\right) = 21.196$$

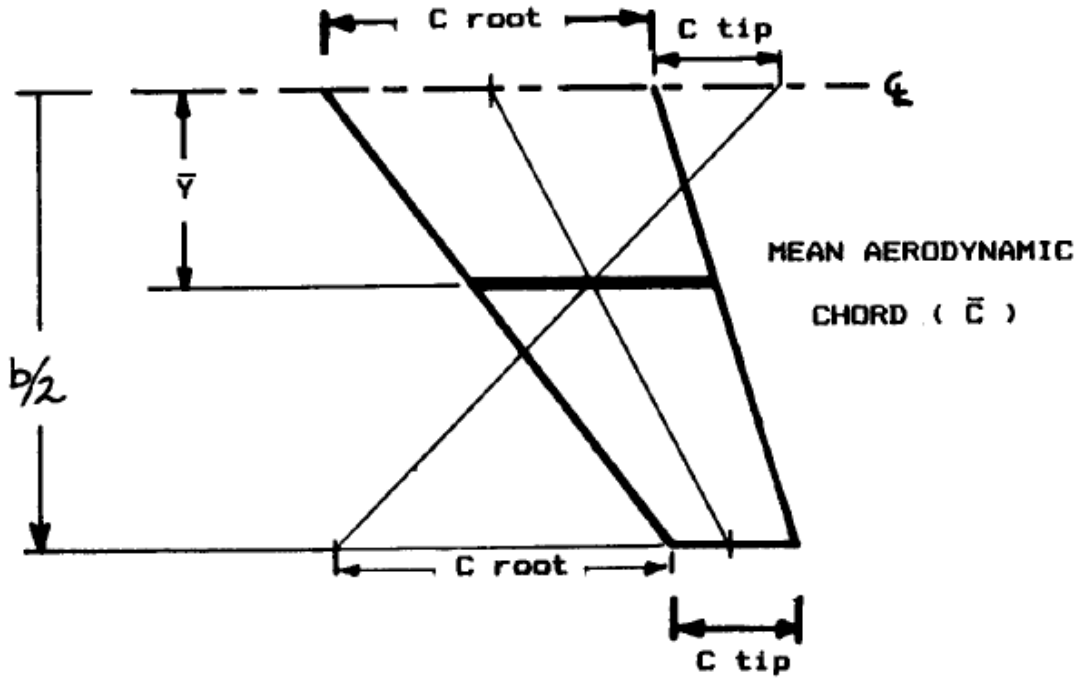

Figure 103: Trapezoidal wing geometry

The typical wing aerodynamic center for subsonic aircraft is given as $0.25\bar{c}$ from Raymer (Raymer, 2012)

Wing aerodynamic center = $0.25\bar{c}$ = 0.25*8.685 = 2.17 (6.7)

The mean geometric chord is calculated by the below equation

Mgc = S/b = 809/98.53 = 8.21 ft (6.8)

Leading-Edge spars can be determined as follows

Along the root chord = $0.20C_r$ = 0.20*11.64 = 2.33 ft

Along the tip chord = $0.20C_r$ = 0.20*4.77 = 0.954 ft

Trailing-Edge spars can be determined as follows

Along the root chord = $0.745C_r$ = 0.745*11.64 = 8.67 ft

Along the tip chord = $0.745C_t$ = 0.745*4.77 = 3.55 ft

6.2.1 Sweep Angle -Thickness Ratio Combination

Wing sweep is mainly used to minimize the adverse effects of transonic and supersonic flow. As the proposed aircraft travels at design Mach number of 0.42 hence, the quarter chord sweep angle is assumed as 0 degrees from the similar airplanes data. The leading-edge sweep angle is calculated by the following equation from Raymer (Raymer, 2012).

$$tan \wedge_{LE} = tan \wedge_{c/4} + \left[\frac{1-\lambda}{A(1+\lambda)}\right] \qquad (6.9)$$

$$tan \wedge_{LE} = \tan(0) + \left[\frac{1-0.41}{12(1+0.41)}\right]$$

$$tan \wedge_{LE} = 2 \text{ degrees}$$

The below figure shows the historical trend line for the leading-edge sweep angle and the maximum Mach number. As per the below figure, the calculated value of leading-edge sweep angle is quite reasonable (Raymer, 2012).

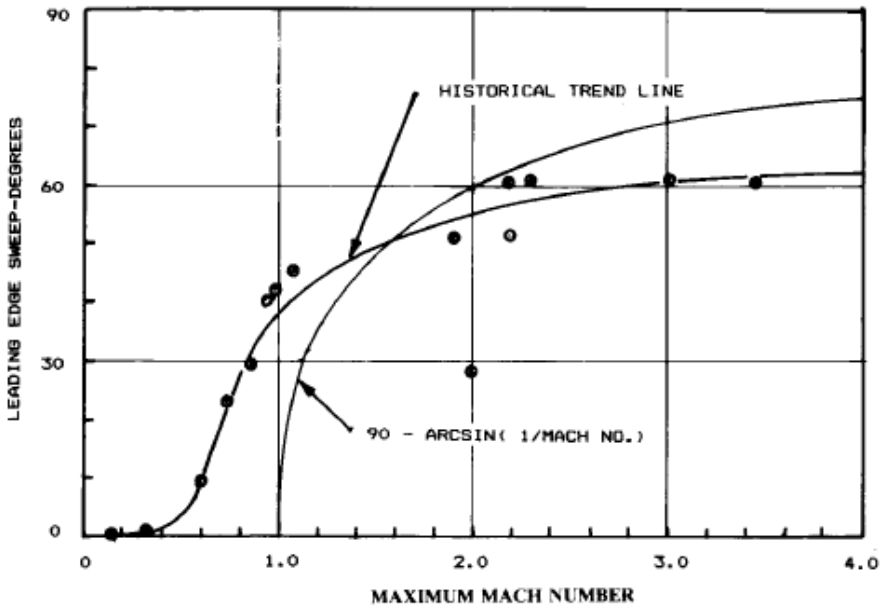

Figure 104: Wing sweep historical trends

The thickness to chord ratio is determined from the below figure from Raymer (Raymer, 2012). The design Mach number for proposed design is 0.42. At M = 0.42, the obtained (t/c) = 0.155 so, it is reasonable to have the following thickness ratios for the proposed design:

$$\text{At wing root, } \left(\frac{t}{c}\right)_r = 0.18$$

$$\text{At wing tip, } \left(\frac{t}{c}\right)_t = 0.15$$

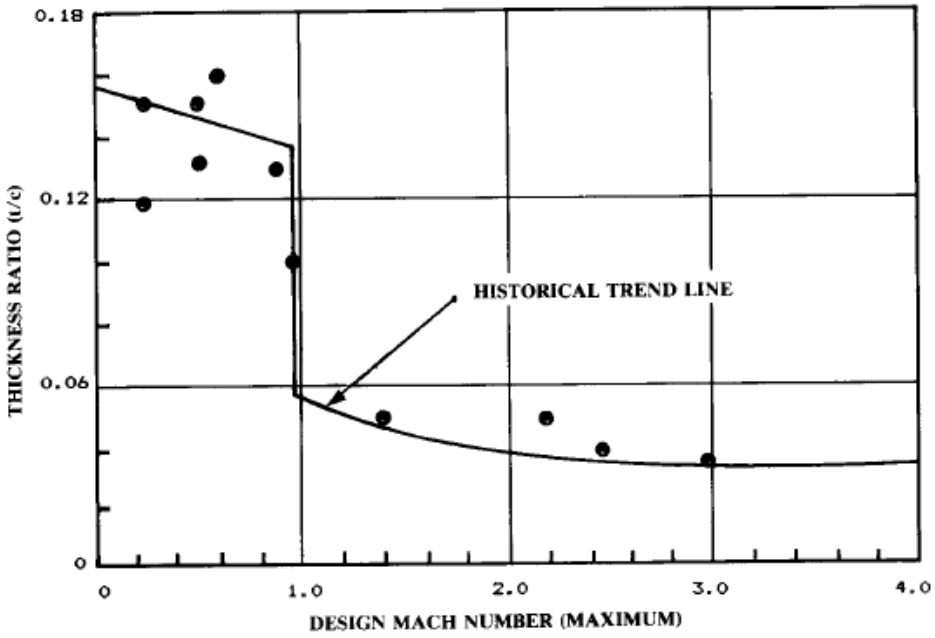

Figure 105: Historical trend of thickness to chord ratio with respect to design Mach number

6.3 AIRFOIL SELECTION

The airfoil thickness ratio has a direct impact on the maximum lift coefficient, drag, stall characteristics and structural weight (Roskam, 2005). The airfoil selection effects the following

- Cruise Speed
- Stall Speed
- Take-off and Landing Distances
- Overall Aerodynamic Efficiency

- **Type of Airfoil**

Based on the above figure, it is reasonable to select an airfoil for wing root with , $\left(\frac{t}{c}\right)_r = 0.18$ and wing tip with , $\left(\frac{t}{c}\right)_t = 0.15$. Therefore, the following airfoils are selected for the proposed design.

Wing Root: NACA 23018

Wing Tip: NACA 23015

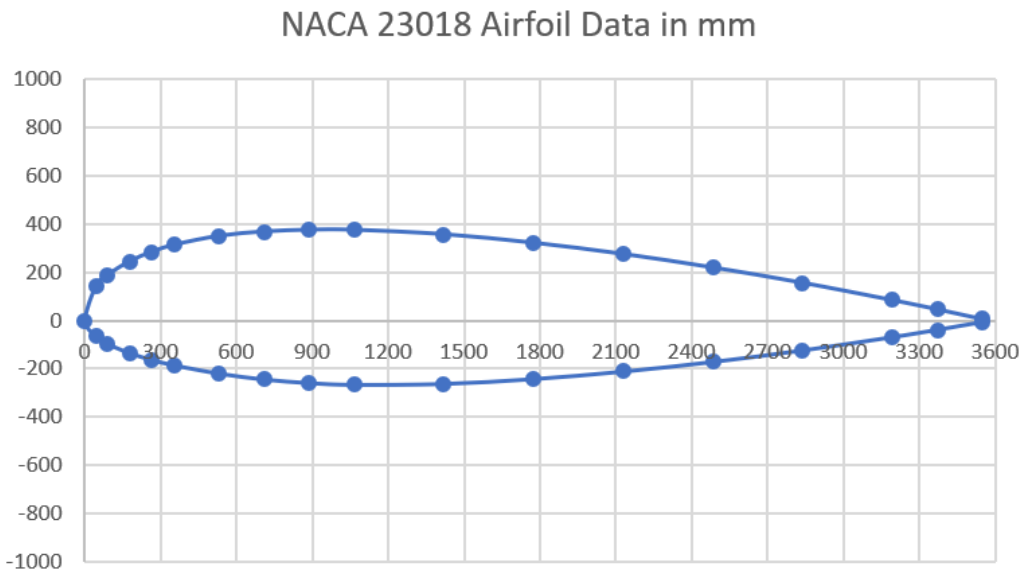

Figure 106: NACA 23018 airfoil

The following graphs are plotted for Reynold's number of 1,000,000 and Ncrit of 9 for just basic idea of NACA 23018 wing root and NACA 23015 wing tip airfoil performance. The maximum lift coefficient increases with increase in Reynold's number and note that the actual calculations of Reynold's number is shown in High-lift devices section. The below graph of C_L versus α for both NACA 23018 and NACA 23015 shows that the proposed wing root airfoil and wing tip airfoil can produce C_L of 1.53 for Reynold's number of 1,000,000 and Ncrit 9.

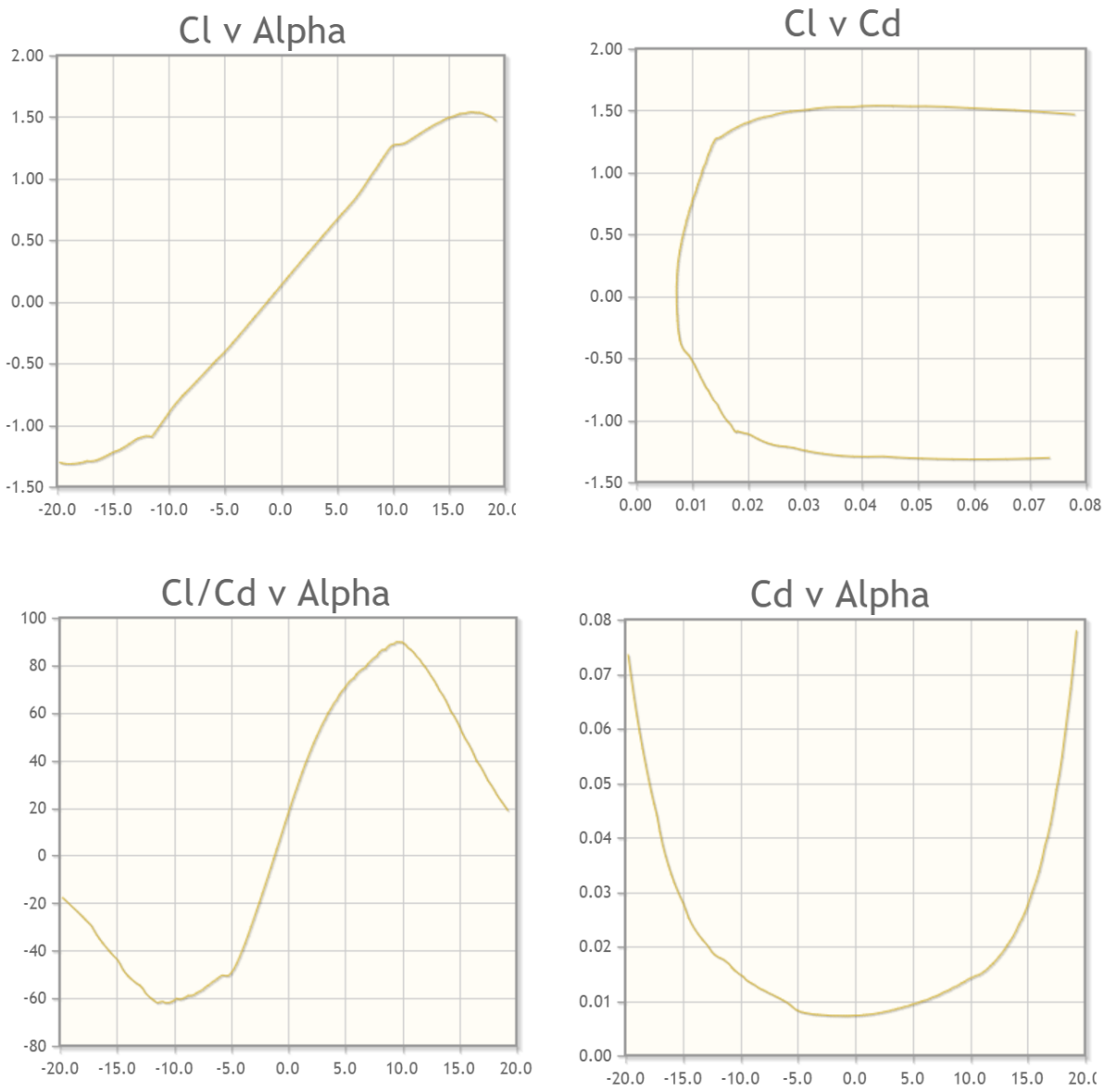

Figure 107: NACA 23018 airfoil performance graphs

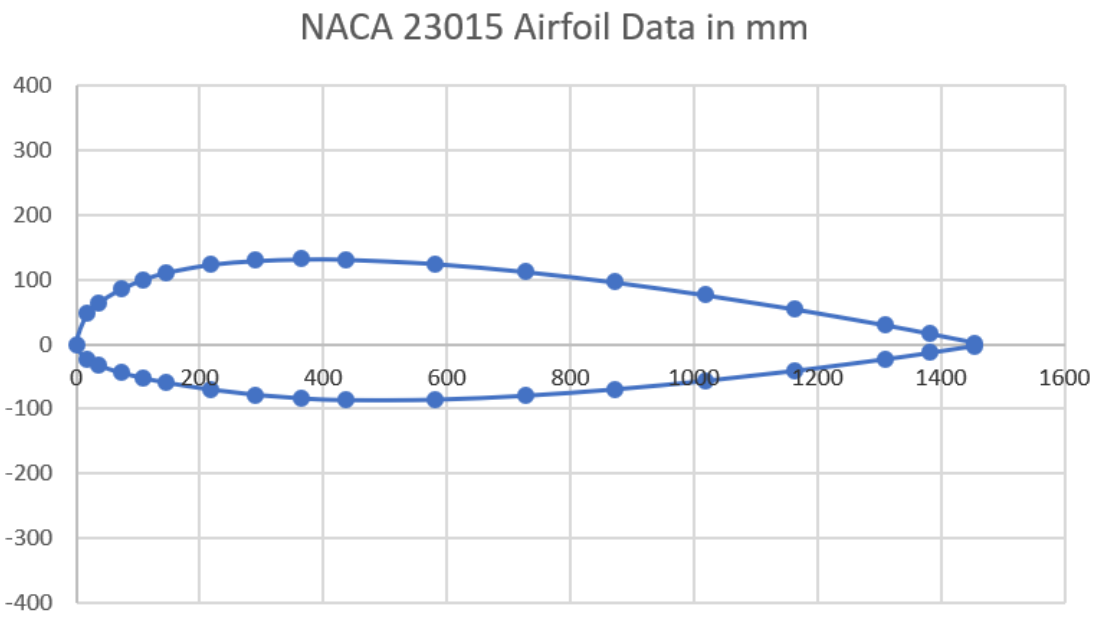

Figure 108: NACA 23015 airfoil

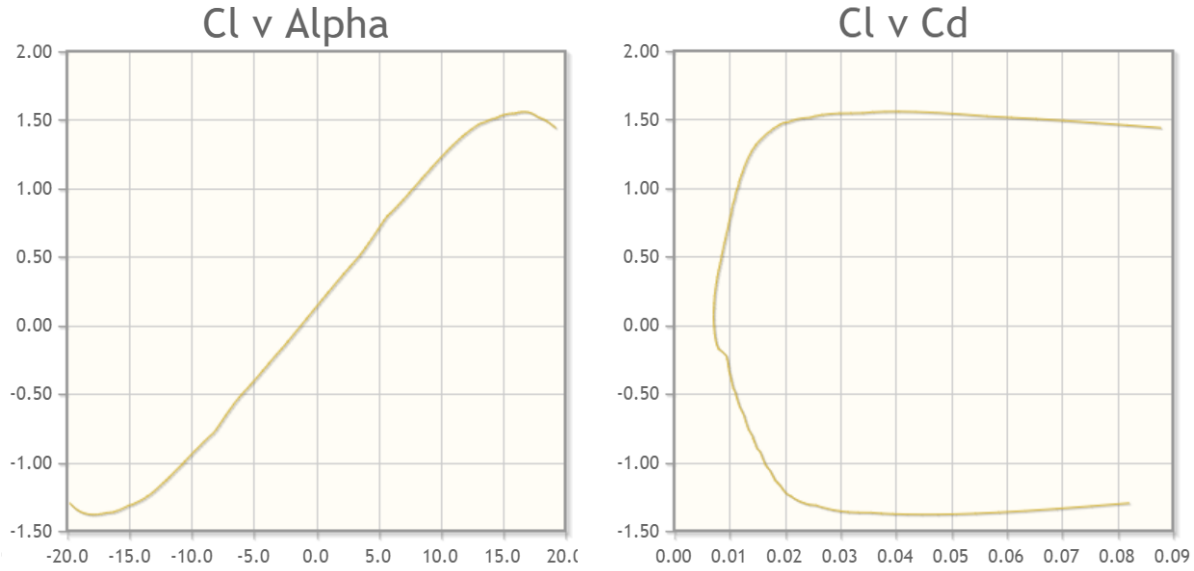

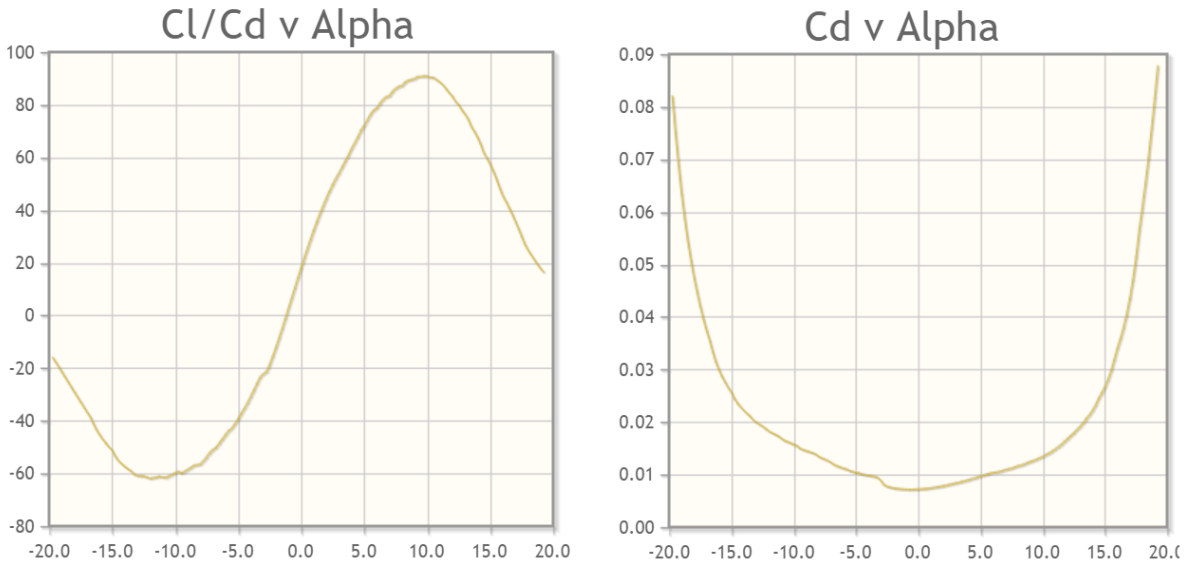

Figure 109: NACA 23015 airfoil performance graphs

- **Incidence Angle**

  The angle of incidence is defined as the angle of the wing chord line with respect to the longitudinal axis of the fuselage. The Roskam data summarizes the effect of wing incidence angle as shown below (Roskam, 2005).

Item	Large i_w	Small i_w
Cruise drag	High	Low
Cockpit visibility	Good	Watch out
Landing attitude in terms of nose gear hitting runway first	Watch out	No problem

Figure 110: Summary of the effect of wing incidence angle

Based on the above figure and comparable aircraft data, it is reasonable to have an incidence angle of 2 degrees which results in low cruise drag and as the proposed design uses high wing, so the cockpit visibility is good.

- **Twist angle**

  The main purpose of the wing twist is to get desired lift distribution pattern or stall characteristics. There are two types of wing twist such as aerodynamic twist and geometric

twist. The aerodynamic twist is defined as angle between zero-lift angle of an airfoil and zero-lift angle of the root airfoil. In aerodynamic twist the airfoil shape varies from wing root to wing tip. The geometric twist is defined as an airfoil having different geometric angles of attack at different spanwise sections. In geometric twist the angle of attack at wing root and wing tip are different. The wing twist is applied primarily to delay the tip stall by changing the wing tip incidence with respect to wing root. The wing twist also reduce wing root bending moment which in turn reduces the wing weight. The proposed design assumes negative angle of incidence at the wing tip and positive angle of incidence at the wing root which results in washout condition.

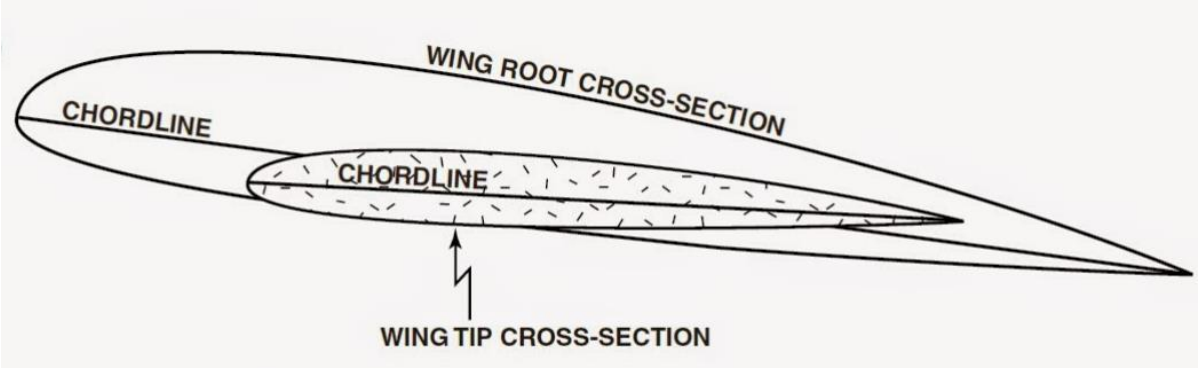

Figure 111: Airfoil washout condition

From the Roskam (Roskam, 2005), the geometric twist is given by

$$\varepsilon_t = i_{W_{tip}} - i_{W_{root}} \qquad (6.10)$$

Assuming the wing tip incidence angle as -1 degree using similar aircraft data and it is already assumed that wing root incidence as 2 degrees. Therefore,

$$\varepsilon_t = -1 - 2 = -3 \text{ degrees}$$

The aerodynamic twist can be determined from the below equation and it is dependent on local zero lift angle which will be varying with spanwise varying chamber (MIT, 2006).

$$\alpha_{aero} \equiv \varepsilon_t - \alpha_{L=0} \qquad (6.11)$$

Where, ε_t and local zero-lift angle $\alpha_{L=0}$ can be changed by a flap deflection and even though we consider a certain flap angle it is hard to determine the local zero-lift angle as it varies from root to tip (MIT, 2006).

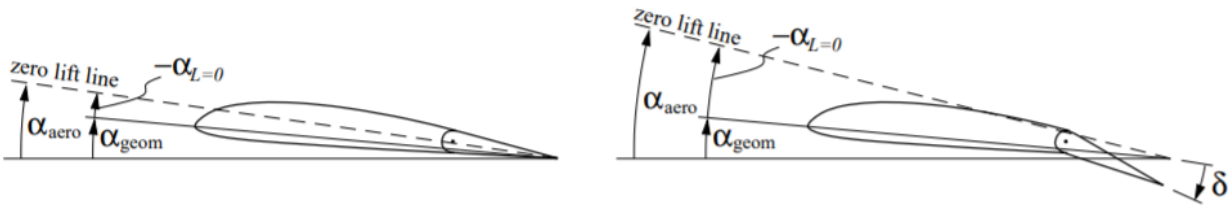

Figure 112: Aerodynamic twist angle definition

6.4 WING DESIGN EVALUATION

The below figure shows the input parameters of the proposed aircraft wing geometry in AAA program using obtained values of aspect ratio, wing area from performance sizing and assumed value of taper ratio and quarter chord angle.

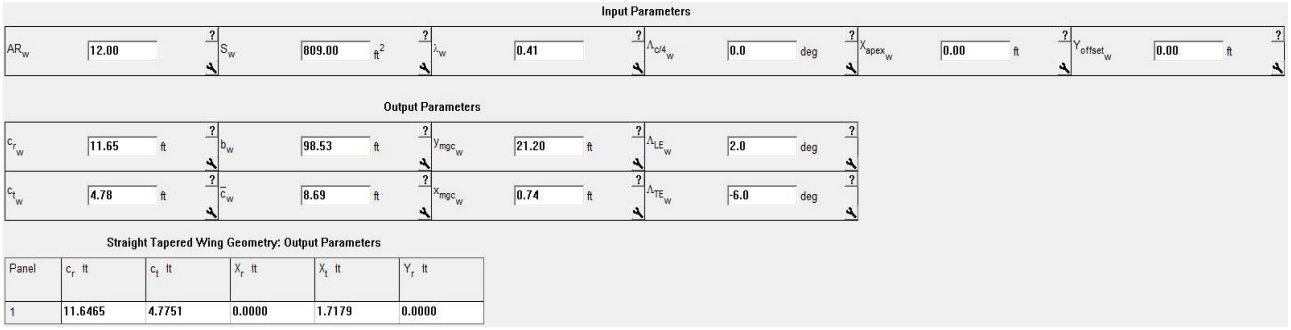

Figure 113: Input parameters of the proposed design wing geometry in AAA

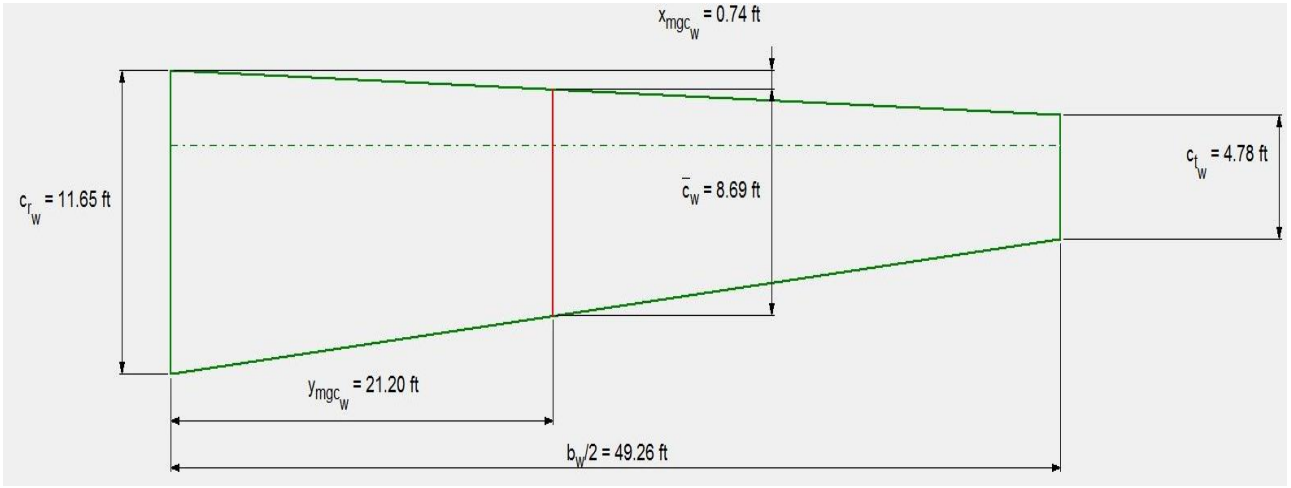

Figure 114: Wing geometry obtained in AAA program

6.5 DESIGN OF HIGH-LIFT DEVICES

The high-lift devices are used to increase the lift coefficient during some phases of the mission. These devices are of two types trailing edge devices i.e flaps and leading-edge devices i.e slats. The high lift devices are selected based on the required maximum take-off lift coefficient and maximum landing lift coefficient. The clean lift coefficient, maximum take-off lift coefficient and maximum landing lift coefficient obtained in performance sizing are as follows

Clean: $C_{L_{max}} = 1.5$

Takeoff: $C_{L_{max_{TO}}} = 2.1$

Landing: $C_{L_{max_L}} = 2.3$

The maximum lift coefficient of the wing for the proposed design which is a short-coupled aircraft is given by

$$C_{L_{max_W}} = 1.1 C_{L_{max}} \tag{6.12}$$

The wing needs to be corrected for the effect of sweep by using cosine rule if the wing sweep angle is between 0 and 35 degrees.

$$C_{L_{max_W}} \text{for Unswept} = \frac{C_{L_{max_W}} \text{for Swept}}{\cos \Delta_{\frac{c}{4}}} \tag{6.13}$$

As the proposed uses 0-degree quarter chord angle so, the above equation becomes

$$C_{L_{max_W}} \text{for Unswept} = \frac{C_{L_{max_W}} \text{for Swept}}{\cos 0}$$

$$C_{L_{max_W}} \text{for Unswept} = C_{L_{max_W}} \text{for Swept} = 1.65$$

The verification needs to be carried whether the wing can produce the required $C_{L_{max_W}}$ for unswept by the following approximation

$$C_{L_{max_W}} = \frac{K_\lambda \left(C_{1_{max_r}} + C_{1_{max_r}} \right)}{2} \tag{6.14}$$

As per the Roskam data (Roskam, 2005), for the λ = 0.41, $K_\lambda = 0.95$. $C_{1_{max_r}}$ and $C_{1_{max_t}}$ can be found out from cambered airfoil graph. The Reynold's number can be calculated by the following equations:

$$\text{At the Root: } R_{n_r} = \frac{\rho V C_r}{\mu} \qquad (6.15)$$

$$\text{At the Tip: } R_{n_t} = \frac{\rho V C_t}{\mu} \qquad (6.16)$$

Using the ρ = 0.002378 Slugs/ft^3, μ = 3.737 x 10^{-7}lb s/ft^2 at sea-level (Engineering, 2003) and V = 286.928 mph. The root chord and tip chord are obtained as 11.64 ft and 4.77 ft.

By substituting the above values in Reynold's number equations, we get the Reynold's number at sea-level as follows:

$$\text{At the Root: } R_{n_r} = \frac{0.002378 * 286.928 * 11.64}{3.737 * 10^{-7}} = 21.2 * 10^6$$

$$\text{At the Tip: } R_{n_t} = \frac{0.002378 * 286.928 * 4.77}{3.737 * 10^{-7}} = 8.7 * 10^6$$

Similarly, using the the ρ = 10.66 x 10^{-4} Slugs/ft^3, μ = 3.217 x 10^{-7}lb s/ft^2 and V = 316.46 mph at cruising altitude (Engineering, 2003)

$$\text{At the Root: } R_{n_r} = \frac{10.66 \text{ x } 10^{-4} * 316.46 * 11.64}{3.217 * 10^{-7}} = 12.2 * 10^6$$

$$\text{At the Tip: } R_{n_t} = \frac{10.66 \text{ x } 10^{-4} * 316.46 * 4.77}{3.217 * 10^{-7}} = 5.0 * 10^6$$

$C_{1_{max_r}}$ = 1.7 and $C_{1_{max_t}} = 1.75$ are obtained from the below figure with $\left(\frac{t}{c}\right)_r = 0.18$ and $\left(\frac{t}{c}\right)_t = 0.15$

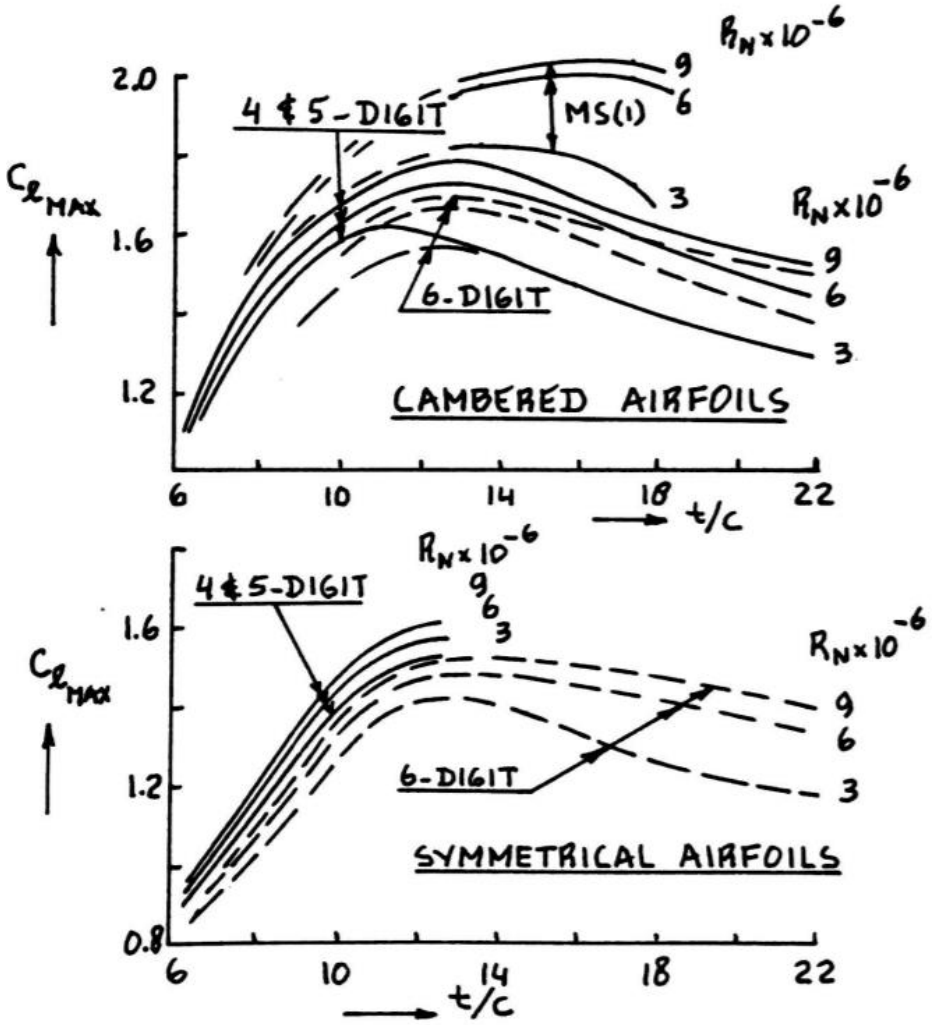

Figure 115: Effect of thickness ratio and reynold's number on section maximum lift coefficient

Therefore, using equation (6.14) we get

$$C_{L_{max_W}} = \frac{0.95(1.75 + 1.7)}{2} = 1.64$$

From equation (6.12), we get

$$C_{L_{max_W}} = 1.1 C_{L_{max}}$$

$$C_{L_{max}} = \frac{C_{L_{max_W}}}{1.1} = \frac{1.64}{1.1} = 1.49$$

The obtained $C_{L_{max}}$ is close enough to assumed clean maximum lift coefficient $C_{L_{max_{clean}}}$ of 1.5.

The incremental values of maximum lift coefficient required to be produced by high-lift devices can be determined by the following equations (Roskam, 2005).

Take-off: $\Delta C_{L_{max_{TO}}} = 1.05\left(C_{L_{max_{TO}}} - C_{L_{max}}\right) = 1.05(2.1 - 1.5) = 0.63$ (6.17)

Landing: $\Delta C_{L_{max_L}} = 1.05\left(C_{L_{max_L}} - C_{L_{max}}\right) = 1.05(2.3 - 1.5) = 0.84$ (6.18)

The obtained flap lift incremental values clearly indicates that they are not very high so, a single slotted flap on starboard and port side of the wing will probably be enough.

With flaps down, the required incremental section maximum lift coefficient can be determined by the below equation (Roskam, 2005)

$$\Delta C_{1_{max}} = \frac{\Delta C_{L_{max}}\left(\frac{S}{S_{wf}}\right)}{K_{\Lambda}} \quad (6.19)$$

Where,

$$K_{\Lambda} = \left(1 - 0.08cos^2\Lambda_{\frac{c}{4}}\right)cos^{3/4}\Lambda_{\frac{c}{4}} \quad (6.20)$$

As the proposed design uses $\Lambda_{\frac{c}{4}} = 0$ so,

$$K_{\Lambda} = 1 - 0.08 = 0.92$$

Assuming two arbitrary values of $\frac{S_{wf}}{S}$ as per the Roskam (Roskam, 2005) Procedure, the following values for take-off flaps and landing flaps are obtained using the equation (6.19) and K_{Λ}.

Table 26: Results of take-off and landing flap incremental maximum lift coefficients for two arbitrary values of $\frac{S_{wf}}{S}$

$\frac{S_{wf}}{S}$	0.3	0.6
Take-off Flaps, $\Delta C_{1_{max}}$	2.28	1.141

Landing Flaps, $\Delta C_{1_{max}}$	3.04	1.52

Assumptions:

As it is already observed that a single slotted flap is enough for the proposed design, the following assumptions are made for the geometry of the flap based on the Roskam data (Roskam, 2005).

$$\frac{Z_{fh}}{c} = 0.1, \qquad \frac{c_{\mathrm{f}}}{c} = 0.25, \qquad \delta_{\mathrm{f_{TO}}} = 20 \text{ deg}, \qquad \delta_{\mathrm{f_L}} = 30 \text{ deg}$$

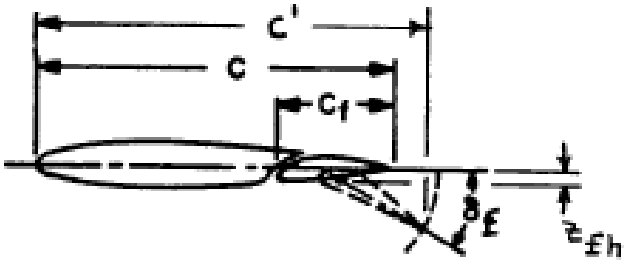

Figure 116: Flap geometry

Take-off:

The flapped section lift curve slope can be determined using the below equation

$$C_{1_{\alpha_{\mathrm{f}}}} = C_{1_{\alpha}} \left(\frac{c'}{c}\right) \qquad (6.21)$$

Where, $C_{1_{\alpha}}$ is assumed to be 2π from the Roskam data (Roskam, 2005) and

$$\frac{c'}{c} = 1 + 2\left(\frac{Z_{\mathrm{fh}}}{c}\right)\tan\left(\frac{\delta_{\mathrm{f}}}{2}\right) \qquad (6.22)$$

By substituting the above assumed values for take-off, we get

$$\frac{c'}{c} = 1 + 2(0.1)\tan\left(\frac{20}{2}\right) = 1.035$$

Therefore, from equation (6.21)

$$C_{1_{\alpha_f}} = 2 * \pi * 1.035 = 6.501$$

For the single slotted flaps,

$$\Delta C_1 = C_{1_\alpha} \alpha_{\delta_f} \delta_f \qquad (6.23)$$

Where, α_{δ_f} can be found from the below figure at take-off flap deflection of 20 deg and $\frac{c_f}{c}$ of 0.25 as 0.5.

From the equation (6.23),

$$\Delta C_1 = 6.501 * 0.5 * 20 * \frac{\pi}{180} = 1.135$$

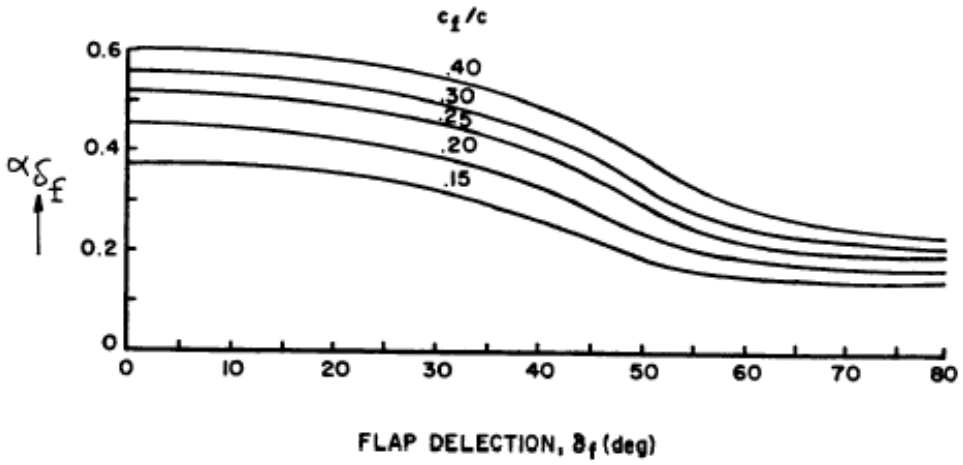

Figure 117: Section lift effectiveness parameter for single slotted flaps

The incremental section lift coefficient due to flaps, ΔC_1 is related to its counterpart $\Delta C_{1_{max}}$ as shown in below figure.

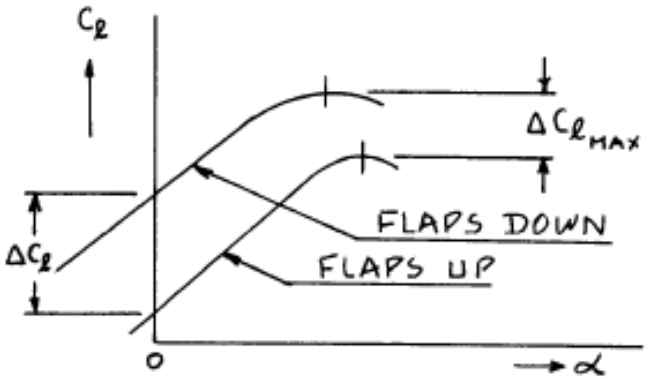

Figure 118: Relation between $\Delta C_{1_{max}}$ and ΔC_1

The Relation between $\Delta C_{1_{max}}$ and ΔC_1 is given by the following equation for preliminary design by Roskam (Roskam, 2005),

$$\Delta C_1 = \left(\frac{1}{K}\right)\Delta C_{1_{max}} \qquad (6.24)$$

Where the value of K can be obtained as 0.93 from the below figure for single slotted flap

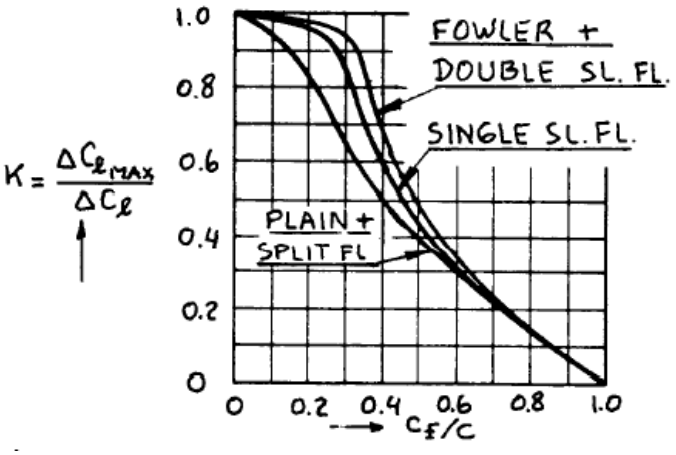

Figure 119: Effect of flap type and flap chord ratio on K

Therefore,

$$1.135 = \left(\frac{1}{0.93}\right)\Delta C_{1_{max}}$$

$$\Delta C_{1_{max}} = 1.055$$

The obtained value of $\Delta C_{1_{max}}$ as 1.055 is within 10% of take-off flaps lift increment value of 1.141 for assumed value of $\frac{S_{wf}}{S}$ as 0.6. Hence, the assumed type of flap, flap deflection angle and $\frac{c_f}{c}$ are reasonable for the take-off condition of the proposed design.

Landing:

The landing calculations are obtained as follows like the take-off calculations with the assumptions of flap geometry mentioned above.

From Equation (6.22), $\frac{c'}{c} = 1 + 2(0.1)\tan\left(\frac{30}{2}\right) = 1.053$

From Equation (6.21), $C_{1_{\alpha_f}} = 2 * \pi * 1.053 = 6.616$

From Equation (6.23), $\Delta C_1 = 6.616 * 0.5 * 30 * \frac{\pi}{180} = 1.696$

From Equation (6.24), $\Delta C_{1_{max}} = 1.696 * 0.93 = 1.578$

The obtained value of $\Delta C_{1_{max}}$ for landing is more than enough when compared to landing flaps lift increment value of 1.52 for assumed value of $\frac{S_{wf}}{S}$ as 0.6.

Summary:

The following parameters summarizes the geometry of the flap

Table 27: Summary of flap geometry

Type of flap	Single Slotted Flap
Ratio of wing flap area to the wing area, $\frac{S_{wf}}{S}$	0.6
Ratio of flap chord to the wing chord, $\frac{C_f}{C}$	0.25
Ratio of $\frac{Z_{fh}}{c}$	0.1

Take-off flap angle,	20 Degrees
Landing flap angle,	30 Degrees

6.6 DESIGN OF LATERAL CONTROL SURFACES

The purpose of lateral control surfaces is mainly for providing lateral stability, i.e rolling motion for the proposed design. The rolling motion is produced by the ailerons which are placed on the trailing edge outboard station of the wing. The data of similar airplanes for aileron span ratio and aileron chord ratio is given by Roskam (Roskam, 2005) as shown below.

Type	Wing Area S ft^2	Wing Span b ft	Vert. Tail Area S_v ft^2	S_r/S_v	x_v ft	$\bar{V}_v$	Rudder Chord root/tip $fr.c_v$	S_a/S	Ail. Span Loc. in/out fr.b/2	Ail. Chord in/out $fr.c_w$
CASA C-212-200										
	431	62.3	77.5	0.41	24.8	0.072	0.41	0.061	.69/1.0	.24/.26
SHORTS										
330	453	74.7	93.1	0.26	27.3	0.075	0.41	0.061	.70/.95	0.27
360	453	74.7	91.4	0.37	33.9	0.091	.39/.36	0.074	.69/.98	0.27
BEECH										
1900*	303	54.5	47.5	0.35	26.5	0.076	.40/.38	0.064	.60/1.0	0.21
B200	303	54.5	52.3	0.29	20.5	0.065	.47/.41	0.059	.60/1.0	0.21
CESSNA CONQUEST										
I	225	44.1	41.3	0.38	17.1	0.071	.46/.38	0.060	.61/.86	.29/.28
II	254	49.3	43.5	0.37	18.7	0.065	.48/.33	0.058	.62/.89	.30/.32
GA Ic	610	78.3	117	0.25	35.4	0.087	.29/.33	0.061	.65/.98	.27/.22
GAF N22B	324	54.2	70.2	0.44	21.6	0.086	.49/.43	0.085	.54/1.0	0.24
Fokker F27-200										
	754	95.2	153	0.30	36.0	0.077	.33/.29	0.050	.69/.98	.31/.29
DeHAVILLAND CANADA										
DHC-6-300	420	65.0	82.0	0.42	25.7	0.077	.35/.44	0.079	.44/.97	0.20
DHC-7	860	93.0	170	0.28	35.7	0.076	.25/.30	0.027	.81/1.0	.27/.31
DHC-8	585	84.0	190	0.26	31.4	0.121	.27/.35	0.031	.80/1.0	.23/.22
EMB-120	409	64.9	74.3	0.38	27.3	0.076	.32/.31	0.084	.63/.97	0.24
BAe 31	270	52.0	83.1	0.26	20.7	0.120	.34/.39	0.061	.59/.97	.28/.30
Metro III	309	57.0	56.0	0.35	27.9	0.089	.37/.56	0.046	.61/.98	.31/.36

* 1900 also has taillets on horizontal tail.

Figure 120: Aileron data for regional turboprop airplanes

The above figure suggests the following aileron dimensions are reasonable:

Aileron Span Ratio Outboard: 0.86 – 1.0

Aileron Span Ratio Inboard: 0.44 – 0.81

Aileron Chord Ratio Outboard: 0.26 – 0.36

Aileron Chord Ratio Inboard: 0.20 – 0.31

Using the above range of data, the proposed design uses one aileron on starboard side of the wing and one aileron on port side of the wing. The proposed design places the aileron on the trailing edge of the wing near to the wing tip as shown below using AAA program.

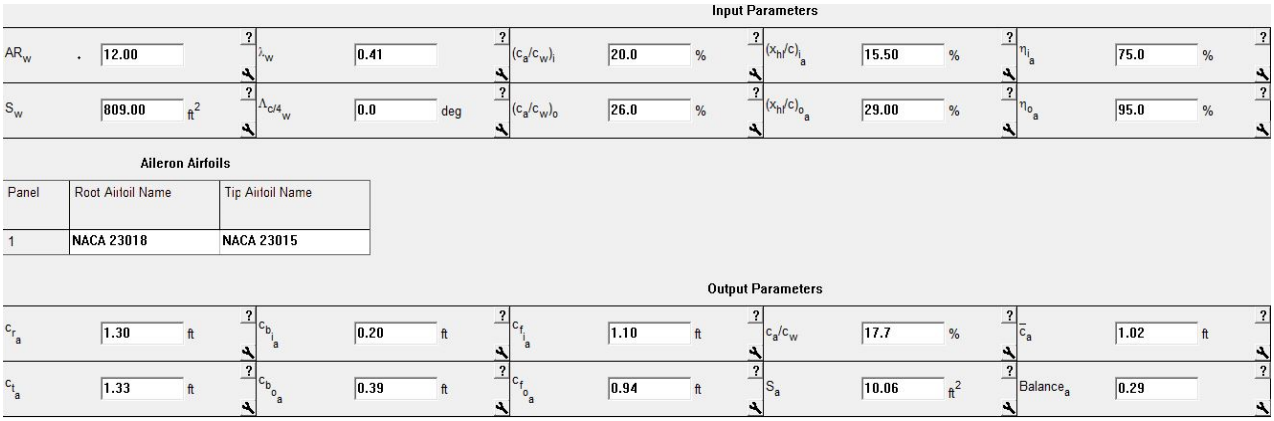

Figure 121: Input parameters for aileron sizing

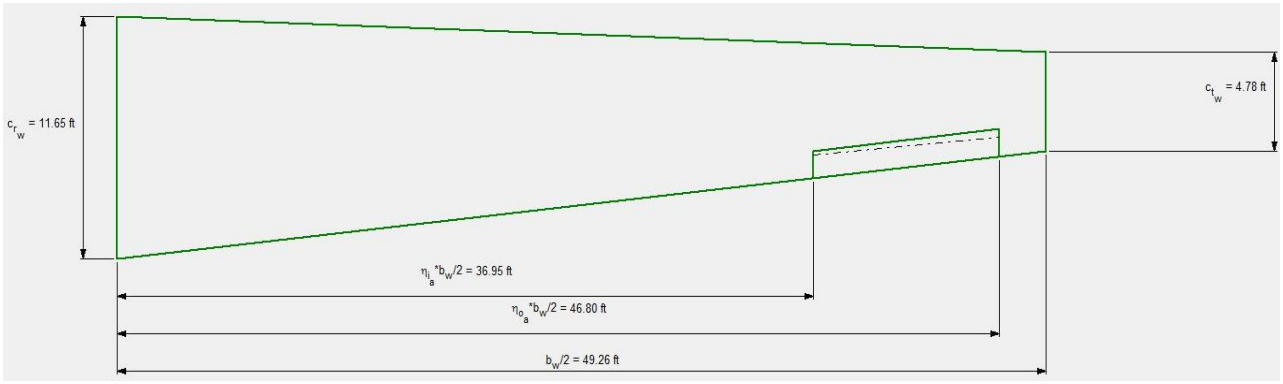

Figure 122: Aileron sizing in AAA program

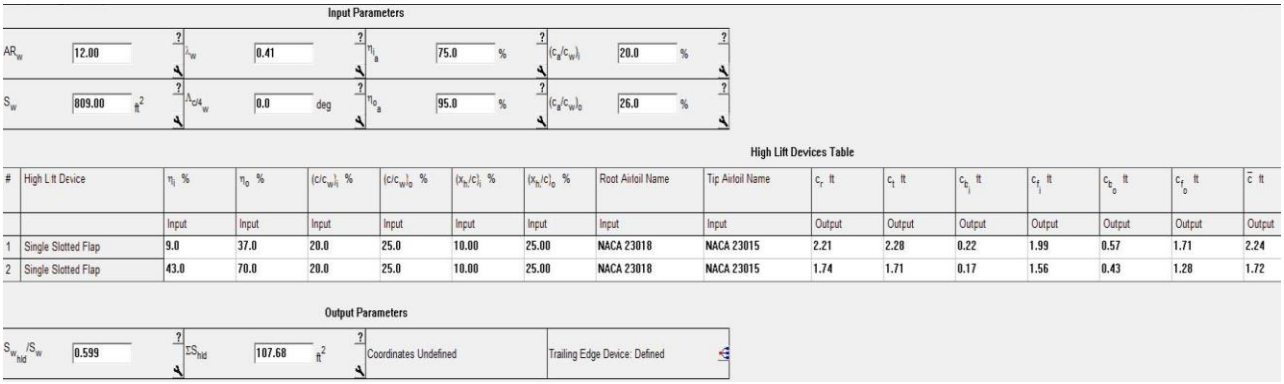

Figure 123: Input parameters of high lift devices

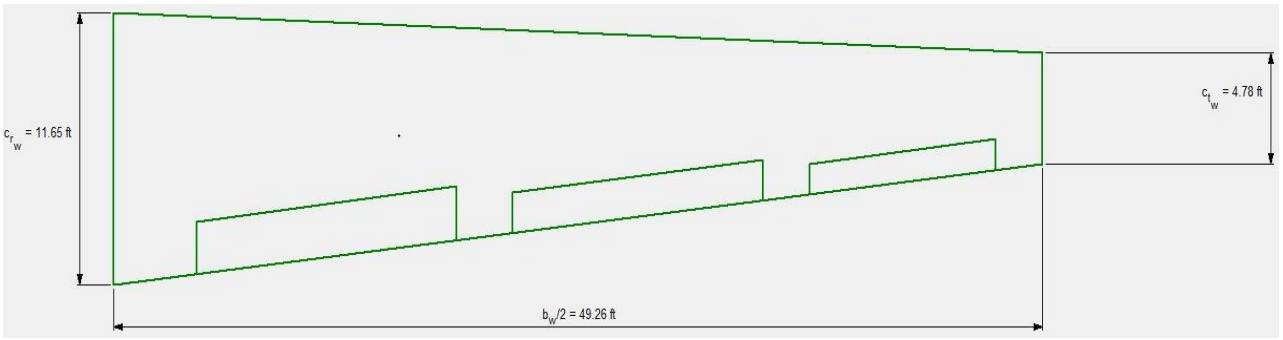

Figure 124: High lift devices sizing in AAA program

6.7 DRAWINGS

The below parameters are obtained from the wing planform design section

Table 28: Parameters of proposed design wing geometry

Span, b	98.53 ft or 30 m
Root Chord, C_r	11.64 ft or 3.55 m
Tip Chord, C_t	4.77 ft or 1.45 m
Mean Aerodynamic Chord, Mac or $\bar{c}$	8.685 ft or 2.65 m
Mean Geometric Chord, Mgc	8.21 ft or 2.5 m
Leading-Edge Sweep Angle	2 degrees
Trailing-Edge Sweep Angle	-6 degrees

Coordinates of Aerodynamic Center (Xac, Yac)	(2.91 ft, 21.196 ft) or (0.89 m, 6.46m)

The wing fuel volume is calculated by using the below equation

$$V_{Wf} = 0.54\left(\frac{S^2}{b}\right)\left(\frac{t}{c}\right)_r\left[\frac{1+\lambda_W\tau_W^{\frac{1}{2}}+\lambda_W^2\tau_W}{(1+\lambda_W)^2}\right] \qquad (6.25)$$

Where,

$$\tau_W = \frac{\left(\frac{t}{c}\right)_t}{\left(\frac{t}{c}\right)_r} = \frac{0.15}{0.18} = 0.833 \qquad (6.26)$$

$$V_{Wf} = 0.54\left(\frac{809^2}{98.53}\right)0.18\left[\frac{1+0.41*0.833^{0.5}+0.41^2*0.833}{(1+0.41)^2}\right] = 491.75\ \text{ft}^3$$

The obtained fuel volume is for the conventional aircraft but as the proposed design uses hybrid design, so only 1891 lbs weight of fuel is used for the mission. The remaining space is empty which is a part of empty weight where this weight can be utilized for batteries.

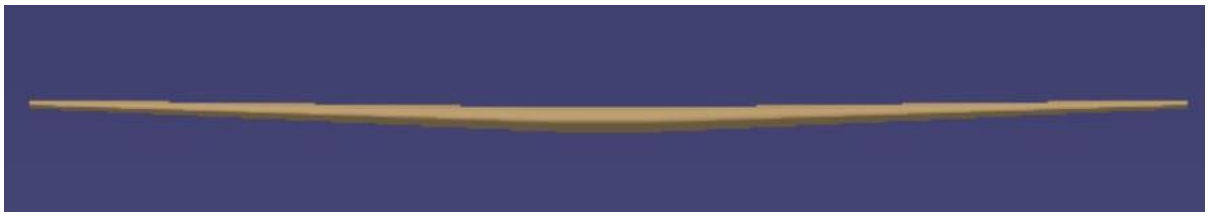

Figure 125: Front view of the wing

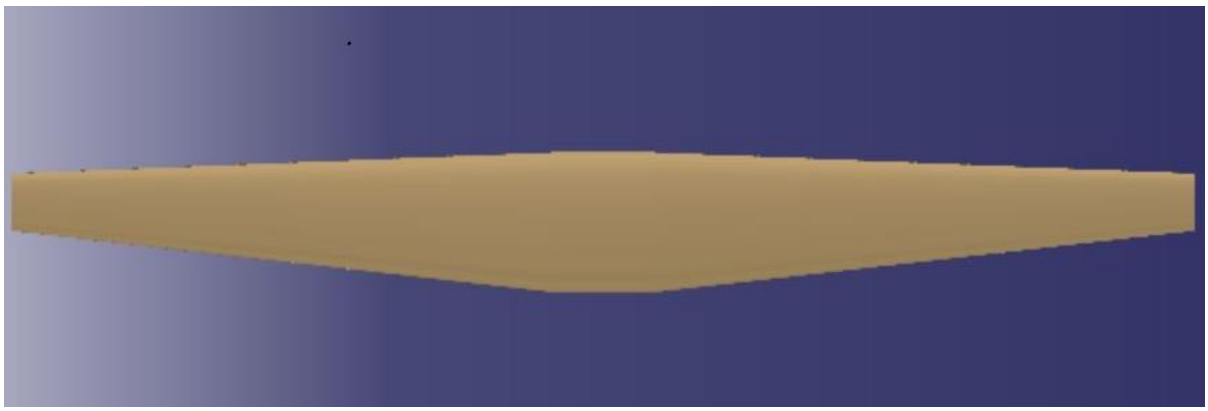

Figure 126: Top view of the wing

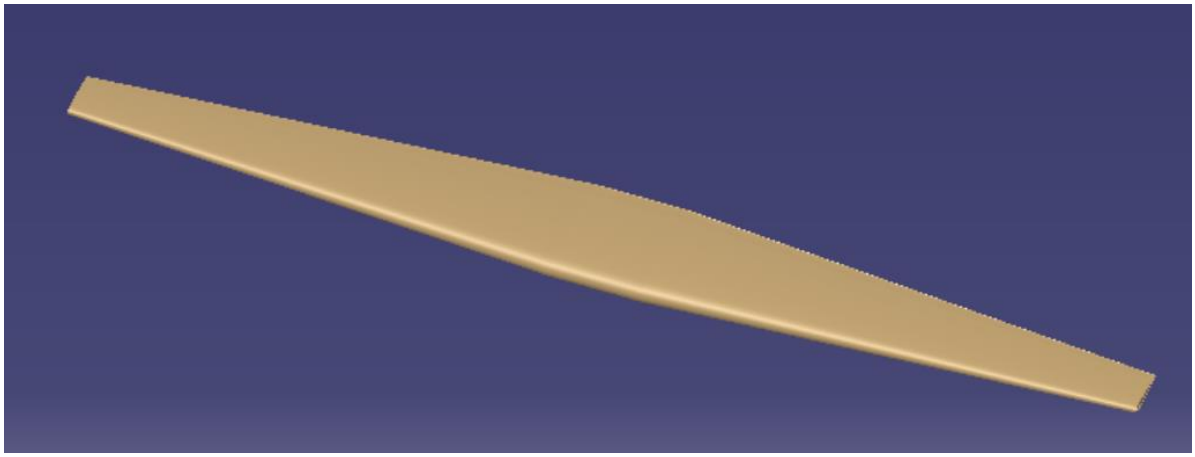

Figure 127: Isometric view of the wing

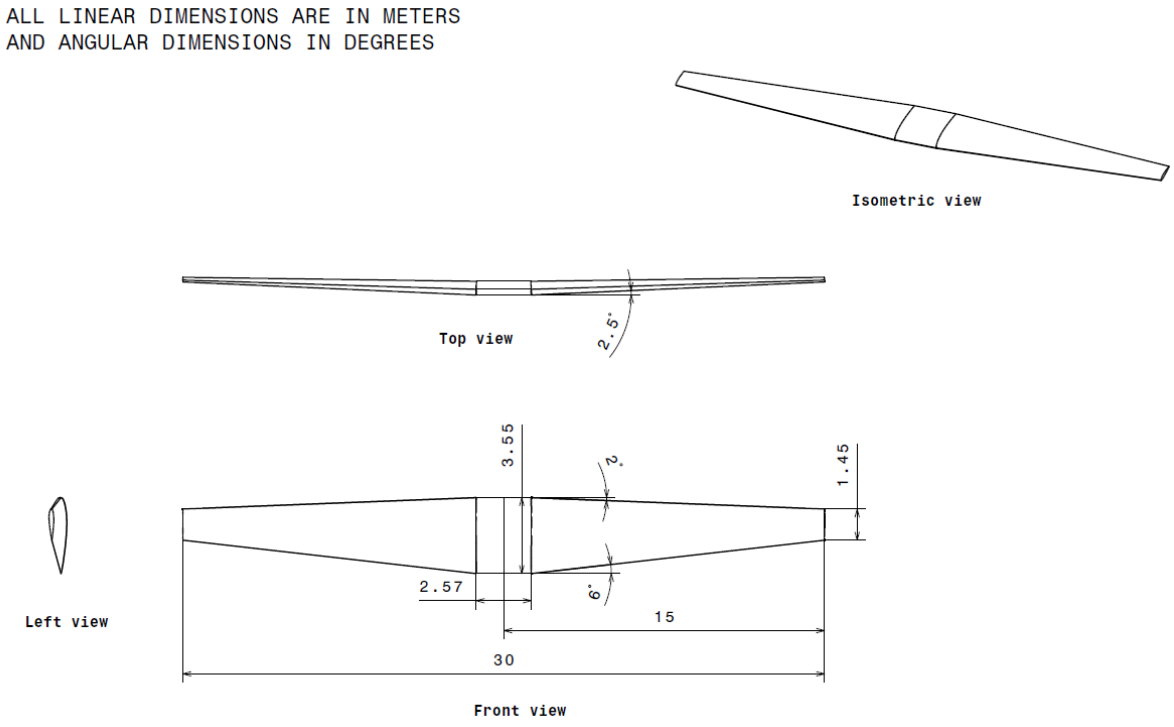

Figure 128: Drawing of the wing

Placement of Wing on Fuselage

The placement of the wing on the fuselage depends on the center of gravity location of wing and the fuselage. According to Raymer, the wing can be placed on the fuselage for subsonic aircraft such that the aircraft center of gravity is at about $0.25\bar{c}$. The x-coordinate of mean

aerodynamic center i.e Xac obtained as 2.91 ft. The center of gravity of fuselage can be calculated by using the below approximate location and the length of the fuselage is obtained as 72.7 ft from fuselage design.

Fuselage C.G = 0.45*length = 0.45*72.7 = 32.17 ft

Wing C.G = 0.40*Mac = 0.40*8.685 = 3.474 ft

The location of wing on the fuselage (Approximately) = 32.17-2.91 = 29.26 ft

Item	Fighters	Transports and bombers	General aviation	Multiplier[a]	Approximate location
Wing	9.0	10.0	2.5	$S_{\text{exposed planform ft}^2}$	40% MAC
Horizontal tail	4.0	5.5	2.0	$S_{\text{exposed planform ft}^2}$	40% MAC
Vertical tail	5.3	5.5	2.0	$S_{\text{exposed planform ft}^2}$	40% MAC
Fuselage	4.8	5.0	1.4	$S_{\text{wetted area ft}^2}$	40–50% length
Landing gear[b]	.033 .045 Navy	.043	.057	TOGW (lb)	–
Installed engine	1.3	1.3	1.4	Engine weight (lb)	–
"All-else empty"	.17	.17	.10	TOGW (lb)	40–50% length

Figure 129: Approximate location of component center of gravity

The wing is placed according to the above calculation and this placement can vary once the stability and control analysis is performed on the proposed design. So, initially the wing is placed on the fuselage approximately to proceed further based on the Raymer data (Raymer, 2012). The drawing of wing placement on fuselage is shown below using CATIA V5 (Computer Aided Three-Dimensional Interactive Application) software. The dimension from nose to the wing leading edge is obtained as 29.2 ft or 8.9 m as shown in below figure.

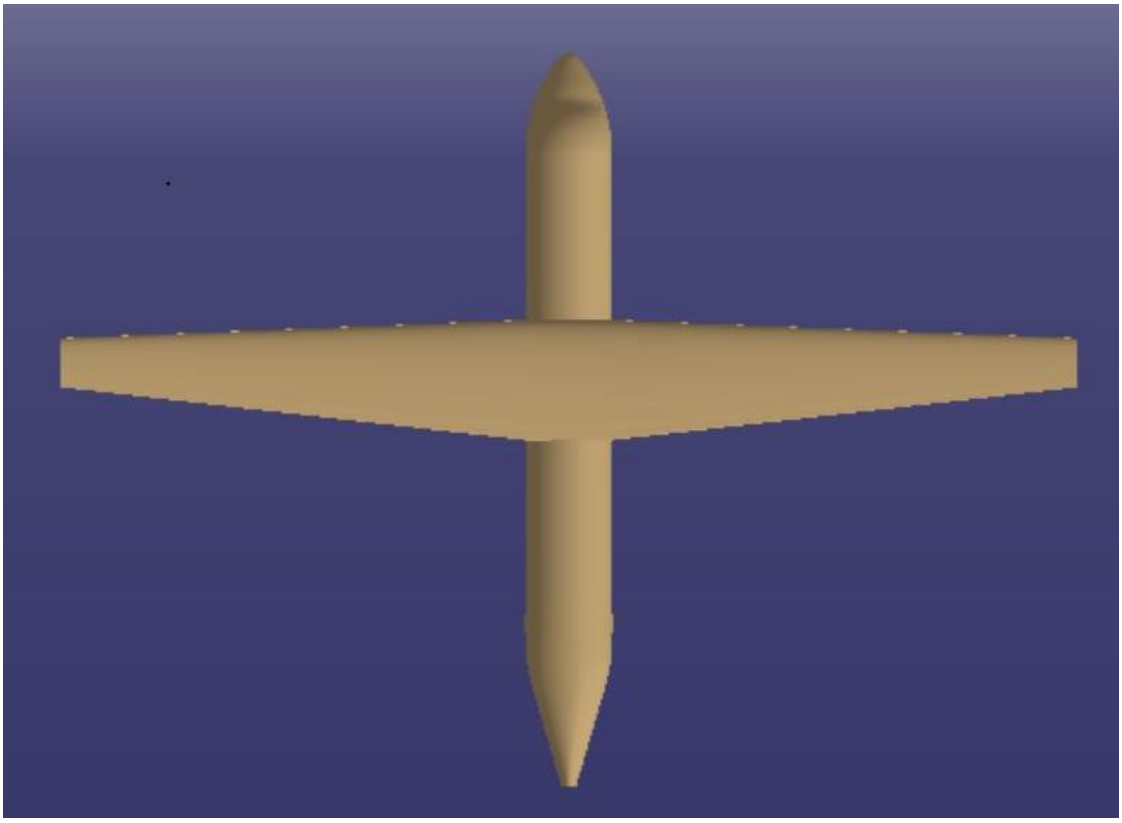

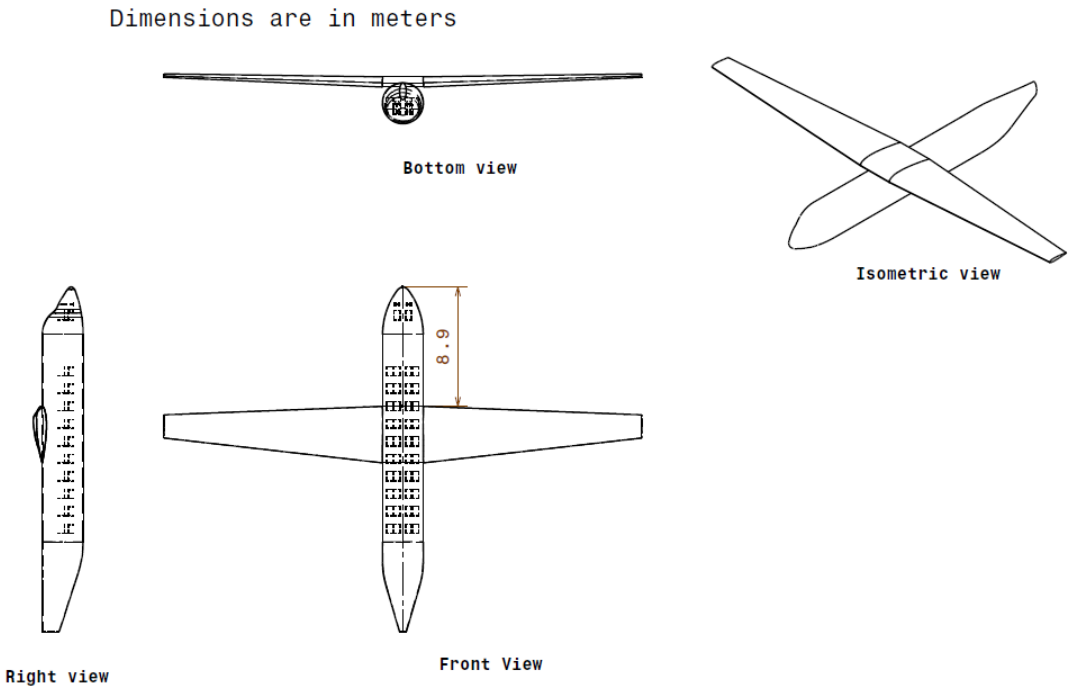

Figure 130: Wing placement on the fuselage

6.8 DISCUSSION

This chapter presented a detailed approach of wing design, lateral control surface and high-lift devices sizing. As we can see the AAA values are exactly matching with the calculated parameters of wing geometry. The lateral control surface sizing is selected within the given range of Roskam data. The high devices are chosen based on the required lift coefficients obtained in performance sizing. Most of the similar regional airplanes have a dihedral angle to provide lateral stability so, it is reasonable to assume a dihedral angle 0f 2.5 degrees for the proposed design. The taper ratio is assumed to be 0.41 for the proposed design where the root chord length and tip chord length found out to be 11.64 ft and 4.77 ft. The proposed design uses two different airfoils for the wing. The root airfoil is thicker than the tip airfoil to get better aerodynamic efficiency. This selection of two different airfoils is quite reasonable when compared with comparable aircraft data where most of the regional airplanes uses two different airfoils. The angle of incidence chosen for the wing root as 2 degrees and wing tip as -1 degree in comparison with comparable aircraft data given by Roskam. The geometric twist obtained as -3 degrees for the proposed wing design. Based on the calculations of lift increment required, single-slotted flap is enough to provide the required lift coefficient during take-off and landing. The complete drawing of proposed design till date is shown in drawings section.

6.9 CONCLUSION

The overall assumed and obtained parameters in wing planform design, lateral control surface and high-lift devices are reasonable based on the required performance of the proposed aircraft. The required maximum lift coefficients during take-off and landing can be obtained by using single-slotted flap on both starboard and port side of the wing. The selected airfoils for wing root and wing tip are reasonable for the obtained thickness to chord ratios and required maximum wing lift coefficient. The aileron sizing is within the range of the given Roskam data.

CHAPTER 7: DESIGN OF THE EMPENNAGE AND THE LONGITUDINAL AND DIRECTIONAL CONTROLS

7.1 INTRODUCTION

This chapter presents a methodology for overall Empennage design with longitudinal and directional controls. The wing planform design is already obtained in the previous chapter with lateral control surface and high-lift devices. Based on the obtained weight sizing, performance sizing, fuselage dimensions, wing sizing parameters, the selection of empennage is carried out with required longitudinal and directional controls. Initially, the selected empennage configuration in chapter 2 i.e configuration selection will be reviewed and then using Roskam procedure (Roskam, 2005), the vertical tail and horizontal tail are designed. The selection of following parameters of vertical and horizontal tails will be presented.

- Sweep Angle
- Taper Ratio
- Aspect Ratio
- Thickness Ratio
- Type of Airfoil
- Dihedral Angle
- Incidence Angle

The designed empennage will be evaluated using AAA (Advanced Aircraft Analysis) program. Once the empennage sizing is completed, the longitudinal and directional controls are selected. The CAD drawings of the overall empennage design will be presented using CATIA V5 (Computer Aided Three-Dimensional Interactive Application) software.

7.2 OVERALL EMPENNAGE DESIGN

The proposed aircraft uses a conventional configuration empennage. The T-tail configuration is selected in chapter 2 for the proposed aircraft as most of the regional turboprop airplanes in the market are using the same configuration. The main reason for selecting T-tail configuration is that the horizontal tail is above most of the effects of downwash from the propeller and as well as airflow from the wings. This allows the elevator for consistent control movements

throughout most of the mission phases as it is operated in undisturbed airflow. The elevator effectiveness can be improved by using T-tail and even the induced drag is reduced because of its position.

Location of the Empennage

The main objective of the tail is to counter the moments produced by the wing and the tail sizing in some way in relation with wing size. The location of the empennage amounts to deciding the empennage moment arms X_v, X_h and X_c.

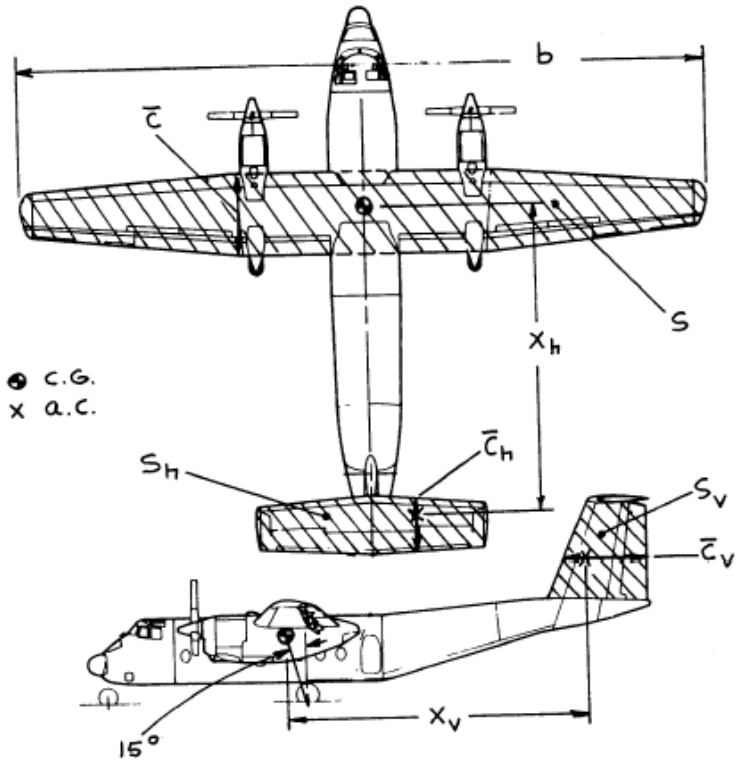

Figure 131: Definition of empennage moment arms

The X_v and X_h are defined in the above figure, whereas X_c is related to canard configuration. There is no canard for the proposed configuration, so the location of empennage is determined only for the T-tail. As per the Raymer (Raymer, 2012), the vertical tail arm is about 50-55% of the fuselage length for aircraft with the engines on the wing. The fuselage length is obtained as 72.7 ft in fuselage design chapter.

Therefore,

$$X_v = 0.50 * \text{length of the fuselage} = 0.50 * 72.7 = 36.35 \text{ ft}$$

For the T-tail horizontal stabilizer location, the following Roskam (Roskam, 2005) data of comparable aircraft is used to select X_h. The value of X_h is assumed as 41.6 ft from the below figure (Roskam, 2005).

$$X_v = 36.35 \text{ ft or } 11.08 \text{ m} \quad (7.1)$$

$$X_h = 41.6 \text{ ft or } 12.68 \text{ m} \quad (7.2)$$

Type	Wing Area S ft^2	Wing mgc $\bar{c}$ ft	Wing Airfoil root/tip NACA*	Hor. Tail Area S_h ft^2	S_e/S_h	x_h ft	$\bar{V}_h$	Elevator Chord root/tip $fr.c_h$
CASA C-212-200								
	431	6.68	653-218	135	0.35	24.9	1.17	.49/.53
SHORTS								
330	453	6.06	NA	83.6	0.33	27.3	0.83	0.50
360	453	6.06	NA	106	0.39	33.0	1.28	0.48
BEECH								
1900	303	5.35	23018/23015	71.3	0.43	30.3	1.33**	.43/.48
B200	303	5.35	23018.5/23011.3	68.0	0.28	24.6	0.91	0.42
CESSNA CONQUEST			*** I airfoils carry -63 mod.					
I***	225	4.73	23018/23009	62.0	0.33	16.4	0.95	.36/.43
II	254	4.98	23018/23009	63.4	0.29	18.0	0.90	.43/.40
GA Ic	610	8.28	NA	134	0.26	36.5	0.97	.29/.32
GAF N22B	324	5.94	23018	78.0	1.00	20.6	0.83	stabilator
Fokker F27-200								
	754	8.43	64-421/64-415	172	0.27	36.0	0.98	.29/.34
DeHAVILLAND CANADA								
DHC-6-300	420	6.50	NA	100	0.35	24.8	0.91	0.47
DHC-7	860	9.45	63A418/63A415	217	0.46	41.6	1.11	.42/.47
DHC-8	585	6.51	NA	154	0.42	36.3	1.47	.41/.43
EMB-120	409	6.57	23018/23012	108	0.39	31.7	1.27	.38/.44
BAe 31	270	5.27	63A418/63A412	84.0	0.46	20.7	1.22	.43/.48
Metro III	309	6.03	65_3A215/64_3A415	76.0	0.28	26.1	1.07	.31/.48

Figure 132: Horizontal tail volume and elevator data for regional turboprop airplanes

Size of the Empennage

The lift produced by the tail is directly proportional to the tail area and the tail effectiveness is proportional to the product of tail area and tail moment arm which leads to tail volume coefficient. Therefore, the tail sizing is all about determining the tail area using the tail volume coefficient and obtained tail moment arm as shown below.

$$\bar{V}_h = \frac{X_h S_h}{S_W \bar{c}} \quad (7.3)$$

$$\bar{V}_V = \frac{X_V S_V}{S_W b} \qquad (7.4)$$

Where,

S_W = Wing area obtained as 809 sq.ft in performance sizing

b = Wing span obtained as 98.53 ft in wing sizing

$\bar{c}$ = Mean aerodynamic chord obtained as 8.685 ft in wing sizing

$\bar{V}_h$= Horizontal tail volume coefficient

$\bar{V}_V$= Vertical tail volume coefficient

The tail volume coefficient is assumed from Roskam data (Roskam, 2005) of comparable aircraft as shown in above figure for horizontal tail and below figure for vertical tail as follows

$$\bar{V}_h = 1.05$$

$$\bar{V}_V = 0.077$$

Type	Wing Area S ft^2	Wing Span b ft	Vert. Tail Area S_v ft^2	S_r/S_v	x_v ft	$\bar{V}_v$	Rudder Chord root/tip $fr.c_v$	S_a/S	Ail. Span Loc. in/out fr.b/2	Ail. Chord in/out $fr.c_w$
CASA C-212-200										
	431	62.3	77.5	0.41	24.8	0.072	0.41	0.061	.69/1.0	.24/.26
SHORTS										
330	453	74.7	93.1	0.26	27.3	0.075	0.41	0.061	.70/.95	0.27
360	453	74.7	91.4	0.37	33.9	0.091	.39/.36	0.074	.69/.98	0.27
BEECH										
1900*	303	54.5	47.5	0.35	26.5	0.076	.40/.38	0.064	.60/1.0	0.21
B200	303	54.5	52.3	0.29	20.5	0.065	.47/.41	0.059	.60/1.0	0.21
CESSNA CONQUEST										
I	225	44.1	41.3	0.38	17.1	0.071	.46/.38	0.060	.61/.86	.29/.28
II	254	49.3	43.5	0.37	18.7	0.065	.48/.33	0.058	.62/.89	.30/.32
GA Ic	610	78.3	117	0.25	35.4	0.087	.29/.33	0.061	.65/.98	.27/.22
GAF N22B	324	54.2	70.2	0.44	21.6	0.086	.49/.43	0.085	.54/1.0	0.24
Fokker F27-200										
	754	95.2	153	0.30	36.0	0.077	.33/.29	0.050	.69/.98	.31/.29
DeHAVILLAND CANADA										
DHC-6-300	420	65.0	82.0	0.42	25.7	0.077	.35/.44	0.079	.44/.97	0.20
DHC-7	860	93.0	170	0.28	35.7	0.076	.25/.30	0.027	.81/1.0	.27/.31
DHC-8	585	84.0	190	0.26	31.4	0.121	.27/.35	0.031	.80/1.0	.23/.22
EMB-120	409	64.9	74.3	0.38	27.3	0.076	.32/.31	0.084	.63/.97	0.24
BAe 31	270	52.0	83.1	0.26	20.7	0.120	.34/.39	0.061	.59/.97	.28/.30
Metro III	309	57.0	56.0	0.35	27.9	0.089	.37/.56	0.046	.61/.98	.31/.36

* 1900 also has taillets on horizontal tail.

Figure 133: Vertical tail volume and rudder data for regional turboprop airplanes

Using the equations (7.3) and (7.4), the horizontal tail and vertical tail areas are calculated as

$$S_h = \frac{\bar{V}_h S_W \bar{c}}{X_h} = \frac{1.05 * 809 * 8.685}{41.6} = 177.34 \text{ sq. ft}$$

$$S_V = \frac{\bar{V}_V S_W b}{X_V} = \frac{0.077 * 809 * 98.53}{36.35} = 168.85 \text{ sq. ft}$$

7.3 DESIGN OF HORIZONTAL STABILIZER

The design of horizontal stabilizer includes the selection of following parameters

- **Aspect Ratio**

  As per the Raymer, the Aspect ratio of the horizontal stabilizer is determined as 50% of the wing aspect ratio which is given by

  $$AR_h = 0.5 * AR_W = 0.5 * 12 = 6 \quad (7.5)$$

  The calculated aspect ratio is within the given range of values of regional turboprop by Roskam as shown in below figure (Roskam, 2005). The aspect ratio is given by

  $$AR_h = \frac{{b_h}^2}{S_h}$$

  Therefore, the span of the horizontal stabilizer is calculated as follows

  $$b_h = \sqrt{AR_h S_h} \quad (7.6)$$

  $$b_h = \sqrt{6 * 177.34} = 32.61 \text{ ft or } 9.94 \text{ m}$$

Type	Dihedral Angle, Γ_h deg.	Incidence Angle, i_h deg.	Aspect Ratio, A_h	Sweep Angle, $\Lambda_{c/4_h}$ deg.	Taper Ratio, λ_h
Homebuilts	+5 - -10	0 fixed to variable	1.8 - 4.5	0 - 20	0.29 - 1.0
Single Engine Prop. Driven	0	-5 - 0 or variable	4.0 - 6.3	0 - 10	0.45 - 1.0
Twin Engine Prop Driven	0 - +12	0 fixed to variable	3.7 - 7.7	0 - 17	0.48 - 1.0
Agricultural	0 - +3	0	2.7 - 5.4	0 - 10	0.59 - 1.0
Business Jets	-4 - +9	-3.5 fixed	3.2 - 6.3	0 - 35	0.32 - 0.57
Regional Turbo-Props.	0 - +12	0 - 3 fixed to variable	3.4 - 7.7	0 - 35	0.39 - 1.0
Jet Transports	0 - +11	variable	3.4 - 6.1	18 - 37	0.27 - 0.62
Military Trainers	-11 - +6	0 fixed to	3.0 - 5.1	0 - 30	0.36 - 1.0
Fighters	-23 - +5	0 fixed to variable	2.3 - 5.8	0 - 55	0.16 - 1.0
Mil. Patrol, Bomb and Transports	-5 - +11	0 fixed to variable	1.3 - 6.9	5 - 35	0.31 - 0.8
Flying Boats, Amph. and Float Airplanes	0 - +25	0 fixed	2.2 - 5.1	0 - 17	0.33 - 1.0
Supersonic Cruise Airplanes	-15 - 0	0 fixed to variable	1.8 - 2.6	32 - 60	0.14 - 0.39

Figure 134: Horizontal tail planform design parameters

- **Taper Ratio**

  Taper ratio is defined as the ratio of wing root chord length to the tip chord length. Taper ratio is mainly for elliptical lift distribution, but it is not a requirement for tail. The tail taper ratio is mainly used for reduction in tail weight. The Taper ratio of horizontal stabilizer is assumed to be 0.6 from the given comparable aircraft data by Roskam as shown above (Roskam, 2005). The root chord of the horizontal stabilizer can be determined by using the below equation

$$C_{r_h} = \frac{2S_h}{b_h(1+\lambda_h)} \qquad (7.7)$$

$$C_{r_h} = \frac{2 * 177.34}{32.61(1+0.6)} = 6.797 \text{ ft or } 2.07 \text{ m}$$

  The tip chord of the horizontal stabilizer is calculated as

$$C_{t_h} = \lambda_h * C_{r_h} = 0.6 * 6.797 = 4.07 \text{ ft or } 1.24 \qquad (7.8)$$

The mean aerodynamic chord of the horizontal stabilizer is determined as

$$\bar{c}_h = \left(\frac{2}{3}\right) C_{r_h} \left(\frac{1 + \lambda_h + {\lambda_h}^2}{1 + \lambda_h}\right) \quad (7.9)$$

$$\bar{c}_h = \left(\frac{2}{3}\right) * 6.797 * \left(\frac{1 + 0.6 + 0.6^2}{1 + 0.6}\right) = 5.55 \text{ ft or } 1.69 \text{ m}$$

The spanwise mean aerodynamic chord location of the horizontal stabilizer is given by

$$\bar{Y}_h = \left(\frac{b_h}{6}\right)\left(\frac{1 + 2\lambda_h}{1 + \lambda_h}\right) \quad (7.10)$$

$$\bar{Y}_h = \left(\frac{32.61}{6}\right)\left(\frac{1 + 2 * 0.6}{1 + 0.6}\right) = 7.473 \text{ ft or } 2.28 \text{ m}$$

- **Sweep Angle**

  The sweep angle is the angle between a perpendicular to the centerline and the leading edge of the wing. As per the Raymer (Raymer, 2012), the leading-edge sweep angle of the horizontal tail is about 5 degrees more than the leading sweep angle of the wing. The obtained leading-edge sweep angle of the wing is 2 degrees. Therefore, the leading-edge angle of the horizontal tail is 7 degrees.

$$\wedge_{LE_h} = 7^o \quad (7.11)$$

  For low speed aircraft, the horizontal tail sweep angle is set to provide a straight hinge line for the elevator, which usually has the right and left sides connected to reduce flutter tendencies.

- **Thickness Ratio**

  The selection of thickness ratio is important to ensure that the critical Mach number for the tails is higher than that of the wing. As per Roskam (Roskam, 2005), the typical thickness ratio for horizontal tail in use is 0.09 to 0.18. The thickness ratio for the horizontal tail is assumed to be 0.12 for the proposed design.

- **Airfoil**

  The horizontal tail airfoil needs to provide positive and negative lift based on the center of gravity location during the mission and hence airfoil needs to be symmetric. The airfoil needs to be selected based on the selected thickness ratio and hence the horizontal tail airfoil is selected as NACA 0012 for both root and the tip.

- **Incidence Angle**

  The incidence angle of the horizontal tail is assumed as 0 degrees from the similar aircraft data given by Roskam (Roskam, 2005).

- **Dihedral Angle**

  The tail dihedral angle is used for lateral stability adjustment and control adjustment. The dihedral angle of the horizontal stabilizer is assumed to be 0 degrees by comparing to the similar aircraft data provided by the Roskam (Roskam, 2005).

7.4 DESIGN OF VERTICAL STABILIZER

- **Aspect Ratio**

  T-tail aircraft have lower vertical aspect ratios to reduce the weight impact of the horizontal tail's location on top of the vertical tail. The Aspect ratio of the vertical stabilizer for the proposed design is obtained from the similar aircraft data as 1.6.

$$AR_V = 1.6 \tag{7.12}$$

  Therefore, the span of the vertical stabilizer is calculated as follows

$$b_V = \sqrt{AR_V S_V} \tag{7.13}$$

$$b_V = \sqrt{1.6 * 168.85} = 16.436 \text{ ft or } 5 \text{ m}$$

Type	Dihedral Angle, Γ_V deg.	Incidence Angle, i_V deg.	Aspect Ratio, A_V	Sweep Angle, $\Lambda_{c/4_V}$ deg.	Taper Ratio, λ_V
Homebuilts	90	0	0.4 - 1.4	0 - 47	0.26 - 0.71
Single Engine Prop. Driven	90	0	0.9 - 2.2	12 - 42	0.32 - 0.58
Twin Engine Prop Driven	90	0	0.7 - 1.8	18 - 45	0.33 - 0.74
Agricultural	90	0	0.6 - 1.4	0 - 32	0.43 - 0.74
Business Jets	90	0	0.8 - 1.6	28 - 55	0.30 - 0.74
Regional Turbo-Props.	90	0	0.8 - 1.7	0 - 45	0.32 - 1.0
Jet Transports	90	0	0.7 - 2.0	33 - 53	0.26 - 0.73
Military Trainers	90	0	1.0 - 2.9	0 - 45	0.32 - 0.74
Fighters	75 - 90	0	0.4 - 2.0	9 - 60	0.19 - 0.57
Mil. Patrol, Bomb and Transports	90	0	0.9 - 1.9	0 - 37	0.28 - 1.0
Flying Boats, Amph. and Float Airplanes	90	0	1.2 - 2.4	0 - 32	0.37 - 1.0
Supersonic Cruise Airplanes	75 - 90	0	0.5 - 1.8	37 - 65	0.20 - 0.43

Figure 135: Vertical tail planform design parameters

- **Taper Ratio**

The Taper ratio of vertical stabilizer is assumed to be 0.6 from the given comparable aircraft data by Roskam as shown above (Roskam, 2005). The root chord of the vertical stabilizer can be determined by using the below equation

$$C_{r_V} = \frac{2S_V}{b_V(1+\lambda_V)} \tag{7.14}$$

$$C_{r_V} = \frac{2 * 168.85}{16.436(1+0.6)} = 12.84 \text{ ft or } 3.91 \text{ m}$$

The tip chord of the vertical stabilizer is calculated as

$$C_{t_V} = \lambda_V * C_{r_V} = 0.6 * 12.84 = 7.7 \text{ ft or } 2.35 \text{ m} \tag{7.15}$$

The mean aerodynamic chord of the vertical stabilizer is determined as

$$\bar{c}_V = \left(\frac{2}{3}\right) C_{r_V} \left(\frac{1+\lambda_V+{\lambda_V}^2}{1+\lambda_V}\right) \tag{7.16}$$

$$\bar{c}_V = \left(\frac{2}{3}\right) * 12.84 * \left(\frac{1 + 0.6 + 0.6^2}{1 + 0.6}\right) = 10.486 \text{ ft or } 3.20 \text{ m}$$

The spanwise mean aerodynamic chord location of the vertical stabilizer is given by

$$\bar{Y}_V = 2\left(\frac{b_V}{6}\right)\left(\frac{1 + 2\lambda_V}{1 + \lambda_V}\right) \quad (7.17)$$

$$\bar{Y}_V = 2\left(\frac{16.436}{6}\right)\left(\frac{1 + 2 * 0.6}{1 + 0.6}\right) = 7.533 \text{ ft or } 2.30 \text{ m}$$

- **Sweep Angle**

  As the proposed aircraft travels at low subsonic speeds, hence low sweep angle is preferred for the vertical tail. The quarter chord sweep angle of vertical tail is assumed as 16 degrees from the comparable aircraft data. The below equation from Raymer is used to calculate the leading-edge sweep angle of the vertical tail (Raymer, 2012).

$$tan \wedge_{LE_V} = tan \wedge_{c/4_V} + \left[\frac{1 - \lambda_V}{A_V(1 + \lambda_V)}\right] \quad (7.18)$$

$$\wedge_{LE_V} = 20^o$$

- **Thickness Ratio**

  The selection of thickness ratio is important to ensure that the critical Mach number for the tails is higher than that of the wing. As per Roskam (Roskam, 2005), the typical thickness ratios for vertical tail in use is 0.09 to 0.18. The thickness ratio for the vertical tail is assumed to be 0.12 for the proposed design.

- **Airfoil**

  The airfoil needs to be selected based on the selected thickness ratio and to maintain the symmetricity of the aircraft about the fuselage longitudinal axis, the airfoil should be symmetric. Hence the vertical tail airfoil is selected as NACA 0012 for both root and the tip.

- **Incidence Angle**

  The incidence angle of the vertical tail is assumed as 0 degrees from the similar aircraft data.

- **Dihedral Angle**

  The dihedral angle of the vertical stabilizer is assumed to be 90 degrees by comparing to the similar aircraft data.

7.5 EMPENNAGE DESIGN EVALUATION

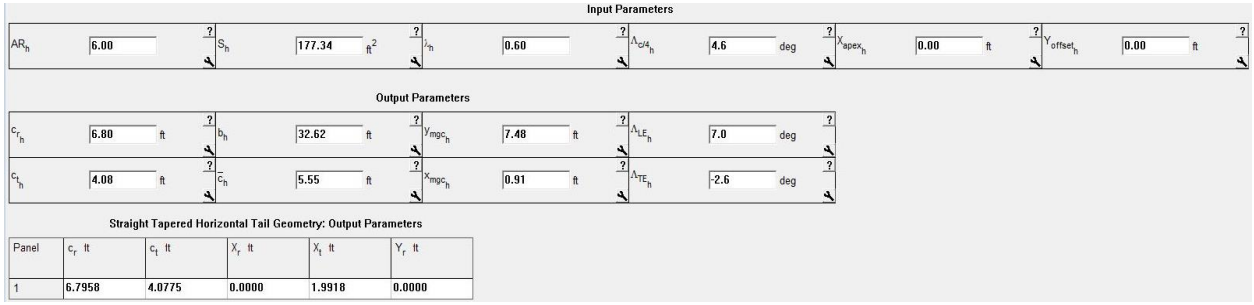

Figure 136: Input parameters of horizontal tail in AAA program

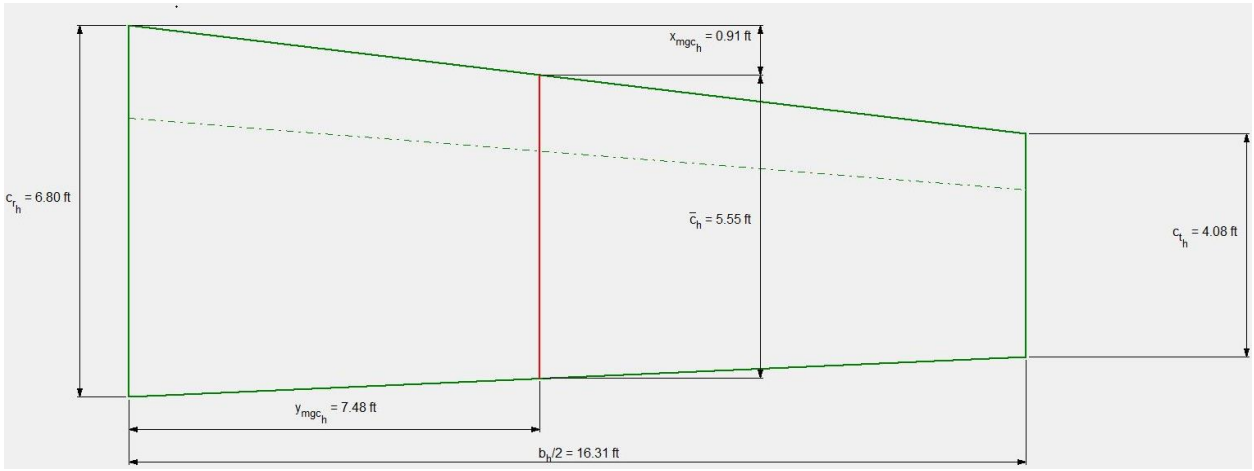

Figure 137: Horizontal tail geometry obtained in AAA program

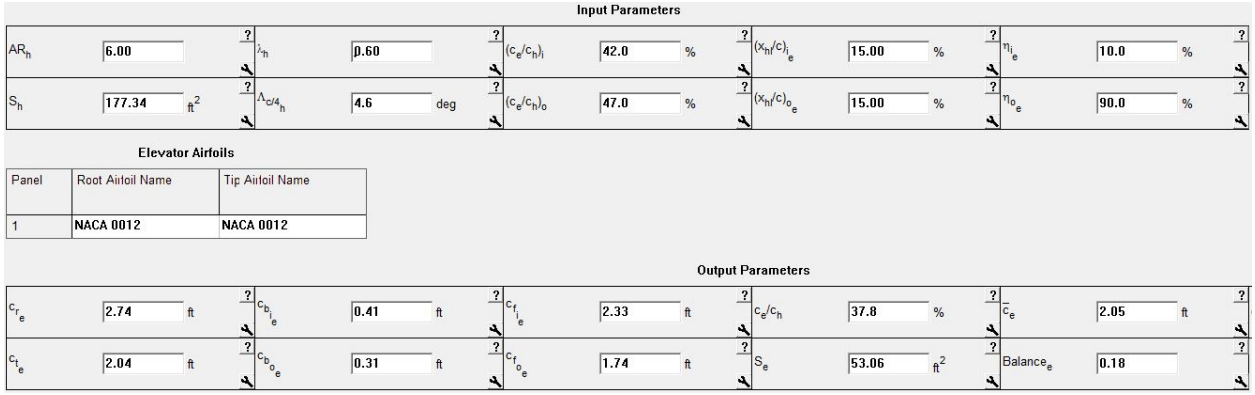

Figure 138: Input parameters of elevator in AAA program

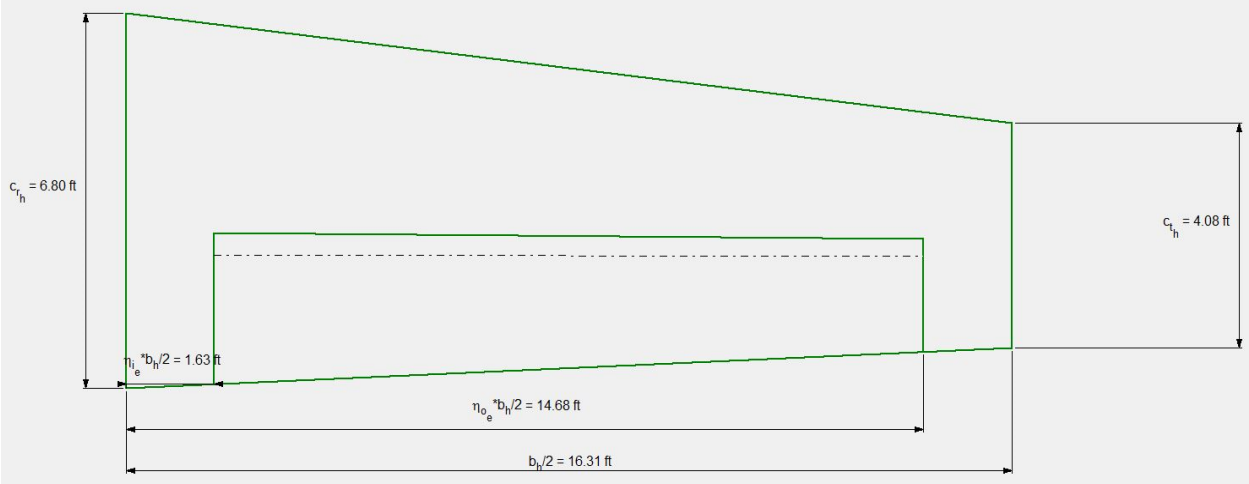

Figure 139: Elevator sizing and location obtained in AAA program

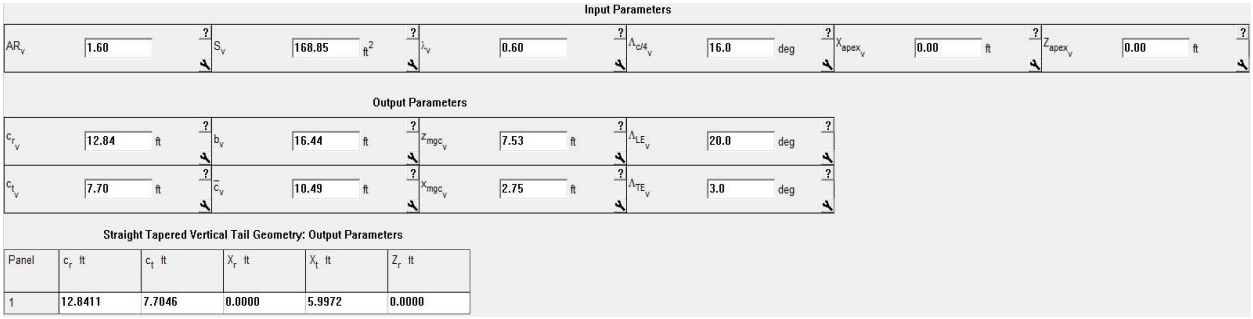

Figure 140: Input parameters of vertical tail in AAA program

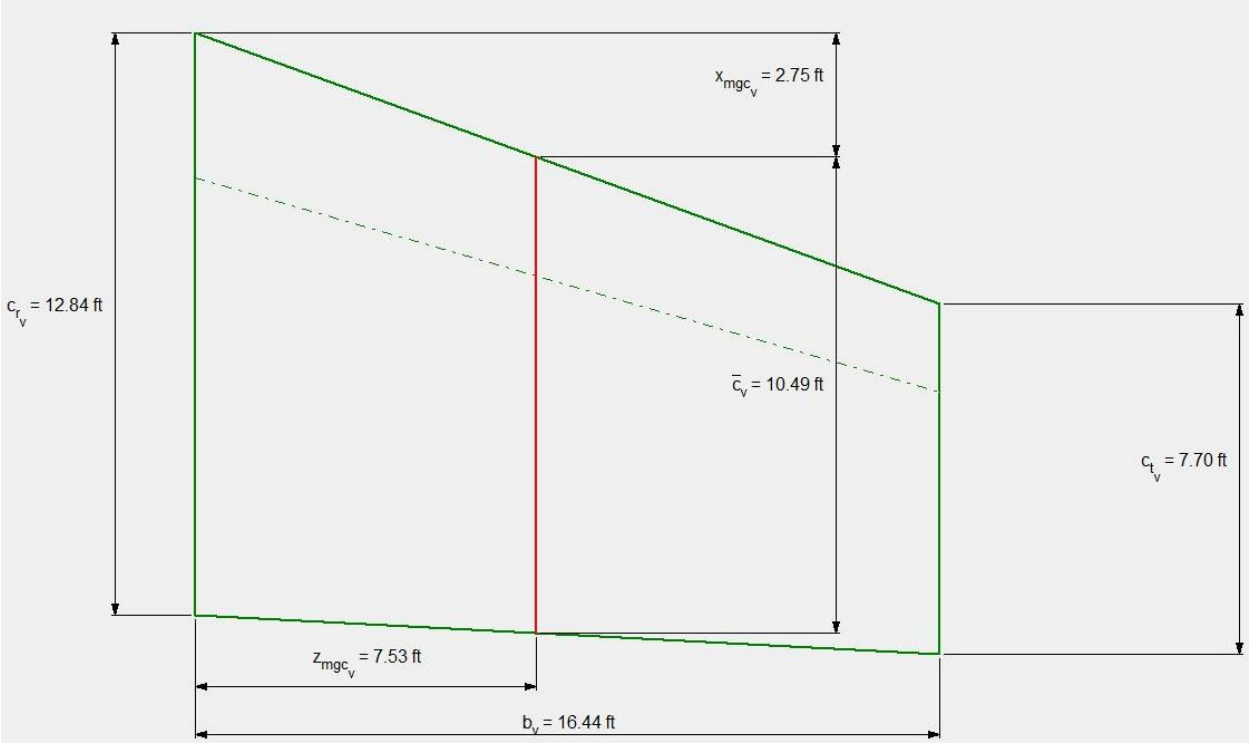

Figure 141: Vertical tail geometry obtained in AAA program

Input Parameters

AR_v	1.60		λ_v	0.60		$(c_f/c_v)_i$	25.0	%	$(x_{hl}/c)_{i_r}$	15.00	%
S_v	168.85	ft^2	$\Lambda_{c/4_v}$	16.0	deg	$(c_f/c_v)_o$	30.0	%	$(x_{hl}/c)_{o_r}$	15.00	%

η_{i_r}	10.0	%									
η_{o_r}	90.0	%									

Rudder Airfoils

Panel	Root Airfoil Name	Tip Airfoil Name
1	NACA 0012	NACA 0012

Output Parameters

c_{r_r}	3.08	ft	$c_{b_{i_r}}$	0.46	ft	$c_{f_{i_r}}$	2.62	ft	c_f/c_v	23.4	%
c_{t_r}	2.47	ft	$c_{b_{o_r}}$	0.37	ft	$c_{f_{o_r}}$	2.10	ft	S_r	31.00	ft^2

$\bar{c}_r$	2.37	ft	
$Balance_r$	0.18		

Figure 142: Input parameters of rudder in AAA program

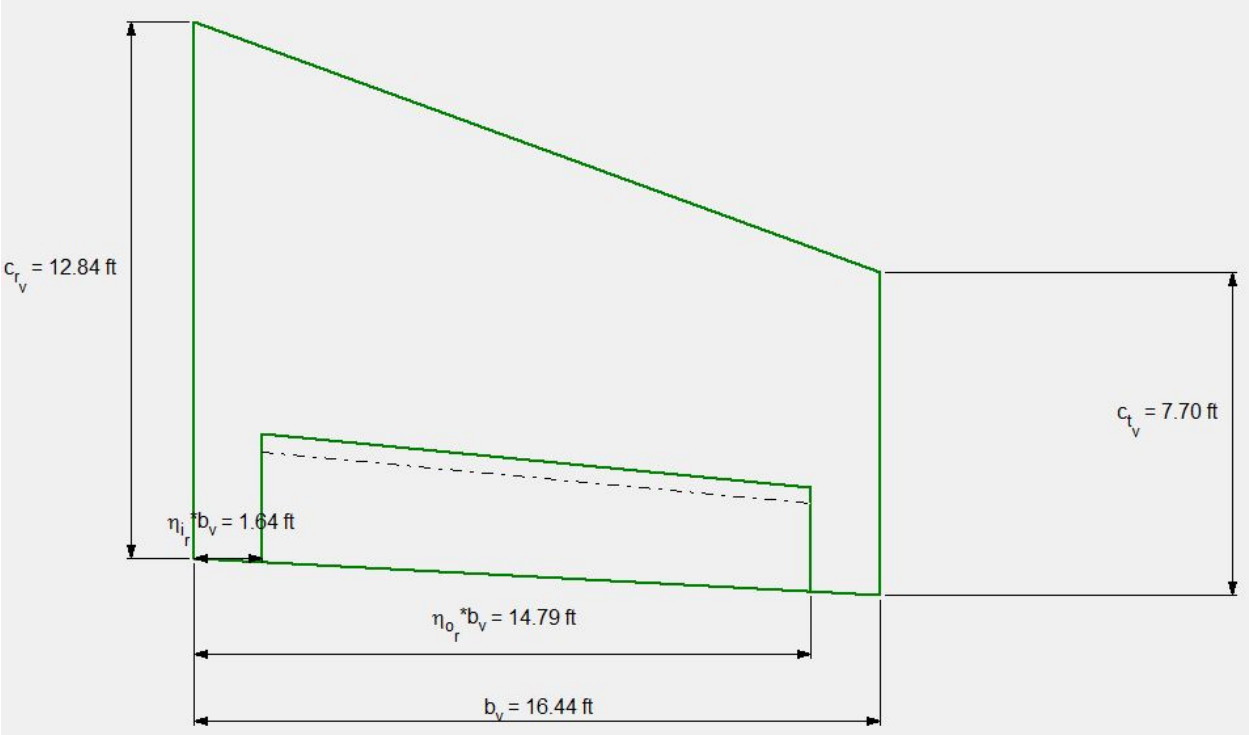

Figure 143: Rudder geometry obtained in AAA program

7.6 DESIGN OF LONGITUDINAL AND DIRECTIONAL CONTROLS

The longitudinal controls in the proposed design are elevators and directional control is rudder. The proposed aircraft uses one elevator on port side and another elevator on starboard side of the horizontal tail and one rudder on the vertical tail like comparable aircraft. Elevators and rudders generally begin at the side of the fuselage and extend to the tip or to 90% of the tail span (Raymer, 2012). Elevators and rudders are typically about 25-50% of the tail chord (Raymer, 2012). The proposed deign elevators and rudder chord are selected within that range of the tail chord. For the T-tail configuration the attachment of horizontal tail on top of the vertical tail is crucial and hence the span of the elevator begins at 10% from the root chord and extend to 90% of the horizontal tail span for the proposed design. Similarly, the rudder starts at 10% from the root and extend to 90% of the vertical tail span. The dimensions of these controls are shown in below CAD drawings.

7.7 CAD DRAWINGS

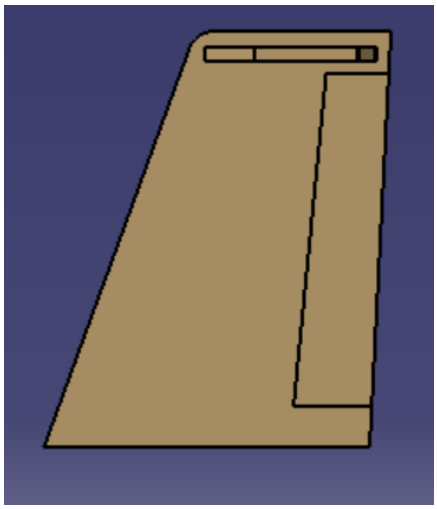

Figure 144: Front view of empennage

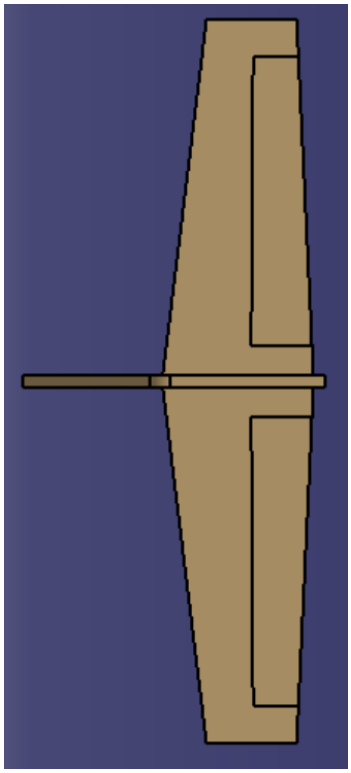

Figure 145: Top view of empennage

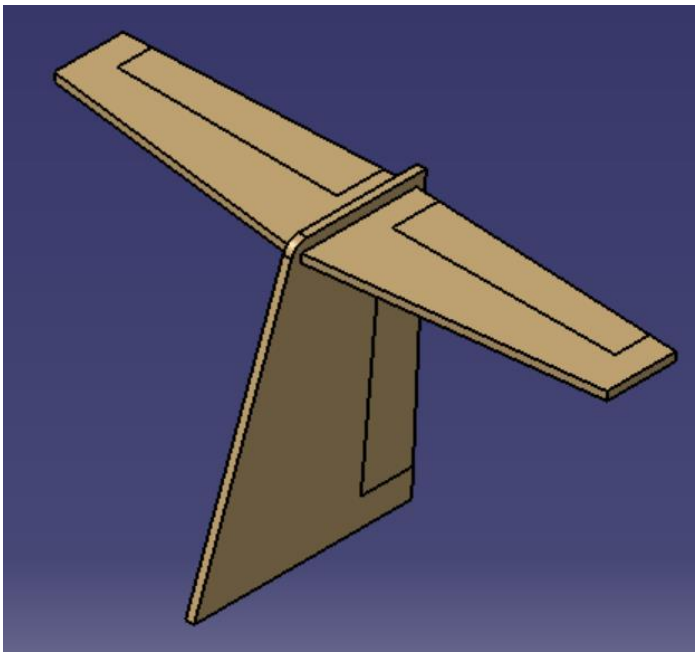

Figure 146: Isometric view of empennage

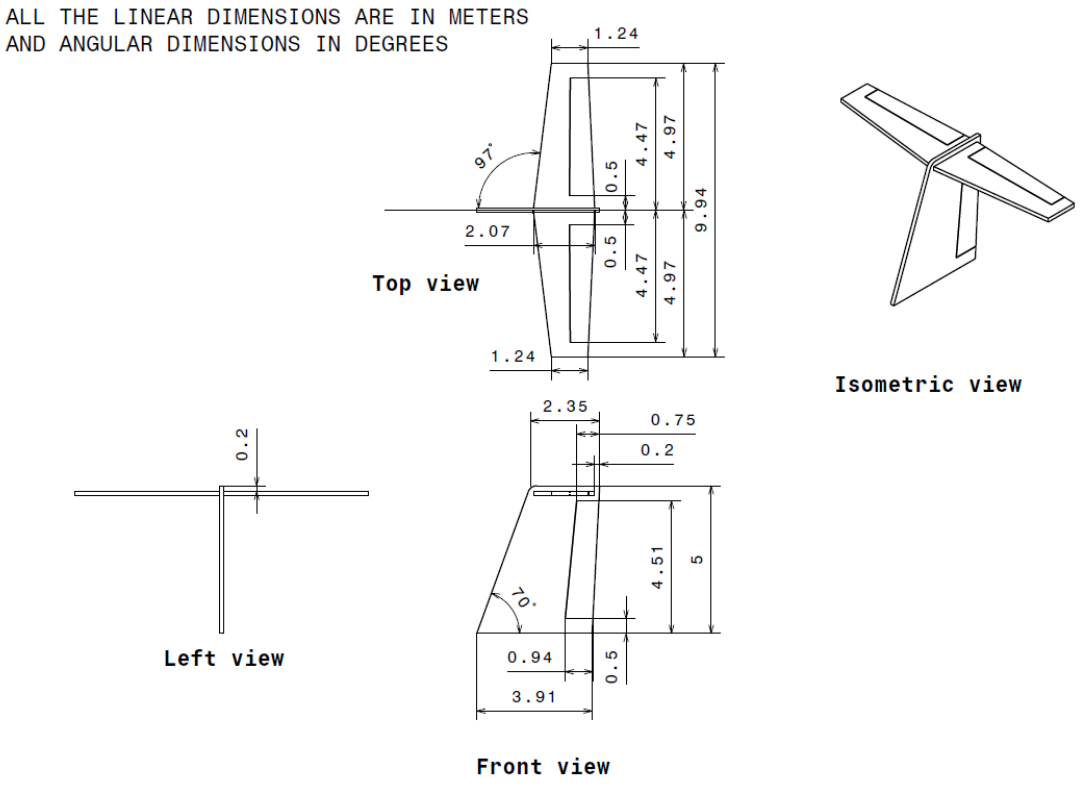

Figure 147: Drawing of empennage with elevators and rudder

Placement of Empennage on the Fuselage

The empennage is approximately placed on the fuselage by using the moment arms. A leading-edge extension is placed for the structural strength between empennage and fuselage as shown below.

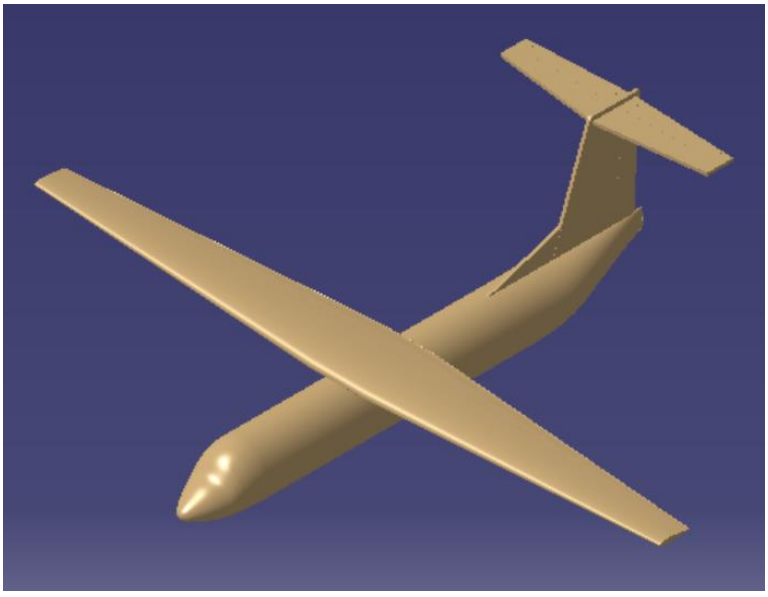

Figure 148: Empennage placement on the fuselage

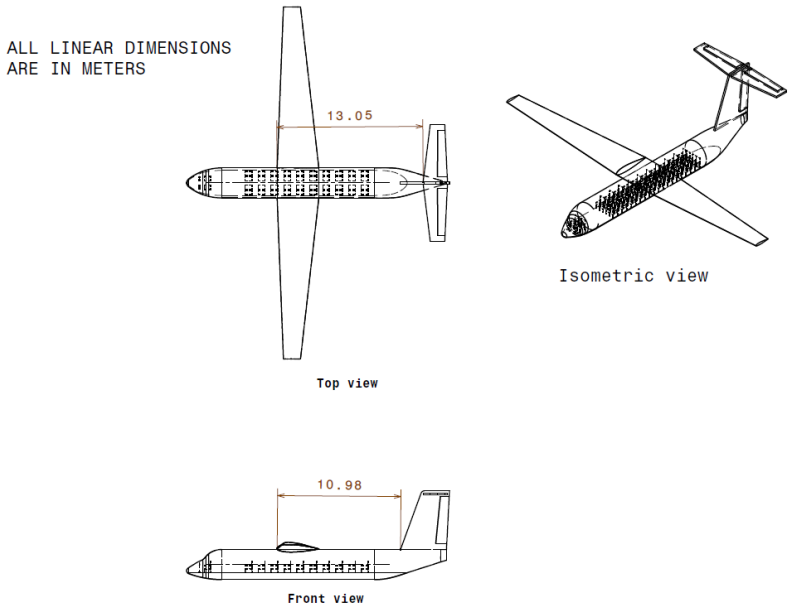

Figure 149: Drawing of empennage placement

7.8 DISCUSSION

This chapter presented a detailed design of Empennage with longitudinal and directional controls by use of Roskam procedure and Raymer equations. The vertical and horizontal tails are designed with assumptions of tail volume coefficient, taper ratio, aspect ratio, dihedral angle, incidence angle, sweep angle which are within the range of data provided by Roskam. The calculated values of span, root chord length, tip chord length, mean aerodynamic chord of both vertical and horizontal tails are perfectly matching with the values obtained in AAA program. The rudder and elevators are designed based on the comparable aircraft data and the typical range provided by the Raymer. The CAD drawings are made based on the data obtained in the design of vertical tail with rudder and horizontal tail with elevators.

7.9 CONCLUSIONS

The proposed design uses a T-tail configuration. The assumptions are quite reasonable by comparing with reference aircraft data and the obtained geometry of empennage by assumptions and manual calculations are closely matching with AAA program. The obtained data satisfies the proposed design mission requirements and with these data we can proceed to landing gear design and stability and control analysis.

CHAPTER 8: LANDING GEAR DESIGN AND WEIGHT & BALANCE ANALYSIS

8.1 INTRODUCTION

This chapter presents a detailed landing gear design and weight and balance analysis. The wing and empennage geometries are already obtained in previous chapters. The following landing gear characteristics are determined based on the obtained mission weights and performance constraints.

- Type, size and number of tires
- Preliminary arrangement
- Retraction feasibility

The fixed landing gear imposes high drag above 150 knots cruise speed of the aircraft. As the proposed aircraft cruise speed is 275 knots and hence, retractable tricycle landing gear is used. Initially, the landing gear is placed based on the center of gravity (CG) range of the aircraft. The CG range is obtained from the estimated weight and balance for an assumed disposition of the landing gear. Once the CG range is obtained, then the landing gear is designed based on the two geometric criteria such as tip-over criteria and ground clearance criteria. The landing gear design requires an iteration process until the actual CG location of the aircraft is obtained.

8.2 ESTIMATION OF THE CENTER OF GRAVITY LOCATION FOR THE AIRPLANE

The landing gear disposition is dependent on the CG location of the proposed aircraft. In this section, the CG location of the major subgroups of proposed aircraft is determined. The center of gravity location for the aircraft is determined using weight and balance method. At this stage, the initial component weight breakdown is determined using the obtained take-off weight. As per the Roskam (Roskam, 2005), using class I weight estimating method, the weight of major airplane components can be expressed as a simple fraction of one of the following weights.

- Gross take-off weight, W_{TO}

- Empty weight, W_E
- Flight design gross weight, GW

The take-off weight and empty weight are already obtained in weight sizing chapter and for civil airplanes the flight design gross weight is same as gross take-off weight. The component weight breakdown is carried out by using the similar airplanes data for weight ratios as shown below.

Table 29: Component weight fractions for similar airplanes and proposed aircraft

Type	**DHC7-102**	**F-27-500**	**F-27-200**	**Proposed Aircraft**
Empty Weight/GW	0.605	0.548	0.537	0.563
Power Plant/GW	0.107	0.110	0.122	0.113
Fixed Equipment Weight/GW	0.169	0.144	0.134	0.149
Wing Group/GW	0.111	0.100	0.104	0.105
Empennage Group/GW	0.030	0.024	0.024	0.026
Fuselage Group/GW	0.106	0.114	0.099	0.106
Nacelle Group/GW	0.042	0.015	0.015	0.024
Landing Gear Group/GW	0.039	0.041	0.042	0.041

The mission weights obtained in chapter 3 are as follows:

Table 30: Mission weights

Take-off Weight, W_{TO} (lbs)	54000
Empty Weight, W_E (lbs)	31926

Payload Weight, W_{PL} (lbs)	8200
Fuel Weight, W_F (lbs)	1891
Crew Weight, W_{crew} (lbs)	820
Operating Empty Weight, W_{OE} (lbs)	33016
Battery Weight, W_{Bat} (lbs)	10893

Using the averaged weight fractions from Table 29, the following preliminary component weights are obtained for the proposed aircraft.

Table 31: Subgroup component weight summary for the proposed aircraft

Component	**First weight estimate (lbs)**	**Adjustment**	**Class I weight (alum.) lbs**
Wing	5670	274	5944
Empennage	1404	68	1472
Fuselage	5742	277	6019
Nacelles	1296	63	1359
Landing gear	2196	106	2302
Power plant	6102	295	6397
Fixed equipment	8046	388	8434
Empty weight	30456	1470	31926
Payload			8200
Crew			820
Fuel weight			1891
Trapped fuel and oil			270
Battery weight			10893
Take-off weight			54000

The sum of weights in the first column yield an empty weight of 30456 lbs instead of desired empty weight of 31926 lbs. The difference is due to round-off errors in the weight fractions used. This difference is distributed to overall items in proportion to their component weights i.e the wing adjusted number is arrived at by multiplying 1470 lbs by 5670/30456. Similarly, all the component weights are adjusted.

Using the obtained geometric parameters of fuselage, wing and empennage, the CG locations can be determined. The length of the nacelle is assumed same as the length of the engine and length of the engine is selected as 7 ft from chapter 4. The location of CG's of major components can be determined as follows using below equations from Roskam (Roskam, 2005).

Table 32: Center of gravity locations of major components

Proposed aircraft components	**Equation**	**CG location from nose**
Fuselage	0.45 * length of the fuselage	32.71 ft
Wing	0.40 * $\bar{c}_w$	28.3 ft
Vertical stabilizer	0.30 * $\bar{c}_V$	65.70 ft
Horizontal stabilizer	0.30 * $\bar{c}_h$	68.71 ft
Nacelle	0.40 * length of the nacelle	22.68 ft

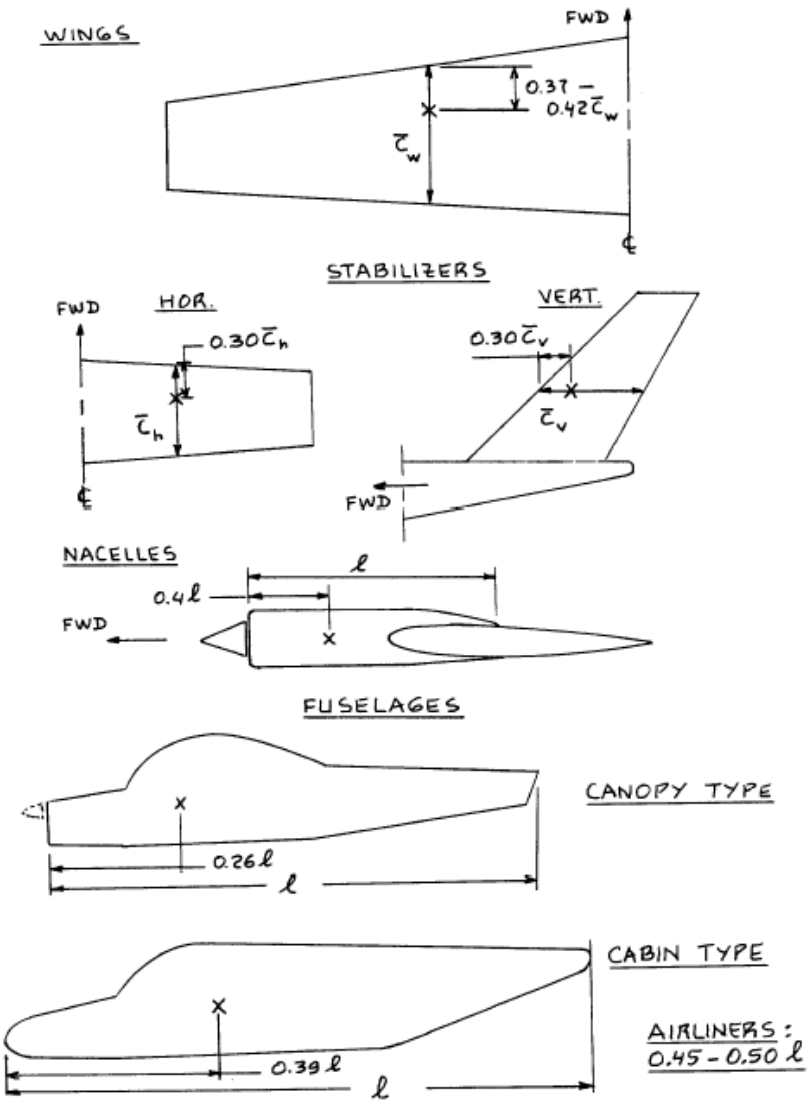

Figure 150: Location of center of gravity of major components

The components weight and coordinate data for the proposed aircraft are shown in below table by assuming the disposition of the landing gear. At this stage taking x and y coordinate data, the range of the CG is determined. The actual CG range is determined once the landing gear is designed, then the z coordinates will be calculated from the ground reference. The empty weight, operating empty weight and take-off weight CG locations are obtained using equations as shown below.

No.	Type of Component	W_i lbs	x_i in.	$W_i x_i$ inlbs	y_i in.	$W_i y_i$ inlbs	z_i in.	$W_i z_i$ inlbs
1.	Fuselage group	W_1	x_1	$W_1 x_1$	y_1	$W_1 y_1$	z_1	$W_1 z_1$
2.	Wing group							
3.	Empennage group							
4.	Engine group							
5.	Landing gear group							
6.	Fixed equipm't group							
	Empty weight: $W_E = \sum_{i=1}^{i=6} W_i$				$x_{cg_{W_E}} = (\sum_{i=1}^{i=6} W_i x_i)/W_E$			
7.	Trapped fuel and oil							
8.	Crew							
	Operating weight empty: $W_{OE} = \sum_{i=1}^{i=8} W_i$				$x_{cg_{W_{OE}}} = (\sum_{i=1}^{i=8} W_i x_i)/W_{OE}$			
9.	Fuel							
10.	Passengers							
11.	Baggage							
12.	Cargo							
13.	Military load							
	Take-off weight: $W_{TO} = \sum_{i=1}^{i=13} W_i$				$x_{cg_{W_{TO}}} = (\sum_{i=1}^{i=13} W_i x_i)/W_{TO}$			

Note: Locations for y_{cg} and for z_{cg} are found from similar equations.

Figure 151: Class 1 weight and balance calculation

Table 33: Components weight and coordinate data for the proposed aircraft

Type of Component	**Weight (lbs)**	**x (ft)**	**Wx (ft.lbs)**	**y (ft)**	**Wy (ft.lbs)**
Wing	5944	28.3	168205.9	0	0
Empennage	1472	67.24	98908.56	0	0
Fuselage	6019	32.71	196904.3	0	0
Nacelles	1359	22.68	30813.34	0	0
Landing gear: Nose gear	460	6.6	3036	0	0
Landing gear: Main gear	1842	32.85	60509.7	0	0
Power plant	6397	22.68	145073.1	0	0
Fixed equipment	8434	32.71	275887.6	0	0
Empty Weight	31926	30.68	979338.5	0	0
Crew: Pilots	410	6	2460	0	0
Crew: Attendants	410	54.72	22436.43	0	0
Trapped Fuel and Oil	270	29	7830	0	0

Operating Empty Weight	33016	30.65	1012065	0	0
Fuel	1891	28.3	53515.3	0	0
Batteries	10893	36.35	395960.6	0	0
Passengers	7000	32.71	228970	0	0
Baggage	1200	32.71	39252	0	0
Take-off weight	54000	32.03	1729763	0	0

The CG locations of major components are shown in below figure of CAD drawing

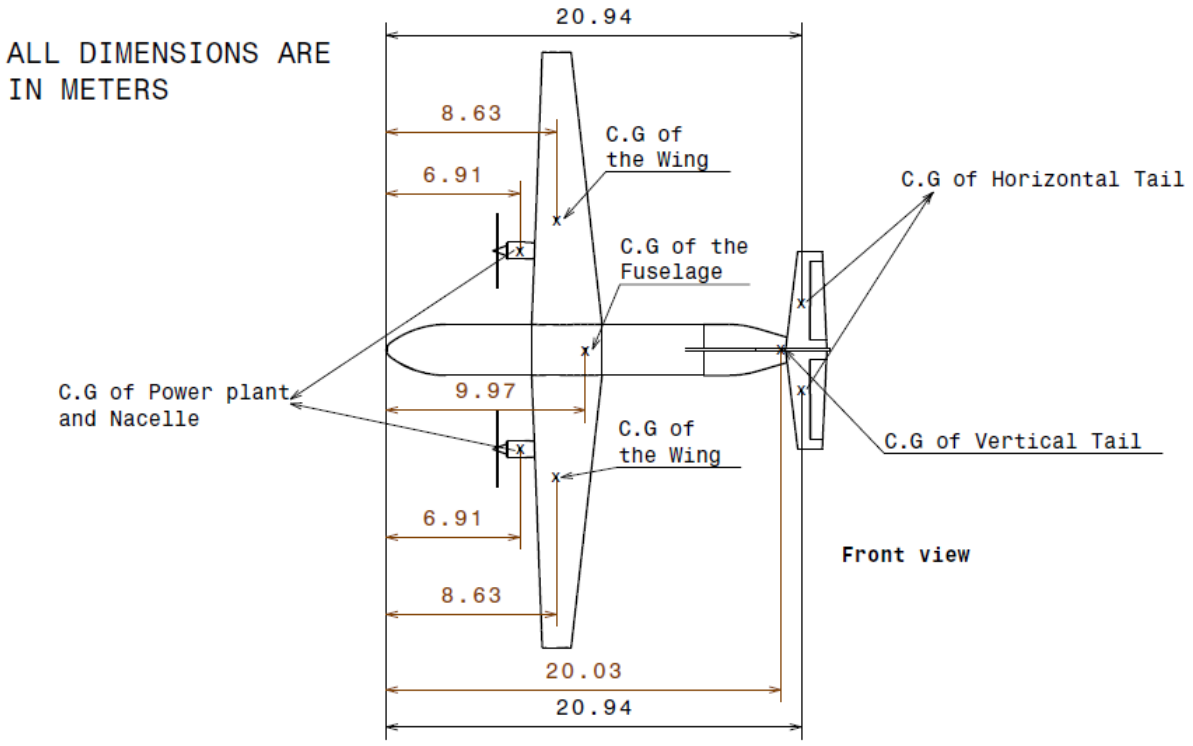

Figure 152: CAD drawing of CG location of major components from nose tip

The CG locations for different loading scenarios are calculated as follows

Table 34: CG locations for different loading scenarios

Loading scenarios	**CG locations from nose (ft)**	**Weight (lbs)**

Empty weight	30.68	31926
Empty weight + crew	30.67	32746
Empty weight + crew + TFO	30.65	33016
Empty weight + crew +TFO+ fuel	30.53	34907
Empty weight + crew + TFO+ batteries	32.07	43909
Empty weight + crew + TFO+ fuel + batteries	31.91	45800
Empty weight + half passengers	30.88	35426
Empty weight + payload	31.09	40126
Empty weight + half luggage	30.71	32526
Empty weight + crew + TFO+ fuel + battery + half payload	31.98	49900
Empty weight + crew + TFO+ fuel + battery + payload	32.03	54000

The CG excursion diagram for different loading scenarios is shown below

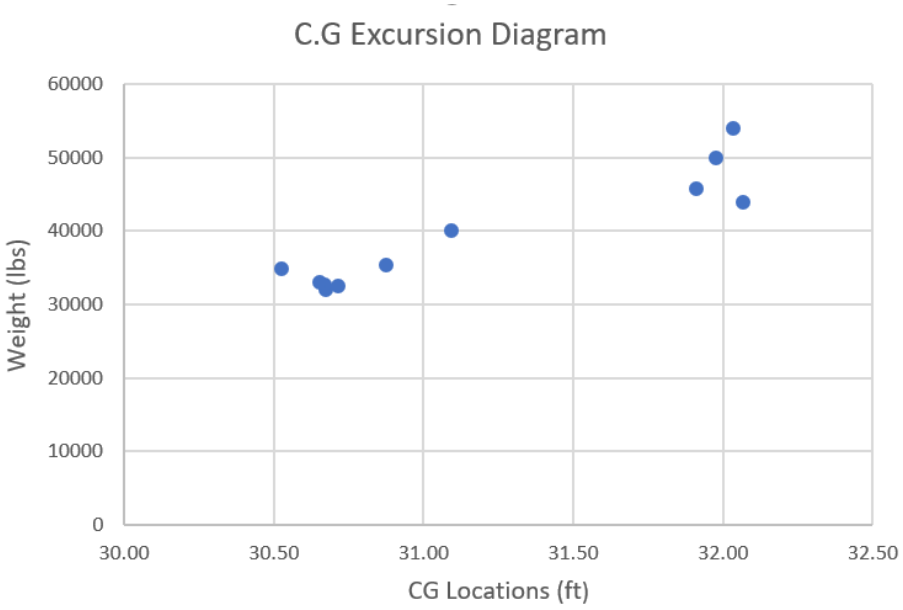

Figure 153: CG excursion diagram

From the above CG excursion diagram the CG range is obtained as follows:

Most forward CG location from the nose of the proposed aircraft: 30.53 ft

Most aft CG location from the nose of the proposed aircraft: 32.07 ft

As per the Roskam (Roskam, 2005), the CG range for regional turboprop airplanes is 12 to 20 inches or 1 to 1.66 ft. The obtained range for the proposed aircraft is 1.54 ft or 18.48 inches.

8.3 LANDING GEAR DESIGN

The retractable tricycle landing gear configuration is selected for the proposed aircraft as the cruise speed is 275 knots and for an ease of ground maneuvering and ground-looping. Most of the civil airplanes are equipped with retractable tricycle landing gears. The landing gear is designed based on the below two geometric criteria.

- Tip-over criteria
- Ground clearance criteria

- **Tip-over Criteria**

Tip-over criteria is classified as

- Longitudinal tip-over criterion
- Lateral tip-over criterion

➢ **Longitudinal tip-over criterion**

According to this criterion, the main landing gear must be behind the aft CG location for tricycle gears. The angle shown in the below figure indicates the usual relation between the aft CG and the main landing gear.

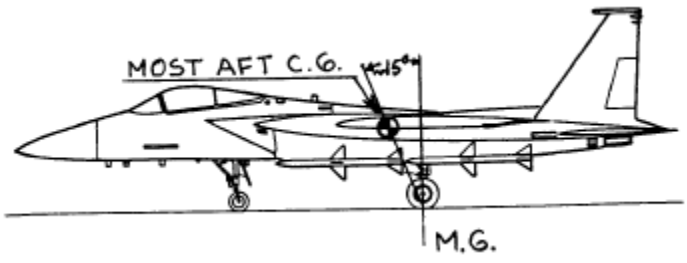

Figure 154: Longitudinal tip-over criterion for tricycle gear

Based on the given longitudinal tip-over criterion for tricycle gears, the proposed aircraft maintaining the longitudinal tip-over is shown below.

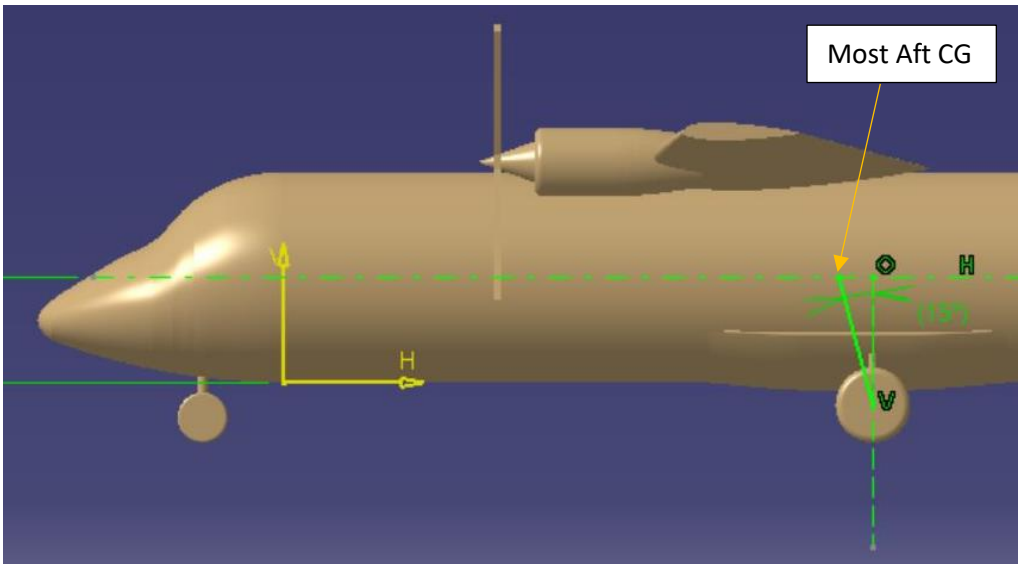

Figure 155: Longitudinal tip-over criterion for the proposed aircraft

- **Lateral tip-over criterion**

The lateral tip-over criterion is given by the below figure and is dictated by angle ψ.

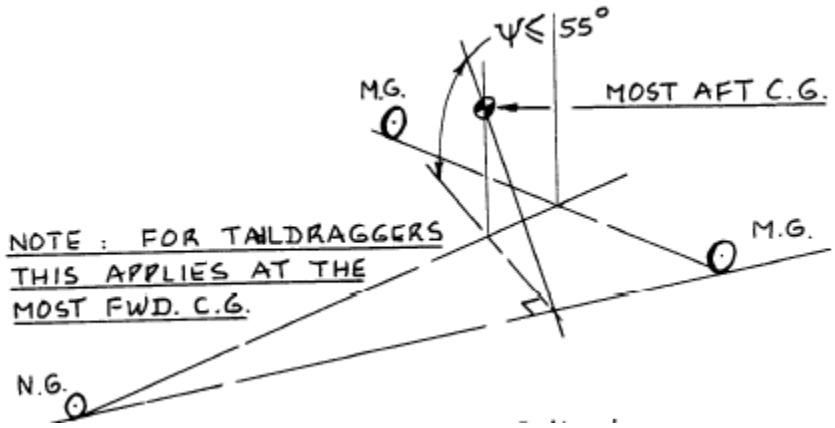

Figure 156: Lateral tip-over criterion for tricycle gear

The proposed aircraft lateral tip-over criterion is shown below

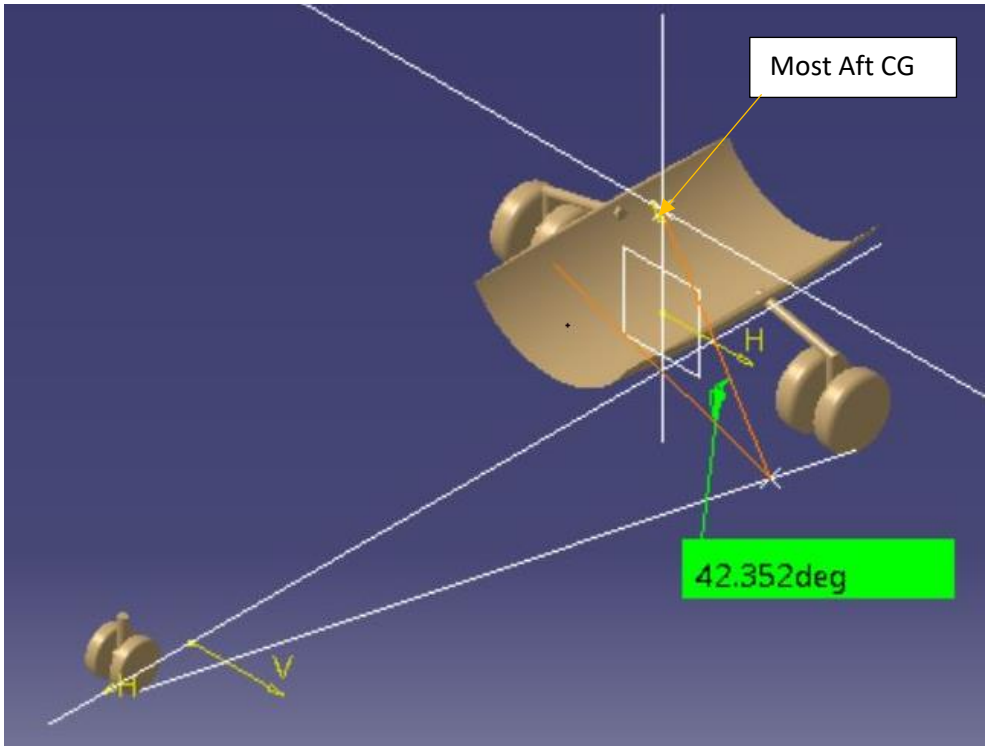

Figure 157: Lateral tip-over criterion for the proposed aircraft

- **Ground Clearance Criteria**

  The ground clearance criteria apply to tricycle gear is classified as

  - Longitudinal ground clearance criterion
  - Lateral ground clearance criterion

➢ **Longitudinal ground clearance criterion**

The longitudinal ground clearance given for tricycle gear is shown below

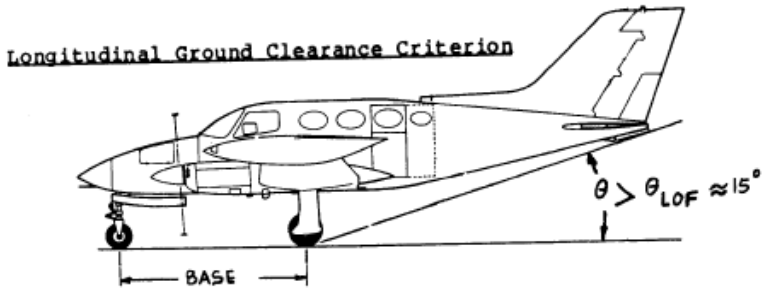

Figure 158: Longitudinal ground clearance criterion for tricycle gear

➢ **Lateral ground clearance criterion**

The lateral ground clearance given for tricycle gear is shown below

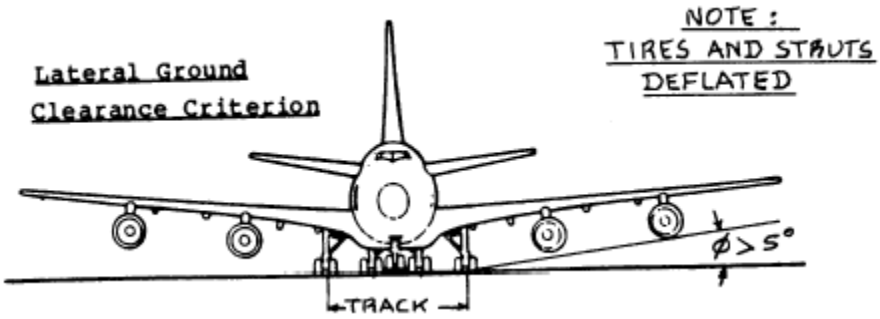

Figure 159: Lateral ground clearance criterion for tricycle gear

The proposed aircraft lateral ground clearance is shown below

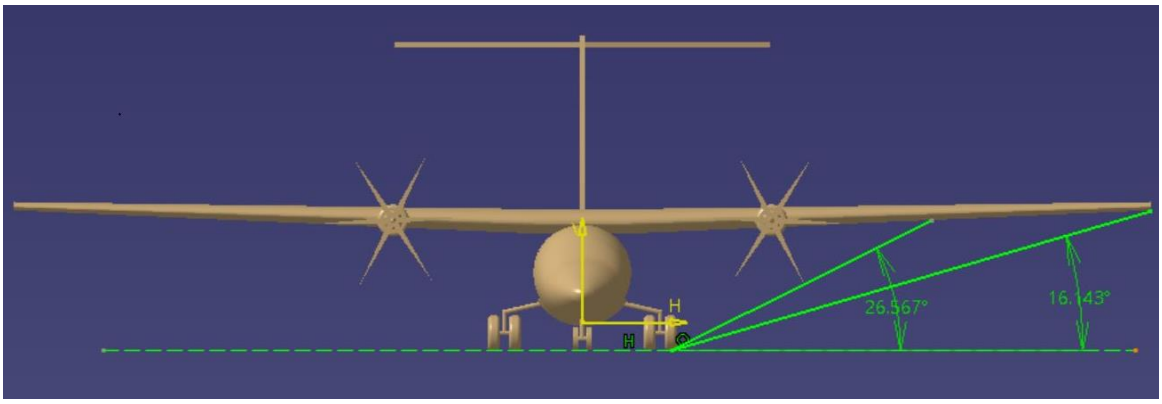

Figure 160: Lateral ground clearance criterion for the proposed aircraft

The landing gear disposition is rightly placed based on the above geometric criteria. As proposed aircraft uses high wing the placement of main landing gear under the wing increases the weight of the landing gear hence, the main landing gear is placed under the fuselage like reference aircraft. Based on the above geometric criteria, the location of the main landing gear struts placed under the fuselage using a fairing under the fuselage.

The maximum static load per strut can be calculated by using the below equations

Nose wheel strut:

$$P_n = \frac{W_{TO} l_m}{l_m + l_n} = \frac{54000 * 1.37}{26.86} = 2750 \text{ lbs} \qquad (8.1)$$

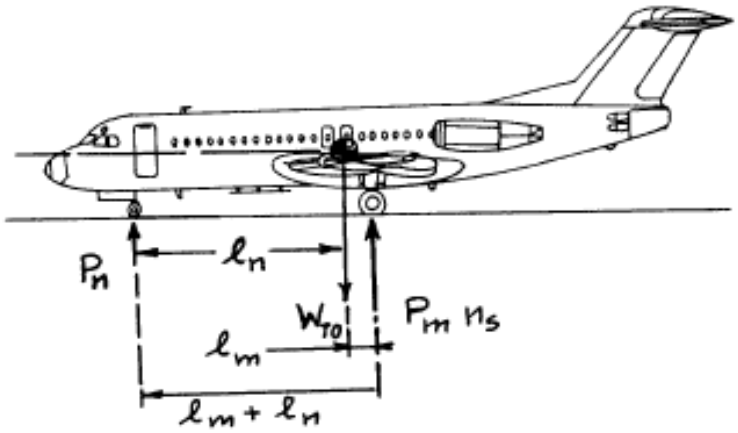

Figure 161: Geometry for static load calculation for tricycle gear

Main gear strut:

$$n_s P_m = \frac{W_{TO} l_n}{l_m + l_n} = \frac{54000 * 25.49}{26.86} = 51251 \text{ lbs} \qquad (8.2)$$

Where $n_s = 2$: two main gear struts are used for the proposed aircraft. One nose gear strut is used for the proposed aircraft based on the above maximum static load calculation.

The gear ratios are determined as

$$\frac{n_s P_m}{W_{TO}} = 0.95 \text{ and } \frac{P_n}{W_{TO}} = 0.05 \qquad (8.3)$$

As per the Roskam data (Roskam, 2005), it is reasonable to assume that two nose wheel tires and two main wheel tires per strut for the proposed aircraft. The main landing gear will have total four wheels and nose landing gear will have two wheels. As per the Raymer (Raymer, 2012), the recommended maximum tire pressure for civil airfield is 120 psi. From the Roskam data (Roskam, 2005), it is reasonable to assume the following wheel dimensions by looking the regional turboprops, transport jets and reference aircraft data (ATR , 2014).

Nosewheel tire: D_t X $b_t = 24$ X 7.7 inches or 2 X 0.6 ft with 68 psi

Main gear tire: D_t X $b_t = 40$ X 14 inches or 3 X 1 ft with 77 psi

The CAD model of proposed aircraft with landing gear disposition is shown below

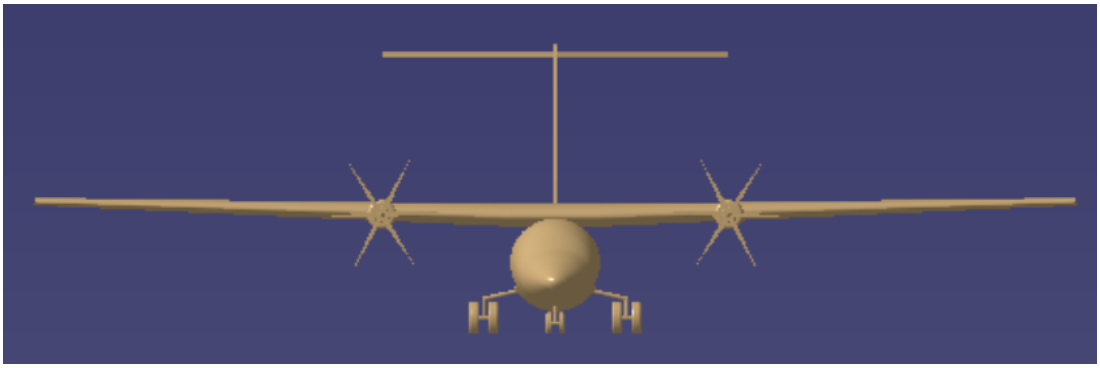

Figure 162: Front view of the proposed aircraft with landing gear disposition

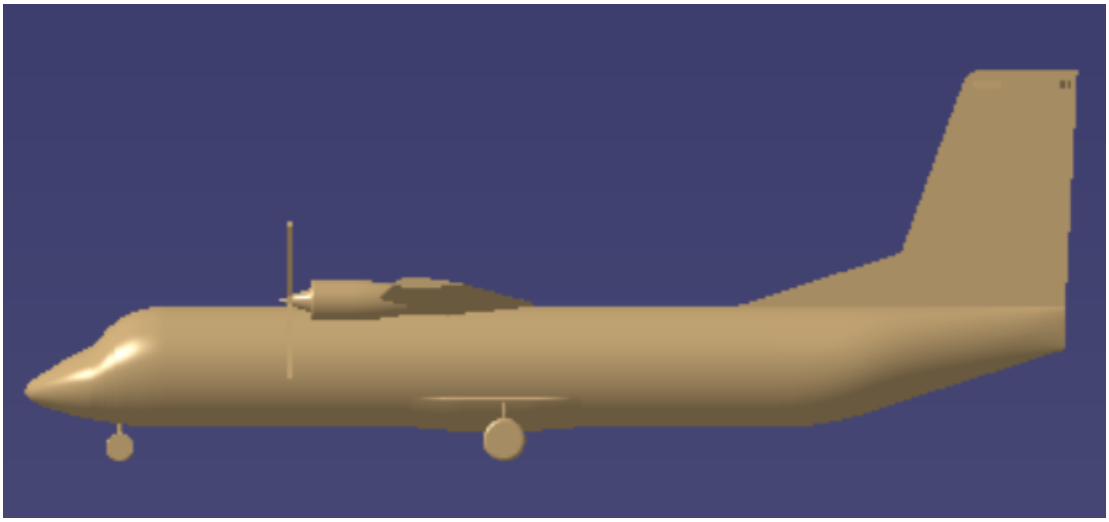

Figure 163: Side view of the proposed aircraft with landing gear disposition

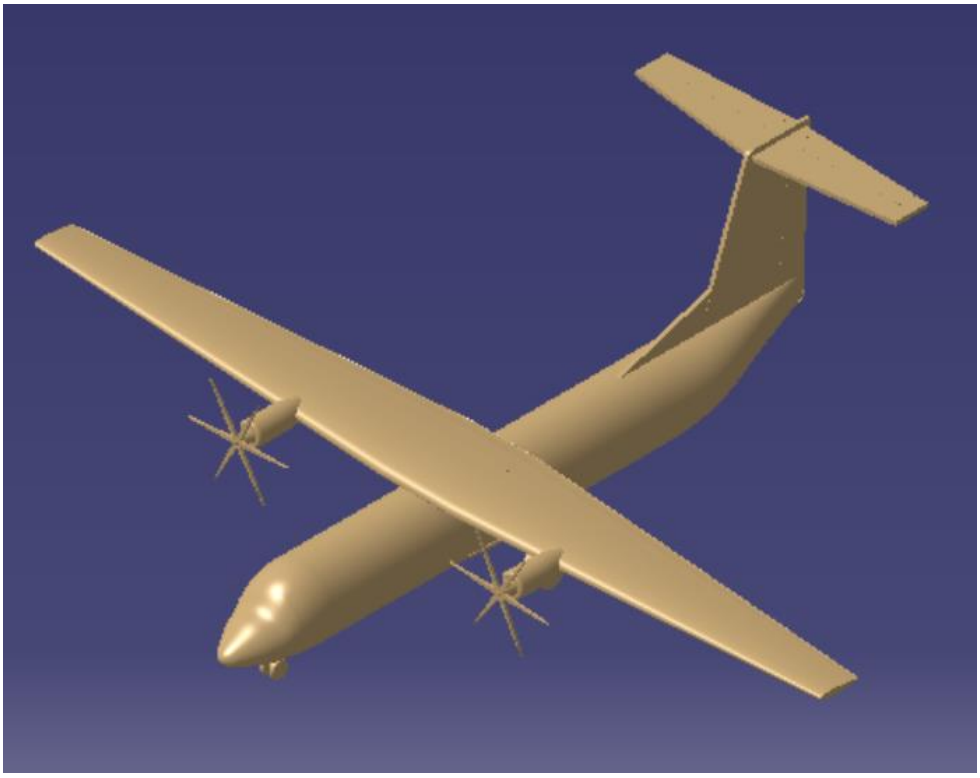

Figure 164: Isometric view of the proposed aircraft with landing gear disposition

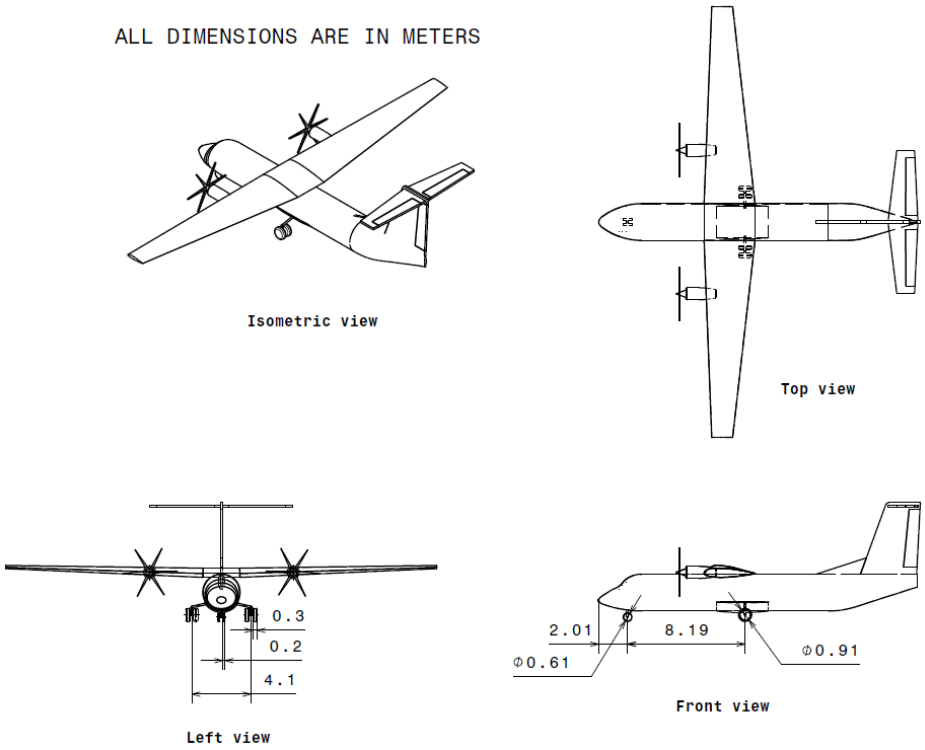

Figure 165: CAD drawing of the proposed aircraft landing gear

The above CAD drawing clearly indicates there is an enough space for retraction of landing gear. The distance between main landing gear struts is 4.10 m or 13.45 ft which is exactly same as reference aircraft ATR-42-600 (ATR , 2014), so there is enough space for retraction of landing gear.

8.4 WEIGHT AND BALANCE

The components final weight and coordinate data is shown below with x, y and z coordinates based on the updated landing gear disposition. The moment arm data for landing gear is updated in the below table.

Table 35: Components final weight and coordinate data

Type of Component	**Weight (lbs)**	**x (ft)**	**Wx (ft.lbs)**	**y (ft)**	**Wy (ft.lbs)**	**z (ft)**	**Wz (ft.lbs)**
Wing	5944	28.3	168205.9	0	0	10.9	64786.01
Empennage	1472	67.20	98908.56	0	0	20.33	29921
Fuselage	6019	32.71	196904.3	0	0	6.6	39726.36
Nacelles	1359	22.68	30813.34	0	0	10.5	14264.81
Landing gear: Nose gear	460	6.6	3036	0	0	2	920
Landing gear: Main gear	1842	33.46	61633.32	0	0	3.14	5783.88
Power plant	6397	22.68	145073.1	0	0	10.8	69082.43
Fixed equipment	8434	32.71	275887.6	0	0	6.6	55666.72
Empty Weight	31926	30.71	980462.1	0	0	8.78	280151.2
Crew: Pilots	410	6	2460	0	0	6.6	2706
Crew: Attendants	410	54.72	22436.43	0	0	6.6	2706
Trapped Fuel and Oil	270	29	7830	0	0	11	2970
Operating Empty Weight	33016	30.69	1013189	0	0	8.74	288533.2
Fuel	1891	28.3	53515.3	0	0	10.9	20611.9
Batteries	10893	36.35	395960.6	0	0	6.6	71893.8
Passengers	7000	32.71	228970	0	0	6.6	46200
Baggage	1200	32.71	39252	0	0	6.6	7920
Take-off weight	54000	32.05	1730886	0	0	8.06	435158.9

The final CAD drawing of components CG location is shown below

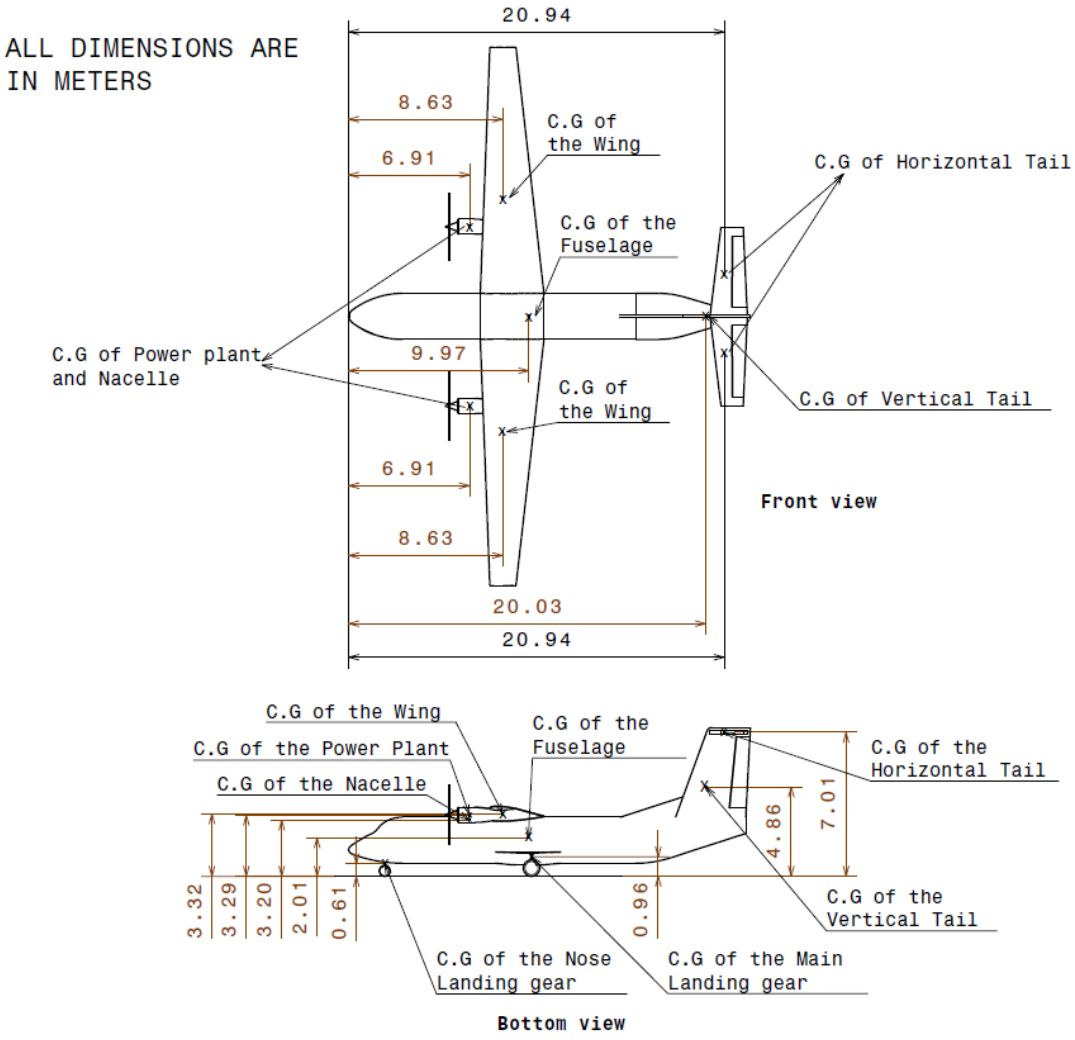

Figure 166: Final CAD drawing of components CG location

8.4.1 CG location for various loading scenarios

The final CG locations are calculated for different loading scenarios as follows

Table 36: Final CG locations for different loading scenarios

Loading Scenarios	**C.G locations from nose (ft)**	**Weight (lbs)**

Empty weight	30.71	31926
Empty weight + Crew	30.70	32746
Empty weight + Crew + TFO	30.69	33016
Empty weight + Crew +TFO+ fuel	30.56	34907
Empty weight + Crew + TFO+ Battery	32.09	43909
Empty weight + Crew + TFO+ fuel + battery	31.94	45800
Empty weight + half passengers	30.91	35426
Empty weight + Payload	31.12	40126
Empty weight + half luggage	30.75	32526
Empty weight + Crew + TFO+ fuel + battery + half payload	32.00	49900
Empty weight + Crew + TFO+ fuel + battery + payload	32.05	54000

The updated CG excursion diagram based on the final CG locations for different loading scenarios is shown below.

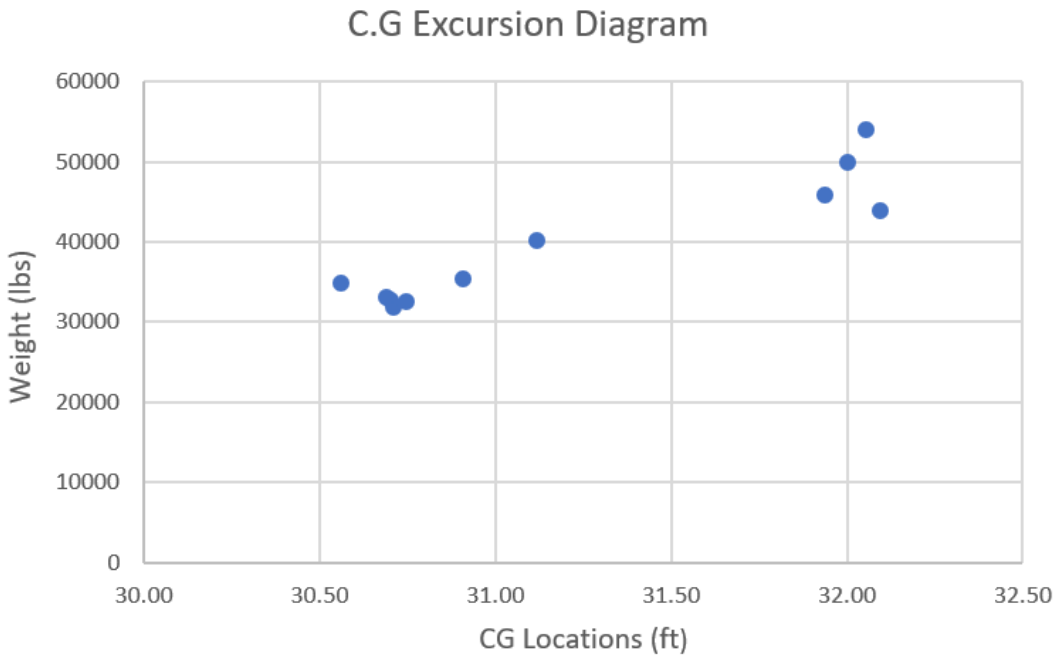

Figure 167: Final CG excursion diagram

Based on the final CG excursion diagram the CG range of the proposed aircraft is determined as

Most forward CG location from nose tip: 30.56 ft

Most aft CG location from nose tip: 32.09 ft

The obtained CG range of 1.53 ft is within acceptable range of 1 ft to 1.66 ft.

8.5 DISCUSSION

This chapter presented a detailed landing gear design using weight and balance method. The landing gear configuration selected for the proposed aircraft is retractable tricycle landing gear. The component weights are obtained by using comparable airplanes weight fractions data. Initially, the weight and balance method for subgroups of aircraft is carried out by assuming the landing gear disposition. The most forward CG location obtained from nose is 30.53 ft and most aft CG location obtained from the nose is 32.07 ft. An iterative process is carried out between the landing gear design and weight and balance satisfying all the geometric criteria. The final obtained most forward CG location from nose is 30.56 ft and most aft CG location from nose is 32.09 ft. The CG range of the proposed aircraft is within acceptable limits of the

comparable aircraft CG range. The complete CAD model and drawing of proposed aircraft is presented in the landing gear section.

8.6 CONCLUSION

The obtained CG range of the proposed aircraft is within acceptable limits of the comparable airplanes CG range given by Roskam (Roskam, 2005). The landing gear configuration selected for the proposed aircraft is retractable tricycle landing gear. The proposed aircraft is said to be stable with minimum variations in CG range. Further stability and control analysis will be carried out with more iterations to obtain exact CG location.

CHAPTER 9: STABILITY AND CONTROL ANALYSIS / WEIGHT & BALANCE-STABILITY & CONTROL CHECK

9.1 INTRODUCTION

This chapter presents a detailed class 1 stability and control analysis for the proposed aircraft configuration. The weight sizing, performance constraints, fuselage design, wing design, empennage design and landing gear design were obtained in previous chapters. The main objective of this chapter is to determine the following stability and control characteristics for the proposed aircraft configuration.

- Static longitudinal stability
- Static directional stability
- Minimum control speed with one engine inoperative

There are two types of stability such as static stability and dynamic stability. The aircraft is said to be statically stable, when it returns to original flight condition after a small disturbance. In dynamic stability, the airplane may converge continuously back to the original steady flight state or it may overcorrect and then converge to the original configuration in an oscillatory manner. Static instability naturally implies dynamic instability, but static stability does not always imply dynamic stability. This chapter presents a longitudinal x-plot and directional x-plot with respect to horizontal tail and vertical tail area. These x-plots are used to determine the changes in horizontal and vertical tail area with respect to changes in aerodynamic center and center of gravity locations of the proposed aircraft.

9.2 STATIC LONGITUDINAL STABILITY

The static longitudinal stability is determined in this section with the help of the following two legs of the X:

- The center of gravity leg represents the rate at which the center of gravity moves with respect to change in horizontal tail area (Roskam, 2005).
- The aerodynamic center leg represents the rate at which the aerodynamic center moves with respect to change in horizontal tail area (Roskam, 2005).

The aft center of gravity location is already obtained in weight and balance analysis and the weight of the empennage is known in the previous chapter. The total empennage weight is obtained as 1472 lbs from the weight and balance analysis. The horizontal tail weight is calculated as 671 lbs with 177.34 sq. ft area. Assuming the weight of the horizontal tail is independent of surface area, then the aerodynamic center is calculated for the proposed aircraft with the following equation:

$$\bar{X}_{a.c_A} = \frac{\left[\bar{X}_{a.c_{wf}} + \frac{\left\{C_{L_{\alpha_h}}\left(1 - \frac{d\varepsilon_h}{d\alpha}\right)\left(\frac{S_h}{S}\right)\bar{X}_{a.c_h}\right\}}{C_{L_{\alpha_{wf}}}}\right]}{F} \tag{9.1}$$

Where,

$$F = \left[1 + \frac{\left\{C_{L_{\alpha_h}}\left(1 - \frac{d\varepsilon_h}{d\alpha}\right)\left(\frac{S_h}{S}\right)\right\}}{C_{L_{\alpha_{wf}}}}\right] \tag{9.2}$$

The CG of the aircraft is obtained by the changing the horizontal tail weight with respect to change in horizontal tail area. The summary of calculated values is given below.

$$\bar{X}_{a.c_{wf}} = 0.12, \qquad C_{L_{\alpha_h}} = 0.072 \text{ deg}^{-1}, \qquad \left(\frac{d\varepsilon_h}{d\alpha}\right) = 0.0291, \qquad \bar{X}_{a.c_h} = 4.916,$$

$$C_{L_{\alpha_{wf}}} = 0.09 \text{ deg}^{-1}$$

The longitudinal x-plot is shown below with horizontal area varying from 0 to 300 sq. ft. Both $\bar{X}_{a.c_A}$ and $\bar{X}_{c.g}$ are plotted as a function of horizontal tail area.

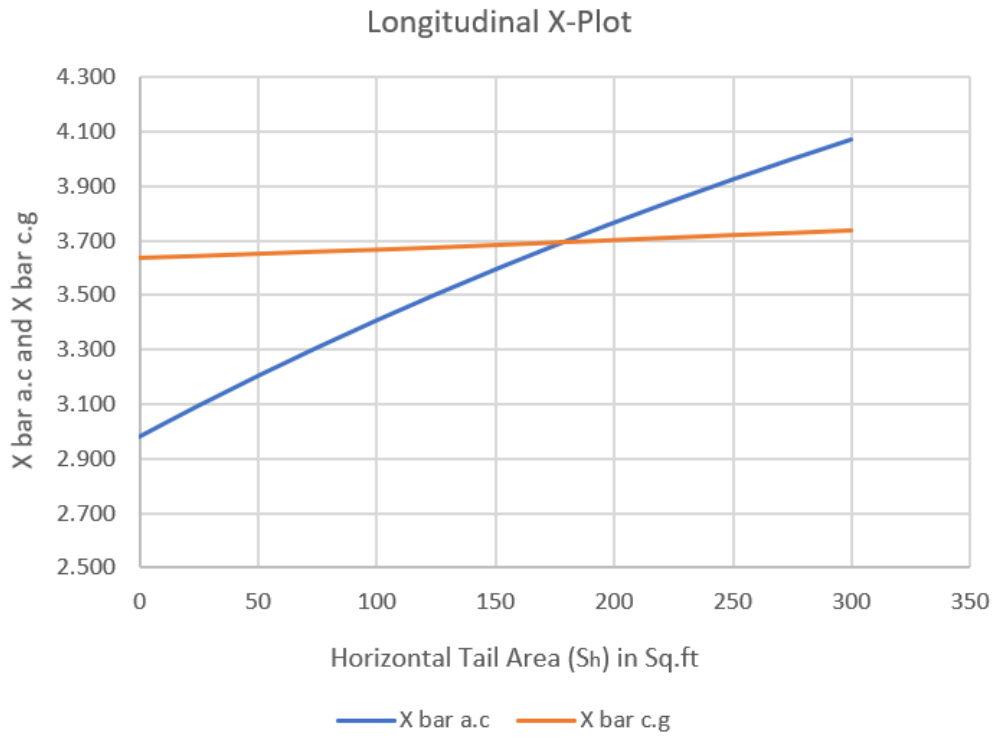

Figure 168: Longitudinal X-plot

The proposed aircraft needs to be inherently stable with static margin of 5 percent as it is a regional turboprop aircraft. The empennage area for a minimum static margin of 5 percent is the design point.

$$\frac{dC_m}{dC_L} = \bar{X}_{c.g} - \bar{X}_{a.c} = -0.05 \qquad (9.3)$$

Zoomed view of longitudinal x-plot is shown below.

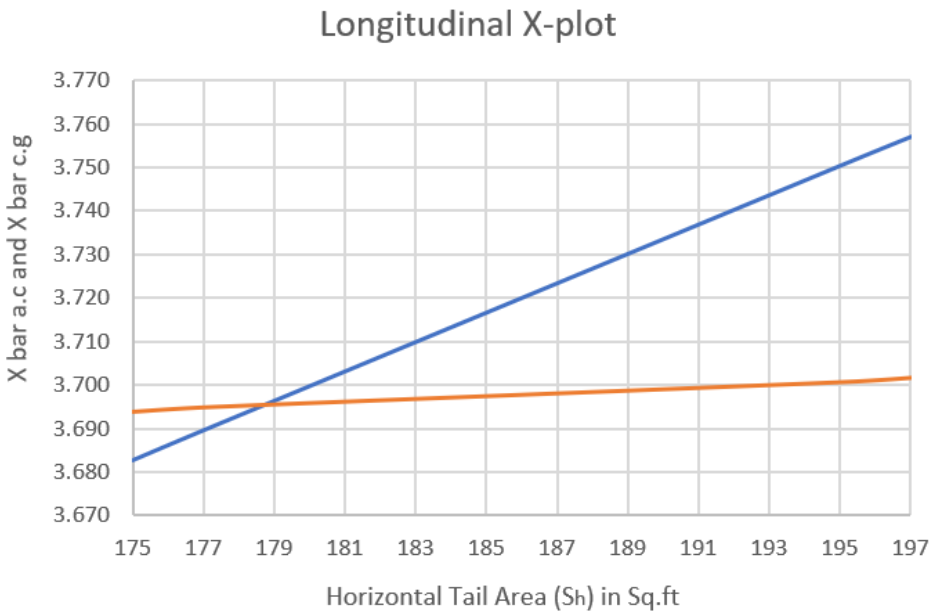

Figure 169: Zoomed view of longitudinal x-plot

The above figure shows the static margin of 5 percent at horizontal tail area of 195 sq. ft and area of horizontal tail obtained in empennage design is 177.34 sq. ft. The allowed difference between both the horizontal tail areas is 10 percent. The difference between the obtained horizontal tail area 177.34 sq. ft and the horizontal tail area obtained from the x-plot 195 sq. ft is 9.9 percent and hence no iteration is required. The difference is within the specified limits of class 1 stability requirements; hence the proposed aircraft is said to be longitudinally stable and the horizontal tail area will be maintained as 195 sq. ft.

9.3 STATIC DIRECTIONAL STABILITY

The static directional stability is determined in this section using directional x-plot with side slip moment coefficient as a function of vertical tail area. The yawing-moment-due-to-sideslip derivative, C_{n_β} also called static directional stability can be determined from the below equation:

$$C_{n_\beta} = C_{n_{\beta_W}} + C_{n_{\beta_f}} + C_{n_{\beta_V}} \qquad (9.4)$$

For preliminary design purposes, the wing contribution is neglected as it is important only at high angles of attack.

$$C_{n_{\beta_W}} = 0 \tag{9.5}$$

The fuselage contribution can be determined from the below equation

$$C_{n_{\beta_f}} = -57.3 K_N K_{R_1} \left(\frac{S_{B_s} l_f}{Sb}\right) \tag{9.6}$$

The vertical tail contribution can be determined from the below equation

$$C_{n_{\beta_V}} = -\frac{\left(C_{Y_{\beta_V}}\right)(l_V \cos\alpha + z_V \sin\alpha)}{b} \tag{9.7}$$

Where,

$$C_{Y_{\beta_V}} = -k_V \left(C_{L_{\alpha_V}}\right)\left(1 + \frac{d\sigma}{d\beta}\right)\eta_V \left(\frac{S_V}{S}\right) \tag{9.8}$$

The summary of calculated values is given below

$k_V = 0.91$, $C_{L_{\alpha_V}} = 0.034\ \text{deg}^{-1}$, $\left(1 + \frac{d\sigma}{d\beta}\right)\eta_V = 0.922$, $C_{Y_{\beta_V}} = -(3.52 * 10^{-5})\, S_V$

$C_{n_{\beta_V}} = (1.182 * 10^{-5}) S_V$

The directional x-plot for the proposed aircraft is shown below based on the obtained calculations

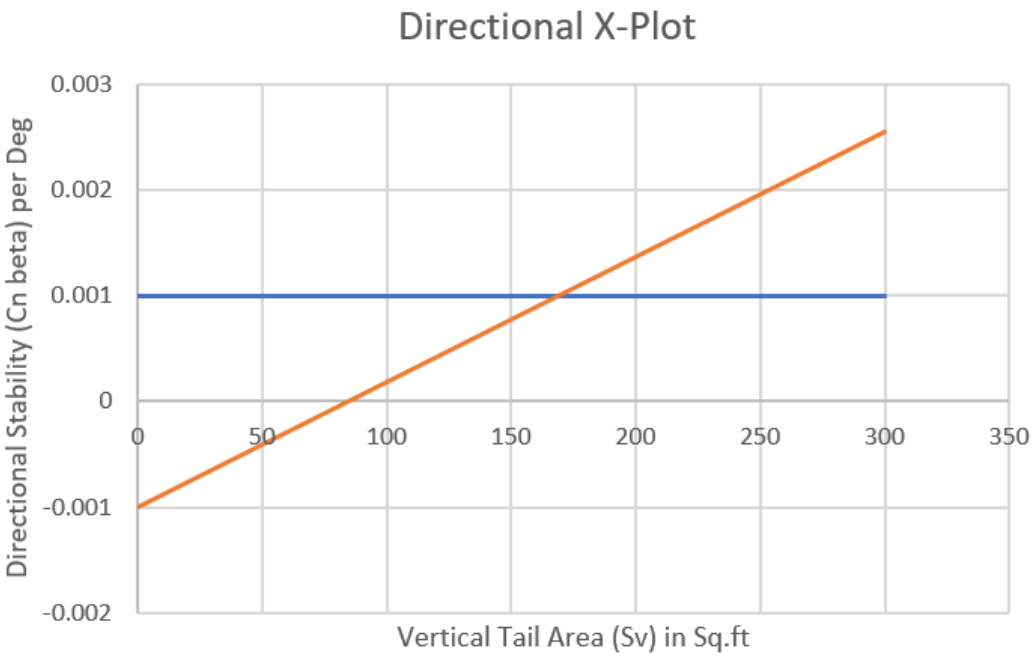

Figure 170: Directional x-plot

The zoomed view of the directional x-plot is shown below

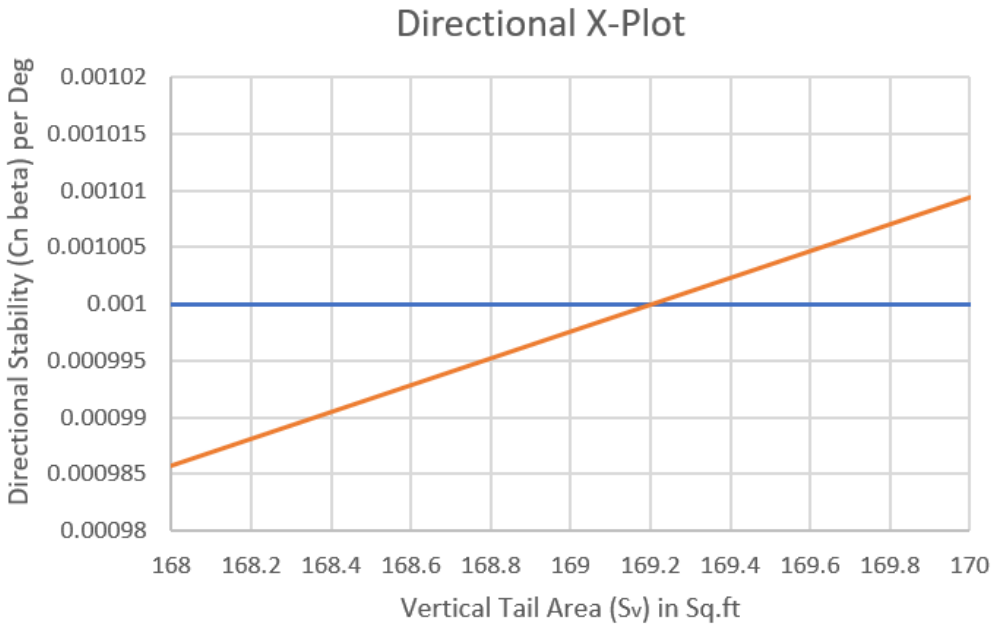

Figure 171: Zoomed view of directional x-plot

The vertical area of 169.2 sq. ft obtained from the directional x-plot at $C_{n_\beta} = 0.001$ as shown in above figure is the design point. The vertical area obtained from the empennage design is 168.85 sq. ft. The difference between both the vertical areas is 0.2 percent which is very less and hence, no iteration is required (Roskam, 2005). The difference is quite negligible in preliminary design of class 1. Hence, the proposed aircraft is directionally stable with negligible variation in vertical tail area.

The critical engine-out yawing moment can be determined from the below equation

$$N_{t_{crit}} = T_{TO_e} y_t \qquad (9.9)$$

The take-off power obtained in performance constraint analysis is 2259 hp for one engine. The take-off power of 2259 hp is converted to take-off thrust of 7016.23 lbs. The y_t is the lateral thrust moment arm of the most critical engine obtained as 16.4 ft from the CAD model as shown below.

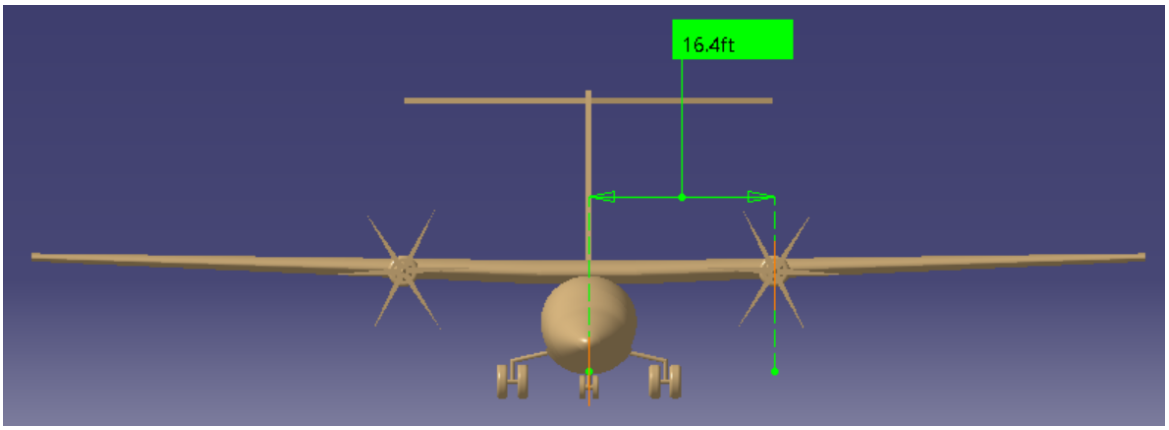

Figure 172: Lateral thrust moment arm

Therefore,

$$N_{t_{crit}} = 7016.23 * 16.4 = 115066 \text{ ft. lbs} \qquad (9.10)$$

The value of drag induced yawing moment due to one engine inoperative can be determined for propeller aircraft with fixed pitch propellers.

$$N_D = 0.25 * N_{t_{crit}} = 28766.5 \text{ ft. lbs} \qquad (9.11)$$

The maximum allowable speed with one engine inoperative is calculated from:

$$V_{mc} = 1.2V_s \tag{9.12}$$

Where, V_s is the landing stall speed which is 91.72 knots obtained from performance constraint analysis.

$$V_{mc} = 1.2 * 91.72 = 110 \text{ knots or } 186 \text{ ft/sec} \tag{9.13}$$

The rudder deflection required to hold the engine out condition at V_{mc} is calculated from

$$\delta_r = \frac{(N_D + N_{t_{crit}})}{\bar{q}_{mc} S b C_{n_{\delta_r}}} \tag{9.14}$$

The summary of calculated values is given below

$$C_{n_{\delta_r}} = -0.079 \text{ deg}^{-1}, \qquad \bar{q}_{mc} = 18.439 \text{ psf}$$

Therefore,

$$\delta_r = -1.238 \text{ degrees}$$

The resulting rudder deflection is within the specified limits of Roskam (Roskam, 2005) and hence, no iteration is required. The proposed rudder and vertical tail sizing are acceptable with one engine inoperative.

9.4 EMPENNAGE DESIGN - WEIGHT AND BALANCE - LANDING GEAR DESIGN - LONGITUDINAL STATIC STABILITY AND CONTROL CHECK

The proposed aircraft static longitudinal stability and static directional stability conditions are satisfied. The horizontal tail area obtained from longitudinal x-plot is within 10 percent difference which indicates the CG travel is close enough to the obtained aft CG location. The vertical tail area obtained from directional x-plot is close enough to the proposed vertical tail area. The required rudder deflection to hold engine-out condition at minimum control speed is acceptable for the proposed aircraft. Both the horizontal tail area and vertical tail area are within acceptable margins and hence, no iteration is required for preliminary design as per class 1 requirements.

9.5 DISCUSSION

The proposed aircraft static longitudinal and static directional stability is determined in this chapter. The longitudinal x-plot is obtained from the change in center of gravity and aerodynamic center location with respect to change in horizontal area. The obtained horizontal tail area at 5 percent static margin is within acceptable limits of class 1 preliminary design. Similarly, the directional x-plot is obtained from the change in yawing-moment-due to sideslip derivative with respect to the vertical tail area. The obtained vertical tail area is very close to the proposed vertical tail area from empennage design. The minimum speed required to control one engine inoperative is determined and rudder deflection at that speed is within acceptable limits.

9.6 CONCLUSION

The static longitudinal x-plot and static directional x-plot clearly indicates that the proposed aircraft is stable both longitudinally and directionally as per class 1 preliminary design requirements. The obtained value of vertical tail area does not require any change but for future work, the horizontal tail area will be sized more precisely to improve the difference.

CHAPTER 10: DRAG POLAR ESTIMATION

10.1 INTRODUCTION

This chapter presents a detailed class 1 method for drag polar estimation of the proposed aircraft. The initial estimation of drag polar equations are already obtained in performance sizing chapter. In this chapter, the initial estimated drag polar equations are compared with the final drag polar values. The airplane zero-lift drag coefficient is calculated by using the equivalent parasite area which will be determined from the total wetted area of the aircraft. The wetted area of each component of the proposed aircraft will be determined and then zero-lift drag will be calculated. The main objective of this chapter is to calculate the drag increment due to flaps and landing gear during take-off and landing. The calculated drag polar equations are then plotted for lift coefficient versus drag coefficient for different configurations.

10.2 AIRPLANE ZERO LIFT DRAG

The airplane zero-lift drag can be determined by calculating the wetted area of the proposed aircraft. The best way to calculate the aircraft wetted area is to split the airplane into components which contribute to wetted area such as

- Wing
- Empennage
- Fuselage
- Nacelles

The wetted area for wing, horizontal tail and vertical tail can be determined from the following equation (Roskam, 2005):

$$S_{wet_{plf}} = 2S_{exp.plf}\left\{1 + \frac{0.25\left(\frac{t}{c}\right)_r (1 + \tau\lambda)}{1 + \lambda}\right\} \qquad (10.1)$$

Where,

$$\tau = \frac{\left(\frac{t}{c}\right)_r}{\left(\frac{t}{c}\right)_t} \text{ and } \lambda = \frac{c_t}{c_r} \qquad (10.2)$$

The exposed wetted area can be determined as shown below

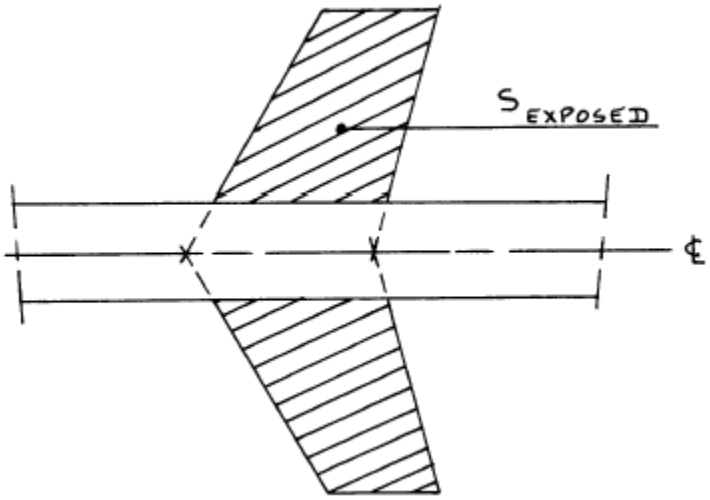

Figure 173: Definition of exposed planform

Calculation of wetted area for wing planform

The wetted area for wing planform is calculated by using the below parameters obtained from previous chapters

Table 37: Parameters of wing planform

Parameters of the wing	**Dimensions**
Root thickness to chord ratio, $\left(\frac{t}{c}\right)_r$	0.18
Tip thickness to chord ratio, $\left(\frac{t}{c}\right)_t$	0.15
Taper ratio, λ	0.41
Wing area, S	809 sq. ft
Tau, τ	1.2

The exposed planform area is calculated by using Figure 173 and CAD model of the proposed aircraft as

$$S_{exp.plf} = 809 - (8.432 * 11.64) = 710.85 \text{ sq. ft} \qquad (10.3)$$

Therefore, by substituting all the above parameters in equation (1), the wetted area of the wing planform is

$$S_{wet_{plf}} = 1485.679 \text{ sq. ft} \qquad (10.4)$$

Similarly, the wetted area of horizontal and vertical tail can be calculated as follows

Calculation of wetted area for vertical tail

Table 38: Parameters of vertical tail

Parameters of the vertical tail	**Dimensions**
Root thickness to chord ratio, $\left(\frac{t}{c}\right)_r$	0.12
Tip thickness to chord ratio, $\left(\frac{t}{c}\right)_t$	0.12
Taper ratio, λ	0.6
Vertical tail area, S_V	168.85 sq. ft
Tau, τ	1

The exposed planform area of the vertical tail is calculated by subtracting the horizontal tail intersection area and fuselage intersection area from the total vertical tail area. The horizontal intersection area obtained from CAD model is 4.18 sq. ft and fuselage intersection area obtained as 2.05 sq. ft.

$$S_{exp.plf} = 168.85 - 4.18 - 2.05 = 162.62 \text{ sq. ft} \qquad (10.5)$$

Therefore, from equation (10.1),

$$S_{wet_{plf}} = 334.99 \text{ sq. ft} \qquad (10.6)$$

Calculation of wetted area for horizontal tail

Table 39: Parameters of horizontal tail

Parameters of the horizontal tail	**Dimensions**
Root thickness to chord ratio, $\left(\frac{t}{c}\right)_r$	0.12

Tip thickness to chord ratio, $\left(\frac{t}{c}\right)_t$	0.12
Taper ratio, λ	0.6
Horizontal tail area, S_V	195 sq. ft
Tau, τ	1

The exposed planform area of the horizontal tail is calculated by subtracting the vertical tail intersection area of 4.18 sq. ft from the total horizontal tail area as follows

$$S_{exp.plf} = 195 - 4.18 = 190.82 \text{ sq. ft} \quad (10.7)$$

Therefore, from equation (10.1),

$$S_{wet_{plf}} = 393.1 \text{ sq. ft} \quad (10.8)$$

Calculation of wetted area for fuselage

The wetted area for fuselage of the proposed aircraft is calculated by using the below equation (Roskam, 2005)

$$S_{wet_{fus}} = \pi D_f l_f \left(1 - \frac{2}{\lambda_f}\right)^{\frac{2}{3}} \left(1 + \frac{1}{{\lambda_f}^2}\right) \quad (10.9)$$

Where,

$$\lambda_f = \frac{l_f}{D_f} \quad (10.10)$$

The below parameters are used to calculate the wetted area for fuselage

Table 40: Parameters of fuselage

Fuselage parameters	**Dimensions**
Length of the fuselage, l_f	72.7 ft
Diameter of the fuselage, D_f	8.43 ft
Fineness ratio, λ_f	8.63 ft

Therefore, from equation (10.9)

$$S_{wet_{fus}} = 1636.02 \text{ sq. ft} \tag{10.11}$$

Calculation of wetted area for nacelles

The below figure shows the geometry of an externally mounted nacelle. The following components of the nacelle contribute to wetted area for the proposed aircraft: fan cowling and the plug. There is no gas generator cowling for the proposed aircraft.

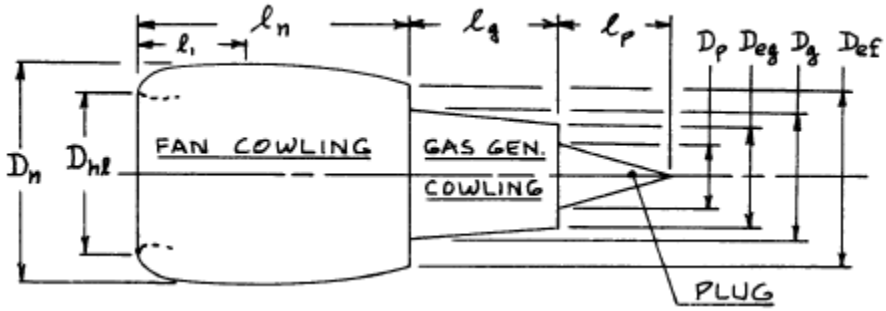

Figure 174: Geometry of nacelle

The wetted area of fan cowling and the plug is calculated by using the below equations (Roskam, 2005):

$$S_{wet_{fan\ cowling}} = l_n D_n \left\{2 + \frac{0.35 l_1}{l_n} + \frac{0.81 l_1 D_{hl}}{l_n D_n} + 1.15\left(1 - \frac{l_1}{l_n}\right)\left(\frac{D_{ef}}{D_n}\right)\right\} \tag{10.12}$$

$$S_{wet_{plug}} = 0.7 * \pi * l_p * D_p \tag{10.13}$$

The below input parameters of the nacelle are used for calculation of the wetted area

Table 41: Parameters of nacelle

Parameters of the nacelle	**Dimensions**
Diameter of the plug, D_p	1.64 ft
Length of the plug, l_p	2.254 ft
l_n	7 ft
D_n	2.75 ft

l_1	3 ft
D_{hl}	1.7 ft
D_{ef}	2.6 ft

By substituting all the above parameters in equation (10.12) and equation (10.13), the following wetted areas are determined for one nacelle.

$$S_{wet_{fan\ cowling}} = 57.48 \text{ ft} \quad (10.14)$$

$$S_{wet_{plug}} = 8.13 \text{ ft} \quad (10.15)$$

The proposed aircraft uses two engines with two nacelles, therefore,

$$S_{wet_{fan\ cowling}} = 2 * 57.48 = 114.96 \text{ ft} \quad (10.16)$$

$$S_{wet_{plug}} = 2 * 8.13 = 16.26 \text{ ft} \quad (10.17)$$

$$S_{wet_{nacelle}} = 16.26 + 114.96 = 131.22 \text{ ft} \quad (10.18)$$

The proposed aircraft uses a fuselage fairing for landing gear retraction hence, as per the Roskam data, the increment of wetted area due to fuselage fairing is assumed to be 40 sq. ft.

The summary of all the components wetted area of proposed aircraft is given below

Table 42: Summary of components wetted area and total wetted area

Component	**Wetted area**
Wing	1485.679 sq. ft
Vertical tail	334.99 sq. ft
Horizontal tail	393.1 sq. ft
Fuselage	1636.02 sq. ft
Nacelles	131.22 sq. ft
Increment due to fuselage fairings	40 sq. ft
Total aircraft	**4021 sq. ft**

The calculated total wetted area of the proposed aircraft is 4021 sq. ft. The equivalent parasite area, 'f' of the proposed aircraft can be obtained from the below figure.

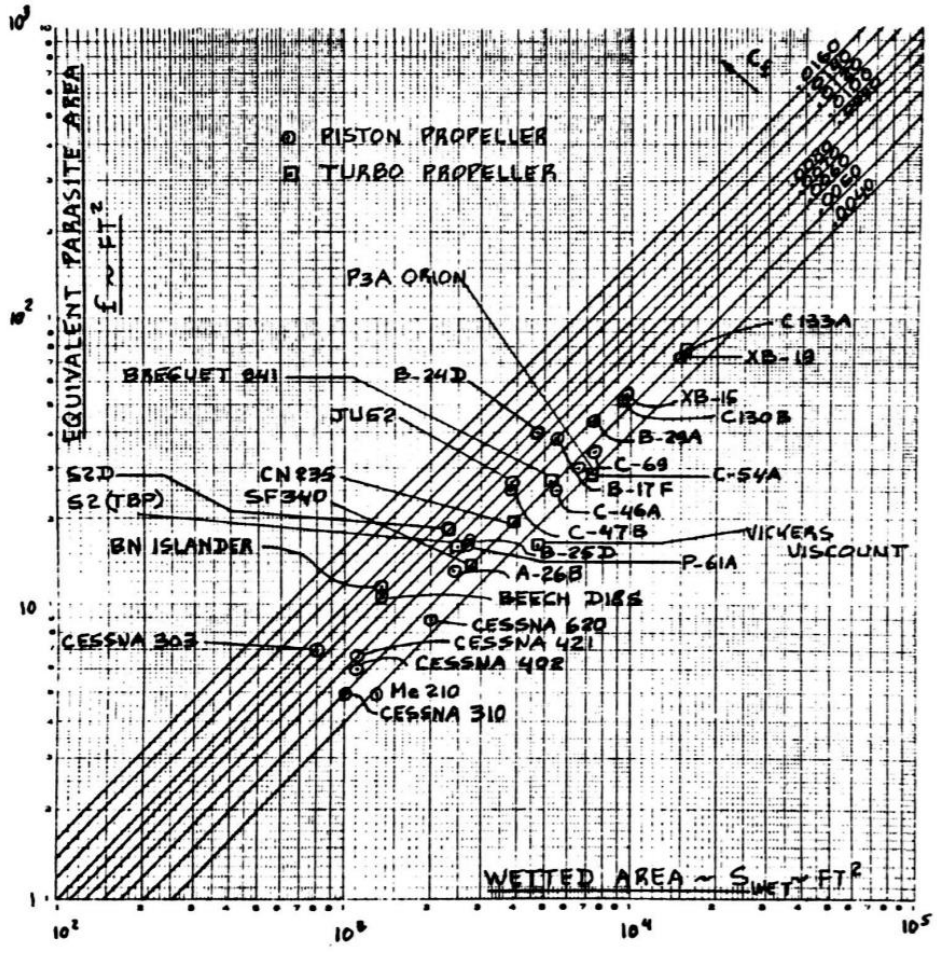

Figure 175: Wetted area versus equivalent parasite area for turbo-prop airplanes

Based on the above figure, the equivalent parasite area 'f' is 20 sq. ft for wetted area of 4021 sq. ft. The clean zero-lift drag coefficient at low speed can be determined from the below equation:

$$C_{D_o} = \frac{\mathrm{f}}{S} \qquad (10.19)$$

Where, f is parasite area and S is the wing area

$$C_{D_o} = \frac{20}{809} = 0.0247 \qquad (10.20)$$

10.3 LOW SPEED DRAG INCREMENTS

10.3.1 High-Lift Device Drag Increments for Take-off and Landing

The flap drag increment for take-off and landing can be determined by using the below data from Roskam (Roskam, 2005).

Configuration	ΔC_{D_o}	e
Clean	0	0.80 - 0.85
Take-off flaps	0.010 - 0.020	0.75 - 0.80
Landing Flaps	0.055 - 0.075	0.70 - 0.75
Landing Gear	0.015 - 0.025	no effect

Figure 176: Estimates for ΔC_{D_o} and e for different configurations

Table 43: Flap drag increment for take-off and landing

Configuration	Aspect ratio	ΔC_{D_o}	e	C_D
Take-off flaps	12	0.015	0.80	$0.0397 + 0.03315\ C_L^2$
Landing flaps	12	0.060	0.75	$0.0847 + 0.03536\ C_L^2$

10.3.2 Landing Gear Drag

The landing gear drag can be obtained as follows

Table 44: Landing gear drag increment

Configuration	Aspect ratio	ΔC_{D_o}	e	C_D
Landing gear	12	0.020	No effect	0.0447

10.4 COMPRESSIBILITY DRAG

The proposed aircraft travels at Mach number 0.41. The compressibility effects are neglected for the proposed aircraft because for Mach number 0.41, the compressibility drag increment is zero as shown below.

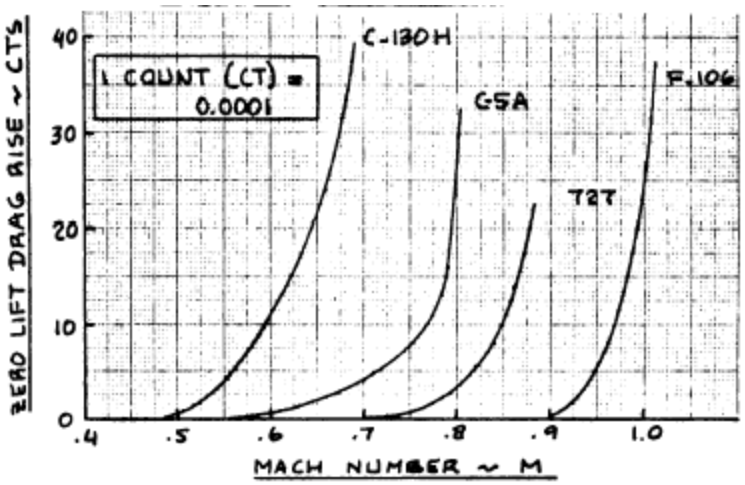

Figure 177: Compressibility drag behavior

10.5 AREA RULING

As per the Roskam (Roskam, 2005), area ruling is applicable for airplanes with Mach number above 0.90. The proposed aircraft travels at Mach number 0.41 and hence, cross-sectional area plot is not required.

10.6 AIRPLANE DRAG POLARS

The aspect ratio of the wing is obtained as 12 and wing area is obtained as 809 sq. ft. The below table is used for the calculation of proposed aircraft drag polar equations.

Table 45: ΔC_{D_o} and e for different configurations

Configuration	ΔC_{D_O}	**e**
Clean	0	0.85
Takeoff Flaps	0.015	0.80
Landing Flaps	0.060	0.75
Landing Gear	0.020	-

The proposed aircraft drag polar equations for different configurations are obtained by using the above table as follows

Table 46: Proposed aircraft drag polar equations

Configuration	C_D
Clean	$0.0247 + 0.0312\ C_L^2$
Takeoff, gear up	$0.0397 + 0.03315\ C_L^2$
Takeoff, gear down	$0.0597 + 0.03315\ C_L^2$
Landing, gear up	$0.0847 + 0.03536\ C_L^2$
Landing, gear down	$0.1047 + 0.03536\ C_L^2$

The graph of proposed aircraft drag polar for different configurations are shown below

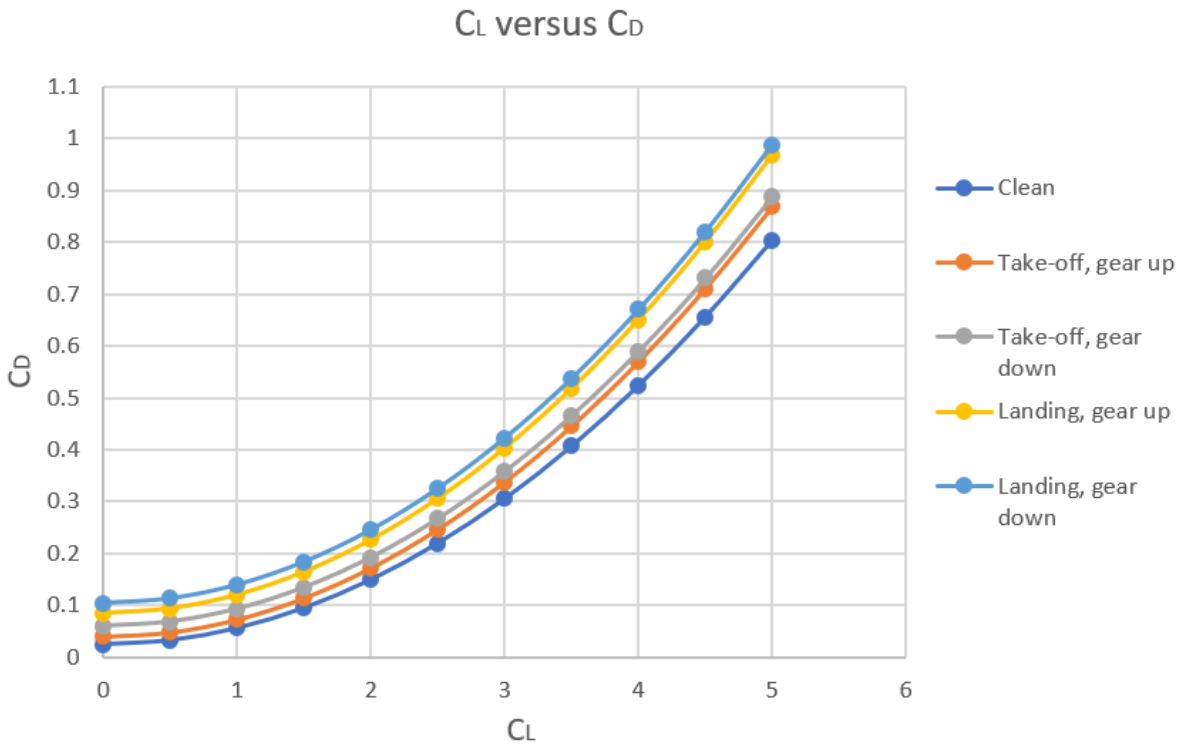

Figure 178: CL versus CD graph for different configurations

10.7 DISCUSSION

This chapter presented a detailed class 1 final drag polar estimation for the proposed aircraft. The high-lift device drag increments for take-off and landing are calculated and landing gear

drag increment was also calculated. The compressibility effects are neglected for the proposed aircraft as for Mach number 0.41, the compressibility drag increment is zero. The proposed aircraft drag polar equations for different configurations are calculated manually and then plotted using excel data. Drag polar estimation is the last step in class 1 preliminary design sequence. The obtained drag polar equations in this chapter can be used in the class II sizing.

10.8 CONCLUSION

The obtained drag polar equations are quite acceptable for class I preliminary design. The class I preliminary design requirements are satisfied and hence, no further change is required for the proposed aircraft.

CHAPTER 11: V-n DIAGRAM

11.1 INTRODUCTION

There are two methods for estimating the component weights and inertias of the airplane in preliminary design. Class I method is already presented in previous chapters. Class II method is based on weight equations for more detailed airplane components and groupings. These equations help us in calculating detailed design configuration parameters. To implement class II method, it is necessary to have a preliminary structural arrangement and V-n diagram. This chapter presents the step by step procedure for constructing V-n diagram of regional hybrid transport aircraft as part of preliminary design sequence II. The V-n diagram presented in this chapter is used in conjunction with class II weight estimation methods.

11.2 METHODS FOR CONSTRUCTING V-n DIAGRAM

V-n diagram is a plot of speed versus load factor and mainly used to determine design limit and design ultimate load factors (Raymer, 2012). V-n diagram defines the strength limitation of an aircraft (Raymer, 2012). There are four factors that affect a V-n diagram such as altitude, maximum gross takeoff weight, symmetry of loading and configuration of aircraft i.e cruise, landing etc. There are many loading scenarios for an aircraft to consider but for class II, we are only going to consider air loads on wing, by taking account into gust and maneuver loads. The class II method considers only flaps-up cases for the construction of V-n diagram (Roskam, 2005). The method for constructing V-n diagram as per FAR 25 includes the calculation of various speeds as shown in below sections.

11.2.1 Calculation of +1g Stall Speed, Vs

The stall speed for FAR 25 aircraft can be determined by using the following equation

$$V_{S_1} = \sqrt{\frac{2\left(\frac{GW}{S}\right)}{\rho C_{N_{max}}}} \qquad (11.1)$$

Where,

GW = flight design gross weight in lbs

S = wing area in sq.ft

ρ = air density in slugs/ft^3

$C_{N_{max}}$= maximum normal force coefficient

The maximum normal force coefficient follows from

$$C_{N_{max}} = \sqrt{(C_{L_{max}})^2 + (C_{D_{at\ C_{L_{max}}}})^2} \tag{11.2}$$

In preliminary design it is acceptable to set

$$C_{N_{max}} = 1.1 C_{L_{max}} \tag{11.3}$$

We know that $C_{L_{max}}$ is 1.5 and W/S is 67 psf from class 1 design calculations, therefore

$$C_{N_{max}} = 1.65$$

From equation (11.1), we get

$$V_{S_1} = 110 \text{ knots}$$

11.2.2 Calculation of Design Limit Load Factor, n_{lim}

The positive design limit load factor or maneuvering limit load factor can be determined from the following equation:

$$n_{lim_{pos}} \geq 2.1 + \left\{\frac{24000}{W + 10000}\right\} \tag{11.4}$$

Where, $n_{lim_{pos}} \geq 2.5$ at all times and need not be greater than 3.8 at W_{TO}

Therefore, $n_{lim_{pos}} = 2.475$ using takeoff weight of 54199 lbs and as it is required $n_{lim_{pos}} \geq 2.5$ at all times, hence

$$n_{lim_{pos}} = 2.5$$

The negative design limit load factor can be determined from

$n_{lim_{neg}} \geq -1.0$ upto V_C and varies linearly from the value at V_C to zero at V_D

11.2.3 Calculation of Design Maneuvering Speed, V_A

The design maneuvering speed can be obtained from

$$V_A \geq V_{S_1}\sqrt{n_{lim}} \tag{11.5}$$

where, n_{lim} is the limit maneuvering load factor at V_C

As $n_{lim_{pos}}$ is 2.5 and V_{S_1} is 110 knots, hence

$$V_A = 110\sqrt{2.5} = 174 \text{ knots}$$

11.2.4 Construction of Gust Load Factor Lines

The gust load factor lines can be constructed by the following equation

$$n_{lim} = 1 + \frac{K_g U_{de} V C_{L_\alpha}}{498\left(\frac{GW}{S}\right)} \tag{11.6}$$

where, K_g is the gust alleviation factor given by:

$$K_g = \frac{0.88\,\mu_g}{5.3 + \mu_g} \tag{11.7}$$

where,

$$\mu_g = \frac{2\left(\frac{GW}{S}\right)}{\rho \bar{c} g C_{L_\alpha}} \tag{11.8}$$

From preliminary design sequence 1, we know gross weight is 54199 lbs, wing area is 809 sq. ft, mean aerodynamic chord of the wing is 8.685 ft and overall airplane lift curve slope, C_{L_α} is 0.107 deg^{-1} or 6.13 rad^{-1}.

At sea-level, g is 32.174 ft/s^2 and ρ is 0.002377 slugs/ft^3

Therefore, by substituting all the values in the above equations, we get

$$\mu_g = 33 \text{ and } K_g = 0.758 \tag{11.9}$$

The derived gust velocity at 25000 ft altitude, U_{de} is determined as follows

For the V_B gust line: $U_{de} = 84.67 - 0.000933\text{h} = 61$ fps (11.10)

For the V_C gust line: $U_{de} = 66.67 - 0.000833\text{h} = 46$ fps (11.11)

For the V_D gust line: $U_{de} = 33.34 - 0.000417\text{h} = 23$ fps (11.12)

Therefore, using equation (11.6), we get

For the V_B gust line: $n_{lim} = 1 + 0.0085V$ (11.13)

For the V_C gust line: $n_{lim} = 1 + 0.0064V$ (11.14)

For the V_D gust line: $n_{lim} = 1 + 0.0032V$ (11.15)

Using the above equations, the gust load factor lines are plotted as shown below

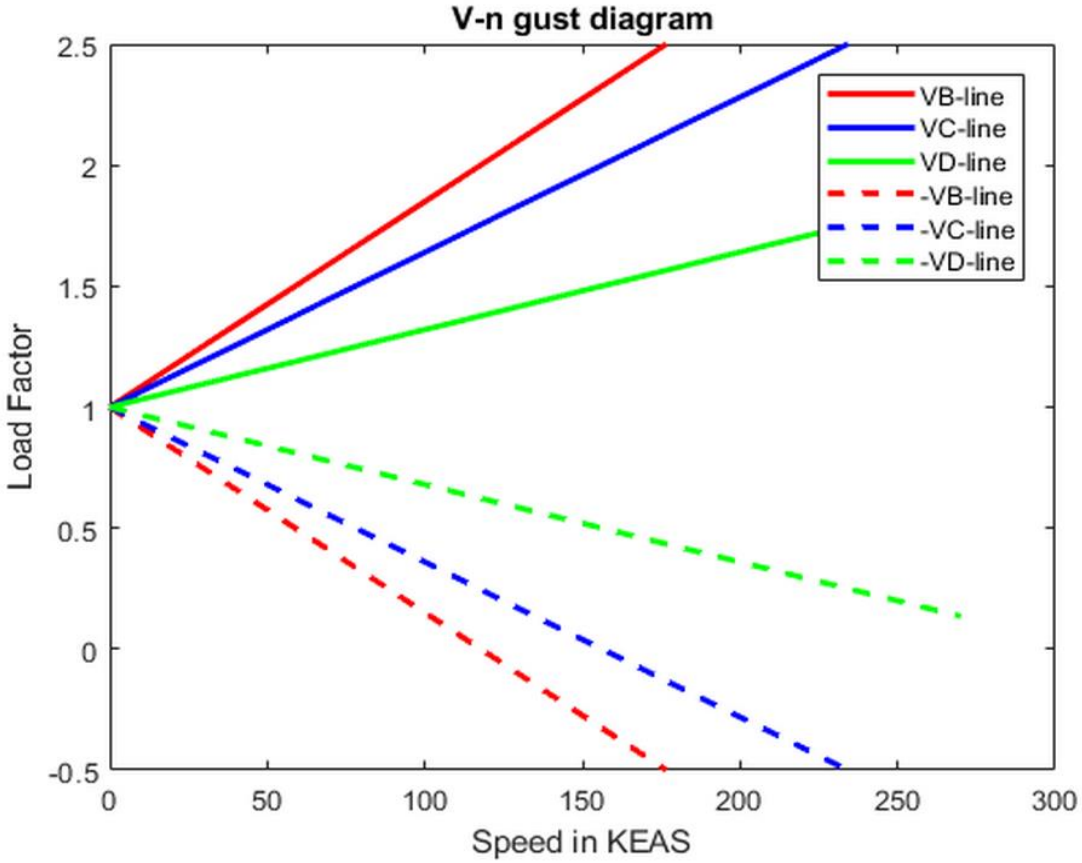

Figure 179: V-n gust load factor lines

11.2.5 Calculation of Design Speed for Maximum Gust Intensity, V_B

Design speed for maximum gust intensity, V_B is determined from the intersection of +1 g stall line and the V_B gust line as shown below (Roskam, 2005). The V_B gust line is obtained from the equation (11.13).

$$V_B = 173 \text{ knots} \quad (11.16)$$

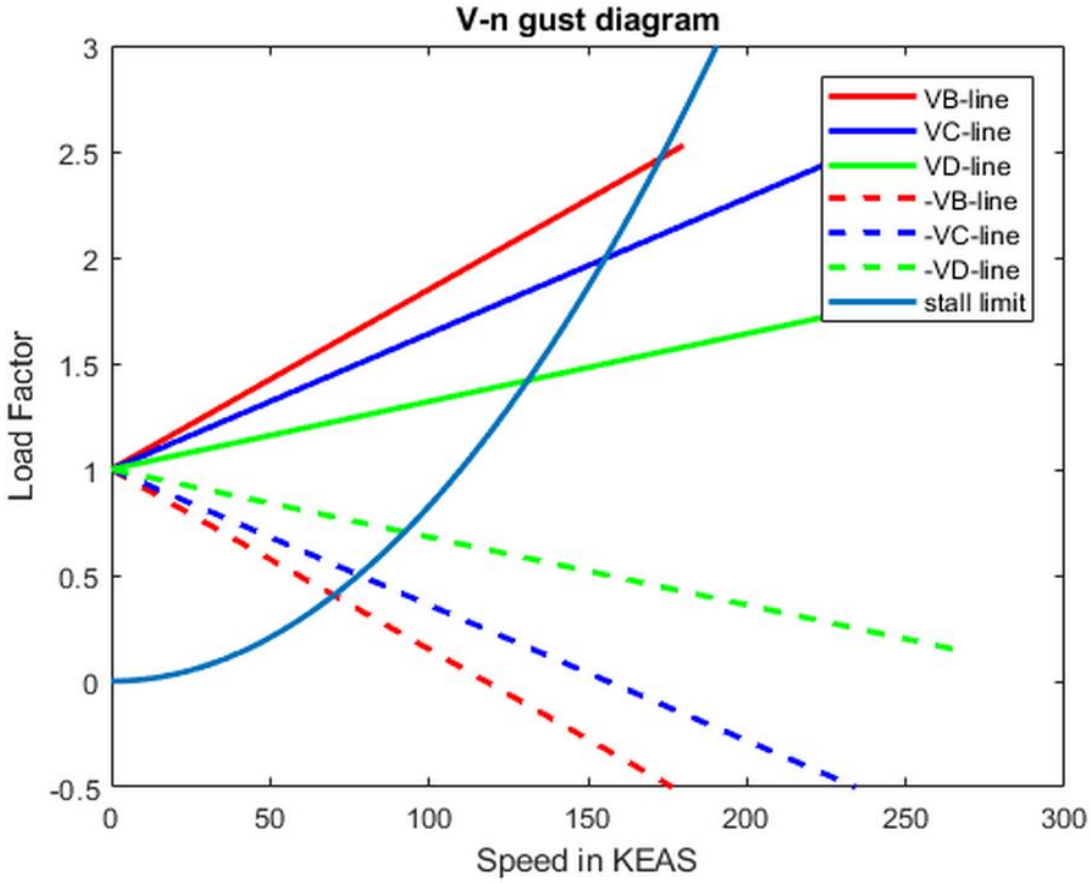

Figure 180: V-n gust diagram

11.2.6 Calculation of Design Cruising Speed, V_C

Design cruising speed must be greater than V_B to provide for inadvertent speed increases likely to occur as a result of severe atmospheric turbulence (Roskam, 2005). V_C can be determined as follows

$$V_C \geq V_B + 43 \text{ kts} \tag{11.17}$$

Therefore,

$$V_C = 173 + 43 = 216 \text{ knots} \tag{11.18}$$

11.2.7 Calculation of Design Driving Speed, V_D

The design driving speed can be calculated by using the below equation

$$V_D \geq 1.25\, V_C \tag{11.19}$$

Therefore,

$$V_D = 270 \text{ knots} \tag{11.20}$$

11.2.8 Calculation of Negative Stall Line

Assuming the $C_{L_{max_{neg}}}$ as -1 for the proposed hybrid design, the $C_{N_{max_{neg}}}$ can be calculated as -1.1 using the equation (11.3). The negative limit load factor is considered as -1 for calculating the negative stall speed using the equation below.

$$V_{S_1} = \sqrt{\frac{2n_{lim_{neg}}\left(\frac{GW}{S}\right)}{\rho C_{N_{max}}}} \tag{11.21}$$

Therefore, by substituting all the values we get

$$V_{S_1} = 134 \text{ knots}$$

11.3 V-n DIAGRAM

V-n diagram is plotted as shown below using all the above equations:

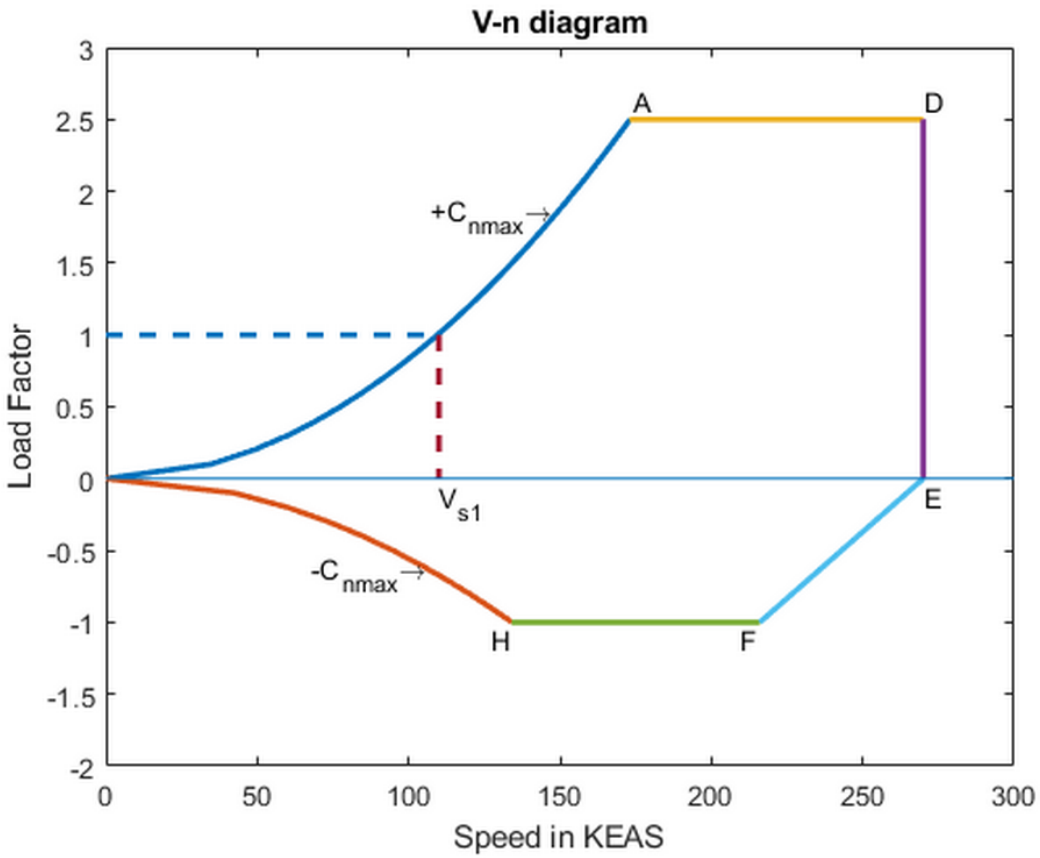

Figure 181: V-n diagram

11.4 DISCUSSION

The obtained V-n diagram represents the proposed design flight operating strength. The maximum positive lift capability and negative lift capability curves are quite important in V-n diagram to determine design limits. Beyond this limit structural damage can occur to the proposed design. The enclosed envelope is the possible limit that the hybrid aircraft can operate without any structural damage. V-n diagram also provides possible combination of airspeeds and load factors for safe operation. The stall speed at +1g is obtained as 110 knots whereas the negative 1g stall speed is obtained as 134 knots. As we can see the maximum positive design limit is +2.5 and negative limit is -1. The airspeed at point A which is also known as maneuver speed, is the minimum airspeed at which the limit load factor can be developed aerodynamically. The airspeed above this point provides positive lift capability enough to damage the proposed aircraft. Hence, it is recommended to be within the envelope for the safe operation of the proposed hybrid aircraft.

CHAPTER 12: CLASS II WEIGHT AND BALANCE

12.1 INTRODUCTION

This Chapter presents the class II weight estimation of the proposed aircraft. Class II methods are based on the weight equations for more detailed airplane components and groupings. Class II weight estimation methods presented in this chapter rely on the preliminary structural arrangement and V-n diagram. The weight and balance of the proposed aircraft is also presented in this chapter.

12.2 CLASS II WEIGHT ESTIMATION

The class II method of weight estimation is applied based on the following details obtained in previous chapters :

- Take-off gross weight
- Wing and empennage design parameters
- Load factor
- Design cruise and/ or dive speed
- Fuselage configuration and interior requirements
- Powerplant installation
- Landing gear design and disposition
- Systems requirements
- Preliminary structural arrangement

The following basic weight definition from preliminary design sequence I will be used:

$$W_{TO} = W_E + W_F + W_{PL} + W_{tfo} + W_{crew} + W_{bat} \quad (12.1)$$

The class II method will focus on estimating the components of empty weight which are defined as:

$$W_E = W_{struct} + W_{pwr} + W_{feq} \quad (12.2)$$

Where,

W_{struct} = structure weight

W_{pwr} = powerplant weight

W_{feq} = fixed equipment weight

Torenbeek method is more appropriate for class II weight estimation of the proposed design and hence Torenbeek equations (Roskam, 2005) are used in below sections.

12.3 CLASS II METHOD FOR ESTIMATING STRUCTURE WEIGHT

The proposed aircraft structure weight mainly consists of the following components:

- Wing, W_W
- Empennage, W_{emp}
- Fuselage, W_f
- Nacelles, W_n
- Landing gear, W_g

$$W_{struct} = W_W + W_{emp} + W_f + W_n + W_g \tag{12.3}$$

Equations for class II structure weight estimation are presented below for the proposed commercial airplane.

12.3.1 Wing Weight

The following equation is used for the estimation of wing weight of the proposed aircraft

$$W_W = 0.0017 W_{MZF} \left(\frac{b}{\cos \Lambda_{\frac{1}{2}}} \right)^{0.75} \left[1 + \left\{ \frac{6.3 \cos \Lambda_{\frac{1}{2}}}{b} \right\}^{\frac{1}{2}} \right] (n_{ult})^{0.55} \left(\frac{bS}{t_r W_{MZF} \cos \Lambda_{\frac{1}{2}}} \right)^{0.30} \tag{12.4}$$

Where,

$$W_{MZF} = W_{TO} - W_F = 54000 - 1891 = 52109\ lbs \tag{12.5}$$

Substituting the parameters obtained in previous chapters such as b = 98.53 ft, $\Lambda_{\frac{1}{2}}$ = 1 deg, t_r= 2.095 ft, S = 809 sq. ft and n_{ult} = 2.5 in the above equation, we get

$$W_W = 5228\ lbs \tag{12.6}$$

12.3.2 Empennage Weight

The empennage weight of the proposed aircraft is expressed as follows

$$W_{emp} = W_h + W_V \tag{12.7}$$

Horizontal tail weight, W_h

The horizontal tail weight for the proposed aircraft can be determined from the following equation

$$W_h = K_h S_h \left[\frac{3.81(S_h)^{0.2} V_D}{\left\{ 1000 \left(\cos \Lambda_{\frac{1}{2}_h} \right)^{\frac{1}{2}} \right\}} - 0.287 \right] \tag{12.8}$$

Where,

$K_h = 1$ for fixed incidence stabilizers

Substituting $\Lambda_{\frac{1}{2}_h} = 3$ deg, $S_h = 195$ sq. ft and $V_D = 270$ knots in the above the equation, we get

$$W_h = 520\ lbs \tag{12.9}$$

Vertical tail weight, W_V

The following equation is used for estimating the vertical tail weight

$$W_V = K_V S_V \left[\frac{3.81(S_V)^{0.2} V_D}{\left\{ 1000 \left(\cos \Lambda_{\frac{1}{2}_V} \right)^{\frac{1}{2}} \right\}} - 0.287 \right] \tag{12.10}$$

Where,

$$K_V = 1 + 0.15 \left(\frac{S_h z_h}{S_V b_V} \right) \tag{12.11}$$

Substituting $S_V = 168.85$ sq. ft, $\Lambda_{\frac{1}{2V}} = 7$ deg, $z_h = 15.518$ ft and b_V = 16.44 ft in above equations, we get $K_V = 1.16$

$$W_V = 509\ lbs \tag{12.12}$$

12.3.3 Fuselage Weight

The following equation is used for fuselage weight estimation

$$W_f = 0.021 K_f \left\{\frac{V_D l_h}{w_f + h_f}\right\}^{\frac{1}{2}} (S_{fgs})^{1.2} \tag{12.13}$$

Where,

$K_f = 1.07$ for a main gear attached to the fuselage

S_{fgs} is obtained from CAD model as 1707.78 sq. ft and using fuselage parameters in the above equation, we get

$$W_f = 4379\ lbs \tag{12.14}$$

12.3.4 Nacelle Weight

The below equation is used for estimating nacelle weight

$$W_n = 0.055\ T_{TO} \tag{12.15}$$

Substituting $T_{TO} = 14029$ lbs, we get

$$W_n = 772\ lbs \tag{12.16}$$

12.3.5 Landing gear Weight

The below equation is used for estimating landing gear weight

$$W_g = K_{g_r}\left\{A_g + B_g (W_{TO})^{\frac{3}{4}} + C_g W_{TO} + D_g (W_{TO})^{\frac{3}{2}}\right\} \tag{12.17}$$

Where,

$K_{g_r} = 1.08$ for high wing airplanes

Substituting the values of main and nose retractable gear of other civil airplanes shown in above table in landing gear weight estimation equation, we get

$$W_g = W_{g_{main}} + W_{g_{nose}} = 1967 + 431 = 2398\ lbs \quad (12.18)$$

The below table shows the class II structural weight estimation of the proposed aircraft.

Table 47: Class II structural weight estimation of the proposed aircraft

Component	**Class I (lbs)**	**Class II (lbs)**	**Use as Class II Estimate (lbs)**
Wing	5944	5228	5586
Empennage	1472	1030	1251
Fuselage	6019	4379	5199
Nacelles	1359	772	1066
Landing gear	2302	2398	2350
Structural weight			**15452**

12.4 CLASS II METHOD FOR ESTIMATING POWERPLANT WEIGHT

The airplane powerplant weight, W_{pwr} will be assumed to consist of the following components:

- Engines
- Air induction system
- Propellers
- Fuel system
- Propulsion system

The below equation is used for powerplant weight estimation

$$W_{pwr} = W_e + W_{ai} + W_{prop} + W_{fs} + W_p \quad (12.19)$$

12.4.1 Engine Weight

The engine weight includes engine, exhaust, cooling, supercharger and lubrication systems.

$$W_e = N_e W_{eng} \tag{12.20}$$

Where, weight per engine W_{eng} is 1720 lbs and there are total two engines for the proposed aircraft. So,

$$W_e = 3440\ lbs \tag{12.21}$$

12.4.2 Propeller Weight

The propeller weight for the proposed design is given by

$$W_{prop} = K_{prop2}(N_p)^{0.218}\left\{D_p P_{TO}(N_{bl})^{\frac{1}{2}}\right\}^{0.782} \tag{12.22}$$

Where,

$K_{prop2} = 0.108$ for Turboprops

Number of propellers, $N_p = 2$

Number of blades, $N_{bl} = 6$

The takeoff power is 4517 hp and diameter of the propeller, D_p is 13 ft. Therefore,

$$W_{prop} = 1357\ lbs \tag{12.23}$$

12.4.3 Fuel System Weight

The fuel system weight of the proposed aircraft is estimated by using the below equation

$$W_{fs} = 80(N_e + N_t - 1) + 15(N_t)^{0.5}\left(\frac{W_F}{K_{fsp}}\right)^{0.333} \tag{12.24}$$

Where,

$K_{fsp} = 6.55\,\frac{lbs}{gal}$ for JP-4

Fuel weight is already obtained in class I as 1891 lbs and the number of separate fuel tanks N_t are two by comparing to the reference aircraft data. Therefore,

$$W_{fs} = 380\ lbs \tag{12.25}$$

12.4.4 Propulsion System Weight

The propulsion system weight is either given as a function of total engine weight and/or mission fuel or by:

$$W_P = W_{ec} + W_{ess} + W_{pc} + W_{osc} \tag{12.26}$$

Where,

$W_{ec} =$ weight of engine controls

$W_{ess} =$ weight of engine starting system

$W_{pc} =$ weight of propeller controls

$W_{osc} =$ weight of oil system and oil cooler

Engine controls

The weight of engine controls for wing mounted turboprops is given by

$$W_{ec} = 56.84 \left\{ \frac{(l_f + b) N_e}{100} \right\}^{0.514} \tag{12.27}$$

Length of the fuselage, l_f is 72.7 ft and wing span is 98.53 ft. Therefore,

$$W_{ec} = 107\ lbs \tag{12.28}$$

Engine starting system

The weight of the engine starting system with turboprop engines using pneumatic starting system is given by the below equation

$$W_{ess} = 12.05 \left(\frac{W_e}{1000} \right)^{1.458} \tag{12.29}$$

Using W_e as 3440 lbs in the above equation, we get

$$W_{ess} = 73\ lbs \tag{12.30}$$

Propeller controls

The weight of propeller controls for turboprop engines can be estimated by using the below equation

$$W_{pc} = 0.322(N_{bl})^{0.589}\left(\frac{N_p D_p P_{TO}}{1000\ N_e}\right)^{1.178} \quad (12.31)$$

By the substituting the obtained values of N_p as 2, D_p as 13 ft, P_{TO} as 4517 hp, N_e as 2 and N_{bl} as 6 from previous chapters, we get

$$W_{pc} = 112\ lbs \quad (12.32)$$

Oil system and oil cooler

The weight of oil system and oil cooler is given by

$$W_{osc} = K_{osc} W_e \quad (12.33)$$

Where,

$K_{osc} = 0.07$ for turboprop engines

Therefore,

$$W_{osc} = 241\ lbs \quad (12.34)$$

The total powerplant weight is calculated as 5710 lbs whereas class I method of powerplant weight estimation is obtained as 6397 lbs. Therefore, the average of both is used as our final class II powerplant weight estimation which is 6053 lbs.

12.5 CLASS II METHOD FOR ESTIMATING FIXED EQUIPMENT WEIGHT

The proposed aircraft assumes the following items in fixed equipment weight:

- Flight control system
- Instrumentation, avionics and electronics
- Electrical system
- Air-conditioning, pressurization, anti- and de-icing system
- Oxygen system

- Auxiliary power unit
- Furnishings
- Baggage and cargo handling equipment
- Paint

12.5.1 Flight Control System

The weight of flight control system is given by the following equation

$$W_{fc} = K_{fc}(W_{TO})^{2/3} \tag{12.35}$$

Where,

$K_{fc} = 0.64$ for airplanes with powered flight controls

Therefore,

$$W_{fc} = 914\ lbs \tag{12.36}$$

12.5.2 Instrumentation, Avionics and Electronics

The weight of instrumentation, avionics and electronics is given by

$$W_{iae} = 120 + 20N_e + 0.006W_{TO} = 484\ lbs \tag{12.37}$$

12.5.3 Electrical System

Electrical system weight is calculated as follows

$$W_{els} = 1163\left\{\frac{W_{fs} + W_{iae}}{1000}\right\}^{0.506} = 1080\ lbs \tag{12.38}$$

12.5.4 Air-Conditioning, Pressurization, Anti- and De-icing systems

Air-conditioning, pressurization, anti- and de-icing systems weight is calculated as follows using the length of the passenger cabin as 42.65 ft.

$$W_{api} = 6.75(l_{pax})^{1.28} = 823\ lbs \tag{12.39}$$

12.5.5 Oxygen System

The weight of the oxygen system is calculated as follows

$$W_{OX} = 20 + 0.5N_{pax} = 42\ lbs \tag{12.40}$$

12.5.6 Auxiliary Power Unit

The weight of auxiliary power unit can be estimated as follows

$$W_{apu} = (0.004 \text{ to } 0.013)W_{TO} \tag{12.41}$$

The proposed aircraft uses battery power and fuel as a combination and hence, it is reasonable to assume minimum value of 0.004.

$$W_{apu} = 0.004\, W_{TO} = 216\ lbs \tag{12.42}$$

12.5.7 Furnishings

The weight of the furnishings can be estimated as follows

$$W_{fur} = 0.211(W_{TO} - W_F)^{0.91} = 4137\ lbs \tag{12.43}$$

12.5.8 Baggage and Cargo Handling Equipment

The baggage and cargo handling equipment include freight pallets with approximate net weight of 262 lbs for handling extra luggage and equipment.

$$W_{bc} = 3S_{ff} = 786\ lbs \tag{12.44}$$

12.5.9 Paint

The weight of the paint for regional proposed aircraft can be estimated as follows

$$W_{pt} = 0.003\, W_{TO} = 162\ lbs \tag{12.45}$$

The total fixed equipment weight is calculated as 8644 lbs whereas class I method of fixed equipment weight is obtained as 8434 lbs. Considering the average, the final class II fixed equipment weight is 8539 lbs.

The class II empty weight is calculated as

$$W_E = W_{struct} + W_{pwr} + W_{feq} = 30044\ lbs \tag{12.46}$$

Comparing the above value with class I estimation of empty weight i.e 31926 lbs, the difference is 6.3 percent. The calculated class II estimates are based on the Roskam (Roskam, 2005) procedure and for hybrid aircraft, the battery handling equipment and battery power generator is not included. Therefore, by assuming battery handling equipment weight as 900 lbs and battery power generator weight as 982 lbs, the

discrepancy of 1882 lbs can be achieved. Hence, the empty weight of 31926 lbs can be used in class II weight estimation.

12.6 WEIGHT AND BALANCE

The class II components weight and coordinate data with x, y and z coordinates are shown below.

Table 48: Class II components weight and coordinate data

Type of Component	Weight (lbs)	x (ft)	Wx (ft.lbs)	y (ft)	Wy (ft.lbs)	z (ft)	Wz (ft.lbs)
Wing	5586	28.3	158083.8	0	0	10.9	60887.4
Empennage: HT	596	68.705	40948.18	0	0	26.35	15704.6
Empennage: VT	655	65.703	43035.46	0	0	18.33	12006.15
Fuselage	5199	32.71	170074.88	0	0	6.6	34313.4
Nacelles	1066	22.68	24177.95	0	0	10.5	11193
Landing gear: Nose gear	446	6.6	2940.3	0	0	2	891
Landing gear: Main gear	1904	33.46	63707.84	0	0	3.14	5978.56
Power plant	7035	22.68	159553.8	0	0	10.8	75978
Fixed equipment	9439	32.71	308749.69	0	0	6.6	62297.4
Empty Weight	31926	30.42	971271.91	0	0	8.75	279249.51
Crew: Pilots	410	6	2460	0	0	6.6	2706
Crew: Attendants	410	54.72	22436.43	0	0	6.6	2706
Trapped Fuel and Oil	270	29	7830	0	0	11	2970
Operating Empty Weight	33016	30.41	1003998.34	0	0	8.71	287631.51
Fuel	1891	28.3	53515.3	0	0	10.9	20611.9
Batteries	10893	36.35	395960.55	0	0	6.6	71893.8
Passengers	7000	32.71	228970	0	0	6.6	46200
Baggage	1200	32.71	39252	0	0	6.6	7920
Take-off weight	54000	31.88	1721696.19	0	0	8.04	434257.21

The class II method calculation of center of gravity locations for different loading scenarios are shown below.

Table 49: Class II method of CG locations for different loading scenarios

Loading Scenarios	C.G locations	Weight
Empty weight	30.42	31926
Empty weight + Crew	30.42	32746

Empty weight + Crew + TFO	30.41	33016
Empty weight + Crew +TFO+ fuel	30.30	34907
Empty weight + Crew + TFO+ Battery	31.88	43909
Empty weight + Crew + TFO+ fuel + battery	31.74	45800
Empty weight + half passengers	30.65	35426
Empty weight + Payload	30.89	40126
Empty weight + half luggage	30.47	32526
Empty weight + Crew + TFO+ fuel + battery + half payload	31.82	49900
Empty weight + Crew + TFO+ fuel + battery + payload	31.88	54000

Based on the above calculated CG locations for different loading scenarios, the class II CG excursion diagram is shown below.

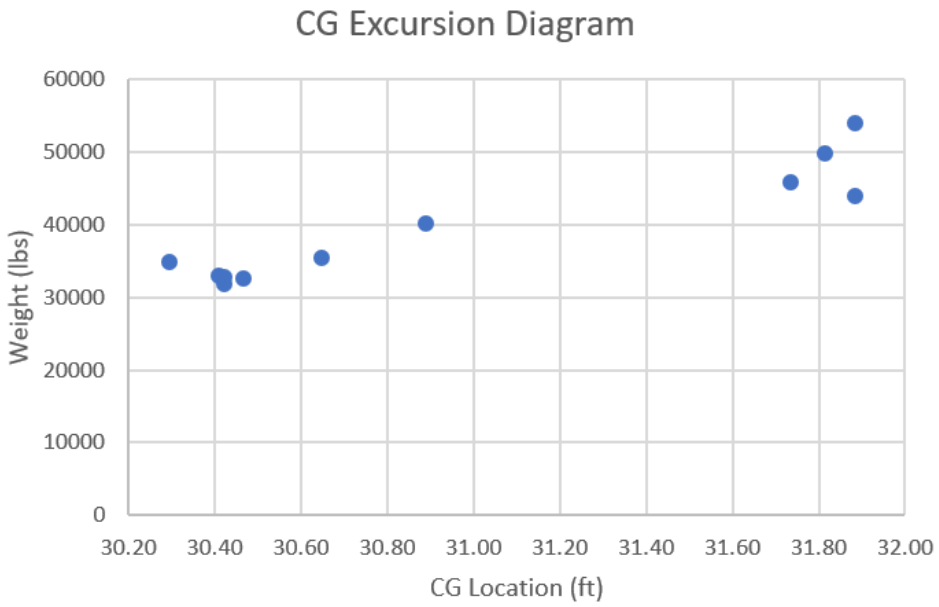

Figure 182: Class II CG excursion diagram

From the above CG excursion diagram the CG range is obtained as follows:

Most forward CG location from the nose of the proposed aircraft: 30.30 ft

Most aft CG location from the nose of the proposed aircraft: 31.88 ft

As per the Roskam (Roskam, 2005), the CG range for regional turboprop airplanes is 12 to 20 inches or 1 to 1.66 ft. The obtained range for the proposed aircraft is 1.58 ft or 18.96 inches.

12.7 DISCUSSION

The class II weight estimation calculations are quite reasonable when compared to the conventional regional reference airplane (ATR Aircraft, 2014). The class I and class II method of weight estimations are almost close. Weight and balance calculations clearly indicates the center of gravity movement is within the given range by Roskam (Roskam, 2005) for regional airplanes. Class II CG range is 1.58 ft whereas class I CG range is 1.53 ft which is close enough.

CHAPTER 13: COST ANALYSIS

13.1 INTRODUCTION

The preliminary design process includes many design decisions which may have significant effect on airplane life cycle cost. It is important for an airplane designer to be aware of these effects to check if their designs are cost-effective. The life cycle cost of the proposed aircraft is categorized into four main cost sources such as

- Research, development, test and evaluation cost
- Acquisition cost
- Operating cost
- Disposal cost

Typically, the operating cost is much larger than the acquisition and disposal cost sources for commercial airplanes. Hence, this chapter presents the operating cost analysis of the proposed aircraft. The operating cost is categorized into direct and indirect operating costs.

13.2 ESTIMATION OF DIRECT OPERATING COST

The direct operating cost of the proposed aircraft is estimated based on the following parameters

- **Block time**

The block time can be expressed as follows

$$t_{bl} = t_{gm} + t_{cl} + t_{cr} + t_{de} \tag{13.1}$$

From performance sizing, the time required to climb and to accelerate to the cruise speed t_{cl} is obtained as 0.30 hours and the time taken to descend, t_{de} is obtained as 0.25 hours.

Where, t_{gm} is the time spent in ground maneuvers expressed as follows:

$$t_{gm} = 0.51(10)^{-6}(W_{TO}) + 0.125 = 0.15 \text{ hours} \tag{13.2}$$

The time spent in cruise, t_{cr} is expressed as follows

$$t_{cr} = \frac{1.06R_{bl} - R_{cl} - R_{de} + R_{man}}{V_{cr}} \tag{13.3}$$

Using the projected horizontal speed of the aircraft during the climb, V_{cl} as 160 knots, descent speed, V_{de} as 125 knots, speed required while maneuvering as required by air traffic control constraints, V_{man} as 275 knots, we get the following distances

$$R_{cl} = V_{cl}t_{cl} = 48\ nm \quad (13.4)$$

$$R_{de} = V_{de}t_{de} = 31\ nm \quad (13.5)$$

$$t_{man} = 0.25(10)^{-6}(W_{TO}) + 0.0625 = 0.076 \text{ hours} \quad (13.6)$$

$$R_{man} = V_{man}t_{man} = 21\ nm \quad (13.7)$$

Also, R_{bl} is considered as 810 nm using the mission specifications and by substituting all the above values in cruise time, we get

$$t_{cr} = 2.91\ hours \quad (13.8)$$

Therefore,

$$t_{bl} = 0.15 + 0.30 + 2.91 + 0.25 = 3.6\ hours \quad (13.9)$$

- **Annual utilization in block hours**

The annual utilization in block hours is expressed as follows

$$U_{ann_{bl}} = 10^3[3.456(t_{bl}) + 2.994 + \{12.289(t_{bl})^2 - 5.6626(t_{bl}) + 8.964\}^{0.5}] \quad (13.10)$$

By substituting t_{bl} as 3.6 hours in the above equation, we get

$$U_{ann_{bl}} = 3271\ hours \quad (13.11)$$

- **Annual block miles**

The annual block miles can be estimated as follows

$$R_{bl_{ann}} = (V_{bl})\left(U_{ann_{bl}}\right) \quad (13.12)$$

Where,

$$V_{bl} = \frac{R_{bl}}{t_{bl}} = \frac{810}{3.6} = 225\frac{nm}{hr} \quad (13.13)$$

Therefore,

$R_{bl_{ann}}$ is 735975 nautical mile per airplane.

13.2.1 Direct Operating Cost of Flying

The direct operating cost of flying is broken down into the following flying cost elements

$$DOC_{flt} = C_{crew} + C_{pol} + C_{ins} + C_{bat} \quad (13.14)$$

Crew cost

The crew cost per nautical mile can be found from

$$C_{crew} = \sum_{j=1}^{j=4} \left[\left(n_{c_j} \right) \left\{ \frac{1 + K_j}{V_{bl}} \right\} \left(\frac{SAL_j}{AH_j} \right) + \left(\frac{TEF_j}{V_{bl}} \right) \right] \quad (13.15)$$

Where,

n_{c_j} is the number of crew members of each type, j. The n_{c_1} stands for captain, n_{c_2} stands for co-pilot and n_{c_3} stands for cabin crew. The proposed design has 1 captain, 1 co-pilot and 2 cabin crew.

K_j is a factor which accounts for vacation pay, cost of training, crew premium, crew insurance and payroll tax which is suggested to use as 0.26.

SAL_j is the annual salary paid to a crew member of type, j. The captain and co-pilot salaries per annum are assumed as 150000 USD and 100000 USD, cabin crew salaries are assumed as 60000 USD each.

AH_j is the number of flight hours per year for a crew member of type j. It is assumed as 900 hours for props for domestic operations.

TEF_j is the travel expense factor associated with each type of crew member, j. It is assumed as USD 7.0 bl/hr for domestic routes.

By substituting the above data, we get

$$C_{crew} = 2.48 \frac{USD}{nm} \quad (13.16)$$

Fuel and oil cost

The direct operating cost of fuel and oil is expressed as follows

$$C_{pol} = 1.05 \left(\frac{W_{F_{bl}}}{R_{bl}} \right) \left(\frac{FP}{FD} \right) \quad (13.17)$$

Where,

$W_{F_{bl}}$ is same as the mission fuel used which is 1513 lbs, FP is the current price of jet fuel which is 2.20 USD/gal. FD is fuel density which is 6.55 lbs/gal for JP-4.

Therefore,

$$C_{pol} = 0.66 \frac{USD}{nm} \tag{13.18}$$

Airframe insurance cost

The airframe insurance cost is determined from the following equation

$$C_{ins} = \frac{\left(f_{ins_{hull}}\right)(AMP)}{\left\{U_{ann_{bl}} V_{bl}\right\}} \tag{13.19}$$

Where,

$f_{ins_{hull}}$ is the annual hull insurance rate which is assumed as 0.030 USD/USD/airplane/year

AMP is the airplane market price, which is assumed as 200,00,000 USD compared to reference aircraft.

Therefore,

$$C_{ins} = 0.82 \frac{USD}{nm} \tag{13.20}$$

Batteries cost

The total required takeoff power is 4517 hp i.e 3368 KW for a range of 810 nm for the proposed aircraft and based on the current market of lithium-sulfur batteries, it is reasonable to assume the battery cost as 0.18 USD/nm.

By substituting all the above costs in direct operating cost of flying, we get

$$DOC_{flt} = 4.14 \frac{USD}{nm} \tag{13.21}$$

13.2.2 Direct Operating Cost of Maintenance

The direct operating cost of maintenance is expressed as follows

$$DOC_{maint} = C_{lab/ap} + C_{lab/eng} + C_{mat/ap} + C_{mat/eng} + C_{amb} \tag{13.22}$$

Labor cost of airframe and systems maintenance

The labor cost of airframe and system maintenance is given by

$$C_{lab/ap} = \frac{1.03\left(MHR_{map_{bl}}\right)\left(R_{l_{ap}}\right)}{V_{bl}} \tag{13.23}$$

Where,

$$MHR_{map_{bl}} = 3.0 + \frac{0.067(W_A)}{1000} \tag{13.24}$$

Airframe weight, $W_A = W_E - N_e W_{eng} = 31926 - (2 * 1720) = 28486\ lbs$ (13.25)

Using W_A as 28486 lbs, we get number of airframe and systems maintenance man hours needed per block hour, $MHR_{map_{bl}}$ as 4.91. The airplane maintenance labor rate per manhour is assumed as 22.60 USD/hr using the data in Roskam (Roskam, 2005). Hence,

$$C_{lab/ap} = 0.5\frac{USD}{nm} \tag{13.26}$$

Labor cost of engines maintenance

The maintenance labor cost per nautical mile of engines can be estimated from

$$C_{lab/eng} = \frac{1.03(1.3)(N_e)\left(MHR_{meng_{bl}}\right)\left(R_{l_{eng}}\right)}{V_{bl}} \tag{13.27}$$

Where, the number of engine maintenance hours needed per block hour per engine, $MHR_{meng_{bl}}$ is expressed as

$$MHR_{meng_{bl}} = \left[\left\{0.4956 + \frac{0.0532\left(\frac{SHP_{TO}}{N_e}\right)}{1000}\right\}\left(\frac{1100}{H_{em}}\right) + 0.10\right] \tag{13.28}$$

The attained number of hours between engine overhauls, H_{em} is assumed as 4000 hours for turbine engines. Using SHP_{TO} as 4517 hp and N_e as 2, we get $MHR_{meng_{bl}}$ as 0.27.

The engine maintenance labor rate per man hour, $R_{l_{eng}}$ is assumed as 22.60 USD/hr.

Therefore,

$$C_{lab/eng} = 0.073 \frac{USD}{nm} \tag{13.29}$$

Cost of maintenance materials for airframe and systems

The cost of maintenance materials for airframe and systems per nautical mile can be estimated from the following equation

$$C_{mat/ap} = \frac{1.03 C_{mat/apblhr}}{V_{bl}} \tag{13.30}$$

Where,

$$C_{\frac{mat}{apblhr}} = \left\{30.0 \left(\frac{CEF_{then\ year}}{CEF_{1989}}\right) ATF + (0.79 * 10^{-5}) AFP\right\} \tag{13.31}$$

Each engine price based on Pratt and Whitney PW127M model; EP is assumed as 995000 USD. Airplane market price AMP is same as the airplane estimated price AEP. Airplane type factor ATF is assumed as 1.0 for the proposed design.

AFP is expressed as follows

$$AFP = AEP - N_e(EP) = 200{,}00{,}000 - (2 * 995000) = 18010000\ USD \tag{13.32}$$

Therefore, $C_{\frac{mat}{apblhr}}$ is obtained as 200 USD/bl hr and hence,

$$C_{mat/ap} = 0.92 \frac{USD}{nm} \tag{13.33}$$

Cost of maintenance materials for engines

The cost of maintenance materials for the engine per nautical mile is estimated from the following equation

$$C_{mat/eng} = \frac{1.03(1.3)(N_e)\left(C_{\frac{mat}{engblhr}}\right)}{V_{bl}} \tag{13.34}$$

Where,

$$C_{mat/engblhr} = \{(5.43 * 10^{-5})(ESPPF) - 0.47\}\left(\frac{1}{K_{H_{em}}}\right) \quad (13.35)$$

The engine spare parts price factor, ESPPF is assumed as 1.50 for the proposed aircraft and $K_{H_{em}}$ for turbine engines is given as

$$K_{H_{em}} = 0.021\left(\frac{H_{em}}{100}\right) + 0.769 = 1.609 \quad (13.36)$$

Therefore, by using ESPPF as 1.50 and $K_{H_{em}}$ as 1.609, we get $C_{mat/engblhr}$ as 50 USD/hr and hence,

$$C_{mat/eng} = 0.60\frac{USD}{hr} \quad (13.37)$$

Applied maintenance burden

The cost of the applied maintenance burden can be estimated as follows

$$C_{amb} = \frac{1.03\left[f_{\frac{amb}{lab}}\left\{\left(MHR_{map_{bl}}R_{l_{ap}}\right)+\left(N_e\, MHR_{eng_{bl}}R_{l_{eng}}\right)\right\}+f_{\frac{amb}{mat}}\left\{C_{\frac{mat}{apblhr}}+\left(N_e\, C_{\frac{mat}{engblhr}}\right)\right\}\right]}{V_{bl}} \quad (13.38)$$

Where,

$f_{\frac{amb}{lab}}$ is assumed as 1.40 and $f_{\frac{amb}{mat}}$ is assumed as 0.70 based on the range given for airlines by Roskam (Roskam, 2005).

Therefore,

$$C_{amb} = 1.75\frac{USD}{nm} \quad (13.39)$$

The total direct operating cost of the maintenance is obtained as follows

$$DOC_{maint} = 3.85\frac{USD}{nm} \quad (13.40)$$

13.2.3 Direct Operating Cost of Depreciation

The direct operating cost of depreciation is expressed as follows

$$DOC_{depr} = C_{dap} + C_{deng} + C_{dprp} + C_{dav} + C_{dapsp} + C_{dengsp} \quad (13.41)$$

Cost of airframe depreciation

The cost of airframe depreciation per nautical mile can be estimated as follows

$$C_{dap} = \frac{F_{dap}\{AEP - (N_e\ EP) - (N_p\ PP) - ASP\}}{DP_{ap} U_{ann_{bl}} V_{bl}} \quad (13.42)$$

The airframe depreciation factor, F_{dap} is assumed as 0.85 and DP_{ap} is assumed as 10 for the proposed aircraft using the below data from Roskam (Roskam, 2005). The price of the propeller is assumed as 65000 USD based on PW 127 M model from Pratt and Whitney. The avionics systems price per airplane of proposed aircraft is assumed as 19,00,000 USD.

Item	Suggested Depreciation Period		Residual Value in Percent	Depreciation Factor*	
Airframe	DP_{ap}	= 10	15	F_{dap}	= 0.85
Engines	DP_{eng}	= 7	15	F_{deng}	= 0.85
Propellers	DP_{prp}	= 7	15	F_{dprp}	= 0.85
Avionics	DP_{av}	= 5	0	F_{dav}	= 1.00
Airplane Spares	DP_{apsp}	= 10	15	F_{dapsp}	= 0.85
Engine Spares	DP_{engsp}	= 7	15	F_{dengsp}	= 0.85

* Depreciation factor =

= [1 - (Residual Value)/(Original Price)]

Figure 183: Depreciation periods and factors

Therefore, by substituting all the values in the above equation, we get

$$C_{dap} = 1.85 \frac{USD}{nm} \quad (13.43)$$

Cost of engine depreciation

The cost of engine depreciation per nautical mile can be determined by using the following equation.

$$C_{deng} = \frac{F_{deng} * N_e * EP}{DP_{eng} * U_{ann_{bl}} * V_{bl}} \quad (13.44)$$

Using the engine depreciation factor, F_{deng} as 0.85 and DP_{eng} as 7 from above table, we get

$$C_{deng} = 0.33\frac{USD}{nm} \tag{13.45}$$

Cost of depreciation of propellers

The cost of depreciation of propellers can be estimated as follows by using the values from the above table.

$$C_{dprp} = \frac{F_{dprp} * N_p * PP}{DP_{prp} * U_{ann_{bl}} * V_{bl}} = 0.021\frac{USD}{nm} \tag{13.46}$$

Cost of depreciation of avionics systems

The cost of depreciation of avionics systems is estimated from:

$$C_{dav} = \frac{F_{dav} * ASP}{DP_{av} * U_{ann_{bl}} * V_{bl}} = 0.52\frac{USD}{nm} \tag{13.47}$$

Cost of depreciation of airplane spare parts

The cost of depreciation of airplane spare parts is estimated from:

$$C_{dapsp} = \frac{F_{dapsp} * F_{apsp}\{AEP - (N_e\ EP)\}}{DP_{apsp} * U_{ann_{bl}} * V_{bl}} = 0.21\frac{USD}{nm} \tag{13.48}$$

Cost of engine spare parts depreciation

The cost of engine spare parts depreciation is estimated as follows

$$C_{dengsp} = \frac{F_{dengsp} * F_{engsp} * (N_e) * (EP) * ESPPF\}}{DP_{engsp} * U_{ann_{bl}} * V_{bl}} = 0.25\frac{USD}{nm} \tag{13.49}$$

Therefore, the total direct operating cost of depreciation is obtained as

$$DOC_{depr} = 3.18\frac{USD}{nm} \tag{13.50}$$

13.2.4 Direct Operating Cost of Landing Fees, Navigation Fees and Registry Taxes

The direct operating cost of landing fees, navigation fees and registry taxes can be expressed as follows

$$DOC_{lnr} = C_{lf} + C_{nf} + C_{rt} \tag{13.51}$$

Direct operating cost due to landing fees

The direct operating cost due to landing fees can be determined from

$$C_{lf} = \frac{C_{aplf}}{V_{bl} * t_{bl}} \tag{13.52}$$

Where,

$$C_{aplf} = 0.002\, W_{TO} = 108 \frac{USD}{nm} \tag{13.53}$$

Therefore,

$$C_{lf} = 0.13 \frac{USD}{nm} \tag{13.54}$$

Direct operating cost due to navigation fees

The direct operating cost due to navigation fees is given by

$$C_{nf} = \frac{C_{apnf}}{V_{bl} * t_{bl}} \tag{13.55}$$

Where,

$C_{apnf} = 0$ USD/flight for domestic operations within USA and hence C_{nf} is 0.

Direct operating cost due to registry taxes

The direct operating cost of registry taxes is expressed as

$$C_{rt} = f_{rt}(DOC) = \{0.001 + (10^{-8}) W_{TO}\} * (DOC) \tag{13.56}$$

Therefore,

$$C_{rt} = 0.00154\ (DOC) \tag{13.57}$$

Hence,

The total direct operating cost of landing fees, navigation fees and registry taxes is obtained as

$$DOC_{lnr} = 0.13 + \{0.00154 * (DOC)\} \quad \frac{USD}{nm} \tag{13.58}$$

13.2.5 Direct Operating Cost of Financing

The direct operating cost of financing is estimated as follows

$$DOC_{fin} = 0.07 * (DOC) \frac{USD}{nm} \tag{13.59}$$

Therefore, the overall direct operating cost is obtained as

$$DOC = 12.20 \frac{USD}{nm} \tag{13.60}$$

13.3 ESTIMATION OF INDIRECT OPERATING COST

The proposed aircraft indirect operating cost can be estimated as follows:

$$IOC = f_{ioc}(DOC) = 0.50 * 12.20 = 6.10 \frac{USD}{nm} \tag{13.61}$$

13.4 ESTIMATION OF TOTAL OPERATING COST

The total operating cost is divided into the following two cost categories

$$C_{OPS} = \sum_{i=1}^{i=n} \left(C_{ops_{dir}}\right)_i (N_{acq})_i + \sum_{i=1}^{i=n} \left(C_{ops_{ind}}\right)_i (N_{acq})_i \tag{13.62}$$

Where,

The number of airplanes acquired by the ith customer, $(N_{acq})_i$ is assumed as 500 for the proposed aircraft for 10 years of operation, $(N_{yr})_i$.

$\left(C_{ops_{dir}}\right)_i$ is the total direct operating cost for the ith airplane customer, expressed as follows

$$\left(C_{ops_{dir}}\right)_i = (DOC)_i (R_{bl_{ann}})_i (N_{yr})_i = 89788950 \frac{USD}{airplane} \tag{13.63}$$

$\left(C_{ops_{ind}}\right)_i$ is the total indirect operating cost for the i[th] airplane customer, expressed as follows

$$\left(C_{ops_{ind}}\right)_i = (IOC)_i(R_{bl_{ann}})_i(N_{yr})_i = 44894475\,\frac{USD}{airplane} \qquad (13.64)$$

Therefore, the total/program operating cost is obtained as follows

$$C_{OPS} = 67 \text{ billion USD} \qquad (13.65)$$

13.5 DISCUSSION

The operating cost analysis of the proposed aircraft includes the estimation of direct operating cost and indirect operating cost. The total operating cost is expressed in terms of total direct, indirect operating costs and the number of airplanes acquired. Direct operating cost includes direct operating cost of flying, direct operating cost of maintenance, direct operating cost of depreciation, direct operating cost of landing fees, navigation fees and registry taxes and direct operating cost of financing.

The results clearly indicate that the direct operating cost is higher compared to indirect operating cost. The overall direct operating cost is obtained as 12.20 USD/nm. Looking at the statistics shown below, direct operating cost consists of 34% of flying, 31.5% of maintenance, 26% of depreciation, 1.5% of landing fees, navigation fees and registry taxes and 7% of financing.

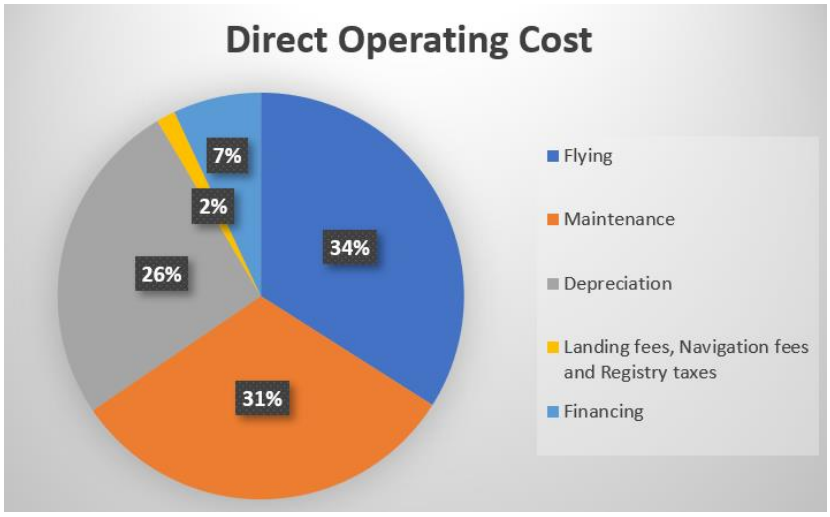

Figure 184: Summary of direct operating cost

Most of the direct operating cost consists of flying maintenance and depreciation. The indirect operating cost is obtained as 6.10 USD/nm. Assuming total 500 proposed airplanes are in acquisition for 10 years of operation, the total operating cost is obtained as 67 billion USD.

REFERENCES

Anticliff, K. R. (2018). Mission Analysis and Aircraft Sizing of Hybrid-Electric Regional Aircraft. *AIAA Technical conference.* AIAA 2018.

ATAG. (2018). *Air Transport Action Group.* Retrieved from ATAG: URL: www.atag.org

ATR . (2014). ATR Family. *ATR Family - ATR Aircraft URL: http://www.atraircraft.com/products_app/media/pdf/FAMILY_septembre2014.pdf*.

ATR. (2014). *ATR Brochure-The Green Power of Tomorrow*. Retrieved from ATR: URL: http://www.atraircraft.com/products_app/media/pdf/Brochure-Environment-2014.pdf.

Babikian, R. (2001). *The Historical Fuel Efficiency Characteristics of Regional Aircraft from Technological, Operational, and Cost Perspectives.* Massachusetts Institute of Technology.

Bombardier Inc. (2017). *Q Series* . Retrieved from Bomabardier Commercial Aircraft: URL: https://commercialaircraft.bombardier.com/themes/bca/pdf/Bombardier_Q_Series_Brochure.pdf

Bradley, M. K. (2015). *Subsonic Ultra Green Aircraft Research: Phase 2 - Volume 2 - Hybrid Electric Design Exploration* . Huntington Beach: NASA.

Cambridge, U. (2014). Hybrid-Electric Plane Successfully Tested in the UK. *URL: https://www.iflscience.com/technology/hybrid-electric-plane-successfully-tested-uk/*.

Engineering, T. (2003). *U.S. Standard Atmosphere*. Retrieved from Engineering ToolBox: URL: https://www.engineeringtoolbox.com/standard-atmosphere-d_604.html

Friedrich, C. (2014). Hybrid-Electric Propulsion for Aircraft. *Journal of Aircraft, Vol. 52 URL: https://arc.aiaa.org/doi/10.2514/1.C032660*(1).

Gary, H. (2018). *Aero International [Regional] ATR-42 and 72 Series Aircraft Chapter.* Retrieved from Saint Paul Airlines : URL: http://stpaulairlines.com/horton.htm

Hepperle, M. (2012). *Electric Flight - Potential and Limitations.* NATO Science and Technology Organization.

Jansen, R. (2017). Overview of NASA Electrified Aircraft Propulsion (EAP) Research for Large Subsonic Transports. *53rd AIAA/SAE/ASEE Joint Propulsion Conference.* Atlanta: AIAA Propulsion and Energy Forum, (AIAA 2017-4701).

Knapp, M. (2018). *Zunum Aero's Hybrid Electric Airplane Aims to Rejuvenate Regional Travel*. Retrieved from IEEE Spectrum: URL: https://spectrum.ieee.org/aerospace/aviation/zunum-aeros-hybrid-electric-airplane-aims-to-rejuvenate-regional-travel.

Luongo, C. A. (2014). Next Generation More-Electric Aircraft: A Potential Application for HTS Superconductors. *URL: https://www.researchgate.net/publication/224557800_Next_Generation_More-Electric_Aircraft_A_Potential_Application_for_HTS_Superconductors*.

MIT. (2006). *Fluids - Lecture 8 Notes*. Retrieved from MIT: URL: https://ocw.mit.edu/courses/aeronautics-and-astronautics/16-01-unified-engineering-i-ii-iii-iv-fall-2005-spring-2006/fluid-mechanics/f08_sp.pdf.

Palt, K. (2017). *CASA C-295 - Specifications - Technical Data/Description*. Retrieved from Flugzeug info.net: URL: http://www.flugzeuginfo.net/acdata_php/acdata_c295_en.php

Palt, K. (2017). *Fokker 50 - Specifications - Technical Data/Description*. Retrieved from Flugzeug info.net: URL: http://www.flugzeuginfo.net/acdata_php/acdata_fokker50_en.php

Pratt and Whitney. (2018). *PW100-150 - Pratt & Whitney*. (Pratt and Whitney Canada) Retrieved from Pratt and Whitney: URL: https://www.pwc.ca/en/products-and-services/products/regional-aviation-engines/pw100-150

Raymer, D. P. (2012). Aircraft Design. In *Aircraft Design: A Conceptual Approach, Fifth Edition.* AIAA Education Series.

Riboldi, F. G. (2016). *An integrated approach to the preliminary weight sizing of small electric aircraft.* Aerospace Science and Technology.

Robertson, C. F. (2015). Hybrid-Electric Propulsion for Aircraft. *Journal of Aircraft, Vol. 52 No. 1 (2015), pp. 176-189 URL: https://arc.aiaa.org/doi/10.2514/1.C032660*(1).

Roskam, D. J. (2005). Airplane Design Part I through VIII. In D. J. Roskam, *Airplane Design* . Lawrence, Kansas: DARcorporation.

Stuckl, S. (2012). VOLTAIR-The All Electric Propulsion Concept Platform-A Vision for Atmospheric Friendly Flight. *28th International Congress of the Aeronautical Sciences URL: https://www.icas.org/ICAS_ARCHIVE/ICAS2012/PAPERS/521.PDF*. ICAS.

Velupillai, D. (2014). T-Tails and Top Technology. *Flight Global URL: https://www.flightglobal.com/FlightPDFArchive/1979/1979%20-%203762.PDF*.

APPENDIX A: Battery Weight Calculation

```
%
% Calculation of battery weight by Riboldi's Method
%
function calculate_battery_weight

    Wto = 54000; % Take-off weight in lbs

    a = -2.3979;
    b = 1;
    c = -0.0866;
    d = 0.8099;

    Cf = 0.004;
    S = 657; % Wing area in sq.ft
    AR = 12; % Aspect Ratio
    e = 0.85; % Oswald Coefficient
    P = 4.77E+14; % Power Density in sq.ft/hr^3
    g = 416696000; % Gravitational force in ft/hr^2
    E = 7.53E+14; % Battery Energy Density in ft^2/hr^2
    np = 0.9;   % Propulsive Effeciency

    Cruise_altitude = 24934; % Cruise Altitude in ft, specified in mission reqs as 7600m
    Vcruise = 1670929; % Velocity Cruise in ft/hr
    density_cruise = 0.034297; % Density Cruise in lb/ft^3

    Vloiter = 1215223.68; % Velocity Loiter in ft/hr
    density_loiter = 0.03539; % Density loiter in lb/ft^3

    Vclimb = 1032942.24; % Velocity climb in ft/hr
    density_climb = 0.056497; % Density climb in lb/ft^3
    rate_of_climb = 81300; % Rate of climb in ft/hr. Assumed from reference aircraft

    range = 4921260; % Range in ft

    Swet = realpow(10, (c + d * log10(Wto))); % Wet area in sq.ft
    f = realpow(10, (a + b * log10(Swet))); % Parasite area in sq.ft
    K = 1/(pi*AR*e);

    CDo = f/S; % zero-lift drag coefficient
    CL_climb = 2*Wto*g/(density_climb*Vclimb*Vclimb*S); % Lift coefficient climb
    CD_climb = CDo + CL_climb*CL_climb*K; % Drag coefficient climb

    CL_cruise = 2*Wto*g/(density_cruise*Vcruise*Vcruise*S); % Lift coefficient cruise
    CD_cruise = CDo + CL_cruise*CL_cruise*K; % Drag coefficient cruise

    CL_loiter = 2*Wto*g/(density_loiter*Vloiter*Vloiter*S); % Lift coefficient loiter
    CD_loiter = CDo + CL_loiter*CL_loiter*K; % Drag coefficient loiter

    Time_loiter = 0.25; % Time to loiter in hrs assumed to be 15mins
    Time_cruise = range/Vcruise; % Time to cruise in hrs
    Time_climb = Cruise_altitude/rate_of_climb; % Time to climb in hrs

    Power_cruise = 0.5*density_cruise*Vcruise*Vcruise*Vcruise*S*CD_cruise; % Power of Crui
se in lb.ft^2/hr^3
    Power_loiter = 0.5*density_loiter*Vloiter*Vloiter*Vloiter*S*CD_loiter; % Power of loit
```

```
er in lb.ft^2/hr^3
    Power_climb = 0.5*density_climb*Vclimb*Vclimb*Vclimb*S*CD_climb; % Power of climb in l
b.ft^2/hr^3

    disp("Power Cruise: " + Power_cruise + " lb.ft^2/hr^3 OR " + lb_sq_ft_per_cubic_hr_to_
kilo_watt(Power_cruise) + " KW");
    disp("Power Loiter: " + Power_loiter + " lb.ft^2/hr^3 OR " + lb_sq_ft_per_cubic_hr_to_
kilo_watt(Power_loiter) + " KW");
    disp("Power Climb: " + Power_climb + " lb.ft^2/hr^3 OR " + lb_sq_ft_per_cubic_hr_to_ki
lo_watt(Power_climb) + " KW");

    Energy_cruise = Power_cruise * Time_cruise; % Energy of cruise in lb.ft^2/hr^2
    Energy_loiter = Power_loiter * Time_loiter; % Energy of loiter in lb.ft^2/hr^2
    Energy_climb = Power_climb * Time_climb; % Energy of climb in lb.ft^2/hr^2

    disp("Energy Cruise: " + Energy_cruise + " lb.ft^2/hr^2 OR " + lb_sq_ft_per_sq_hr_to_k
ilo_watt_hr(Energy_cruise) + " KWh");
    disp("Energy Loiter: " + Energy_loiter + " lb.ft^2/hr^2 OR " + lb_sq_ft_per_sq_hr_to_k
ilo_watt_hr(Energy_loiter) + " KWh");
    disp("Energy Climb: " + Energy_climb + " lb.ft^2/hr^2 OR " + lb_sq_ft_per_sq_hr_to_kil
o_watt_hr(Energy_climb) + " KWh");

    battery_weight = max([(Energy_cruise + Energy_climb + Energy_loiter)/E, max([Power_cli
mb, Power_cruise, Power_loiter])/P])/np;
    disp("Battery Weight: " + battery_weight + " lbs");
end

function kw = lb_sq_ft_per_cubic_hr_to_kilo_watt(value)
    kw = value*9.03208807E-13/1000;
end

function kwh = lb_sq_ft_per_sq_hr_to_kilo_watt_hr(value)
    kwh = value*9.03208807E-13/1000;
end
```

```
Power Cruise: 2.623198997415625e+18 lb.ft^2/hr^3 OR 2369.2964 KW
Power Loiter: 1.826501827901566e+18 lb.ft^2/hr^3 OR 1649.7125 KW
Power Climb: 1.518420124965518e+18 lb.ft^2/hr^3 OR 1371.4504 KW
Energy Cruise: 7.725908340822153e+18 lb.ft^2/hr^2 OR 6978.1085 KWh
Energy Loiter: 4.566254569753915e+17 lb.ft^2/hr^2 OR 412.4281 KWh
Energy Climb: 4.656861918313679e+17 lb.ft^2/hr^2 OR 420.6119 KWh
Battery Weight: 12761.1332 lbs
```

APPENDIX B: MATLAB Code for Performance Constraints Matching Plot

```
% Performance Constraints Analysis Matching Graph
function plot_all_perf_objectives
    S_TOFL = 1367; % Takeoff field length in meters
    THRUST_TO_POWER_CONST = 2.9;
    sigma = 1;
    S_FL = 1300; % Landing field length in meters
    density = 0.002377; % Density in slugs/ft^3

    TOP_25 = S_TOFL*3.28084/37.5;

    figure
    title('Matching Graph');
    xlabel('(W/S)_{TO} (lb/ft^2)', 'Fontsize',12);
    ylabel('(W/P)_{TO} (lb/hp)', 'Fontsize',12);
    CL_values = [1.5 1.7 1.9 2.1];

    for CL = CL_values
        ws_takeoff = 20:1:100;
        wp_takeoff = (THRUST_TO_POWER_CONST*TOP_25*sigma*CL)*realpow(ws_takeoff, -1);
        hold on
        plot(ws_takeoff, wp_takeoff)
    end

    ylim([0 50]);

    V_A = realpow(S_FL*3.28084/0.3, 0.5);
    disp("Approach speed: " + V_A);
    landing_stall_speed = V_A*1.68781/1.3; % Landing stall speed in ft/sec
    disp("Stall speed: " + landing_stall_speed);
    CL_values = [1.9 2.1 2.3 2.5];

    for CL = CL_values
        ws_landing = ((landing_stall_speed^2)*0.5*density*CL)/0.972;
        wp_landing = [0 50];
        hold on
        plot([ws_landing ws_landing], wp_landing)
    end

    disp("FAR 25.111(OEI) Ratio: " + wp_ws_ratio_far_25111);
    ws = 20:1:100;
    wp = wp_ws_ratio_far_25111*realpow(realpow(ws, 0.5), -1);
    hold on
    plot(ws, wp, '--');

    disp("FAR 25.121(OEI) transition segment Ratio: " + wp_ws_ratio_far_25121_gear_down);
    ws = 20:1:100;
    wp = wp_ws_ratio_far_25121_gear_down*realpow(realpow(ws, 0.5), -1);
    hold on
    plot(ws, wp, '--');

    disp("FAR 25.121(OEI) second segment Ratio: " + wp_ws_ratio_far_25121_gear_up);
    ws = 20:1:100;
    wp = wp_ws_ratio_far_25121_gear_up*realpow(realpow(ws, 0.5), -1);
    hold on
    plot(ws, wp, '--');
```

```
    disp("FAR 25.121(OEI) en-route climb Ratio: " + wp_ws_ratio_far_25121_flaps_retracted)
;
    ws = 20:1:100;
    wp = wp_ws_ratio_far_25121_flaps_retracted*realpow(realpow(ws, 0.5), -1);
    hold on
    plot(ws, wp, '--');

    disp("FAR 25.119(AEO) Ratio: " + wp_ws_ratio_far_25119_gear_down);
    ws = 20:1:100;
    wp = wp_ws_ratio_far_25119_gear_down*realpow(realpow(ws, 0.5), -1);
    hold on
    plot(ws, wp, '--');

    disp("FAR 25.121(OEI) Ratio: " + wp_ws_ratio_far_25121_approach_flaps);
    ws = 20:1:100;
    wp = wp_ws_ratio_far_25121_approach_flaps*realpow(realpow(ws, 0.5), -1);
    hold on
    plot(ws, wp, '--');

    Ip = 1.7;
    sigma = 1;
    ws = 20:1:100;
    wp = ws/(sigma*Ip^3);
    plot(ws, wp);

    set(findall(gcf, 'type', 'line'), 'linewidth', 1.5);

    lgd = legend('CL TO = 1.5', 'CL TO = 1.7', 'CL TO = 1.9', 'CL TO = 2.1', 'CL Landing =
 1.9', 'CL Landing = 2.1', 'CL Landing = 2.3', 'CL Landing = 2.5', 'FAR 25.111(OEI)', 'FAR
 25.121(OEI) transition segment', 'FAR 25.121(OEI) second segment', 'FAR 25.121(OEI) en-ro
ute climb', 'FAR 25.119(AEO)', 'FAR 25.121(OEI)', 'Cruise Speed');
    lgd.FontSize = 5;
end

%
% Takeoff flaps, landing gear retracted, FAR25.111(OEI)
%
function wp_ws_ratio = wp_ws_ratio_far_25111
    velocity_ratio = 1.2; % V2/Vs_TO
    np = 0.85; % Propeller Efficiency
    clmax_takeoff = 1.7; % Takeoff lift coefficient
    cdo = 0.0489; % Zero-lift drag coefficient
    aspect_ratio = 12;
    e = 0.8; % Oswald coefficient
    cgr = 0.012; % Climb gradient
    sigma = 1;

    cl = clmax_takeoff/(velocity_ratio*velocity_ratio);
    k = get_k(aspect_ratio, e);
    cd = cdo + k*cl^2;
    lift_to_drag_ratio = cl/cd;
    cgrp = (cgr + (1/lift_to_drag_ratio))/(cl^0.5);
    wp_ws_ratio = (18.97*np*(sigma^0.5))/cgrp;
end

%
```

```
% Takeoff flaps, landing gear down. FAR 25.121(OEI)
%
function wp_ws_ratio = wp_ws_ratio_far_25121_gear_down
    velocity_ratio1 = 1.1; % VLOF/Vs_TO
    velocity_ratio2 = 1.2; % V2/Vs_TO
    np = 0.85; % Propeller Efficiency
    clmax_takeoff = 1.7; % Takeoff lift coefficient
    cdo = 0.0689; % Zero-lift drag coefficient
    aspect_ratio = 12;
    e = 0.8; % Oswald coefficient
    cgr = 0; % Climb gradient
    sigma = 1;

    cl = clmax_takeoff/(velocity_ratio1^2);
    k = get_k(aspect_ratio, e);
    cd = cdo + k*cl^2;
    lift_to_drag_ratio = cl/cd;
    cgrp = (cgr + (1/lift_to_drag_ratio))/(cl^0.5);
    wp_ws_ratio1 = (18.97*np*(sigma^0.5))/cgrp;

    cl = clmax_takeoff/(velocity_ratio2^2);
    k = get_k(aspect_ratio, e);
    cd = cdo + k*cl^2;
    lift_to_drag_ratio = cl/cd;
    cgrp = (cgr + (1/lift_to_drag_ratio))/(cl^0.5);
    wp_ws_ratio2 = (18.97*np*(sigma^0.5))/cgrp;

    wp_ws_ratio = max(wp_ws_ratio1, wp_ws_ratio2);
end

%
% Takeoff flaps, landing gear retracted FAR 25.121(OEI)
%
function wp_ws_ratio = wp_ws_ratio_far_25121_gear_up
    velocity_ratio = 1.2; % V2/Vs_TO
    np = 0.85; % Propeller Efficiency
    clmax_takeoff = 1.7; % Takeoff lift coefficient
    cdo = 0.0489; % Zero-lift drag coefficient
    aspect_ratio = 12;
    e = 0.8; % Oswald coefficient
    cgr = 0.024; % Climb gradient
    sigma = 1;

    cl = clmax_takeoff/(velocity_ratio*velocity_ratio);
    k = get_k(aspect_ratio, e);
    cd = cdo + k*cl^2;
    lift_to_drag_ratio = cl/cd;
    cgrp = (cgr + (1/lift_to_drag_ratio))/(cl^0.5);
    wp_ws_ratio = (18.97*np*(sigma^0.5))/cgrp;
end

%
% Flaps retracted, Landing gear retracted, FAR 25.121(OEI)
%
function wp_ws_ratio = wp_ws_ratio_far_25121_flaps_retracted
    velocity_ratio = 1.25; % V2/Vs_TO
    np = 0.85; % Propeller Efficiency
```

```
    clmax_takeoff = 1.5; % Takeoff lift coefficient
    cdo = 0.0339; % Zero-lift drag coefficient
    aspect_ratio = 12;
    e = 0.85; % Oswald coefficient
    cgr = 0.012; % Climb gradient
    sigma = 1;

    cl = clmax_takeoff/(velocity_ratio*velocity_ratio);
    k = get_k(aspect_ratio, e);
    cd = cdo + k*cl^2;
    lift_to_drag_ratio = cl/cd;
    cgrp = (cgr + (1/lift_to_drag_ratio))/(cl^0.5);
    wp_ws_ratio = (18.97*np*(sigma^0.5))/cgrp;
end

%
% Landing flaps, Landing gear down, FAR 25.119 (AEO)
%
function wp_ws_ratio = wp_ws_ratio_far_25119_gear_down
    velocity_ratio = 1.3; % V2/Vs_TO
    np = 0.85; % Propeller Efficiency
    clmax_takeoff = 2.1; % Takeoff lift coefficient
    cdo = 0.1139; % Zero-lift drag coefficient
    aspect_ratio = 12;
    e = 0.75; % Oswald coefficient
    cgr = 0.032; % Climb gradient
    sigma = 1;

    cl = clmax_takeoff/(velocity_ratio*velocity_ratio);
    k = get_k(aspect_ratio, e);
    cd = cdo + k*cl^2;
    lift_to_drag_ratio = cl/cd;
    cgrp = (cgr + (1/lift_to_drag_ratio))/(cl^0.5);
    wp_ws_ratio = (18.97*np*(sigma^0.5))/(cgrp*(0.972^1.5));
end

%
% Approach Flaps, FAR 25.121(OEI)
%
function wp_ws_ratio = wp_ws_ratio_far_25121_approach_flaps
    velocity_ratio = 1.5; % V2/Vs_TO
    np = 0.85; % Propeller Efficiency
    clmax_takeoff = 1.9; % Takeoff lift coefficient
    cdo = 0.0864; % Zero-lift drag coefficient
    aspect_ratio = 12;
    e = 0.75; % Oswald coefficient
    cgr = 0.021; % Climb gradient
    sigma = 1;

    cl = clmax_takeoff/(velocity_ratio*velocity_ratio);
    k = get_k(aspect_ratio, e);
    cd = cdo + k*cl^2;
    lift_to_drag_ratio = cl/cd;
    cgrp = (cgr + (1/lift_to_drag_ratio))/(cl^0.5);
    wp_ws_ratio = (18.97*np*(sigma^0.5))/(cgrp*(0.972^1.5));
end
```

```
function k = get_k(aspect_ratio, e)
    k = 1/(3.14*aspect_ratio*e);
end
```